Early-age cracking of concrete

A study into the influence of stress relaxation on early-age cracking of concrete structures under imposed deformations

TU Delft

J.R. van Bokhorst

Early-age cracking of concrete

A study into the influence of stress relaxation on early-age cracking of concrete structures under imposed deformations

By

J. R. van Bokhorst

in fulfilment of the requirements for the degree of

Master of Science
in Structural Engineering

at the Delft University of Technology,
to be defended publicly on Wednesday April 29, 2020 at 14:00.

Thesis committee:	Prof. dr. ir. E. Schlangen,	TU Delft, chairman
	Dr. ir. M. Luković,	TU Delft
	Dr. ir. B. Šavija,	TU Delft
	Ir. J.C. Galjaard RO,	VWICC

TU Delft

Preface

Before you lies the report of my master thesis “Early-age cracking of concrete: A study into the influence of stress relaxation on early-age cracking in concrete structures under imposed deformations”. It has been written in fulfilment of the requirements for the degree of Master of Science in Structural Engineering at the Delft University of Technology.

I was engaged in this research in the period from September 2019 to April 2020. The subject of my master thesis was formulated in cooperation with VolkerWessels Infra Competence Centre (VWICC) and prof.dr.ir. Erik Schlangen. I have a great interest in infrastructure projects and in particular concrete structures. For me, the subject of my thesis therefore is an interesting mix between fundamental research and engineering practice. The combination of performing laboratory tests at the university, using finite element models and doing measurements in practice made that I found my research challenging but also very interesting.

I want to express my gratitude to the members of my thesis committee prof.dr.ir. Erik Schlangen, dr.ir. Mladena Luković, dr.ir. Branko Šavija and ir. Hans Galjaard RO for their excellent advice, guidance and support throughout the period I was working on my master thesis. I want to thank Hans Galjaard in special, for he was, in his role of daily supervisor, always willing to debate issues, share insights and support me in my daily work. Partly because of this, I can look back on my period at VWICC with good feelings.

Finally, I want to thank my family and friends for their support and interest in my work, you kept me motivated to keep doing my best and bring my research to a successful conclusion.

I hope you enjoy your reading.

J.R. van Bokhorst
Nijkerk, April 2020

Abstract

When hardening concrete is subjected to imposed deformations, stresses may develop. If at any point in time this stress exceeds the tensile strength of the material, the concrete will crack. Early-age cracking of concrete structures may lead to issues related to durability, serviceability and aesthetics. During hardening of concrete the material properties are still in development. This means that to be able to assess the risk of early-age cracking for a specific case, understanding of the hydration process and the stress- and strength development is required. Besides, concrete is a viscoelastic material which means that stresses are affected by mechanisms of creep- and relaxation. The right approach for assessing the risk of early-age cracking in concrete structures is yet to be determined and the effects of creep and relaxation on the stress development during hardening remain subject of debate.

The aim of this study was to gain more insight in the effect of stress relaxation on early-age cracking of concrete structures under imposed deformations. For this purpose, the following research question was formulated:

"How can early-age cracking in concrete under imposed deformations be analysed taking into account stress relaxation and what is the applicability of the models used?"

To be able to answer this research question, first the relevant processes and mechanisms that play a role in the hardening of concrete had to be discussed in more detail. The state-of-the-art of the subject was discussed as well as the methods to take into account viscoelastic material behaviour in the analysis.

Next, the research was narrowed down by considering a single case from engineering practice. It was decided to consider a dive-under that was being constructed near Zwolle, the Netherlands. This dive-under consists of multiple segments which are all constructed in the same manner by first casting the slab and subsequently casting the walls on top. The hardening process of the walls corresponds to a typical imposed deformations case as is also described in literature.

In order to assess the risk of early-age cracking for the selected case, finite element software was used. The hardening process of the walls of the dive-under was modelled by considering a cross-section of the wall and slab. A parameter study was carried out to gain more insight in the effect of altering the different input parameters of the analysis on the resulting stress- and strength development during hardening.

Also, creep data which could be found in literature was analysed and the Maxwell chain model was adopted to be able to model the viscoelastic material behaviour. The Maxwell chain model consists of units of springs and dampers connected in series. When using several of these units in parallel, the viscoelastic material behaviour can be simulated. Evaluation of the Maxwell chain model was needed to be able to use the available creep data in the analysis.

Because the outcome of the analysis was dependent on many input parameters, several laboratory tests were carried out at the Stevin laboratory of the TU Delft. This was done for the specific concrete mixture that was also being used in the construction of the walls of the dive-under. The aim of these tests was on the one hand to simulate the hardening process of the wall of the dive-under and on the other hand to determine the strength- and stiffness development of the material over time. Also, the autogenous deformations were measured in a ADTM test. The results of the tests were analysed and could subsequently be used to improve the accuracy of the finite element model regarding the risk of early-age cracking.

Then, by making use a finite element model of the TSTM test and comparing the outcome of this analysis with the results of the actual TSTM test, the viscoelastic material behaviour of the concrete could be derived. It was found that the effects of creep- and stress relaxation at early-ages were initially underestimated and new creep curves were derived. An average early-age creep factor for the stress in a governing point in the bottom of the wall of around 2.4 was found.

Next to the laboratory testing and computational models, temperature measurements and visual inspections were done in practice on a segment of the dive-under. The temperature measurements could directly be used to improve the model. The aim of the visual inspections was to determine whether early-age cracking would actually occur in the walls of the dive-under. During the inspections it was found that early-age cracking did not occur in any of the inspected walls. Cracking of the walls was eventually observed, however not within the time period that was regarded for early-age cracking. The results of the inspections were then used to be able to make judgements on the accuracy and suitability of the model for the assessment of the risk of early-age cracking.

By making use of the collected data, the derived material properties and the temperature measurements from practice, the assessment of the risk of early-age cracking could be performed more accurately. This resulted in a figure which showed the stress- and strength development over time for a governing point in the cross-section of the wall. Based on information found in literature, a global risk of early-age cracking of the wall could then be determined.

When comparing the results of the above described finite element analysis with the results of the visual inspections, it was found that the results of the model did not correspond to the observations from practice. The output of the analysis suggested a high risk of early-age cracking, while in reality early-age cracking did not occur in any of the inspected walls. Possible causes for this difference were subsequently discussed.

In the end, conclusions were drawn on the accuracy of the analysis, the material properties that were determined through laboratory testing and the effect of viscoelastic material behaviour on the risk of early-age cracking of the walls. It was found that the material behaviour at early-ages (the first 48 hours) is very important for the overall stress development. Also, the results of the laboratory testing suggested that the effects of creep- and stress relaxation are generally underestimated in this period. Moreover, it was concluded that early-age autogenous swelling is of significant influence on the stress development over time. This period of swelling prior the autogenous shrinkage is however not taken into account in the current Eurocode.

More research is needed into the (viscoelastic) material behaviour at early-ages. In this way the creep curves as proposed in this research can be verified. The fact that cracking of the walls only occurred at higher ages, suggests that the effect of stress relaxation at higher ages is limited. This behaviour should be investigated in more detail. Also, the research methods that are used in this study should also be combined for more cases in the future. Using the combination of a computational model, laboratory tests and observations from practice creates the necessary conditions to be able to draw well-founded conclusions on the accuracy of the used models and the material behaviour in practice. Testing methods should be developed/improved to be able to measure material behaviour at very early ages.

Table of contents

List of abbreviations

ACI	American concrete institute
ADTM	Autogenous deformation testing machine
BFS	Blast furnace slag
CEB	Comité Euro-International du Béton
CPT	Cone penetration test
CSH	Calcium Silicate Hydrate
CTE	Coefficient of thermal expansion
FEA	Finite element analysis
FEM	Finite element model
FIB	Fédération Internationale du Béton
HSC	High strength concrete
ITZ	Interfacial transition zone
JSCE	Japan Society of Civil Engineers
KNMI	Koninklijk Nederlands Meteorologisch Instituut
LVDT	Linear variable differential transformer
ODE	Ordinary differential equation
OPC	Ordinary Portland cement
RH	Relative humidity
SP	Superplasticizer
TSTM	Temperature stress testing machine
ULS	Ultimate limit state
UHPFRC	Ultra high performance fibre reinforced concrete

List of symbols

Latin letters

a	Transfer coefficient at the boundary of the element	$[Wm^{-2}°C^{-1}]$
C	Cement dependent factor in 'de Vree' equation	[-]
c	Subgrade modulus of the soil	$[N/mm^3]$
c_T	Specific heat	$[J/kg * K]$
d	thickness of the formwork layer at the boundary of the concrete element	$[m]$
E_{cm}	Mean Young's Modulus	$[N/mm^2]$
f_{ck}	Characteristic concrete compressive strength	$[N/mm^2]$
f_{cm}	Mean compressive strength of concrete	$[N/mm^2]$
f_{ctm}	Mean tensile strength	$[N/mm^2]$
G	Solar radiation function	$[W/m^2]$
J	Radiation function for at a boundary of the element	$[Jm^2s^{-1}]$
J	Creep compliance	$[1/MPa]$
M	Maturity of the concrete	$[°Ch]$
n	Factor for time dependent behaviour	[-]
Δp	Change in pore pressure	$[N/mm^2]$
q	Heat flux from concrete to the environment	$[Jm^2/s]$
q_{solar}	Heat flux regarding solar radiation	$[Jm^2/s]$
R	Universal gas constant	$[kJ/molK]$
R	Degree of restraint	[-]
r	Meniscus radius in capillary pore	$[mm]$
s_{CEM}	Factor for cement type classification	[-]
T	Absolute temperature of the concrete	[°C]
T_e	External absolute temperature	[°C]
T_r	Reference temperature for maturity calculations	[°C]
T_0	Initial mix temperature	[°C]
t	Time	$[h]$
ΔT	Change in temperature	[°C]
Δt	Time increment	$[s]$
w	Wind speed	$[m/s]$
Q	Apparent activation energy	$[kJ/mol]$

Greek letters

α_{bs}	Factor for cement type classification	[-]
α_c	Coefficient of thermal expansion	[1/°C]
α_h	Degree of hydration	[-]
$\beta\,(t)$	Time dependent function	[-]
γ	Surface tension of pore water	$[N/mm]$
γ	Safety against cracking	[-]
ε	General strain	$[mm/mm]$
ε_a	Emissivity coefficient for long wave radiation to the surface	[-]
ε_{au}	Autogenous strain	$[mm/mm]$
ε_{ca}	Autogenous strain	$[mm/mm]$
ε_{cr}	Creep strain	$[mm/mm]$

ε_r	Emissivity coefficient for short wave radiation	[-]
ε_s	Emissivity coefficient for long wave radiation from the surface	[-]
ε_T	Thermal strain	$[mm/mm]$
λ_c	Thermal conductivity	$[W/mK]$
μ	Viscosity of a linear damper	$[hN/mm^2]$
ρ_c	Specific mass of concrete	$[kg/m^3]$
σ	General stress	$[N/mm^2]$
σ	Radiation coefficient	$[Wm^{-2}K^{-4}]$
τ	Retardation time	$[h]$
$\Psi(t,T)$	Relaxation factor	[-]

List of figures

1 Introduction

1.1 Concrete as a construction material

Concrete is the most widely used construction material in the world. The first evidences of concrete being used as a construction material go back to around 5000BC. Although not the inventors, it were the Romans that around 200BC first used concrete as a construction material on a wide scale (Giatech Scientific, 2017). The Romans used a mixture of volcanic ash, lime and seawater to create a durable concrete (Kohlstedt, 2017). They used this concrete to amongst others build arched structures utilising the concretes high compressive strength. Today, more than 2000 years later, some of these construction are still in great condition.

figure 1 Colosseum, Rome. Example of durable roman concrete (Smithsonian, 2011; The American society of mechanical engineers, 2017)

Concrete is an artificial rock type characterised by its high compressive strength and low tensile strength. Concrete is brittle material and can in the essence be created from the basic ingredients: cement (binder), water and aggregates. The type of cement (e.g. Portland cement or Blast furnace slag cement), the ratio between the amount of water and cement and the type of aggregates used will largely determine the properties of the hardened concrete (Reinhardt, 1985).

Because in engineering practice concrete is not only loaded in compression but is also loaded in tension, steel reinforcement is put in in the form of bars, wires and/or fibres. Under tension the concrete will crack, transferring the force to the reinforcement by means of bond forces. The reinforcement is then loaded in tension. Because steel is a ductile material with high tensile strength, the reinforced concrete will be able to withstand tensile stresses and will not fail in a brittle way. Although cracking of the reinforced concrete is needed to activate the steel, the type and width of the cracks should be controlled. This is because cracks can have a negative influence on the water tightness, aesthetics and durability of the reinforced concrete (Bamforth, 2007).

Early-age cracking may also occur. This means that the concrete already cracks in the first days after casting, before external loads are applied. This type of cracking is strongly related to hardening of the concrete, which is the consequence of the hydration process. During hydration the concrete is subject to imposed deformations, which when restrained can cause stresses to occur in the concrete. Because during hardening the material properties of the concrete are still developing, early-age cracking may occur when at any point in time the tensile strain capacity is exceeded. Complicating factor here is the fact that the hydration induced stresses may be reduced over time due to relaxation effects. A detailed time dependent analysis is needed to analyse the behaviour of hardening concrete and to determine whether the early-age cracking is likely to occur. Performing such an analysis is part of this research (van Breugel et al., 1996).

There are various recent developments in the field of concrete science, where higher strength classes are reached by lowering water/cement ratios and additives- and admixtures are used to be able to design a workable and functional concrete for many different purposes (van Breugel et al., 2017). These developments complicate the analysis of hardening concrete. On the other hand, research is being done on the influence of hardening shrinkage and stress relaxation on early-age cracking of concrete, while no consensus on these subjects has been reached yet. Determining the magnitude of these effects is one of the main goals of this study.

1.2 Imposed deformations in hardening concrete

1.2.1 The concept of imposed deformations

The concept of imposed deformations can best be explained by the example of the prismatic bar below. The bar is subjected to a uniform temperature drop, which will cause it to shorten. If the bar is able to deform freely, no stresses will develop, as can be seen in fig. 2.a. However, if the bar is clamped at both sides like in fig. 2.b, this deformation is being restrained. In this case the bar will not shorter and tensile stresses will develop. This restrained deformation is called “imposed deformation”. This term thus refers to the situation of the free shortening of the bar and the restoring force that is needed in case the deformation is restrained (van Breugel et al., 1996).

In this example temperature change is the cause of imposed deformations, but in practice there are several other causes like shrinkage, swelling, moisture gradients etc.

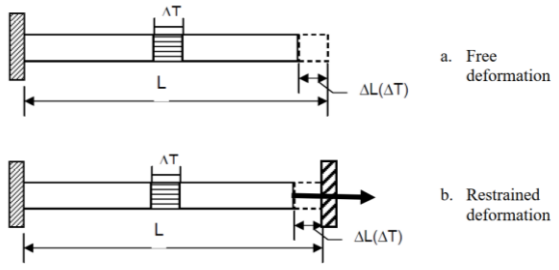

figure 2 Prismatic bar under imposed deformation (van Breugel et al., 1996).

1.2.2 Imposed deformations and the hydration process

Imposed deformations also occur as part of the hydration process. When cement and water are mixed, a chemical reaction will take place resulting in crystallisation and binding of the water and cement particles. This is called hydration. Hydration results in an irregular porous structure containing different types of crystals (e.g. CSH, $Ca(OH)_2$ etc.) surrounding the aggregates (Reinhardt, 1985). This is an exotherm process which means that heat is being released. Heating and subsequent cooling of the concrete will cause thermal strains.

Next to thermal strains there will also be hardening shrinkage in the concrete, which is closely related to movement and binding of water in the cement paste. There are two types of hardening shrinkage, namely chemical shrinkage and autogenous shrinkage. Chemical shrinkage represents an internal volume reduction due to the formation of a capillary pore structure in the concrete. Hardly any external volume changes occur, resulting in negligible stresses on macro scale. Autogenous shrinkage however does result in external volume changes. The most used hypotheses to explain this mechanism can best be described as follows: autogenous shrinkage is the result of the binding of water during the hydration process, emptying the pore structure. One of the consequences of this self-desiccation process it that it results in capillary “suction forces” as can be seen in figure 3. These

forces are supposed to form a large contribution to the external shrinkage and effects of creep and relaxation of the cement paste (van Breugel et al., 2017).

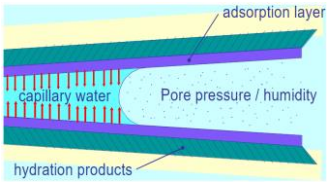

figure 3 Principle of capillary suction (van Breugel et al., 2017).

Whether the thermal- and shrinkage induced strains will cause stresses in the concrete depends first of all on the degree of restraint. In practice there will always be some degree of restraint which will subsequently result in stresses. A distinction should however be made between internal- and external restraint. Because the thermal strains will not be uniformly distributed over the cross-section, parts that want to expand or shrink relative to other parts will be restrained. This is called internal restraint and can be further explained by means of the element in figure 4. Here the temperature development of a hardening massive concrete element can be seen. As the concrete hardens and the rate of hydration increases (phase 1), heat is built-up in the centre zone of the element resulting in temperature differentials over the element as can be seen in the figure. The thermal expansion of the centre zone is restrained by the outer zone causing tensile stresses in the outer zone. When hydration slows down and the concrete starts to cool (phase 2), the centre cools down more compared to the concrete in the outer zone. The corresponding thermal shrinkage of the inner zone is then restrained by the concrete in the outer zone, causing tensile stresses in the centre zone of the cross-section during cooling (Bamforth, 2007).

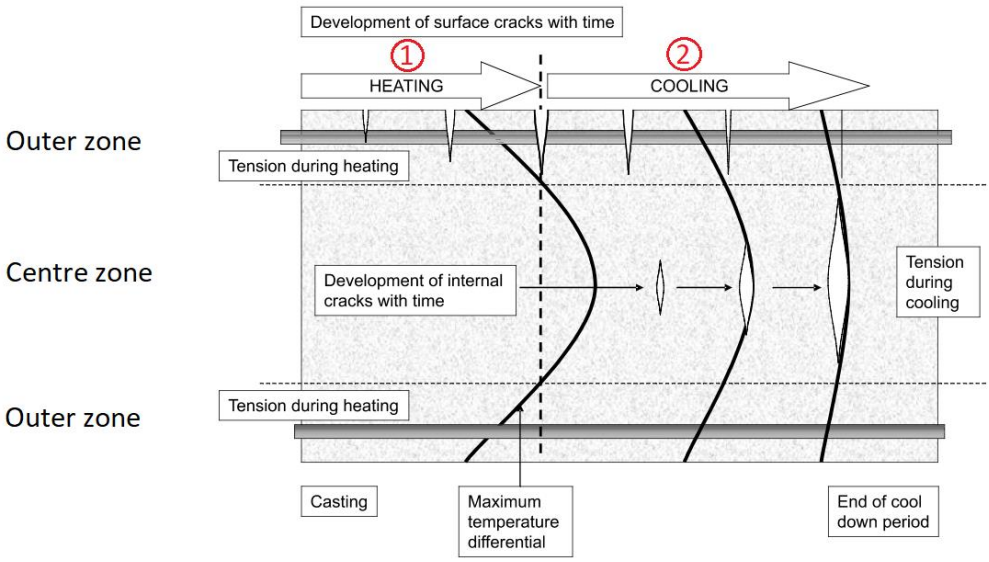

figure 4 Internal- and external restraint in a massive concrete section (Bamforth, 2007).

External restraint of hardening concrete occurs when a new concrete element is cast against an already hardened concrete element. When hydration slows down and the newly cast element starts to cool down, it wants to shrink. This shrinkage is however restrained by the already hardened concrete to which the new element is connected. This restrained shrinkage causes tensile stresses in the young concrete as can be seen in figure 5 (van Breugel et al., 1996).

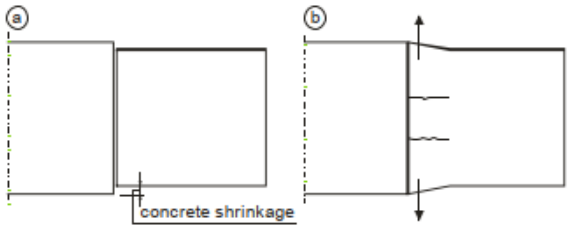

figure 5 Example of external restraint. A freshly casted wall against hardened concrete (van Breugel et al., 1996).

In practice external- and internal restraints occur simultaneously. Which means that stresses due to imposed deformations will always occur. The magnitude of these stresses and whether these stresses will lead to early-age cracking depend on many other factors which will be analysed later in this research.

1.3 Early-age cracking of concrete

As stated before, early-age cracking of concrete occurs when the concrete cracks during hardening before structural loading is applied. In the early stages of hardening, the material properties of the concrete are still developing. On the one hand the tensile strength of the concrete is developing, while on the other hand stresses due to imposed deformations are also developing. If at any point in time the tensile stresses become higher than the tensile strength of the concrete, the concrete will crack. This means that there is a "race" in time between stress and strength as can be seen in figure 6. In reality the tensile strength- and stress can during hardening only be evaluated with a certain probability. Therefore in practice statements can only be made on the 'probability of cracking' (van Breugel et al., 1996.

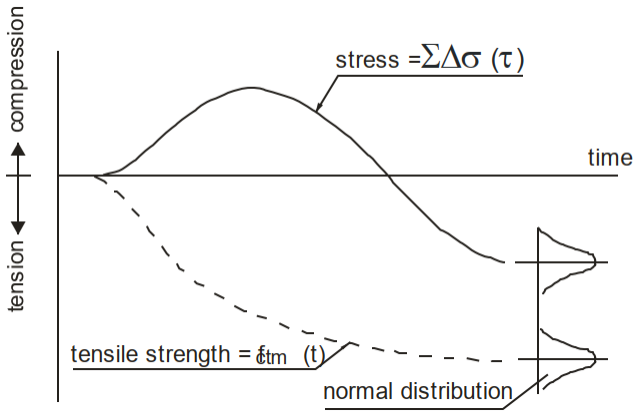

figure 6 Stress and strength development in hardening concrete (van Breugel et al., 1996).

Furthermore, stresses in concrete are subject to relaxation effects, which influence the magnitude of the stress during hardening. Stress relaxation is a phenomenon which is caused by changes in the microstructure of the material and is influenced by the stiffness- and temperature of the concrete. The actual magnitude of the effect of relaxation on the stress development during hardening however remains subject of debate. There are several mechanical models that can be used to take this viscoelastic material behaviour into account which will be discussed in more detail later in this study. Moreover, assessing the effect of stress relaxation on the probability of early-age cracking is part of this study.

1.4 Imposed deformations and design

In practice, imposed deformations will occur in all concrete structures. When these imposed deformations cause early-age cracking of the structure, this will generally generate a developing crack pattern. This means that imposed deformations will have limited impact on the load bearing capacity of the structure and thus will not be taken into account in the Ultimate Limit State (ULS) (NEN-EN 1992-1-1). Because the analysis of early-age cracking requires detailed and time-dependent calculations using numerical calculations tools, in practice it is often chosen to use simplified approaches to reduce the probability of early-age cracking.

For some applications early-age cracking may lead to issues related to durability and/or serviceability. For instance liquid retaining walls in reservoirs rely on their water tightness, which could be lost due to early-age cracking. Also, cracking could in some environments lead to durability problems in the form of, for instance, chloride penetration induced corrosion of the reinforcement. For these structures a detailed analysis on the stress- and strength development of the concrete over time could be needed. In this analysis stress relaxation effects should also be taken into account which makes the analysis even more complicated (Bouquet, 2019). When such an analysis is carried out, the risk of cracking is evaluated using a stress criterion from probabilistic calculations to reach the required safety level against cracking.

1.4.1 Codes and standards

As stated before, imposed deformations are generally not regarded in the ULS. This means that in the Eurocode the concrete is often assumed to be free of stresses when structural loading is applied (Bouquet, 2019).

The Eurocode- and Model Code give some guidance on the calculation of autogenous shrinkage. In the Eurocode a calculation method is proposed where the amount of autogenous shrinkage is based solely on the strength class of the concrete. The Model Code however also includes the cement type in the autogenous shrinkage calculations. Published research shows that the cement type has a significant effect on the magnitude of the shrinkage, which is not considered in the Eurocode (Bamforth, 2007).

The stresses that develop at early-ages are not added in the total crack width calculation for structural loading in the Eurocode, as they are assumed to be self-equilibrating due to creep effects.[1] There is however limited guidance on material behaviour in time in both the Eurocode and the Model Code. For instance, information on how to deal with time dependent processes like developing material properties and stress relaxation is limited. A general factor of 0,65 is assumed to account for relaxation effects on stresses caused by imposed deformations (NEN-EN 1992-1-1).

It can therefore be concluded that the Eurocode- and Model Code provide little to no guidance on how to deal with time dependent behaviour of concrete, while on the other hand for several types of concrete structures a detailed analysis is required to determine the risk of early-age cracking. This raises the question whether a better insight could be gained in the different processes that influence the probability of cracking. Also, the effects of stress relaxation and autogenous shrinkage on the stress development during hardening should be investigated in more detail. When is done, the assessment of the risk of early-age cracking due to imposed deformations can be performed more accurately which could lead to a more adequate design.

[1] This may change in the updated version of the Eurocode, where a factor for early-age cracking could be added

1.5 Research question and objectives

First of all, the different processes regarding hardening of concrete, imposed deformations and stress relaxation will be discussed in more detail in a literature study. As described above, consensus about the effects of relaxation on stresses in hardening concrete has not yet been reached and further understanding of this time dependent process is therefore required. Also, more insight in the development- and magnitude of autogenous shrinkage over time is required to be able to assess the risk of early-age cracking. In literature however, little to no guidance is found on the detailed analyses that are required to describe the complex behaviour of hardening concrete. Besides, the hydration induced stresses are mostly disregarded in the design. The research question is therefore formulated as follows:

"How can early-age cracking in concrete under imposed deformations be analysed taking into account stress relaxation and what is the applicability of the models used?"

The main objective here is to describe the relevant hardening processes and use an appropriate model for stress relaxation in a finite element analysis. This will be done for a specific case where the results of the finite element analysis will be compared to observations from practice. Besides, the aim is to draw conclusions on the effects of autogenous shrinkage and stress relaxation in relation to the hardening process and early-age cracking. In the end conclusions will be drawn on the accuracy of the model and recommendations will be made on further research needed to be able to assess the risk of early-age cracking in more detail in the future.

1.6 Research approach and strategy

To be able to answer the research question a certain strategy will be followed. The study can therefore be subdivided in the following activities:

- Performing a literature study to gain more insight in the relevant processes regarding early-age cracking and imposed deformations in hardening concrete
- Definition of the case study and setting up a finite element model for this specific case
- Performing a parameter study to gain more insight in the effects of variations of the different input parameters of the model on the results of the analysis
- Analysis of creep data and viscoelastic material models to be able to take into account stress relaxation effects in the analysis
- Laboratory testing at the TU Delft to simulate the hardening process of the case study and to determine several relevant material properties
- In-situ measurements and inspections to validate the results of the finite element analysis
- Comparison between the results of the laboratory testing, measurements, inspections and finite element analyses to be able to draw conclusions on the accuracy of the input parameters and applicability of the models used. The aim here is to determine a set of model properties that give results that are agreement with observed behaviour from the practical case.

1.7 Outline of the report

The previously discussed subactivities of the study are elaborated in different chapters in the report. The outline of the total report is displayed here schematically where the different chapters can be seen together with their global content.

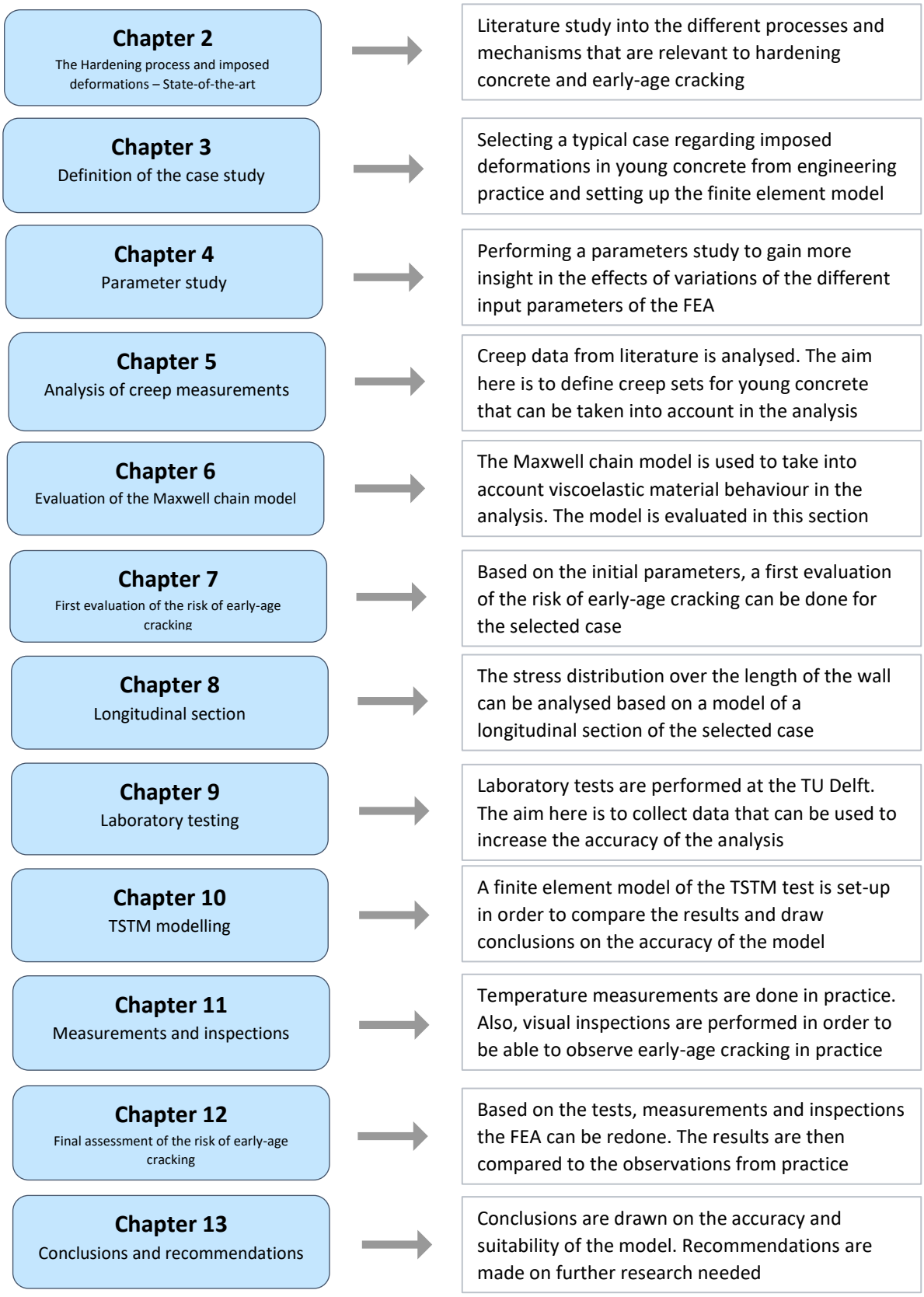

2 The Hardening process and imposed deformations – State-of-the-art

In this section the results of the literature study are discussed. As is already mentioned in the introduction, the literature study is performed to gain a better understanding in the different processes and material properties relevant to hardening of concrete and early-age cracking. Besides, imposed deformation and mechanisms of stress formation in hardening concrete are discussed. The literature study is performed to in the end be able to adequately assess the risk of early-age cracking for a selected case.

2.1 The hydration process

To gain a better understanding in the processes and mechanisms behind hardening of concrete and the development of strength- and stresses, the hydration process should be discussed in more detail. Hydration is the well-known consequence of mixing cement and water, which initiates the hardening process by means of dissolution- and crystallisation of the cement. As crystallisation continues, the concrete gains strength and stiffness. Hydration is an exotherm process which means that heat is being released. There are many factors that influence the strength development, the amount of heat release and subsequent temperature rise of the concrete. These factors will also be discussed in more detail here.

2.1.1 Hydration of cement

The most commonly used cements are ordinary Portland cement (OPC) and cements that are based on Portland cement but also contain other types of binders like Blast furnace slag cement. Portland cement is produced by heating and milling of the raw materials, resulting in the formation of cement clinkers. In table 1 the clinker components of Portland cement can be seen together with their weight percentage.

Chemical Name	Chemical formula	Shorthand Notation	Weight percent
Tricalcium silicate(alite)	$3CaO{\cdot}SiO_2$	C_3S	55
Dicalcium silicate (belite)	$2CaO{\cdot}SiO_2$	C_2S	18
Tricalcium aluminate	$3CaO{\cdot}Al_2O_3$	C_3A	10
Tetracalcium aluminoferrite	$4CaO{\cdot}Al_2O_3{\cdot}Fe_2O_3$	C_4AF	8
Calcium sulfate didydrate (Gypsum)	$CaSO_4{\cdot}2H_2O$	$C\bar{S}H_2$	6

Table 1 Typical composition of Portland cement (Mindess, 2003).

As stated before, hydration starts when cement comes in contact with water causing the cement to dissolve and crystals to be formed. Through hydration concrete starts gaining stiffness and strength. During this process heat is released. Several different stages of the hydration process can be distinguished as can be seen in figure 7 (Reinhardt, 1985; Kim, 2010).

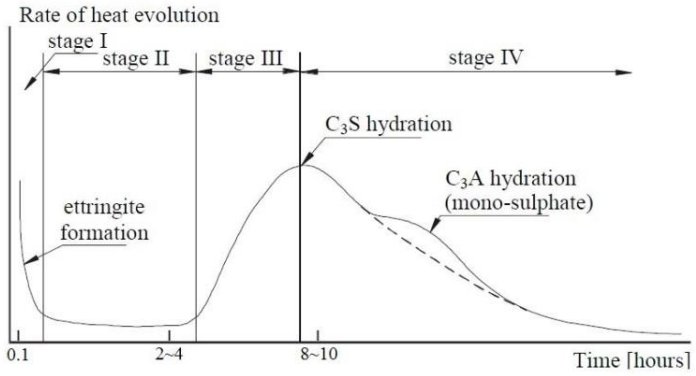

figure 7 Different stages in rate of heat evolution over time (Kim, 2010).

- Stage I: dissolution stage

Directly after contact with water a small part of the C_3A is dissolved and reacts with gypsum to form ettringite. This reaction only last for a couple of minutes and stops when a layer of ettringite has formed around the cement particles stopping the water from reaching the cement and thus from hydrating. The ettringite formation in this stage has little effect on the strength of the concrete.

- Stage II: dormant period

The ettringite crystals are in this stage still relatively small and therefore do not yet bridge between the cement particles. This causes the concrete to keep its consistency and workability. In the dormant period the rate of hydration is very low and the strength does not increase.

- Stage III: acceleration stage

The hydration accelerates as the C_3S dissolves and hydrates forming calcium silicate hydrate (CSH) crystals. The rate of hydration and heat release rapidly increases and the concrete begins to set. The formed CSH from the C_3S is responsible for rapid early strength formation and thus in this stage the strength starts to increase. Also the C_2S starts to hydrate, however this clinker component hydrates at a slower rate giving high strength in the long-term.

- Stage IV: deceleration stage

In this stage the rate of hydration starts to decrease again as most of the hydrated particles have formed and grow in thickness. Also ettringite is converted resulting in the formation of mono-sulphates

- Stage V: steady stage

In this stage the rate of hydration is low as the pores have become smaller due to the outward growth of the hydrated particles which makes it is harder for the water to reach the un-hydrated cement. This causes hydration to continue over the lifetime of the concrete while never reaching full hydration.

As for the strength contribution of the different clinker components it can be stated that the C_3S gives high early strength, while the C_2S gives low early strength but on the long-term catches up with the C_3S (after ~ 1 year). The C_3A and C_4AF do hardly contribute to the strength development but the fact that they control the course of the hydration process makes them important. The strength contributions of the different clinker components can also be seen in figure 8. In the end a concrete design that requires high early strength should thus contain a large C_3S fraction and visa

versa. In this way the strength- and heat development can be controlled by adjusting the mix design (van Breugel et al, 2017; Fairbairn et al., 2013; Reinhardt, 1985).

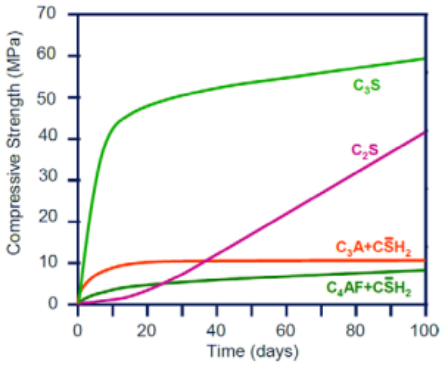

figure 8 Strength contributions of different clinker components during hardening over time (Punkki, 2010).

As stated before the CSH crystals give the strength to the concrete. They form sheeted layers of crystals, with water in between. This water is called the interlayer water. With formation of the hydration products water is chemically bound, resulting in a porous structure of the cement paste. At the edges of the pores water is physically adsorbed by the CSH sheets. Several models for the structure of the hydrated cement paste can be found in literature. In figure 9 the model as proposed by Feldman and Sereda (1968) can be seen (van Breugel et al, 2017; Reinhardt, 1985).

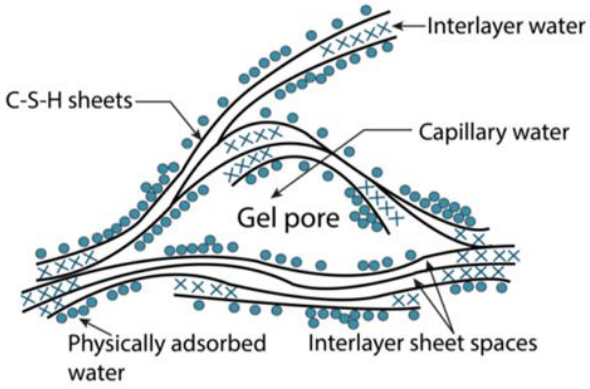

figure 9 Probable structure of hydrated silicates based on Feldman and Sereda (1968) (Fairbairn et al., 2013).

2.1.2 Adiabatic temperature rise

In case all the during hydration produced heat is used for heating of the concrete itself and no heat is lost to the environment, the hydration process is called adiabatic. The adiabatic temperature rise can be determined experimentally and results in an adiabatic curve where the temperature rise is plotted versus the hydration time. An example of such a curve can be seen in figure 10. The adiabatic curve is input for calculation software to be able to calculate the temperature distribution in the concrete during hardening. The shape of the curve mainly depends on the concrete mixture and the casting temperature and is often provided by the cement producer (van Breugel et al., 1996).

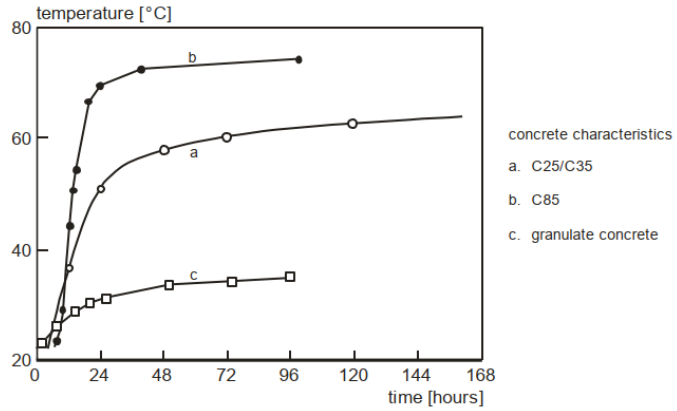

figure 10 Examples of the adiabatic temperature rise for different concrete mixtures (van Breugel et al., 1996).

In practice the course of the temperature rise in the concrete during hardening will not be adiabatic, but will be semi-adiabatic. This means that after adiabatic rising of the temperature some of the heat is lost to the environment which cools down the concrete and slows down the rate of hydration.

2.1.3 Types of cement

Next to Portland cement which consists of the clinker components as discussed above, there are several other types of cement with each of them having different properties. However most of these cements have a certain mass percentage of clinker components. In Eurocode NEN-EN 197-1 the composition, specifications and conformity criteria for common cements can be found. The five main types can also be seen in table 2 (NEN-EN 197-1).

Main type	Name	Clinker %	Other main components
CEM I	Portland cement (PC)	95-100	-
CEM II	Portland composite cement	65-94	Various additions
CEM III	Blast furnace slag cement	5-64	Blast furnace slag
CEM IV	Pozzolan cement	45-89	Pozzolanic material
CEM V	Composite cement	20-64	Mix of blast furnace slag and pozzolan and/or fly ash

Table 2 Main cement types and their general composition (NEN-EN 197-1).

CEM III is often used in the Netherlands. Blast furnace slag (BFS) is a by-product from the oil industry. BFS is used in CEM III cement by replacing part of the clinker by BFS. To be able to start hydration, the slag needs an activator which comes from the hydrated clinker component. In general the strength development of BFS is slower compared to that of Portland cement which means that also the heat production is lower. The effect can also be seen in figure 11 where the total heat generated decreases with increasing slag content (Bamforth, 2007; van Breugel et al., 2017).

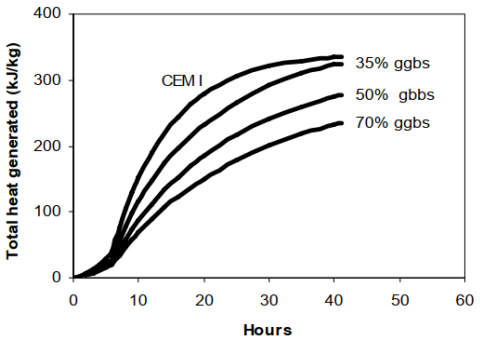

figure 11 Effect of slag content in concrete mixture on total heat generation over time (Bamforth, 2007)

In general it can be stated that by replacing part of the clinker components (especially C_3S and C_3A), the rate of hydration and heat production can be controlled. By controlling the heat production the hydration induced stresses can be controlled and thus the risk of cracking can be controlled.

2.1.4 Influences on heat development and temperature rise

There are several factors that influence the heat development and subsequent temperature rise of the concrete. To be able to properly analyse the hydration induced thermal deformations, these factors have to be discussed.

2.1.4.1 Cement type, content and fineness

As discussed above, the type of cement used in the concrete mixture influences the heat production during hardening. BFS cement for instance generally has lower heat production compared to PC. Also the influence of the different clinker components on heat production has been discussed.

Next to the type of cement, also the cement content and fineness are of influence to the rate of heat production. The cement content is expressed as the mass of cement per unit of volume $[kg/m^3]$. With a higher cement content, there will be greater heat production per unit of volume and thus also a greater temperature rise (Bamforth, 2007). This effect can also be seen in a raise in temperature development in the adiabatic curve. UHPFRC for instance have a relatively high cement content compared to ordinary concrete, the effect of this increased cement content can be seen in figure 12.

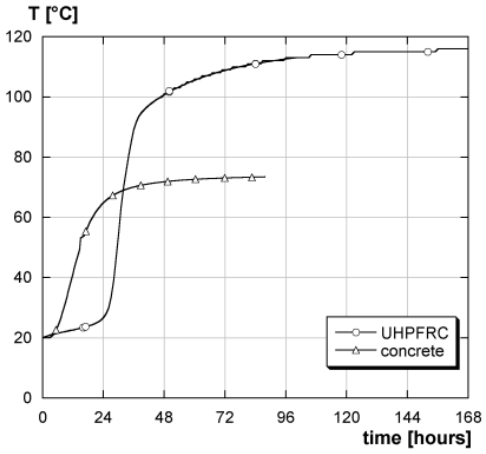

figure 12 Effect of increasing the cement content on the total heat generation over time (Habel, 2004).

The fineness of the cement is expressed by the Blaine-value which denotes the specific surface of the cement per unit of weight $[m^2/kg]$. Cements with a high Blaine-value have a high fineness. A fine cement has a higher rate of reaction and thus greater heat release due to the large reaction surface of the cement particles. This effect can be seen in figure 13.

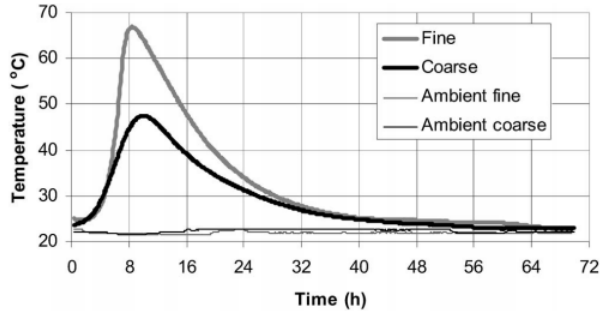

figure 13 Effect of the cement fineness on the total heat generation over time (Bentz et al., 2008).

2.1.4.2 Additives

As stated before the amount of heat production can be controlled by altering the concrete mixture. This can be done by changing the cement type but can also be achieved by using additives. Here some commonly used additives and their effect on the heat production are discussed.

2.1.4.2.1 Fly ash

Fly ash is a by-product from the burning of coal and is often used in concrete to be able to reduce the w/c ratio due to the fact that fly ash acts as a retarder in the hydration process and subsequent strength development. The use of fly ash as an additive in the concrete mix thus has the effect of reducing the heat development. This effect is confirmed by experiments as can be seen in figure 14.

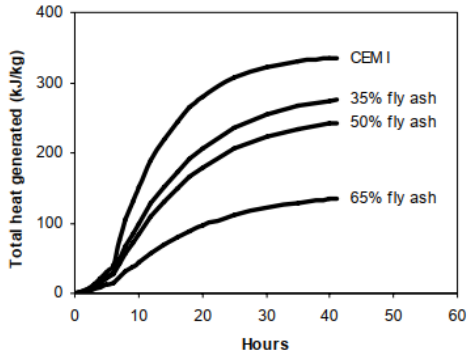

figure 14 Effect of fly ash content on the total heat generation over time (Bamforth, 2007).

2.1.4.2.2 Silica fume

Silica fume is commonly used in HSC as an additional binder. Literature shows that the heat production of silica fume is similar to that of Portland cement. The use of silica fume as an admixture thus has little effect on the amount of heat released (Bamforth, 2007).

2.1.4.3 Casting temperature

The temperature of the concrete mixture when casting turns out to be of influence to the magnitude of temperature rise during hardening. As a general rule it can be stated that the mix temperature is $\sim 5\ ^{\circ}C$ higher compared to the ambient air temperature (Bamforth, 2007). This means that during casting in the winter period the temperature of the concrete mixture will be significantly lower compared to the mix temperature in the summer period. Literature shows that a high mixture temperature will lead to a lower temperature rise and vice versa. This effect can also be seen in figure 15.

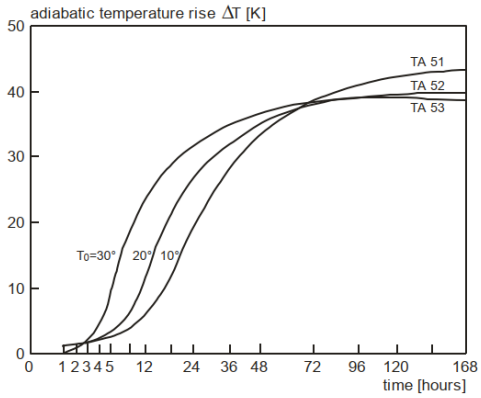

figure 15 Effect of initial mix temperature on the adiabatic temperature rise (van Breugel et al., 1996).

2.1.4.4 Geometry

As stated before, in practice the temperature rise will not be adiabatic, but semi-adiabatic due to temperature losses to the environment. The geometry of the concrete section is an important factor in the determination of the temperature rise during hardening. The temperature rise in the concrete is the results of the difference between the incoming and outgoing heat flux and is location dependent. The temperature rise is therefore not uniform over the cross-section. As one can imagine, at a location close to the edge of the cross-section the heat loss to the environment will be greater and the temperature rise will thus be lower. The opposite holds for the centre of the cross-section, where the temperature rise will be greater and will be almost adiabatic. Due to the greater temperature rise, the rate of hydration will also be greater in the centre of the section. To be able to evaluate the maturity or degree of hydration in a certain location, the actual temperature in that location should be measures/calculated. This effect is illustrated in figure 16.

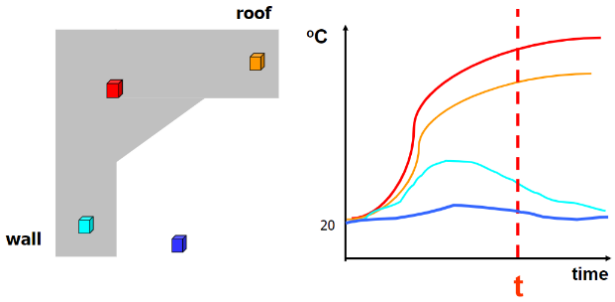

figure 16 Difference between adidabatic and semi-adiabatic tempearure rise in a concrete cross-section (van Breugel et al., 2017).

2.1.4.5 Boundary conditions

The temperature distribution is calculated by solving the heat diffusion equation in the concrete domain which depends on the internal heat production and the outgoing heat flux to the environment. The outgoing heat flux depends on the boundary conditions of the hardening concrete which are discussed in this section.

2.1.4.5.1 Formwork and windspeed

The heat flux as a result of convection at an edge boundary of the hardening concrete depends on the type of formwork used and the wind speed. As for the formwork the type of material, the number of layers and the layer thickness are important. The higher the heat conductivity $\lambda\ [W/mK]$ of the material, the higher the outgoing heat flux will be. As for the wind speed it can be stated that the higher the wind speed $w\ [m/s]$, the higher the cooling effect (heat flux) at that boundary will be. In general the heat flux $q\ [Jm^2/s]$ at a boundary is described as follows (van Breugel et al., 1996; Femmasse B.V., 2006):

$$q\ = a(T - T_e) \tag{2.1}$$

Where a is the transfer coefficient at the boundary $[Jm^{-2}s^{-1}{}^{\circ}C^{-1}]$ or $[Wm^{-2}{}^{\circ}C^{-1}]$, T is the concrete temperature at the boundary $[^{\circ}C]$ and T_e is the external temperature, which varies over time $[^{\circ}C]$.

When a boundary without any present formwork is considered, the free transfer coefficient should be used which depends only on the wind speed:

$$a_{free} = \begin{matrix} 5.6 + 4.0w & for\ w \leq 5\ m/s \\ 7.2w^{0.78} & for\ w > 5\ m/s \end{matrix} \tag{2.2}$$

If however any formwork is present at the boundary, the following calculation method is proposed for calculating the transfer coefficient a:

$$\frac{1}{a} = \frac{1}{a_{free}} + \sum_{s=1}^{n} \frac{1}{a_s} \tag{2.3}$$

In which:

$$a_s = \frac{\lambda}{d} \tag{2.4}$$

In the latter expression λ is the thermal conductivity of the formwork material and d is the thickness of the layer $[m]$. n is the number of formwork layers present at the boundary.

2.1.4.5.2 Solar radiation

Especially in the summer period, the solar radiation may have significant impact on the hydration process in the form of the radiation heat flux. The effect of solar radiation may lead to an additional temperature increase in the concrete of 10°C or higher (van Breugel et al, 1996). Therefore the solar radiation should be taken into account when assessing the risk of early-age cracking. The heat flux related to solar radiation can be described as follows (Femmasse B.V., 2006):

$$q_{solar} = -\varepsilon_r J + \sigma[\varepsilon_s (T + 273)^4 - \varepsilon_a (T_e + 273)^4] \tag{2.5}$$

Where:

$\varepsilon_r = the\ emissivity\ coefficient\ for\ short\ wave\ radiation\ [-]$
$\varepsilon_s = the\ emissivity\ coefficient\ for\ long\ wave\ radiation\ from\ the\ boundary\ surface\ [-]$
$\varepsilon_a = the\ emissivity\ coefficient\ for\ long\ wave\ radiation\ to\ the\ boundary\ surface\ [-]$
$J = the\ radiation\ function\ for\ the\ particular\ boundary\ [Jm^2 s^{-1}]$
$\sigma = the\ radiation\ coefficient = 5.77 * 10^{-8}\ Jm^{-2} s^{-1} K^{-4}$

Here ε_r depends on the colour of the surface, and standard values can be retrieved from a table. ε_s depends on the type of material and standard values can again be retrieved from a table. In the end ε_a depends on ε_s and the amount of present clouds and is described as:

$$\varepsilon_a = \varepsilon_s * c_1 \tag{2.6}$$

Where $c_1 = 0.82$ for a cloudless sky and $c_1 = 0.94$ for a cloudy sky.

The radiation function J depends on the solar radiation G $[W/m^2]$ and can be described by a periodical function in time with an implemented cut-off criterion to ensure that no negative radiation can occur in the analysis. A sinusoidal function can be used to describe the day-night cycle with respect to heat radiation.

2.1.4.5.3 External temperature

The external temperature T_e [℃] is an input parameter in the equation for the convection heat flux at the edge boundaries on the concrete and formwork. The external temperature is naturally not a constant and follows a day-night cycle. The average temperature depends on the geological location and the time of the year as it will be lower during the winter and higher during the summer. In the evaluation of the concrete temperature in the FEA the external temperature can be modelled using periodical functions like for instance a sinusoidal function as can be seen in figure 17 (Femmasse B.V., 2006). In this example the average external temperature is 6 ℃ and the amplitude is 3 ℃ as used to be typical for casting during winter in the Netherlands in the past. The frequency of the of the sinusoidal function is $[1/day]$ as it resembles a day-night cycle.

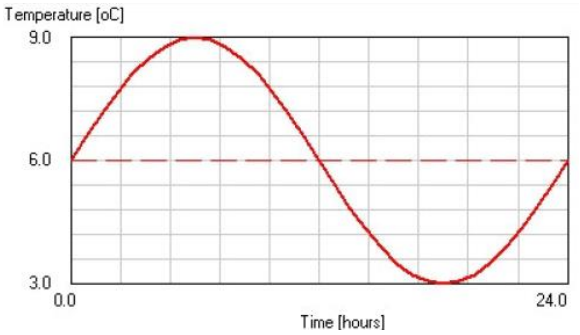

figure 17 Example of a period temperature curve showing the day-night cycle

2.1.5 Measures to reduce temperature differentials during hardening

In the section above the relevant factors that influence the heat development and temperature rise in the concrete are discussed. However heat development in itself is not a problem, it are the temperature differentials (in space and time) and restrained thermal deformations that will cause stresses in the hardening concrete on structural level. Later in this research there will be elaborated on thermal deformations and restraints. In this section several measures that can be taken to reduce the temperature differentials and thus the risk of cracking of the concrete during hardening are discussed briefly. Assessment of the effects of these measures however lies outside the scope of this research.

2.1.5.1 Precooling of the concrete mixture

As discussed before, during hydration heat is released and the temperature of the concrete rises. The maximum temperature in the core of the concrete and the temperature differential with respect to the environment can be reduced by cooling the mixture before casting. There are two methods that can be used: cooling the mix components separately before mixing or cooling the total mixture after mixing but before casting. Cooling of the total mixture can for instance be done by injection with liquid nitrogen (Fairbairn et al., 2013; Bamforth, 2007).

2.1.5.2 Post-cooling during hardening

Post-cooling of the concrete can be achieved by using an embedded cooling pipe system with water- or air circulation. By using this system the internal temperature of the concrete during hardening can be controlled. Post-cooling proves to be a cost-effective measure for casting massive concrete sections (Fairbairn et al., 2013; Bamforth, 2007).

2.1.5.3 Insulation

During hardening the centre of the concrete section hardens under near-adiabatic conditions while at the edges there will be semi-adiabatic conditions due to heat loss to the environment through convection and conduction resulting in lower temperatures at the edges. This means that there will be a temperature differential over the cross-section of the element which could lead to stress formation. To reduce this temperature differential it is often chosen to use insulation at the concrete edges which reduces the outgoing heat flux at this location. There are several methods to provide the necessary insulation like for instance using a formwork material with a lower thermal conductivity (plywood instead of steel) or using insulation blankets (Fairbairn et al., 2013).

2.1.5.4 Construction phasing

In the end the construction phasing can be of large influence on the temperature development in hardening concrete. This has to do mainly with the dimensions of casting blocks and the time interval between casting of adjacent blocks (Fairbairn et al., 2013). The effects of variations in these parameters can however only be assessed properly by using numerical analysis (Bamforth, 2007).

2.2 Maturity concepts

The development of mechanical properties of young concrete is often described by means of the maturity concept. Instead of the degree of hydration, an equivalent time is calculated that indicates the state of hydration of the concrete based on the temperature history, relative to development at a certain reference temperature (Reinhardt, 1985). The maturity is therefore also referred to as 'equivalent hydration period' or 'equivalent age at reference curing temperature'.

Saul et al (1951) was first to propose the maturity method where the maturity M was expressed as the product of temperature and time, taking into account the temperature history of the concrete (de Schutter, 2003):

$$M = \int_0^t (T(t) - T_0)dt \tag{2.7}$$

Where:

$$T(t) = the\ temperature\ of\ the\ concrete\ at\ age\ t$$
$$T_0 = the\ temperature\ belong\ which\ no\ hardening\ will\ occur$$

A couple of years later the method of equivalent age t as mentioned in the introduction of this section was proposed as an alternative to Saul's formula (Chengju, 1989):

$$t_{eq} = \int_0^t \gamma(T)dt \tag{2.8}$$

Where $\gamma(T)$ is the temperature dependent affinity ratio with respect to a certain reference temperature T_r which is often set to 20°C.

2.2.1 Arrhenius function

Later it was found that the hardening process is not a linear function of the curing temperature, and a new non-linear approach to the affinity ratio function was proposed by, amongst others, Arrhenius (de Schutter, 2003):

$$\gamma(T) = e^{\frac{Q}{R}\left(\frac{1}{273+T_r} - \frac{1}{273+T(t)}\right)} \tag{2.9}$$

Where:

$$Q = the\ apparent\ activation\ energy\ hydration\ \left[\frac{kJ}{mol}\right]$$
$$R = the\ universal\ gas\ constant\ = 0.00831446\ \left[\frac{kJ}{mol\ K}\right]$$
$$T(t) = the\ time\ dependent\ temperature\ of\ the\ concrete\ [°C]$$
$$T_r = the\ reference\ temperature\ [°C]\ (\ often\ 20\ °C\ is\ used\ )$$

The activation energy takes into account the temperature sensitivity of the hydration process. The higher the activation energy, the higher the temperature sensitivity. The following expressions can be used for determining the activation energy (Chengju, 1989):

$$\begin{aligned} Q &= 33.5\ kJ/mol \quad && for\ T \geq 20°C \\ Q &= 33.5 + 1.47 * (20 - T)\ kJ/mol \quad && for\ T < 20°C \end{aligned} \tag{2.10}$$

Next to the Arrhenius function, there are several other proposed functions for the affinity ratio. Nevertheless, the Arrhenius function as presented by Hansen and Pedersen is most used in engineering practice. As described above, using the maturity concept results in an equivalent

concrete age t. However, to be able to predict the early-age strength and stiffness development based on this equivalent age, experimentally obtained relations are needed.

In research by Z.P. Bažant (1988), the maturity equation was complemented by a second term which takes into account the effect of the moisture potential (humidity) of the concrete on the maturing process. The total equation for maturity $M(t)$ then becomes (Femmasse B.V., 1996):

$$M(t) = \int_0^t e^{\frac{Q}{R}\left(\frac{1}{273+T_r} - \frac{1}{273+T(t)}\right)} * \frac{1}{1+(a_c - a_c h)^{b_c}} dt \tag{2.11}$$

Where:

$$h = moisture\ potential\ [-]$$
$$a_c = coefficient$$
$$b_c = coefficient$$

2.2.2 Method 'de Vree'

Next to the Arrhenius function as non-linear alternative to the relation between maturity and strength, several other methods were proposed which are referred to as 'weighted maturity methods'. One of these methods is called the Dutch method 'De Vree'. According to this method, the weighted maturity can be determined with the following expression (van Breugel et al., 2017):

$$M_w = \sum \Delta t * T * C^n \tag{2.12}$$

Where:

$$\Delta t = the\ time\ increment\ in\ hours$$
$$T = the\ temperature\ in\ °C\ for\ the\ time\ increment$$
$$C = is\ a\ cement\ dependent\ factor$$

The weighted maturity is thus determined be summing the area increments $\Delta t * T$ $[°Ch]$ multiplied by the weight values C^n. The principle can also be seen in figure 18.

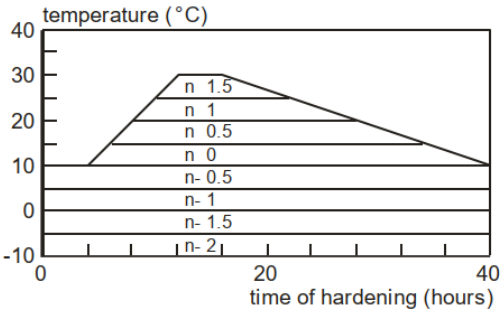

figure 18 Principe of the method 'de Vree' (van Breugel et al., 1996).

This method is often used in building practice where the in-situ strength of the concrete is calculated using temperature measurements and a 'maturity computer' which calculates the maturity of the concrete over time. The strength can subsequently be determined based on predetermined relations between maturity and strength.

The maturity concept can be used in practice to determine the mechanical properties of the concrete as a function of time. Next to the maturity concept, there is another common method for determining the material properties called the degree of hydration concept. When using the degree of hydration (α) for determining the compressive strength of concrete, an adiabatic hydration curve corresponding to the specific concrete is needed. Also, the temperature development during

hardening should be measured. In this way the degree of hydration concept is similar to using the maturity concept. In the remainder of this research it is chosen to use the maturity concept over the degree of hydration concept and therefore the latter will not further be discussed.

2.2.3 Development of material properties

To be able to use the maturity concept for determining the concrete strength development, the relationship between the maturity of the specific concrete and the compressive strength should be determined in advance. This can be done in an experimental way by determining the compressive strength of specimens that are hardening at a constant curing temperature. Such a curve is called a 'calibration curve' (van Breugel et al., 1996).

Various different functions are proposed to determine the strength-maturity relation. A commonly used function is the one proposed by Plowman (1956), who proposed a simple logarithmic relation (Chengju, 1989):

$$f_{cm} = a + b \log(M) \tag{2.13}$$

Where:

$f_{cm} = the\ mean\ compressive\ strength\ of\ the\ concrete$
$M = the\ maturity$
$a, b = constants\ that\ depend\ upon\ the\ cement\ type\ and\ w/c\ ratio\ of\ the\ concrete$

In figure 19 an example of such a calibration curve can be seen.

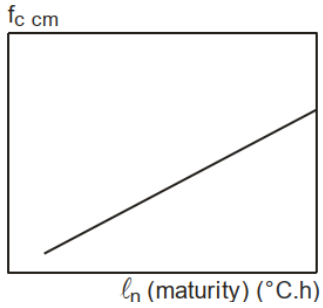

figure 19 Calibration curve for relation between strength and maturity (van Breugel et al., 1996).

When the calibration curve is known, the early-age compressive strength of the concrete at time t can be determined as follows:

- Determine the temperature of the concrete by measuring or calculating the temperature during hardening
- Calculate the maturity M (or equivalent age t_{eq}) at time t
- Use the predetermined relation between the compressive strength and maturity to determine the concrete compressive strength at time t

Next to the compressive strength, the development of the tensile strength and stiffness can also be determined based on the maturity.

2.2.3.1 NEN-EN 1992-1-1

Methods for determining the mechanical properties of concrete as function of time using the maturity concept can also be found in standards and codes. There are several international codes written by for example the ACI, CEB and JSCE. Here the methods as described by the Eurocode are discussed in more detail.

NEN-EN 1992-1-1 gives guidance regarding the development of material properties in time. The expressions are based on experiments and the 28-day properties of the concrete. Using this method the development of mechanical properties can be determined as function of the maturity (in the form of the equivalent age). The general expression is given as:

$$X(t) = \beta_c(t)^n * X_{28} \tag{2.14}$$

Where:

$$\beta_c(t) = a\ function\ that\ expresses\ the\ development\ over\ time$$
$$X_{28} = the\ mechanical\ property\ at\ 28\ days$$
$$n = a\ parameter$$

In the Eurocode an exponential time-development function is proposed:

$$\beta_c(t) = e^{s_{CEM}\left(1-\sqrt{\frac{28}{t}}\right)} \tag{2.15}$$

Where s_{CEM} is a coefficient which depends on the strength class of cement and t is the concrete age in days.

2.2.3.1.1 Compressive strength

Based on the proposed method by EN 1992-1-1, the mean compressive strength at time t can be expressed as follows:

$$f_{cm}(t) = \beta_c(t) * f_{cm,28} \tag{2.16}$$

Where the material factor $n = 1$ and $f_{cm,28}$ is the 28 day mean compressive strength of the concrete.

2.2.3.1.2 Tensile strength

In the same way the tensile strength can be expressed as follows:

$$f_{ctm}(t) = \beta_c(t)^{\frac{1}{2}} * f_{ctm,28} \tag{2.17}$$

Where the material factor $n = \frac{1}{2}$ and $f_{ctm,28}$ is the 28 day mean tensile strength of the concrete.

2.2.3.1.3 Stiffness

The same function can also be used for describing the development of the Young's Modulus. In this case the factor $n = \frac{1}{3}$ is used. The expression becomes:

$$E_{cm}(t) = (\beta_c)^{\frac{1}{3}} * E_{cm,28} \tag{2.18}$$

Where $E_{cm,28}$ is the 28-day mean Young's Modulus of the concrete.

For the calculation methods as proposed by standards like the NEN-EN 1992-1-1 holds that they are less accurate compared to e.g. maturity relations and calibration curves derived from experiments. Especially the development of tensile strength is stronly influenced by curing conditions, structural dimensions and internal stresses, which together cause a large scatter in tensile strength development. This is also observed in literature where a large scatter of the factor n is found for the development of the tensile strength (Fairbairn et al., 2013). Nevertheless the proposed calculation methods are adopted by the Eurocode.

2.3 Thermal properties of concrete

The thermal response of hardening concrete to the hydration process consists of temperature- and volume changes. The magnitude of the response depends on the thermal properties of the concrete. These thermal properties however change over time. This complicates the determination of the relevant parameters needed for evaluation of the response. In this section these parameters and their magnitude are discussed in more detail.

2.3.1 Thermal conductivity

The rate at which heat is transferred through the concrete is determined by the thermal conductivity (Bamforth, 2007). The thermal conductivity is denoted as λ_c $[W/mK]$.

The magnitude of thermal conductivity mainly depends on the aggregate type and the moisture content of the concrete. The thermal conductivity is therefore not constant, but changes in time due to changes in moisture content of the concrete. The thermal conductivity increases with increasing moisture content due to fact that water has a higher conductivity compared to air. With increasing moisture content the pores fill with water increasing the conductivity. As for aggregates it can be stated that the thermal conductivity is different for each aggregate type, and that the thermal conductivity of the concrete increases linearly with the volume fraction of aggregates as the aggregates have the highest thermal conductivity of the components in the concrete mix. In the end it was also found that age has little effect on the thermal conductivity (Kim et al., 2002).

In general the magnitude of thermal conductivity lies within the range from 1.0 to 2.5 $[W/mK]$ (Bamforth, 2007). The actual value of the thermal conductivity is different for each concrete and can only be determined through experiments. Nevertheless some guidance on the thermal conductivity in practice is found in literature. In table 3 and table 4 proposed values for use in early-age concrete modelling can be seen for different aggregate types and moisture contents.

Aggregates	Thermal conduction λ_c of concrete with different types of aggregates	
	[kJ/(m^2 K h)]	[W/(m K)]
Quartzite	12.6	3.5
Dolomite	15.6	3.2
Limestone	9.4 – 11.9	2.6 – 3.3
Granite	9.4 – 9.7	2.6 – 2.7
Rhyolite	7.9	2.2
Basalt	6.8 – 7.9	1.9 – 2.2

Table 3 Thermal conductivity and of concrete for different types of aggregates (van Breugel et al., 1996).

Aggregate type	**Thermal conductivity of concrete (W/m.K)**	
	Sand and aggregate from same rock type	Aggregate from defined rock type with siliceous sand
Quartzite and siliceous gravels with high quartz content	2.9	2.9
Granite, gabbros, hornfels	1.4	2.0
Dolerite, basalt	1.3	1.9
Limestone, sandstone, chert	1.0	1.8

Table 4 Thermal conductivity of concrete for different aggregate types by Clauser and Huenges (1995) (Bamforth, 2007).

As can be seen from the tables above, there are relatively large differences in proposed values for the thermal conductivity. Therefore, as is stated before, the only way to accurately determine the thermal conductivity of a specific concrete mixture is through testing.

2.3.2 Thermal capacity

The thermal capacity $[\,J/m^3 * K\,]$, also known as heat capacity, refers to the amount of energy needed $[\,J]$ to increase a volume of concrete $[m^3]$ by one unit of temperature $[K]$. The thermal capacity is calculated as the product of the specific heat and specific mass:

$$\rho_c * c_T \tag{2.19}$$

Where ρ_c is the specific mass of the concrete $[kg/m^3]$ and c_T is the specific heat of the concrete $[J/kg * K]$. Here these components will be discussed briefly.

Like the thermal conductivity, the specific heat is mix dependent and determined by the specific heat of the different components and their volume fraction. This means that the aggregates are of great influence on the total specific heat. However also the water content is of great influence because the specific heat of water is relatively high compared to that of the other components (Bamforth, 2007). This means that also the specific heat is affected by changes in internal relative humidity during hardening. Nevertheless the specific heat is usually assumed constant and the specific heat of ordinary concrete lies within the range from 0.84 to 1.17 $[k\,J/kgK]$ (Neville, 2011).

Literature presents a relatively large variation in the specific heat. However accurate evaluation of the specific heat is necessary as the specific heat has significant influence on the temperature rise of the structure and thus the stresses. In fact a certain percentage of variation in the specific heat may lead to an equal percentage of variation in the computed thermal stresses in the structure (Fairbairn et al., 2013).

The specific heat is also a function of the degree of hydration, as its magnitude lowers with increasing degree of hydration. In figure 20 the relationship between early-age specific heat, w/c ratio and cement content can be seen as presented by literature.

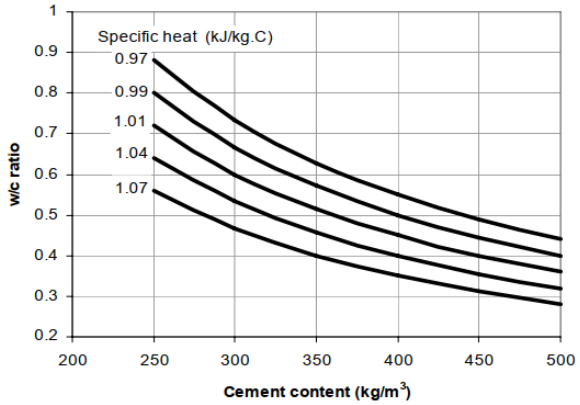

figure 20 Relation between cement content, w/c ratio and specfic heat (Bamforth, 2007).

2.3.3 Coefficient of thermal expansion

The coefficient of thermal expansion (CTE) is used to describe the volume change as a result of changes in temperature. The coefficient of thermal expansion is denoted as α_c and it describes the linear volume change per unit of temperature change $[1/°C]$.

The magnitude of the CTE depends on the CTE's of the individual components of the concrete mixture. Because the aggregates generally are the largest volumetric part, they also have the biggest influence on the magnitude of the CTE of the concrete. Values depending on the type of aggregate can be found in literature some of which can be seen in table 6.

Aggregate type	Gravel	Granite	Limestone	LWAC with natural sand
Thermal expansion coefficient (με/°C)	13	10	9	9

Table 5 Coefficient of thermal expansion for concrete with different types of aggregates (Bamforth, 2007).

Besides the fact that the CTE changes with the mix design, the CTE for hardening concrete is not a constant but changes over time as a function of the maturity and the moisture state. In the early-ages of hardening, the CTE of the concrete is dominated by the CTE of water, which is much higher. This results in a relatively high CTE in the heating phase of the hydration process. This effect is confirmed by literature as can be seen in figure 21. It can however be argued that in this stage the concrete also has very low stiffness, which reduces the resulting stresses. Furthermore in the early-stages relaxation effects will cause most stresses to be relieved (van Breugel et al., 1996). Therefore it seems reasonable to adopt a constant value for The CTE of hardening concrete.

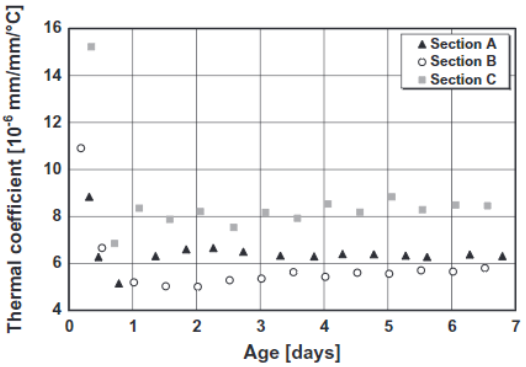

figure 21 Time-dependency of the coefficient of thermal expansion (Yeon et al., 2013).

Values for the CTE are also proposed in standards and codes, which can be used when there is no further information available. In general a constant value for the CTE is adopted, ignoring the effects of the concrete mixture and the time dependency.

- In the CEB-FIP Model Code 2010 (and the Eurocode) a CTE of $10\ \mu\varepsilon/°C$ is proposed for normal weight concrete and a CTE of $8\ \mu\varepsilon/°C$ is proposed for LWAC
- In the ACI 2001 standard a CTE of 11 $\mu\varepsilon/°C$ is recommended for all concrete
- In CIRIA C660 by P. Bamforth a CTE of 12 $\mu\varepsilon/°C$ is recommended as it is argued that an underestimation of the CTE can have a significant influence on the early-age stress calculations.

2.4 Imposed deformations in hardening concrete

In the introduction of this study the concept of imposed deformations was discussed. Also, the imposed deformations that are relevant in hardening concrete were discussed briefly. Imposed deformations are (partially) restrained deformations that as a result of the restraining cause stresses. In the assessment of early-age cracking it are imposed thermal- and hardening shrinkage deformations that cause concrete stresses to develop during hardening. In this section these deformations are discussed in more detail.

2.4.1 Thermal deformations

2.4.1.1 Temperature development in time

In the section on the hydration process the heat- and temperature development in hardening concrete are discussed. As discussed, in the centre of a concrete element the temperature development will be close to adiabatic while on the edges of the element the temperature development will be semi-adiabatic due to heat transfer to the environment. This causes the centre of the elements to have a higher temperature increase during the heating phase compared to the edges. This can be seen in figure 22 where the temperature distribution and development of a wall cast on an already hardened base during hardening can be seen. In the graph on the right the difference between the temperature development of the core of the wall and the outer zone of the wall can be seen. The temperature rise in the outer zone of the wall is smaller and the temperature development is influenced by the day-night temperature cycle.

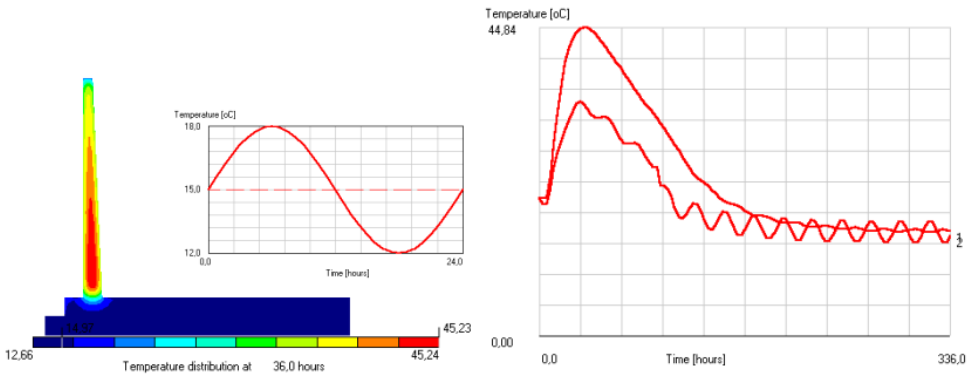

figure 22 Example of heat development over time during hardening for a concrete cross-section (van Beek et al., 2001).

When hydration starts, the heat development will initially be low due to the dormant period as is already discussed before in the section on the hydration process. When the hydration subsequently accelerates, the rate of heat production increases which causes temperature rises in the concrete. After a certain period the rate of hydration will decrease which causes the rate of heat production to decrease as well. The heat flux to environment will become larger than the rate of heat production and the concrete will start to cool until equilibrium with the environment is reached. In figure 23 another typical temperature curve of a concrete element during hardening can be seen. In this figure also the influence of the section thickness can be seen as the temperature rise in the concrete increases with the section thickness.

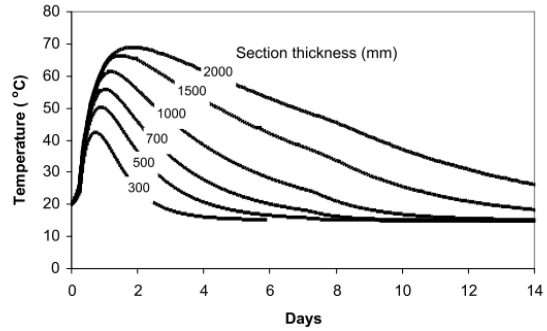

figure 23 Effect of section thickness on total temperature increase during hardening (Bamforth, 2007).

2.4.1.2 Thermal strains

Up till now only the temperature development over time has been discussed. It are however the thermal strains that will cause stresses as they are being (partially) restrained. The types and degree of restraint will be discussed later. For now it is of importance to describe the relation between temperature changes and thermal strains ε_T. This relation is as follows:

$$\varepsilon_T = \alpha_c * \Delta T \tag{2.20}$$

Where α_c $[1/°C]$ is the linear coefficient of thermal expansion and ΔT $[°C]$ is the temperature change. The magnitude of α_c has already been discussed in the section on thermal properties. As can be seen from the equation above there is a linear relation between the temperature change and thermal strains. From this is can be concluded that the thermal strain curve has the same shape as the temperature curve as shown in the figures above.

However the thermal strains will (partially) be restrained, resulting in the formation of stresses. A distinction can be made between internal- and external restraint. Restraining effects will be discussed in more detail in the section on stress formation due to imposed deformations. For now it is sufficient to state that the measured thermal strains will be lower compared to the free thermal strains resulting in stress formation. This effect can be seen in figure 24 where the difference between the free- and measured thermal strains are shown.

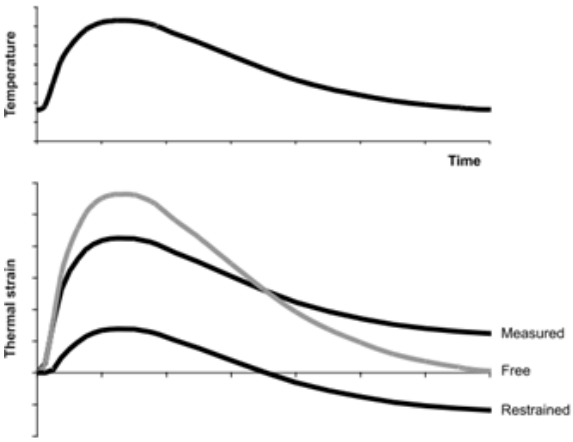

figure 24 Temperature development over time and the corresponding thermal strains (Bamforth, 2007).

As described above, the thermal strains follow from the thermal properties of the concrete and the temperature changes over time. The temperature development over time depends on many factors and can be calculated using finite element software. The software is used to solve the partial differential equation describing heat transfer under transient conditions (Fick's second law).

2.4.2 Shrinkage deformations

2.4.2.1 Drying shrinkage

Drying shrinkage is the result of moisture transport from the concrete to its surroundings. This causes 'drying' of the internal pore system and an increase of the capillary 'suction' forces in the pores (van Breugel et al., 2017). The results is external volume changes over time. The magnitude of shrinkage depends mainly on the dimensions the element, the relative humidity of the surroundings and the w/c ratio of the concrete. Although the final value of the drying shrinkage may be substantial, it develops relatively slow over time. This means that in the first days after casting, the amount of drying shrinkage will be low as can be seen in figure 25. For this reason, drying shrinkage can generally be ignored in the assessment of early-age cracking (Bamforth, 2007). Hence in this research drying shrinkage will also not be taken into account and the focus will be on thermal- and hardening deformations.

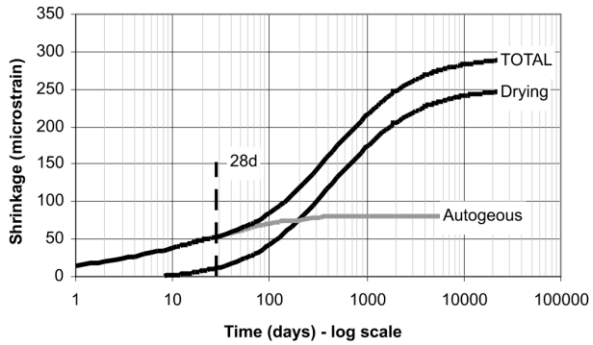

figure 25 The effect of drying shrinkage w.r.t. the total shrinkage over time (Bamforth, 2007).

2.4.2.2 Hardening shrinkage

Next to thermal deformations there will also be hardening shrinkage in concrete, which is closely related to the movement and binding of water in the cement paste. Hardening shrinkage can be subdivided into two types, namely chemical shrinkage and autogenous shrinkage. Chemical shrinkage represents an internal volume reduction due to the formation of a capillary pore structure in the concrete. The total volume of the hardened cement paste is smaller than the sum of the volumes of the different components of the fresh paste, because water is chemically bound in the hydration process resulting in internal empty pores. Hardly any external volume changes occur, resulting in negligible stresses on macro scale (van Breugel et al., 2017). For this reason, chemical shrinkage is not taken into account in this analysis, as we are only interested in deformational changes that cause stresses and thus affect the probability of cracking.

Autogenous shrinkage however does result in external volume changes. Autogenous shrinkage is defined as an external volume change occurring without any moisture transfer to the environment (Holt, 2001). When these deformations are restrained, stresses will occur. All concrete experiences autogenous shrinkage, however the effects are larger for concrete with a low w/c ratio (<0.4) in which there is a shortage of available water for hydration. In general the existence of autogenous shrinkage is recognized, but historically it has not been common practice to include the effects of autogenous shrinkage in the design. Also the magnitude of autogenous shrinkage turns out to be relatively hard to predict. For these reasons the effect of autogenous shrinkage on early-age cracking could benefit from further research (Bamforth, 2007). In this research autogenous deformations will be included in the assessment of early-age cracking, where results of laboratory tests will be used as input for the calculations.

2.4.2.2.1 Mechanisms of autogenous shrinkage

A lot of research has been done on autogenous shrinkage over the past years. It can be concluded that there exists a relationship between the relative humidity of the pore structure and autogenous shrinkage, which means that autogenous shrinkage is in this way related to chemical shrinkage (Holt, 2001; Lu et al., 2014). During hardening water is chemically bound by the hydration products, reducing the relative humidity of the pore structure over time. Although there is consensus about the relationship between relative humidity of the pore structure and autogenous shrinkage, the actual mechanism behind autogenous shrinkage remains subject of debate. Moreover, recent research shows that autogenous shrinkage could in part also be the result of effects of creep. However, there are three principal hypotheses as to what are the driving mechanisms (Lu, 2019; Lura et al., 2003):

1. **Hydrostatic tension in capillary water**

Capillary pores are partially filled with water. When the relative humidity of the internal pore structure decreases, the radius of the meniscus at the surface between pore water and air decreases, which causes an increase in capillary tension force as can be seen in figure 26. The change in pore pressure can be calculated using the following relation:

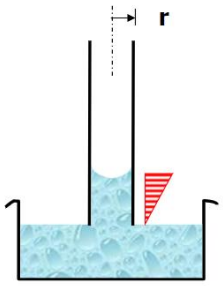

figure 26 Capillary tension force as function of the radius of the meniscus (van Breugel et al., 2017).

$$\Delta p = \frac{2\gamma}{r} \tag{2.21}$$

Where:

$\Delta p = the\ change\ in\ pore\ pressure\ \left[\frac{N}{mm^2}\right]$
$\gamma = the\ surface\ tension\ \left[\frac{N}{mm}\right]$
$r = meniscus\ radius\ [mm]$

The capillary tension forces cause an external volume reduction of the concrete (Lu, 2019). This mechanism seems to be the major contributor for a RH range between 80 – 100%. However in recent studies the validity of the concept of capillary tension forces causing autogenous shrinkage has been doubted (van Breugel et al., 2017).

2. **Changes in disjoining pressure**

Disjoining pressure occurs between two solid particles in the cement paste. The disjoining pressure depends on the distance between the particles and develops in the region of hindered adsorption between the two particles. This is the region where the distance between the particles is smaller than twice the thickness of the adsorbed water layer as can be seen in figure 27. There is a positive relation between changes in the thickness of the adsorbed water layer and the disjoining pressure. When the relative humidity of the capillary pores decreases, the thickness of the adsorbed water layer decreases and as a result the disjoining pressure will also decrease. This causes an external

volume reduction (Lu, 2019). This mechanism seems to be dominant for a RH range between 40 – 80%. The quantification of shrinkage due to changes in disjoining pressure turns out to be rather difficult due to the inhomogeneous microstructure of the concrete (van Breugel et al., 2017).

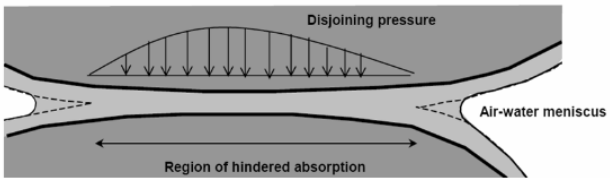

figure 27 Principle of disjoining pressure (van Breugel et al., 2017).

3. Changes in surface tension of solid gel particles

All solid gel particles experience a certain surface tension. This surface tension is a function of the thickness of the adsorbed water layer surrounding the particle. During hydration, water is chemically bound in the hydration products which reduces the relative humidity of the pore structure. The reduction of RH causes a decrease in thickness of the adsorbed water layer, which then causes an increase of surface tension of the solid gel particles. This means that the solids are loaded in compression which results in a volume reduction. This mechanism is dominant for a range of RH of the pore system between 0 – 40% (Lu, 2019; van Breugel et al., 2017).

It can be concluded that the 'self-drying' of the internal pore system is the driving force that results in a volume reduction (van Breugel et al., 2017). The amount of autogenous shrinkage is determined by a combination of the mechanisms as mentioned above. The contributions of each mechanism will however change with changing relative humidity and thus over time, which makes the evaluation complicated. Measurements are needed to be able to validate the models and to be able to determine the magnitude of autogenous shrinkage accurately in the design.

2.4.2.2.2 Autogenous swelling

In the early stages of hardening, i.e. the first hours after casting, 'autogenous' swelling of the cement matrix may occur, which means swelling of the matrix without any moisture exchange with the environment. This effect increases for concretes higher w/c ratio (Bamforth, 2007). There are several mechanisms that have been proposed to account for swelling of the matrix.

1. Formation of crystals of calcium hydroxide and/or ettringite

The ions present in the pore water will crystallize, grow and may exert a force on the pore wall. The most common crystallised salt in the concrete pore structure is calcium hydroxide, but also the formation of ettringite may have this effect. This pressure may cause a volume increase of the cement paste (Lu, 2019; Lura et al., 2003).

2. Microcracking

Microcracking is also one of the driving mechanisms behind autogenous swelling. Because of internal microcracking, the external volume of the concrete may increase (van Breugel et al., 2017).

3. Hydration expansion

During the hydration process, the solid cement particles dissolve and form smaller hydration products which together occupy a larger volume than the single cement particle as can be seen in figure 28. This causes a volume increase of the cement paste (van Breugel et al., 2017).

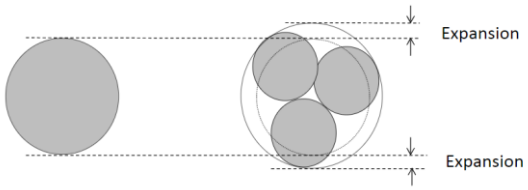

figure 28 principle of autogenous swelling

In practice the swelling- and shrinkage mechanisms occur simultaneously. The magnitude of the swelling mechanisms is generally larger in the early stages, causing overall swelling followed by overall autogenous shrinkage of the concrete as can be seen in figure 29.

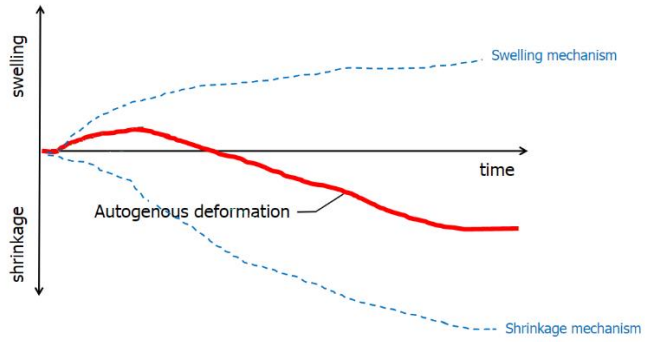

figure 29 Example of autogenous deformations over time (van Breugel et al., 2017).

2.4.2.2.3 Influences on autogenous shrinkage

As autogenous shrinkage is defined as shrinkage occurring without any moisture exchange with the environment, this implicates that autogenous shrinkage cannot be controlled on the building site by altering for instance the external curing method or time. The magnitude of autogenous shrinkage is thus solely based on the mix design of the concrete (Holt, 2001). Here the parameters that most influence the magnitude of autogenous shrinkage are discussed.

- Water/cement ratio

One of the factors that has most influence on the magnitude of autogenous shrinkage, is the w/c ratio, which is closely related to strength. In general autogenous shrinkage occurs in concretes of all w/c ratios. However a significant increase in the magnitude is observed for concretes with w/c ratios ≤ 0.4 (Mors, 2011). This has several causes that are all related to the pore structure of the concrete. Generally when the w/c ratio is lower than around 0.4, there is insufficient water available for full hydration. This results in a more dense capillary pore structure, where the magnitude of the menisci induced hydrostatic tension increases, and thus the autogenous shrinkage increases (Tazawa et al., 1995). Besides, with lower w/c ratio the relative humidity in the pore structure will be lower, increasing changes in disjoining pressure and surface tension in the gel particles. This will also increase the amount of autogenous shrinkage (Lu, 2019). In figure 30 the influence of w/c ratio on the magnitude of autogenous shrinkage can be seen.

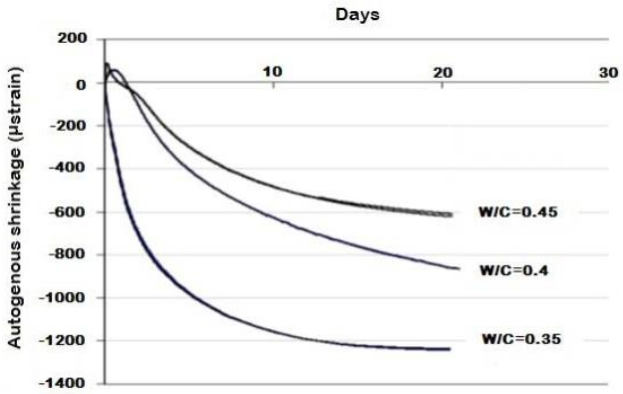

figure 30 The effect of the w/c ratio on the amount of autogenous shrinkage of Portland cement pastes by Wei (2008) (Lu, 2019).

- Binder type and composition

The binder type and composition also have a large influence on the magnitude of autogenous shrinkage in concrete. The primary type of cement that is used (e.g. BFS or OPC) and its clinker composition are both of large influence. Also the use of admixtures like fly ash and silica fume will have an effect on the amount of autogenous shrinkage.

Ordinary Portland Cement:
For ordinary Portland cement the clinker mineral composition is important. According to Jensen (2000), increasing the C_3A or gypsum content causes a significant reduction of autogenous shrinkage, while the C_3S and C_2S content do not seem to have a large impact (Jensen, 2000). These findings are shown in figure 31. Also, during hydration of C_3A and C_4AF ettringite is formed. Ettringite formation goes along with expansion of the cement gel, which reduces the effect of autogenous shrinkage. This means that increasing the C_4AF content will also cause of reduction of autogenous shrinkage (Lu, 2019).

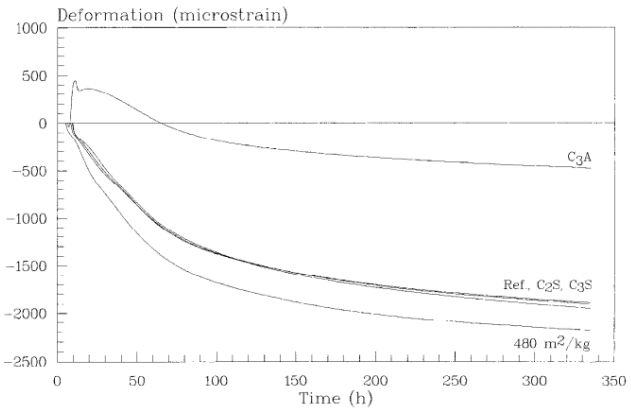

figure 31 Autogenous deformations for the different clinkers in Portland cement (Jensen, 2000).

Blast Furnace Slag cement:
The use of Blast Furnace Slag cement as partial replacement of Portland cement will result in reduced heat production during hardening and in a finer pore structure. A finer concrete will increase the capillary action in the pores resulting in an increase of autogenous shrinkage. This effect is confirmed by experiments and the results can be seen in figure 32 (Lu, 2019; Bamforth, 2007; Lee et al., 2006).

Silica fume:
The use of silica fume in concrete increases the amount of autogenous shrinkage. Silica fume is typically used in high strength concretes, which in general have large autogenous shrinkage. The amount of silica fume used increases this effect. This is also confirmed by experiments and the results can be seen in figure 32 (Lu, 2019; Bamforth 2007).

Fly ash:
Fly ash is a rest-product of the burning of coal and is often used to increase the durability of concrete. Fly ash has a relatively low reactivity and will thus hydrate slower compared to OPC. Corresponding to this also the change in relative humidity of the pore structure will be slower, reducing the amount of autogenous shrinkage (Lu, 2019). This effect is confirmed by experiments and the results can again be seen in figure 32.

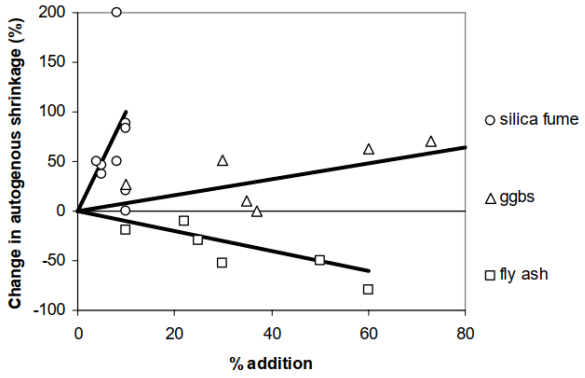

figure 32 Effect of fly ash and GGBS on the amount of autogenous shrinkage (Bamforth, 2007).

Superplasticizers:
Superplasticizers are often used in concretes with low w/c ratio to increase the workability of the mixture. They have the effect of increasing the cement dispersion and rate of hydration. Experiments performed by Holt (2001) show that the use of SP increases the amount of autogenous shrinkage in the concrete as can be seen in figure 33.

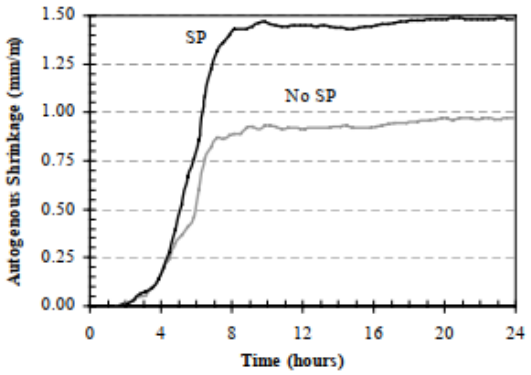

figure 33 The effect of superplacticizers on the amount of autogenous shrinkage (Holt, 2001).

- Aggregates

As mentioned before, aggregates act as internal restraint in concrete. This means that shrinkage of the cement paste is being restrained by the aggregates resulting in stress formation. This reduction of shrinkage of the cement paste depends on the stiffness of the aggregates used. Increasing the stiffness of the aggregates results in a reduction of autogenous shrinkage (Mors, 2011). The

difference in magnitude of autogenous shrinkage for cement mortar and concrete can be seen in figure 34.

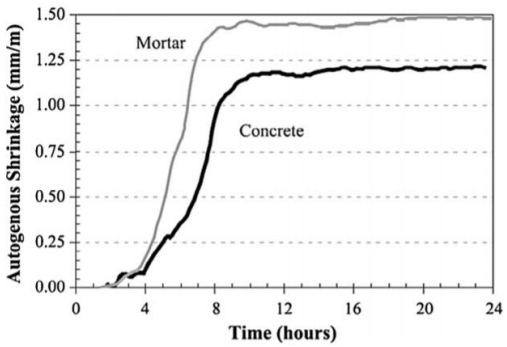

figure 34 The effect of aggregates on the amount of autogenous shrinkage (Wu, 2017).

2.4.2.2.4 Reducing autogenous shrinkage

Although autogenous shrinkage can by definition not be reduced by curing measures taken on the building site, there are several ways to mitigate the effects of autogenous shrinkage. Here some of these measures are discussed.

- Internal curing

Because there is a close relationship between the relative humidity of the pore structure and autogenous shrinkage, the way to mitigate autogenous shrinkage can be sought in this area. Using for instance Saturated Light Weight Aggregates, large changes in the relative humidity of the pore structure can be avoided because additional moisture is stored in the porous aggregates. This moisture is released during hardening and becomes available to stabilize the humidity of the pore structure, reducing autogenous shrinkage. In the same way Super Absorbing polymers can be used as means of internal curing (Bentz et al., 2010).

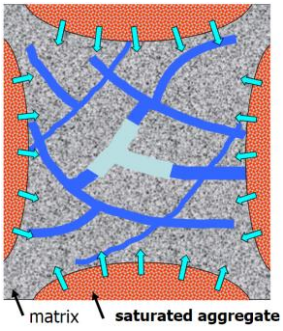

figure 35 Principle of saturated aggregates to reduce the capillary tension forces (van Breugel et al., 2017).

2.4.2.2.5 Magnitude of autogenous shrinkage

As discussed in the sections above, consensus has not yet been reached on the actual mechanisms behind autogenous shrinkage. Besides, calculations on the different mechanisms (on micro- and meso scale) are difficult and can only be performed using advanced numerical calculation methods. For this reason in engineering practice analytical expressions are used to evaluate autogenous shrinkage in hardening concrete as a function of time. Most of these expressions are based on experimental results. However in practice the calculated values often deviate significantly from each other and also from measured values on autogenous shrinkage (Lu, 2019; Mors 2011; Naghdi, 2013). In this research, autogenous shrinkage curves will be used as input for the finite element models. To be able to accurately consider autogenous shrinkage in the analysis, first of all the different

autogenous shrinkage calculation models that are proposed in literature should be discussed. Comparisons should then be made between the results of these calculation methods and available measurement data on autogenous shrinkage. This is done in this section.

2.4.2.2.5.1 Analytical calculations methods

There are several different analytical calculation methods proposed in literature. Some can be found in codes and standards like EN 1992-1-1 Design of concrete structures or the JSCE Specification 2002 (Japan Society of Civil Engineers). Others can be found in literature where analytical expressions are derived from measurements on autogenous shrinkage. In this section some analytical calculations methods will be discussed and compared.

- **Eurocode**

In the Eurocode NEN-EN 1992-1-1 Design of concrete structures, a method is proposed for calculating autogenous shrinkage based on measurements on OPC concrete. In the Eurocode it is stated that autogenous shrinkage occurs in concrete of all w/c ratios and that it is a linear function of the w/c ratio. Also, the Eurocode states that autogenous shrinkage has to be taken into account only when fresh concrete is casted against already hardened concrete. The autogenous shrinkage strain is defined as follows:

$$\varepsilon_{ca}(t) = \beta_{as}(t) * \varepsilon_{ca}(\infty) \tag{2.22}$$

In which:

$$\varepsilon_{ca}(\infty) = 2{,}5 * (f_{ck} - 10) * 10^{-6} \tag{2.23}$$

And:

$$\beta_{as}(t) = 1 - e^{-0{,}2t^{0{,}5}} \tag{2.24}$$

Where t is given in days and f_{ck} is the characteristic compressive strength in N/mm^2.

- **Japan Society of Civil Engineers (JSCE)**

In the JSCE Specification 2002 a method for calculating autogenous shrinkage for concretes with $0.20 \leq \frac{w}{c} \leq 0.65$ is formulated. Based on experimental data, the prediction model was proposed by the JCI Committee (RILEM Workshop Shrinkage of concrete 2000). In this method the amount of autogenous shrinkage depends on the w/c ratio, the type of cement and the time of setting which is related to the early-age stiffness development. The autogenous shrinkage strain is defined as follows:

$$\varepsilon'_{as}(t) = \gamma * \varepsilon'_{as,\infty} * \beta(t) * 10^{-6} \tag{2.25}$$

In which the ultimate amount of autogenous shrinkage is defined as:

$$\begin{aligned} \varepsilon'_{as,\infty} &= 3070 * e^{-7.2\left(\frac{w}{c}\right)} \quad for \quad 0.2 \leq \frac{w}{c} \leq 0.5 \\ \varepsilon'_{as,\infty} &= 80 \qquad\qquad\quad for \quad \frac{w}{c} > 0.5 \end{aligned} \tag{2.26}$$

And

$$\beta(t) = 1 - e^{-a(t-t_s)^b} \tag{2.27}$$

Here γ is a factor for the type of cement (equal to unity for Portland cement), t is the time in days and t_s is the setting time in days. Guidance as to what the value for γ should be when a different binder is used, is however not given. Expressions are proposed for evaluating the factors a and b:

$$a = 3.27 * e^{-6.83*\frac{w}{c}} \quad (2.28)$$

$$b = 0.251 * e^{2.49*\frac{w}{c}} \quad (2.29)$$

According to a research performed by Naghdi (2013), where calculation models were compared with results from experiments, this model turned out to be most accurate of all models analysed.

- **CIRIA C660**

In British publication CIRIA C660 written by P.B. Bamforth (2007) on early-age crack control in concrete, it is stated that the type of cement has a large impact on the magnitude of autogenous shrinkage, while the Eurocode does not take this into account. Also, published data on autogenous shrinkage is discussed in which the amount of autogenous shrinkage measured is significantly underestimated by the calculations according to the Eurocode. This effect increases for higher strength classes.

In CIRIA C660 research as performed by Beroghel-Bouny and Kheirbeck (2000) is discussed, in which measurements have been carried out on concretes with w/c ratios varying between 0.25 and 0.6. Here a calculation method is proposed which also takes into account early-age swelling of concretes with relatively high w/c ratio. However Bamforth concludes that due to the high amount of uncertainty in the determination of autogenous shrinkage, early-age swelling should not be taken into account in the design. In the end the autogenous shrinkage strain can be calculated according to Beroghel-Bouny and Kheirbeck (2000) using the following expression:

$$\varepsilon_{ca} = \left(240t^{0.15} - 650\left(\frac{w}{c}\right)\right) * 10^{-6} \quad (2.30)$$

- **CEB-FIP MC 2010**

In the CEB-FIP Model Code 2010 an approach for calculating autogenous shrinkage is proposed. In this approach the autogenous shrinkage depends on cement type, compressive strength and concrete age. The autogenous shrinkage strain is expressed as:

$$\varepsilon_{au(t)} = \varepsilon_{nau}(f_{cm,28}) * \beta_{au}(t) \quad (2.31)$$

In which:

$$\varepsilon_{nau}(f_{cm,28}) = -\alpha_{au}\left(\frac{\frac{f_{cm,28}}{10}}{6+\frac{f_{cm,28}}{10}}\right)^{2.5} * 10^{-6} \quad (2.32)$$

And

$$\beta_{au}(t) = 1 - e^{-0.2\sqrt{t}} \quad (2.33)$$

Where α_{au} is a coefficient which depends on the early strength class of cement, which can be taken from table 7 from EN 1992-1-1, t is the concrete age in days and $f_{cm,28}$ is the 28 day concrete mean compressive strength.

Early strength class of cement (according to EN 197-1)	α_{bs}
High early strength: Class R	600
Ordinary early strength: Class N	700
Low early strength: Class L	800

Table 6 NEN-EN 1992-1-1 table B.1 Early-age strength classifictation for cement

In the document CEN/TC 250/SC 2 a draft version for the revision of the Eurocode EN 1992-1-1 2018 D3 is discussed. Here the calculation method for autogenous shrinkage is modified and the calculation method according to CEB FIP MC 2010 is adopted. This means that in the new Eurocode the above described approach will become standard.

- **M. Mazloom et al. (2004)**

In a research on the effect of silica fume on mechanical properties on HSC by Mazloom et al. (2004), measurements were done on the amount of autogenous shrinkage in different test specimens. The following expression was determined using regression analysis which depends on the amount of silica fume and the age of the concrete:

$$\varepsilon_{sh}(t) = \frac{t}{0.3SF+12.6+t} * 516 * y_s * 10^{-6} \quad (2.34)$$

In which:

$$y_s = 0.014SF + 0.39 \quad (2.35)$$

Here SF is the silica fume percentage and t is the age of the concrete in days.

There are several other proposed calculation methods for quantifying autogenous shrinkage, however most research focusses on the cement paste instead of the concrete. This makes those methods less suitable for this research.

A comparison between the different calculation methods can be seen in figure 36 below. Here the different models are used to calculate the autogenous shrinkage for a random concrete mixture. The following input is used in the evaluation of the models:

- Concrete strength class: C45/55
- $f_{cm} = 53\ N/mm^2$
- $f_{ck} = 45\ N/mm^2$
- $\alpha_{au} = 700\ (\ Class\ N\ )$
- $w/c\ \ ratio\ = 0.446$
- $\gamma = 1.0$
- $SF = 0\%$

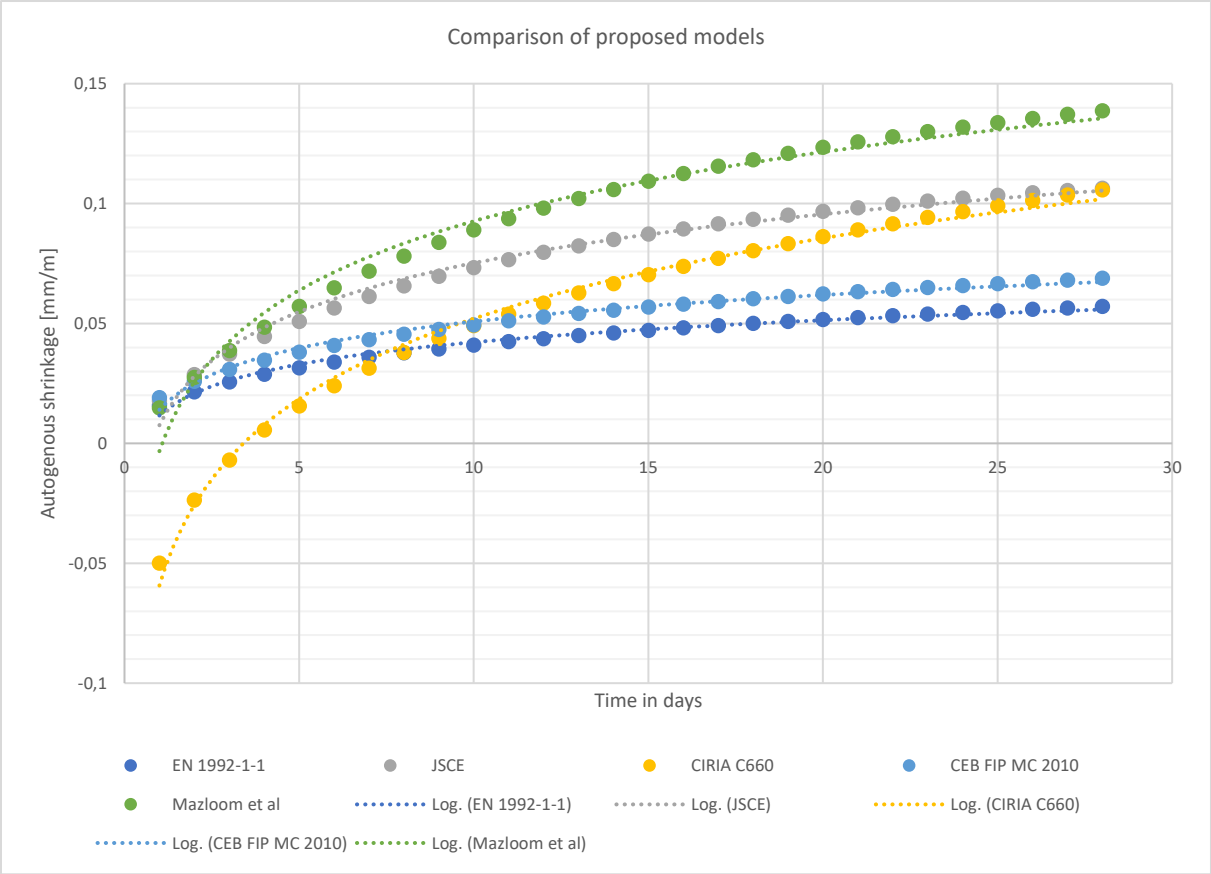

figure 36 Comparion between different calculation methods for the amount of autogenous shrinkage over time

As can be seen from the figure above, there is a relatively large scatter in the results of the different calculation models. It can be concluded that the calculation models according to the Model Code and the Eurocode result in significantly lower values compared to the other methods. Also, CIRIA C660 is the only standard which includes autogenous swelling.

2.4.2.2.5.2 Measurements on Autogenous shrinkage

To be able to verify the proposed calculation models and to be able to accurately model autogenous shrinkage in the Finite Element calculations, measurements on autogenous shrinkage in concrete are needed. As stated before, literature mainly focusses on autogenous shrinkage in the cement paste, which differs from shrinkage of the total concrete due to internal restraints. The available data from literature regarding measurements on autogenous shrinkage in concrete is discussed here and comparisons are made with proposed models from literature as discussed in the section above.

- R. Mors, TU Delft

In a master thesis by R. Mors (2011) performed at the Microlab of the TU Delft, measurements were done on autogenous shrinkage in concrete containing BFS. Several mixtures were tested and in the end the results were compared with the proposed calculation models by EN 1992-1-1 and JSCE Specification 2002. The result can be seen in figure 37. According to R. Mors, the total shrinkage is predicted quite accurately, however the subdivision between autogenous- and drying shrinkage is not correct. The measured autogenous shrinkage was underestimated significantly by the Eurocode. The ratios between the measured values and predicted values by the Eurocode for all mixtures lie within the range of 3 to 5. The calculation method as proposed by the JSCE also underestimates the amount of autogenous shrinkage, however not to the same extent as the Eurocode.

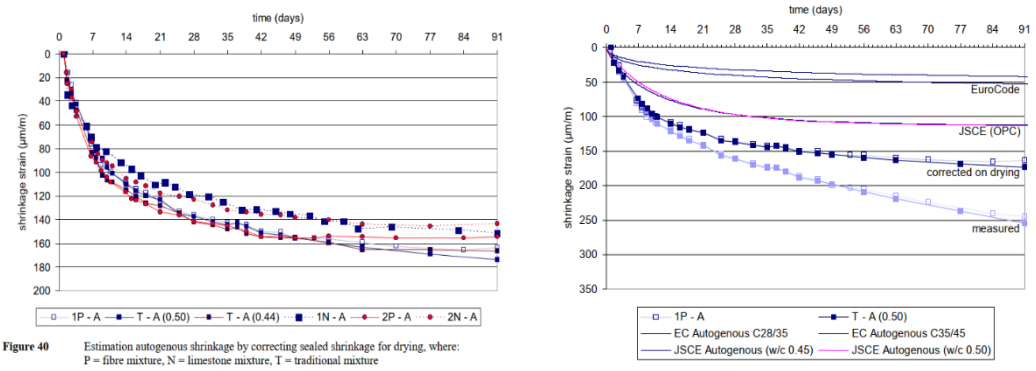

Figure 40 Estimation autogenous shrinkage by correcting sealed shrinkage for drying, where: P = fibre mixture, N = limestone mixture, T = traditional mixture

figure 37 Results of measurements of autogenous shrinkage and comparisons with calculation methods (Mors, 2011).

- R. Naghdi, Zanjan University (2013)

R. Naghdi measured autogenous shrinkage in nine HPC mixtures (relatively low w/c) with silica fume added in some of the mixtures. The results were compared with several proposed calculation models from research. The results show a significant increase in autogenous shrinkage with the addition of silica fume. This is in line with earlier discussed literature by P. Bamforth (2007). Also, an increase in cement content has the effect of increasing the amount of autogenous shrinkage. The results can be seen in figure 38.

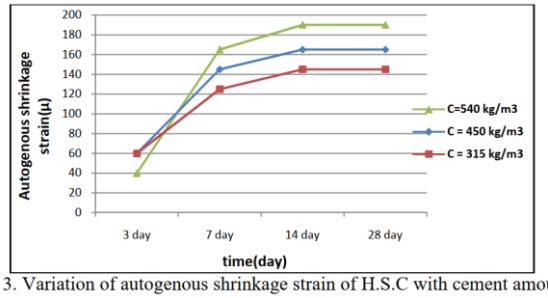

Fig 3. Variation of autogenous shrinkage strain of H.S.C with cement amount

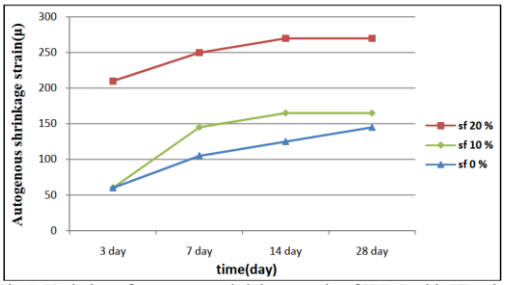

Fig 4. Variation of autogenous shrinkage strain of H.S.C with SF ratio

figure 38 Amount of autogenous shrinkage for different concrete mixtures (Naghdi, 2013).

In the end, from the comparison between the measurements and the results from the proposed calculation models it can be concluded that the JCSE 2002 Model gave the most accurate results. The predictions made by the Eurocode again proved to significantly underestimate the magnitude of the measured autogenous shrinkage.

2.5 Stresses due to imposed deformations

In the previous section the relevant imposed deformations in hardening concrete are discussed. As these imposed deformations are by definition (partly) restrained, they will result in stress formation in the concrete. When the stresses exceed a certain limit, the risk of cracking will increase. In assessing the risk of cracking it is therefore important to determine the magnitude of these stresses. In this section the restraining mechanism behind stress formation due to imposed deformations in hardening concrete will be discussed.

2.5.1 Concrete as a multiscale material

For evaluation of the stresses in hardening concrete it is essential to determine the length scale on which the analysis will be carried out. As for concrete there are three different length scales that can

be distinguished: the micro, meso and macro scale. The length scale on which the analysis will be carried out determines the way in which the concrete will be modelled and each length scale thus has different implications for the analysis and results. In figure 39 a visualisation of the correlation between the different length-scales can be seen.

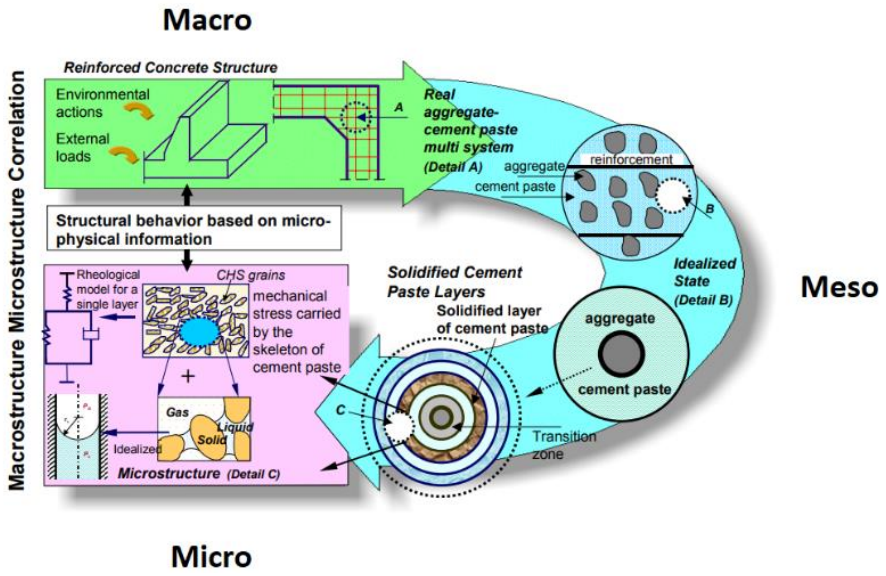

figure 39 Visualisation of the correlation between the different length-scales (Maekawa et al. 2003).

2.5.1.1 Micro

When concrete is regarded at micro-scale it consist out of cement particles, reaction products (e.g. CSH crystals) and the internal pore structure as parts of the cement paste. When evaluating at this level the internal restraint between the different particles in the cement paste can be modelled and the stresses can be evaluated acting between the different particles. The length scale for this model is about 10^{-8} to 10^{-4} m (Maekawa et al. 2003).

2.5.1.2 Meso

On the meso-scale concrete is regarded as an heterogenous three-phase material consisting of the aggregates, cement paste matrix and the interfacial transition zone (ITZ) which all have different sizes and properties. The ITZ is a generally weaker- and thin cement layer at the surface of the aggregates. An advantage of modelling on this scale is that the material eigenstresses due to internal restraints caused by the aggregates can be modelled which can result in internal microcracking. The disadvantage however is that relatively detailed information about the concrete constituents is needed which is not always available in practice. The length scale for this model is about 10^{-4} to 10^{-2} m (Bouquet, 2019; Maekawa, 2003).

2.5.1.3 Macro

On the macro-scale concrete is regarded as an homogenous material, which means that it has uniform composition and properties throughout its volume. All properties are weighted averages derived from its internal components and their composition. The advantage of macro modelling is that the models are relatively simple which enables entire concrete structures to be analysed. A disadvantage of macro modelling is the fact that internal restraints on the meso scale are disregarded which means that material eigenstresses and subsequent microcracking are not taken into account (Maekawa et al. 2003). The length-scale for this model is from 10^{-2} m up to tens of meters.

In this study the focus is on effects of imposed deformations on concrete structures, which means that entire concrete structures will have to be modelled. It follows that this will be done by analysing concrete on the macro-scale. Modelling on the macro-scale has certain limitations as discussed above but is considered the most convenient for the purpose of this study.

2.5.2 Degree of restraint

In the introduction it was already mentioned that when thermal- and shrinkage strains are restrained, stresses will occur. The magnitude of the stresses consequently depends on the degree of restraint. There are two types of restraints that occur simultaneously, but have different origins and effects. The different types of restraints and the way in which they cause stress formation will here be discussed in more detail.

2.5.2.1 Internal restraint

A distinction can be made between internal restraint acting on the meso-scale and external restraint acting on the macro-scale. On the meso scale internal restraint is the consequence of differences in stiffness and thermal properties between the cement paste and the aggregates. When the cement paste deforms, this deformation is partially restrained by the aggregates which results in stresses. This type of restraint is called 'material restraint' and the subsequent stresses are called 'material eigenstresses' and can lead to microcracking. This effect is shown schematically in figure 40 (Bouquet, 2019). However in this study the concrete is considered on the macro-scale with the consequence of not taking the material eigenstresses into account.

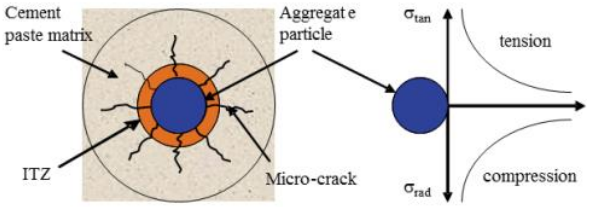

figure 40 Example of stress formation due to internal restraints on the meso scale (Bouquet, 2019).

There will also be internal restraint on the macro scale. This type of restraint is a consequence of differentials in thermal strains over the concrete element can best be explained by means of a massive concrete element. This is done in the introduction in relation to figure 4. In case of a symmetric temperature distribution these compressive- and tensile stresses will be in equilibrium and the concrete will therefore not deform. By definition these stresses are called 'structural eigen stresses' (Bouquet, 2019).

2.5.2.1.1 Eigenstresses

In the section above the term 'eigenstresses' was mentioned. Eigenstresses are stresses that follow from the residual part of a temperature distribution that is in complete equilibrium and therefore does not cause deformations but will cause eigenstresses. These stresses occur due to internal restraint and will thus also occur without any external restraints. An example of a temperature gradient over a wall which in part leads to eigenstresses can be seen in figure 41 (van Breugel et al., 1996; Bouquet, 2019).

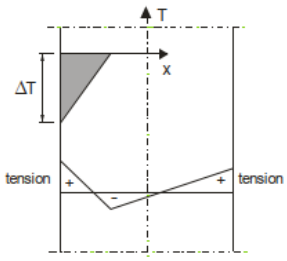

4.5a Cooling at one side

figure 41 Eigenstresses due to thermal gradients over a cross-section (van Breugel et al., 1996).

The temperature distribution in the figure above can be divided into a mean temperature, a temperature gradient and the 'eigen temperatures' which lead to eigenstresses.

2.5.2.2 External restraint

2.5.2.2.1 General

Next to internal restraints there are external restraints. These external restraints are imposed by adjoining structures which form fixed boundaries at the edges of the young concrete and restrain deformations of during hardening. The degree of restraint $R\ [-]$ determines the magnitude of the stresses and is generally expressed as:

$$R = \frac{Actual\ imposed\ stress}{Imposed\ stress\ at\ full\ restraint} \tag{2.36}$$

The degree of restraint varies between 0 and 1 and thus between stress free deformations and full degree of restraint which means that all deformation is restraint and the imposed stress is maximum. The degree of restraint is an essential parameter in the stress evaluation. Accurate determination of the degree of restraint is relatively difficult as it is primarily determined by the dimensions and the differences in stiffness between the adjacent elements which varies over time. Also the degree of restraint is not constant over the element but decreases with distance from the fixed boundary. The degree of restraint is therefore often determined using numerical calculation methods (Al-Gburi, 2015). In figure 42 the stresses over time for varying degree of restraint can be seen for the centre of a hardening concrete wall on a slab with semi-adiabatic temperature conditions. As can be seen, the stress increases with increasing degree of restraint.

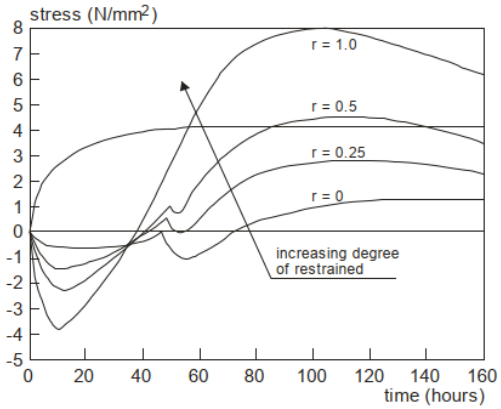

figure 42 The effect of the degree of restraint on the stress formation over time (van Breugel et al., 1996).

2.5.2.2.2 Types of external restraint

For the typical case of casting a wall on top of an already hardened slab there are several configurations of external restraints. There are three basic cases which can be described: one edge base restraint, two perpendicular edge restraint and three edge restraint. All three basic cases have their own restraint distribution (Al-Gburi, 2015). In figure 43.a the restraint distribution of a wall with one edge base restraint can be seen. It can be seen that the degree of restraint decreases with increasing distance from the base edge. At some distance from the base edge the restraint will become zero again and subsequently also the stresses will become zero. The length/height ratio is thus of influence on the distribution of the degree of restraint. If the height of the wall is more or equal to half of the wall length, the restraint at the top will be close to zero. However, independently of the length/height ratio, near the connection interface between wall and slab there will always be full restraint. This effect can also be seen in figure 43.b.

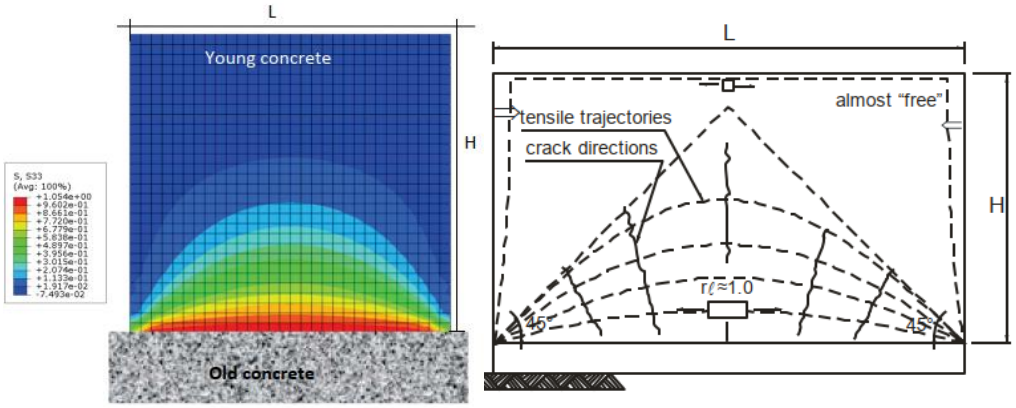

figure 43 Tensile trajectories in a concrete wall due to external restraints (Al-Gburi, 2015;van Breugel et al., 1996).

2.5.2.3 Reducing the restraint

From a design perspective it is desirable to reduce the stresses that occur due to imposed deformations during hardening. This can be achieved by reducing the degree of external restraint. There are many measures that can be taken to accomplish this, some of which will be mentioned briefly here (Al-Gburi, 2015).

- Altering the casting sequence
- The use of construction joints to allow for deformations
- Shortening casting lengths to reduce restraint over height of the wall
- Reducing the stiffness of the base to allow the wall to warp
- Reduce boundary fixation

2.5.3 Stress development during heating- and cooling phase

As hydration starts, heat will develop in the concrete which causes it to expand. Besides, the stiffness of the concrete increases and stresses will develop due to the internal- and external restraints. The stress development over time is different for each location in the cross section. The restrained expansion initially causes compressive stresses in the centre of the concrete and tensile stresses in the outer zone of the concrete as already discussed. When the cooling phase of the hydration process starts, the concrete will start to shrink and because a part of this shrinkage is being restrained tensile stresses will develop. These tensile stresses will increase over time until the concrete is in thermal equilibrium with its surroundings. The stress curve over time in the centre of the concrete section has a typical shape which follows the temperature development as can be seen in figure 44 where measurements are done on a fully restrained hardening prismatic bar for different

initial temperatures. In figure 44.a the temperature development over time can be seen and in figure 44.b the stress development over time can be seen.

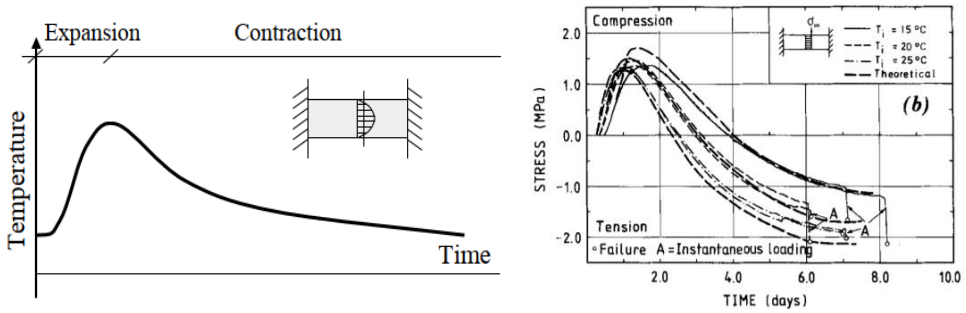

figure 44 Typical stress curve over time for restrained hardening (Al-Gburi, 2015).

2.5.3.1 Effect of shrinkage

Unlike the temperature strains, the shrinkage strains on the macro-scale are uniformly distributed over the concrete element (except for drying shrinkage). A single shrinkage curve is used for modelling of the shrinkage induced stresses in the hardening concrete. As the shrinkage is assumed to be uniform over the concrete element, internal restraints will not be present and the only restraint is external. The stress contribution of the shrinkage strains will follow the same time dependent curve as the shrinkage. As discussed before in this study only autogenous shrinkage will be taken into account as drying shrinkage will have little effect in young concrete. In figure 45 an example of stress formation due to several imposed shrinkage curves can be seen. It should be noted that in this example a nonlinear analysis is performed where post peak behaviour is included. In this nonlinear analysis cracking of the concrete causes a redistribution of forces and a reduction in stress.

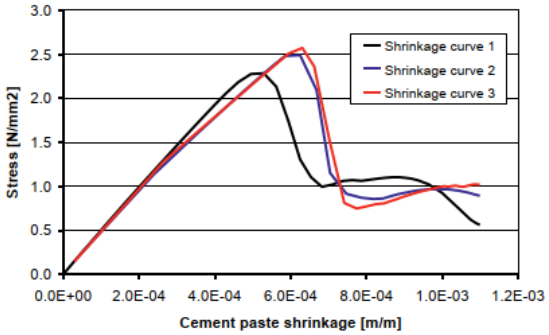

figure 45 Stress formation over time due to imposed shrinkage for a non-linear analysis (Bouquet, 2019).

A more detailed analysis of the stress formation due to imposed thermal- and shrinkage deformations in concrete structures will be performed when carrying out the parameter study using finite element software. Here the effect of thermal- and shrinkage strains will be analysed in more detail by discussing stress- and strength development in time for several governing locations in the element. The stresses that develop during hardening are also reduced by relaxation effects. This will be discussed in more detail in the next section.

2.6 Creep and stress relaxation

Concrete as a material is subjected to creep and relaxation effects which makes it a viscoelastic material. Creep is defined as the increase in deformation over time under constant loading and relaxation is defined as a decrease in stress over time under constant deformation. Despite the fact

that the effects are different, both phenomena are driven by the same mechanisms which take place in the microstructure of the material (Reinhardt, 1985). Creep and stress relaxation occur in all concrete, which means that stresses that develop during the early stages of hardening will be reduced by relaxation effects. This results in a reduction of the tensile stresses that develop during hardening which has a positive effect on the probability of early-age cracking. In figure 46 below the effect of creep and relaxation is visualized. In the figure on the left the strain due a constant stress can be seen. Here the subdivision between the elastic- and creep strain can be seen. In the figure on the right the effect of stress relaxation can be seen where the stress due to a constant strain decreases gradually over time.

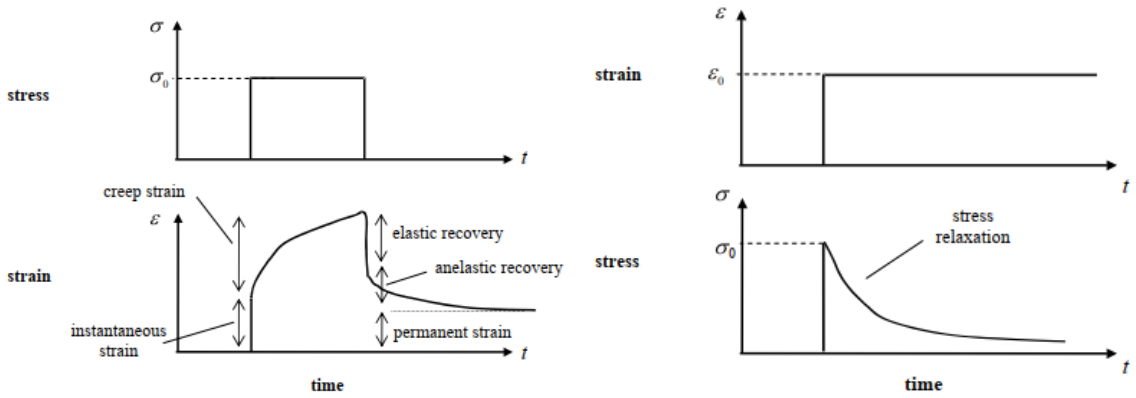

figure 46 Visualisation of the effects of creep and stress relaxation over time (Kelly, 2015).

To include the relaxation effect in the stress calculations during the hardening process, the total stress is calculated in an incremental way where the principle of superposition is assumed to hold (van Breugel et al., 1996). The magnitude of the stress relaxation varies of time and depends on many factors like for instance the type of cement and the maturity of the concrete at the moment of application of the load. Because creep and relaxation are interrelated, the magnitude of stress relaxation can be deducted from the creep behaviour of the material. Creep data can be found in literature for a wide range of concrete mixtures and loading ages.

However as was stated in the introduction of this study, the magnitude of the relaxation effects during the hardening of concrete remains subject of debate and in engineering practice often a single reduction factor is used to account for stress relaxation during hardening. In this study it is therefore aimed to analyse the effects of stress relaxation on early-age cracking in more detail. The principles of creep and stress relaxation, the mechanisms that lie behind it, the method for taking relaxation into account in the stress calculations and the model that is used in the FEA will be discussed in this section in more detail.

2.6.1 Mechanisms

According to H.W. Reinhardt (1985) there are two mechanisms responsible for creep- and relaxation effects. The first mechanism finds its origin in the movement of the evaporable water in the cement paste, where water redistributes inside the capillary pore system. This creep takes place when the concrete is loaded with a very short loading time. Therefore it is called the short-time creep.

The long-term creep finds its origin in the viscoelastic behaviour of the gel particles (Calcium silicate hydrates, CSH). Because of the inhomogeneous structure of these particles in the cement paste, during loading of the concrete stress peaks will occur causing bonds between the particles to be broken. These particles will shift and create new bonds in the shifted state resulting in a

redistribution of gel particles. This redistribution is facilitated by the presence of physically bound water, which enhances the shift of particles that are located next to the capillary pores and which are thus less bound to the cement paste. Following this model, any disturbance of the structure of water in the concrete paste like a temperature rise or moisture change, will increase the creep effects.

The long-term creep can be subdivided in the basic creep and transient creep, where the basic creep is a function of the moisture content and temperature, while the transient creep is a function of the change in temperature and moisture content. Part of the creep will be irreversible, namely the redistribution of the gel particles in the shifted phase. There is also a reversible part of the creep. This reversible part comes from elastic deformation of the gel particles, which returns to a state of equilibrium after release of the load. This is visualized in figure 46 (Reinhardt, 1985; van Breugel, 1980).

S.J. Lokhorst (2001) compares outcomes of several other researches into the mechanisms behind creep and relaxation. Some contradictory results are found but all proposed mechanisms have in common that they are related to changes in the microstructure of the cement paste, where time dependent behaviour plays an important role.

2.6.2 Influences on creep and stress relaxation

Abundant research has been performed on the influencing factors of creep and relaxation. Although some of the research focusses on influences on creep and others on influences on relaxation, the results will be similar since both effects originate from the same mechanisms (Reinhardt, 1985). In this research the focus is on factors that influence the behaviour of young concrete. This means that factors that influence the long term creep such as moisture content, loading cycles and humidity of the surroundings will not be mentioned here.

Concrete mixture:

Type of cement: BFS cement experiences less creep compared to Portland cement according to Reinhardt (1985). This is however contradicted by S.J. Lokhorst (2001) who states that BFS cements experience larger early-age relaxation and creep compared to Portland cement based concrete. In another study on the effect of partial Portland cement replacement the following graph is found which suggest a reduction in creep- and relaxation effects for increasing BFS content. Overall it can be concluded that the effect of BFS cement on creep remains subject of debate and also depends on the fraction of blast furnace slag cement in the total cement.

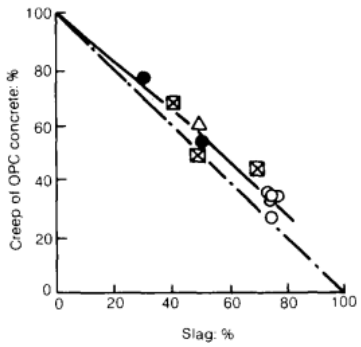

figure 47 Effect of BFS content on the creep of OPC concrete (Bamforth, 1980)

- There is a linear relationship between the *cement content* and the amount of creep. This is due to the fact that part of the creep occurs in the ITZ (Interfacial Transition Zone) which is the layer between the cement paste and aggregate.

- The *fineness* of the cement also seems to have an influence on the amount of creep. There are however contradictory statements found in literature on this effect (Lokhorst, 2001).
- The *water/cement ratio* largely influences the amount of creep. Because a higher w/c ratio results in a less dense concrete, moisture transfer occurs easier, which contributes to the amount of creep (Lokhorst, 2001).
    - $\varepsilon_{cr} \sim \left(\frac{w}{c}\right)^2$ (2.37)
- In general the aggregates have a higher stiffness compared to the cement paste. This means that when the cement paste wants to deform, it is internally restrained by the aggregates. This also holds for creep effects. According to Neville (1997), the *volume percentage of aggregates* in the concrete can be related to the amount of creep. The higher the relative amount of aggregates, the less creep will occur.
- There exists an inversely proportional relation between the *maturity* of the concrete and the amount of creep. I.e. young concrete creeps more than hardened concrete (Bamforth, 2007). This is confirmed by van Breugel et al. (1996) as can be seen in figure 48 where the relaxation factor $\Psi(t,\tau)$ is calculated according to a general formula for young concrete. The fact that hardening concrete creeps more compared to hardened concrete again stresses that a more accurate evaluation of the creep- and relaxation effects is important in the assessment of early-age cracking (as is part of this study).

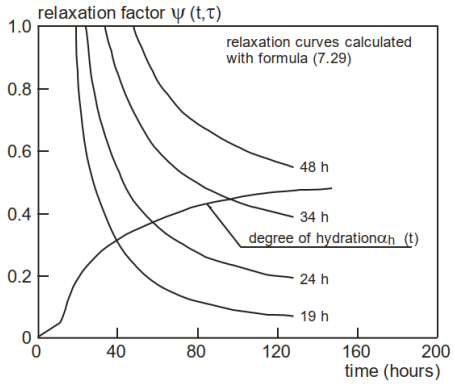

figure 48 Time- and maturity dependency of the relaxation factor (van Breugel et al., 1996).

- Research shows that some *additives* in concrete also have an influence on the amount of creep, however the assessment of these effects lies outside the scope of this research.

Boundary conditions:

- Increasing the temperature of the concrete increases the mobility of the gel particles, which in turn increases the creep effects. During hydration the temperature of the concrete rises, which increases the amount of creep and relaxation. Compressive stresses that develop during the heating phase in the very early stages when the maturity is also low, are thus largely reduced due to relaxation effects (Lokhorst, 2001; Bamforth, 2007). The opposite holds for tensile stresses during the subsequent cooling phase.

In the end it can be concluded that for this study namely the type of cement, the maturity of the concrete and the temperature are the most relevant parameters that influence the creep and relaxation behaviour. It is therefore important to incorporate the effects of these parameters in the calculations.

2.6.3 Creep measurements

As discussed in the introduction of this chapter, creep data can be found in literature. Creep measurements are performed on concrete by measuring the deformations after application of a constant load at a specific concrete age. This is often done for multiple ages at loading to be able to draw conclusions on the changes in viscoelastic behaviour of concrete during aging. There are different types of creep that can be measured. Generally the 'basic creep', 'drying' creep or 'total creep' is measured.

The magnitude of the creep is often expressed as the creep compliance or the specific creep. The creep compliance $J\ [1/MPa]$ is defined as the total load strain per unit of stress and is the sum of the elastic strain and the specific creep (Page et al., 2007). As stated before, the magnitude of the creep that is found depends on many factors related to both the concrete mixture and the boundary conditions.

Because creep and stress relaxation are related, creep measurements can be used as input for the analysis to be able to take stress relaxation into account. This can be done by making use of rheological models such as the Maxwell chain model which describe the viscoelastic material behaviour and consist of a system of springs and dampers. This will be discussed in more detail later.

Below some typical results of creep measurements are displayed. In the first graph basic creep data as measured by Ohnuma (1983) can be seen. Here the specific creep is measured for a concrete containing Ordinary Portland Cement with a 28-day compressive strength $f_{cm} = 25\ MPa$. The ages at loading are respectively 3, 7 and 28 days. As can be seen from the graph, there exists an inversely proportional relation between the maturity of the concrete and the creep. In the second graph basic creep data as measured by Lee (2006) can be seen. Here the creep compliance is measured for a concrete containing Ordinary Portland Cement with a 28-day compressive strength $f_{cm} = 57\ MPa$. The ages at loading are respectively 1, 3, 7 and 28 days.

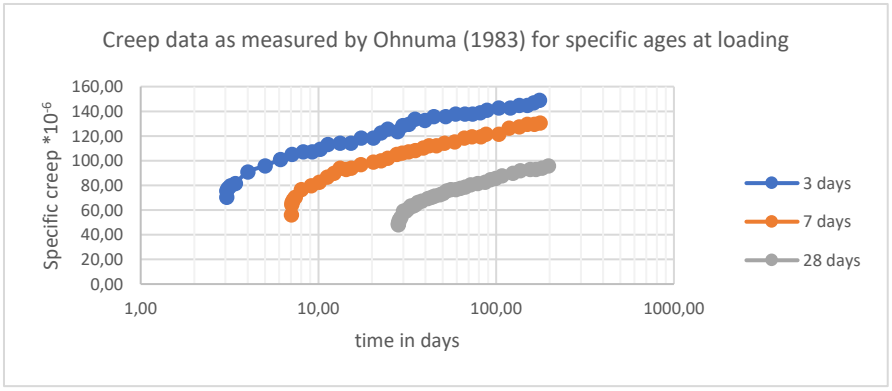

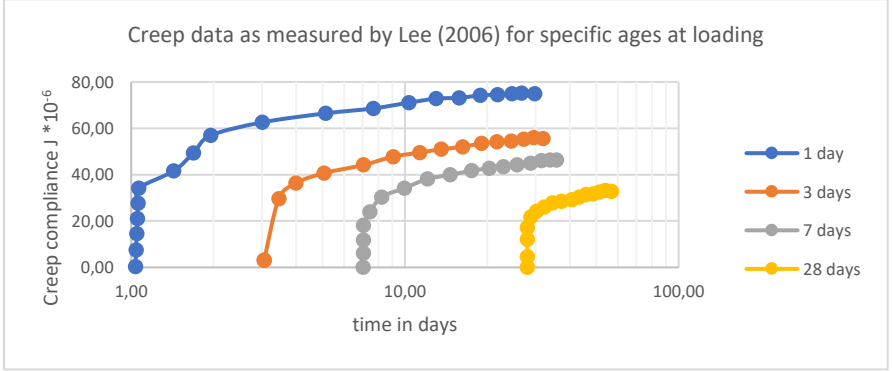

figure 49 Examples of results of creep measurements on young concrete (Bažant et al., 2014).

As stated before in the introduction of this research, the magnitude of the creep- and relaxation effects in hardening concrete remains subject of debate. As can be concluded from analysing creep data from literature, there is wide spread in creep values as can also be seen in figure 49 above. Especially for hardening concrete this range is relatively wide. Without available data on early-age viscoelastic behaviour regarding the concrete of interest it remains relatively difficult to accurately evaluate the stresses in the concrete during hardening. Determining the magnitude of stress relaxation during hardening more accurately is therefore part of this study.

2.6.4 Maxwell chain model

To be able to include viscoelastic material behaviour in Finite element software, mechanical models are used. These mechanical models consist of systems of linear elastic springs and linear viscous dash-pots (dampers) (Kelly, 2015). There are several models that can be used like the Kelvin model, the Burger's model and the Maxwell chain model. The models differ in the configuration of the springs and dampers which determines the response of the system.

In this study the Maxwell chain model will be used. This mechanical model consists of units of springs and dampers connected in series as can be seen in the figure below. The spring has a stiffness E and the damper has a viscosity μ.

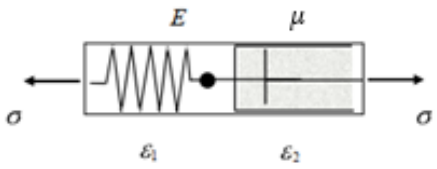

figure 50 Mechanical model for a single Maxwell unit (Kelly, 2015).

The constitutive relation for a Maxwell unit can be derived using the equilibrium conditions corresponding to a system connected in series. This is done in appendix B and the resulting standard form can be written as:

$$\sigma + \tau\dot{\sigma} = \mu\dot{\varepsilon} \tag{2.38}$$

With $\tau = \frac{\mu}{E}$ is the retardation time of the damper in hours.

In figure 51 the creep-recovery response of the Maxwell chain model can be seen. As can be seen, at the moment of application of the load there is an elastic strain response corresponding to the linear spring which will be equal to σ_0/E. The strain response increases over time at a constant strain rate corresponding to the linear viscous damper. After removal of the load there will be an immediate elastic recovery corresponding to the linear spring. In this model there is no inelastic recovery, which means that a permanent strain remains. In reality however there could be some inelastic recovery.

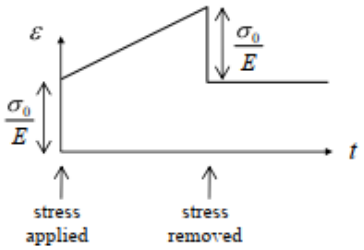

figure 51 Creep-recovery response of the Maxwell chain model (Kelly, 2015).

To describe the viscoelastic behaviour of the material, several Maxwell units in parallel are used. Generally 4 to 5 units are needed to accurately describe the material behaviour (Reinhardt, 1985). In figure 52 such a scheme can be seen. Each unit has its own retardation time and stiffness as the Young's modulus (stiffness) of the concrete is distributed over the different units by means of coefficients. The retardation time of a specific unit is generally set as 10^{k-1} where k is the number of the unit that is regarded. Because the viscoelastic behaviour of hardening concrete changes over time, the distribution coefficients are not constant but change for each maturity of the concrete. This means that a set of distribution coefficients is defined for each maturity of the concrete. Changes in viscoelastic behaviour during hardening of the concrete are in this way modelled using an aging Maxwell chain model.

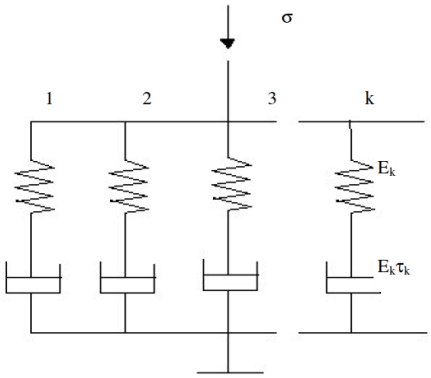

figure 52 Mechanical scheme of the general Maxwell chain model consisting of multiple units in parallel (Femmasse B.V., 1996).

In figure 52 above a Maxwell chain model consisting of k units connected in parallel can be seen. This system has to be evaluated in order to be able to analyse the effect of variations of the distribution coefficients and to be able to compare the model output to actual creep data. To solve such a system of Maxwell units one has to solve a system of first order ordinary differential equations. The initial conditions can be retrieved from the static system at $t = 0$ by making use of the properties of a parallel system:

$$\sigma(t) = \sum_{i=1}^{k} \sigma_i(t) \tag{2.39}$$

$$\varepsilon(t) = \varepsilon_1(t) = \ldots = \varepsilon_k(t) \tag{2.40}$$

After the initial conditions have been found the system can be solved. This is done by making use of the Laplace method. Making use of the Laplace method reduces the system of ODE's to a system of algebraic equations which can be solved using substitution or other methods from linear algebra. In appendix B a system of two Maxwell units is solved by hand. Besides the derivation of a system of 5 Maxwell units is performed including the formulation of the initial conditions needed to solve the system.

Solving of the system results in total strain curves which depend on the concrete stiffness (related to maturity) and the distribution coefficients. In figure 53 the total strain response to a unit of stress (creep compliance) for a maturity at loading of 24 hours can be seen. The distribution coefficients are defined according to the Maxwell chain data as displayed in table 8.

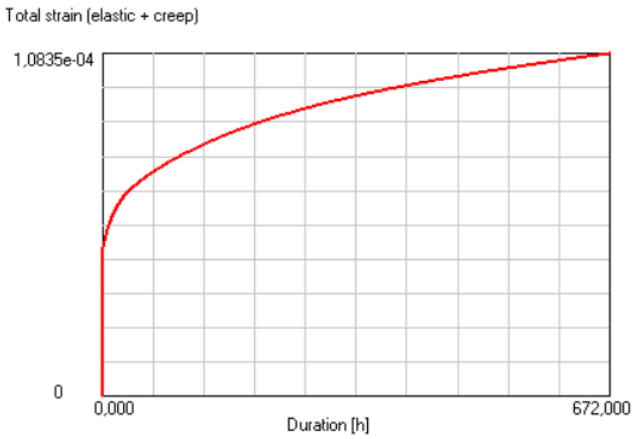

figure 53 Example of a total strain response to one unit of stress for a maturity at loading of 24 hours.

As stated before, the distribution coefficients corresponding to the different Maxwell units vary for increasing maturity (and E-modulus). This is assembled in a so-called Maxwell chain data file as can be seen in table 8 below. In this data file the distribution coefficients are defined for several maturities. To obtain the distribution coefficients for other maturities, interpolation can be used. The Maxwell chain data is presented here corresponds to 'average creep' material behaviour and is provided by the TU Delft.

Maxwell Chain Data Retardation times with distribution coefficients

Maturity	E-modulus	1,0	10,0	100,0	1000,0	10000,0	100000,0
[hours]	[MPa]	[hours]	[hours]	[hours]	[hours]	[hours]	[hours]
0	500	0,0000	0,0000	0,2000	0,8000	0,0000	0,0000
12	16685	0,0000	0,3000	0,2000	0,3000	0,2000	0,0000
24	21943	0,0000	0,2500	0,2500	0,2000	0,3000	0,0000
72	29021	0,0000	0,2000	0,2500	0,1500	0,4000	0,0000
168	33112	0,0000	0,2000	0,1500	0,2000	0,4500	0,0000
336	35628	0,0000	0,2000	0,1000	0,2000	0,5000	0,0000
672	37521	0,0000	0,1500	0,1500	0,1000	0,6000	0,0000
1344	38920	0,0000	0,1500	0,1000	0,1500	0,6000	0,0000
2688	39941	0,0000	0,1000	0,1500	0,0500	0,7000	0,0000

Table 7 Example of Maxwell chain data for 'average creep' behaviour (TU Delft, 2019).

It could be of interest to use actual creep measurement data when analysing the hardening process of a specific concrete. To be able to do this the distribution coefficients for a specific maturity at loading have to be altered to fit the creep data.

2.6.5 Stress calculation procedure

For this study it is relevant to discuss the stress calculation procedure that is used in the Finite element analysis in which stress relaxation is taken into account. As stated in the introduction, analysing the stress- and strength development for hardening concrete is relatively complex due to the fact the material properties (including viscoelastic behaviour) vary over time. This means that the response of the material is different for each point in time. To be able to take these effects into account, the principle of superposition is used for the calculations. In this section the details of the stress calculations using the principle of superposition are discussed briefly as not all expressions are derived in detail.

With the use of the principle of superposition a linear constitutive relation is assumed, which is valid under a couple of predefined conditions regarding the stress range, unloading, moisture content distribution during creep and sudden stress increases at later ages. The superposition principle states

that the response to two or more strains, is equal to the sum of the responses to each of the strains taken individually.

A constitutive relation for viscoelastic material behaviour which relies on the method of superposition is proposed by Bažant (1988), where the stress $\sigma(t)$ at time t can be calculated by summation of the stress history increments at times τ, which can be described as $R(t,\tau) * \mathrm{d}\varepsilon(\tau)$. The total stress at time t will then be:

$$\sigma(t) = \int_0^t R(t,\tau) * (d\varepsilon(\tau) - d\varepsilon^0(\tau)) \tag{2.41}$$

This integration formula yields the constitutive relation of the ageing viscoelastic material with time dependent properties in which $R(t,\tau)$ is the relaxation function which is related to the response of the Maxwell chain model (Bažant, 1989). The total response can be obtained by summation of the functions over the units of the model. This is done via a Dirichlet-series containing exponential functions. In this way an expression for the relaxation formula can be derived, in which the material properties remain time dependent (Reinhardt, 1985):

$$R(t,\tau) = \sum_{k=1}^{m} E_k * e^{-\frac{\Delta t}{\tau_k}} \tag{2.42}$$

Where:

$m =$ the number of Maxwell units
$\tau_k =$ the retardation time of stress reduction for unit k
$\Delta t =$ the duration of the time interval
$E_k =$ the stiffness of the spring element for unit k

The two equations above can be evaluated in an incremental way where it is assumed that the incremental strain rate is constant in the time interval from t^i to t^{i+1}. The total stress at the end of the time interval i can then be calculated using the following expression where the stress contributions of the m Maxwell units are summed up (Femmasse B.V., 1996):

$$\sigma^{i+1} = \sum_{k=1}^{m} \left(\frac{\tau_k}{\Delta t} E_k \left(1 - e^{-\frac{\Delta t}{\tau_k}} \right) \right) \Delta\varepsilon^i + \sum_{k=1}^{m} \sigma_k^i e^{-\frac{\Delta t}{\tau_k}} \tag{2.43}$$

Where:

$\sigma^{i+1} =$ the total stress at the end of time interval i
$\sigma_k^i =$ the stress in Maxwell unit k at the beginning of time interval i
$\Delta\varepsilon^i =$ the total strain increment for time interval i

For small retardation times τ_k , the factor $e^{-\frac{\Delta t}{\tau_k}}$ will be small. From the equation above can be seen that the stress contribution from the Maxwell unit σ_k^i to the next time step will therefore be small as well. In other words, a large part of the stress corresponding to this unit will not be taken into account in the next timestep and has thus vanished due to relaxation effects. So, units with short retardation times give large stress relaxation. This means that for units with high retardation times there will be less relaxation.

In figure 54 below a schematic representation of the stresses as calculated using the superposition principle can be seen. In the graph the stress contribution for each time step i can be seen. The total stress is calculated by summing over the different stress increments. As can be seen in the graph, the

stresses of the different increments decay over time due to relaxation effects. The total stress at for instance $t = 2$ is then equal to the sum of the remainders of the stress increments (in red).

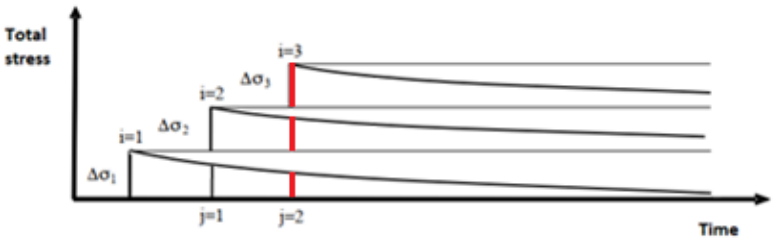

figure 54 Schematic representation of the superposition princple used in the calculation of the total stress (Bouquet, 2019).

2.7 Early-age cracking

In the previous sections the different mechanisms and processes that are relevant to the evaluation of the risk of early-age cracking are discussed. The main purpose of discussing these mechanisms and processes is to in the end be able to evaluate the probability of early-age cracking. In this section early-age cracking is discussed. First the probability of cracking is discussed. Second the different types of cracks are discussed followed by the consequences of the occurrence of these cracks. Then measures for mitigating crack risk in design are briefly discussed as many of these are already discussed in the previous sections. In the end early-age cracking in engineering practice is discussed where the design methods regarding imposed deformations and early-age cracking are reviewed as they are used in engineering practice.

2.7.1 Probability of cracking

In general it can be stated that if at any point in time during hardening the tensile stress exceeds the tensile strength, the concrete will crack. As however stated in the Model Code 2010: “the phenomena of cracking are of highly probabilistic nature”. It is therefore common practice to speak of a certain probabilistic safety against cracking in terms of a likelihood of the mean tensile strength being greater than the tensile stress in the concrete. The stress and strength are often described using normal distributions as can be seen in figure 55. Here the stress- and strength development of hardening concrete can be seen. The probability of cracking is then determined using statistics (van Breugel et al., 1996).

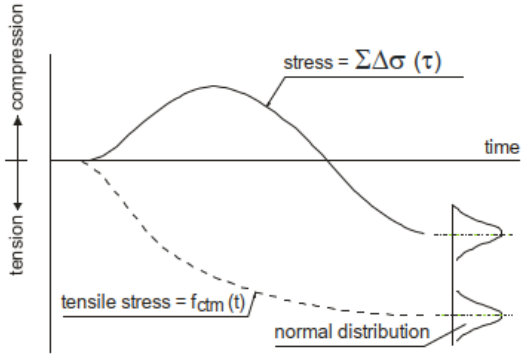

figure 55 Schematic representation of the probability of cracking (van Breugel et al., 1996).

2.7.1.1 Crack criteria

Judging the probability of cracking is often done using a certain criterion. There are three different types of crack criteria: stress criterion, strain criterion and temperature criterion. The temperature criterion limits the temperature difference over a cross-section. If this temperature difference

remains below a certain value, the safety against cracking is assumed to be sufficient. This criterion is however the least reliable. In practice the stress criterion is preferred.

2.7.1.1.1 Stress criterion

Based on a large number of experiments a stress criterion is developed. Using this method the safety against cracking is expressed as a limit for the tensile stress as function of the mean tensile strength. If for example the tensile stress is limited to $0.5 * f_{ctm}$, the probability of cracking is 0.02% and the safety against cracking $\gamma = \left(\frac{f_{ctk}}{\sigma ctk}\right) = 1.22$. In this study this stress criterion will be used as is in line with van Breugel, 1996. When the tensile stress remains below this limit, the safety against cracking is sufficient and the probability of cracking is negligible (van Breugel et al., 1996). In figure 56 the stress development in hardening concrete can be seen in 'green'. The strength development can be seen in 'red'. The stress criterion is implemented in 'orange'. From this example it can be concluded that this particular element has a high risk of early-age cracking.

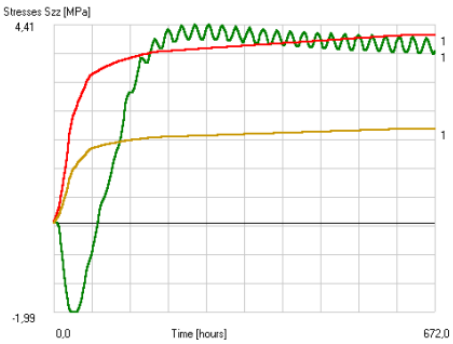

figure 56 Typical stress vs strength diagram for hardening concrete under imposed deformations

The stress criterion can only be used is the stress- and strength development in time during hardening are known. It is therefore needed to perform detailed numerical calculations using finite element software. This will also be part of this study.

2.7.2 Types of cracks

There are several types of cracks that could occur in hardening concrete. Four types will be distinguished here as can be seen in figure 57 (Al-Gburi, 2015):

- 1: Surface cracks developed during the heating phase

In the acceleration phase of the hydration process the temperature in the core of the element rises substantially. The temperature rise in the outer zones is limited due to the exchange of heat with the surroundings. As a result the thermal expansion of the core of the element is internally restrained by the outer zones causing tensile stresses in the outer zones. This may result in surface cracks in the outer zone during the heating phase.

- 2: Through cracks developed during the heating phase

Besides, thermal expansion of the hardening concrete is restrained externally by the already hardened concrete. In the interface zone between the two elements this restrained expansion may cause tensile stresses in the hardened concrete and could lead to cracking.

- 3: Through cracks developed during the cooling phase due to internal restraints

Because the core of the hardening concrete element experiences a greater temperature rise during the acceleration phase of the hydration process, the core will subsequently experience a greater

temperature drop and contraction during the cooling phase. The shrinkage of the core of the element is internally restrained by the outer zones resulting in tensile stresses in the core of the hardening element. Subsequently through cracks may occur in this phase.

- 4: Through cracks developed during the cooling phase due to external restraint

Similar to the heating phase, in the cooling phase thermal shrinkage of the young concrete is restrained by the older concrete in the interface zone between the two elements. This restrained shrinkage may cause tensile stresses to develop in the young concrete. Because the material properties of the young concrete are still in development, the tensile stress could at any point in time exceed the tensile strength which leads to cracking of the young concrete.

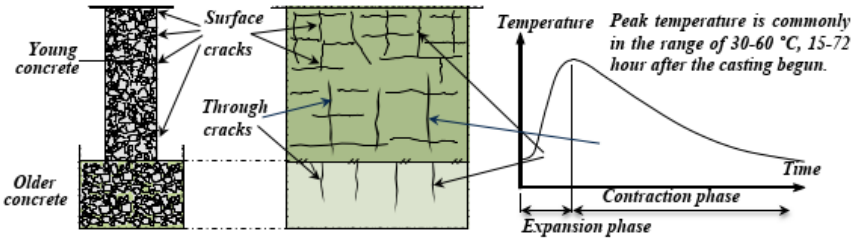

figure 57 Different types of cracks regarding early-age cracking (Al-Gburi, 2015).

Autogenous shrinkage occurs (almost) homogenously over the concrete element. As a result the autogenous shrinkage may counteract the thermal expansion induced compressive stresses and may thus have a beneficial effect in the heating phase. However during the cooling phase the autogenous shrinkage contributes to the tensile stress formation and thus the risk of early-age cracking.

Next to the different types of early-age cracks, there are several different cracks patterns that can be distinguished as can be seen in figure 58. The crack pattern that will occur depends on the boundary conditions of the freshly casted element. From mechanics it is known that cracks will form perpendicular to the tensile stress trajectories. This results in different crack patterns for base- and end-restrained concrete elements.

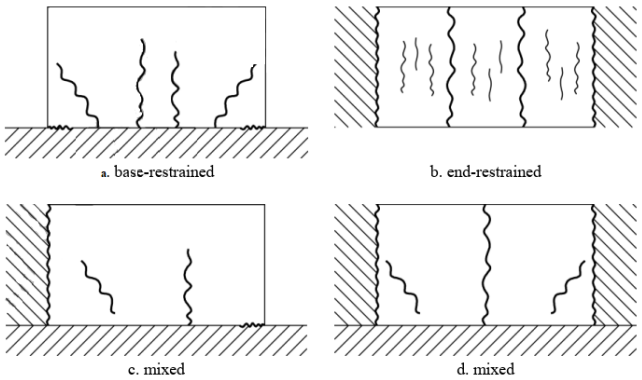

figure 58 Different types of restraints and corresponding crack patterns (Al-Gburi, 2015).

2.7.3 Consequences of early-age cracking

Cracking of concrete structure is in principle not a problem as it is needed to activate the reinforcement during loading. However when cracking occurs unpredictably or the crack widths become too large, problems may arise. As discussed in the introduction of this study this also holds

for early-age cracking as it may lead to issues regarding durability, serviceability and aesthetics. (P. Bamforth, 2006)

If predicted correctly, early-age cracking can be controlled by means of adequate reinforcement design. By adding reinforcement the crack widths and spacing can be controlled. When early-age cracking is however not designed for in an adequate way, problems may arise. With regard to durability the early-age cracks widths should be limited. In the Eurocode maximum crack widths are recommended for several exposure classes. Exceedance of these recommended values may lead to durability issues like carbonation or chloride-induced rebar corrosion.

Next to cracks that cause durability issues there are cracks that affect the concrete's serviceability. Through cracks for instance may jeopardise the water tightness of concrete structures. This is especially important for water-retaining structures with a high tightness class in which no leakage is permitted. In the end early-age cracking may also lead to cracks that are unacceptable from an aesthetic perspective. Although this is a highly subjective aspect, it should be taken into account in the design (van Breugel et al., 2017).

To be able to come up with an adequate design regarding early-age cracking in concrete due to imposed deformations, a time-dependent numerical analysis is needed in which the different processes and mechanisms in relation to stress- and strength development are taken into account. This should be done to prevent problems regarding durability, serviceability and aesthetics. Performing such an analysis is part of this study. In practice however, such analyses are not always performed and simplified methods are used to take into account imposed deformations.

2.7.4 Reducing the risk of early-age cracking

Next to the consequences of cracking, it is also relevant to briefly discuss measures that can be taken to mitigate the risk of early-age cracking. In the first paragraph of this section and in the sections on temperature development and autogenous shrinkage some of these measures are already discussed. Nevertheless the most common measures that can be taken are mentioned again here (Bamforth, 2007):

- Changes in mix design (see paragraph 2.1 of this section):
  - Aggregate type, shape and size. The aggregates form a large volume fraction of the concrete and thus have a large contribution to the material properties
  - Cement type. As already discussed the cement type, content and fineness influence the heat development during hydration
  - Additives. The use of additives like fly ash may have a positive effect on the heat production during hydration

- Construction method:
  - Type of formwork and striking time. For large sections it is important to use formwork with high insulation properties and a long striking time to reduce the temperature gradients over the cross-section. Also insulation blankets can be used at the surfaces where no formwork is present.
  - Pre-cooling of the mix. When the mix temperature at casting is reduced, also the temperature peak will be reduced
  - Post-cooling during hardening. An internal cooling-pipe system may be used to reduce the temperature increase in the core of the hardening element
  - Movement joints allow for free deformations and therefore reduce the amount of restrained deformations. This reduces the stresses in the concrete.

- Construction sequence. The construction sequence may be of influence on the temperature- and stiffness differences between the adjacent elements.

2.7.5 Design with additional reinforcement

In the past sections several ways to reduce the risk of early-age cracking have been discussed. For instance a temperature criterion can be used and it can be decided to apply post-cooling of the concrete mixture to reduce the temperature differentials over the cross-section during hardening. In some cases however it could be undesirable or impossible to use such measures. In these cases it can be decided to accept the risk of early-age cracking and to add additional reinforcement to control the crack widths. Such a method is also described in CIRIA C660 by P. Bamforth and will also be described in a coming CROW report on early-age cracking and design. Here the restrained thermal- and autogenous strain is calculated based on analytical expressions and graphs. A constant creep coefficient is used to account for stress relaxation. The additional reinforcement needed to control the crack width is then calculated from the early-age crack inducing strain ε_{cr} .

It can be stated that the method as described above is based on several assumptions regarding material behaviour and imposed deformations and will therefore be relatively conservative and inaccurate. A more accurate evaluation of the concrete stresses during hardening can be obtained through finite element modelling of the hardening process, which is part of this study.

3 Definition of the case study

The goal of this research is to gain more insight in the mechanisms behind early age cracking to in the end be able to draw conclusions on the risk of early-age cracking in relation to stress relaxation and autogenous shrinkage. It is difficult to investigate this in a general way, which means that the problem should be narrowed down. This is done by reducing the problem to a specific case for which the analysis is performed. By selecting a specific case which is relevant in answering the research question, conclusions can be drawn on the relationship between modelling of the hardening process and the actual behaviour of the construction.

The selection of a case that would be relevant to the research was narrowed down by taking into account the 'big five' of imposed deformations as described by K. van Breugel et al. (2018). In cooperation with VWICC it is decided to aim for a case in which fresh concrete is casted against already hardened concrete. For this typical case imposed deformations will develop in the fresh concrete during hardening due to the restraining effect of the already hardened concrete. This can also be seen in the figure below.

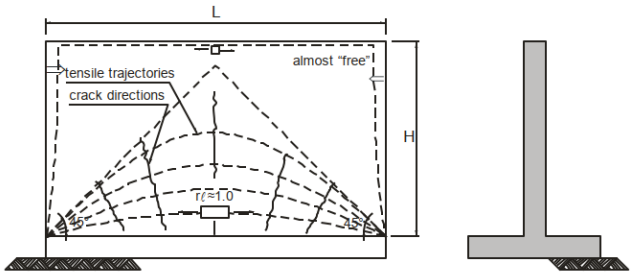

figure 59 Typical case of imposed deformations where a wall is casted against an already hardened slab.

3.1 Dive-under Herfte

A suitable case was found where walls are casted on top of an already hardened slab. A dive-under is currently being built as part of the project Zwaluw- Zwolse Alliantie to create a grade separation for two railway tracks as can be seen in figure 61. The dive-under is built-up out of several segments which are constructed consecutively. This is done by first constructing the slab and then casting the walls on top.

The walls are relatively thick but nevertheless it was decided in the design that active cooling during hardening will not be used. The imposed deformations could lead to cracking and therefore additional reinforcement is used to control the crack widths. The fact that the walls are relatively thick and the absence of any cooling techniques increases the risk of early-age cracking. This makes that this is a relevant case to review in this research. In figure 60 such a segment can be seen.

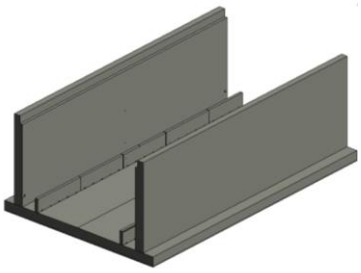

figure 60 Walls and slab of a segment of the dive-under.

The construction of the dive-under already started in 2019. Nevertheless after analysing the building schedule it was found that the construction of the walls of segment 11 to 16 would start in January 2020. This makes that these segments are suitable to review as part of this case-study. In figure 61 an overview of the segments as part of the dive-under can be seen.

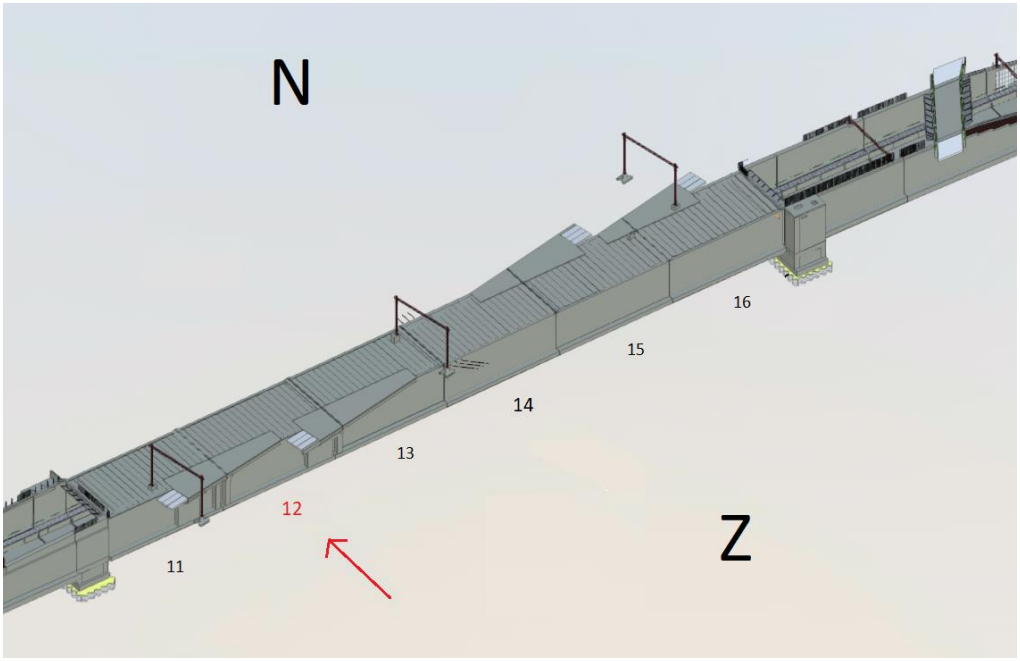

figure 61 Overview of segment 11 to 16 of the dive-under and indication of the Southern wall of segment 12.

In relation to the schedule of this research it was found that the construction of Southern wall of segment 12 would be most suitable to review in more detail. The construction schedule of this wall can be seen in table 9 below.

Activity	Duration in days	Begin date	End date
Preparing of formwork	10	31-1-2020	19-02-2020
Preparing of reinforcement	6	6-02-2020	13-02-2020
Cleaning	1	14-02-2020	14-02-2020
Casting of the concrete wall	1	15-02-2020	15-02-2020
Hardening	3	17-02-2020	19-02-2020
Demoulding	1	20-02-2020	20-02-2020

Table 8 Construction schedule for the Southern wall of segment 12 (VWICC).

In figure 62 a cross-section of a segment of the dive-under can be seen. In this cross-section also the prefab prestressed beams can be seen. These beams will be placed on top of the walls after hardening and are therefore not relevant to this study. The relevant dimensions of the walls and slab are as follows:

- Height of the wall = 7100 mm
- Thickness of the wall = 800 mm
- Thickness of the slab = 800 mm
- Width of the segment of = 15.000 mm
- Length of the segment = 24.000 mm

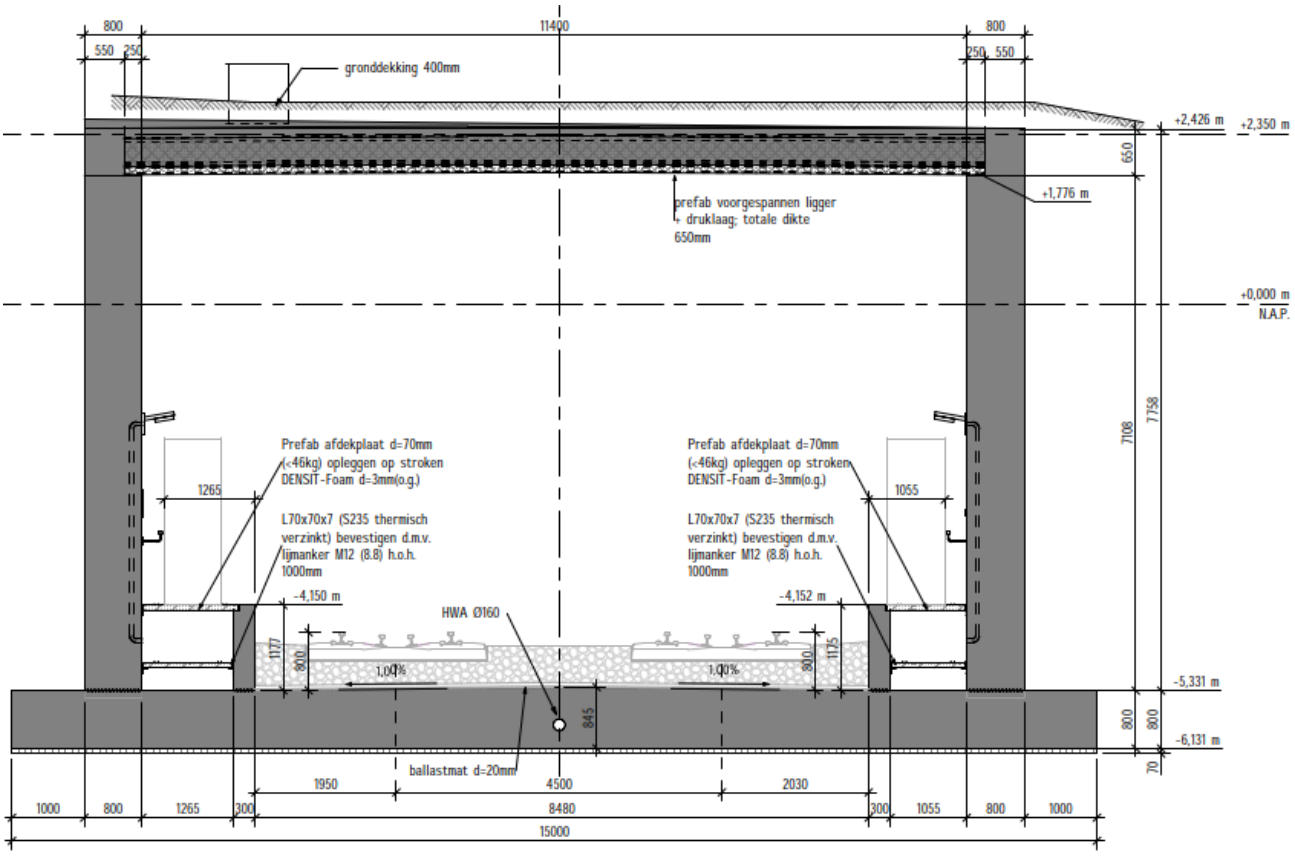

figure 62 Cross-section of the dive-under segment.

3.2 Concrete mixture

Here some basic properties of the concrete of the walls can be seen. More details on the concrete mixture can be seen in the section on laboratory testing. It should be noted that the specific details on the concrete mixture are considered as confidential by Mebin B.V. and can therefore not be published here.

Property:	**Value/remarks:**
Cement manufacturer	ENCI B.V.
Concrete manufacturer	Mebin B.V.
Concrete strength class	C30/37
Binder type	CEM III/B 42,5 N

Table 9 Basic properties of the concrete mixture for casting of the walls of the dive-under.

3.3 Cross-sectional modelling of the wall

The hardening process of the wall will be modelled using finite element software called MLS Heat. The aim here is to accurately model the hardening process and imposed deformations acting on the wall to in the end be able to assess the risk of early-age cracking of the walls. This is done by first modelling the cross-section of the wall and slab and determining the mechanical boundary conditions and then determining all the required input parameters needed to perform the finite element calculations. These parameters will all be determined for the case of the dive-under near Zwolle. In the end also a longitudinal section of the wall will be modelled based on the results of the cross-sectional modelling. This will be discussed in more detail after the first assessment of the risk of early-age cracking based on the cross-sectional model is complete.

3.3.1 Model

The cross-section of the walls and slab of a segment of the dive-under is modelled by making use of a symmetry axis. In this way only half the cross-section has to be modelled which reduces the model size and computation time. Because initially only the cross-sectional plane is modelled, development of the stresses over the length of the wall are not regarded. The situation of fully developed stresses is modelled which is valid for large part of the wall except for both ends (over the length of the wall). The stress state at the ends of the wall will however not be governing in the assessment of early-age cracking as the length/height ratio of the wall is sufficient for external restraint to develop fully (van Breugel et al., 1996).

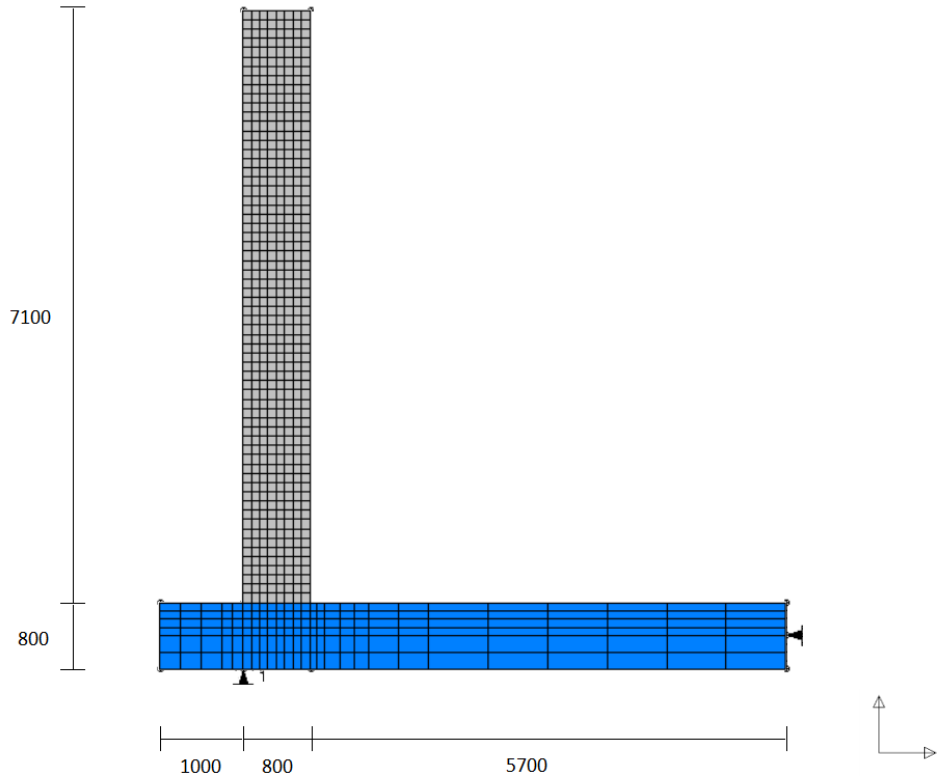

figure 63 Cross-sectional model of the wall and slab of a segment of the dive-under.

The model can be seen in figure 63 above. In this figure the relevant dimensions of the model can be seen together with the mesh. The mechanical- and kinematic boundary conditions can to a large extent be seen in this figure and can best be summarized as follows:

- One point support underneath the wall to restrain vertical displacements at this point.
- One line support along the symmetry axis of the slab which restraints displacements in x-and y-direction at the symmetry axis.
- A situation of plane strain is modelled. For a situation of plane strain holds that the only non-zero strain components act in one plane, in this case the cross-sectional plane. This means that the strain in the outward z-direction ε_{zz} is assumed to be equal to zero. The strain vector then becomes:

$$strain\ vector = \varepsilon = \begin{bmatrix} \varepsilon_{xx} \\ \varepsilon_{yy} \\ \gamma_{xy} \\ \varepsilon_{zz} \end{bmatrix} = \begin{bmatrix} \varepsilon_{xx} \\ \varepsilon_{yy} \\ \gamma_{xy} \\ 0 \end{bmatrix}$$

- Because use is made of symmetry, rotation around the vertical y-axis is fixed. Rotation around the x-axis is free and dilatation in the z-direction is also free.
- The steel reinforcement that is present in the cross-section is not modelled. Because a viscoelastic analysis will be performed without including any damage- or fracture models, the material behaviour after the moment of cracking is not taken into account and therefore the reinforcement does not have to be modelled.

In the end a mesh refinement study has been performed to ensure that the mesh fineness is sufficient. This can be seen in Appendix E.

3.3.2 Input parameters

After the model is finished, the initial input parameters that are required to perform the finite element analysis have to be determined. The different input parameters are discussed in more detail in the literature study. Here initial values are determined for this specific case based on graphs, tables and expressions from codes and literature. However, later in this study, several input parameters will be determined more accurately through laboratory testing

3.3.2.1 Thermal properties

- **Thermal capacity**

The thermal capacity is the product of the density and the specific heat c_T $[\,kJ/kg * K]$. The density of the concrete is assumed to be $\rho_c = 2400\ kg/m^3$. The specific heat can be retrieved from tables and is determined to most likely be equal to: $c_T = 1.04\ kJ/kg * K$. The thermal capacity then becomes: $\rho_c * c_T = 2400\ kg/m^3 * 1.04\ kJ/kg * K = 2496\ kJ/m^3K$ (Bamforth, 2007).

- **Thermal conductivity**

The thermal conductivity depends on the type of aggregate used. In this case it is quartzite. According to K. van Breugel et al. (1996) the thermal conductivity then becomes $3.5\ W/mK$. However according to P. Bamforth (2007) the thermal conductivity becomes $2.9\ W/mK$. As an initial guess it is decided to use $3.0\ W/mK$.

- **Coefficient of thermal expansion**

According to K. van Breugel et al. (1996) the coefficient of thermal expansion for concrete containing quartzite is 12.1 με/℃. However according to P. Bamforth (2007) a value of 12.0 με/℃ should be used when a more accurate value has not been measured. It is decided to use a coefficient of thermal expansion of 12 με/℃.

3.3.2.2 Concrete mix properties

- **Adiabatic evolution**

The adiabatic evolution has been proposed by VWICC. The adiabatic evolution that is used will most likely be relatively accurate for concrete containing CEMIII/B 42,5N and can be seen in figure 64.

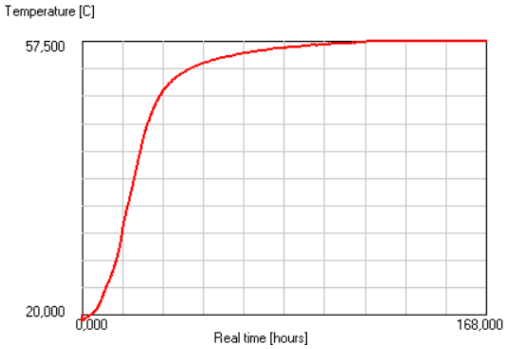

figure 64 Adiabatic evolution for a concrete mixture containing CEM III/B 42,5N

- **Activation energy**

The activation energy Q for concrete containing blast furnace slag cement is derived from literature and is assumed to be $50\ kJ/mol$ (Wu et al., 1983; Barnett et al., 2006; Fernandez-Jimenez et al., 1997).

- **Young's modulus development**

The development of the Young's modulus is derived from the 28-day Young's modulus as is proposed by NEN-EN 1992-1-1. This is done for concrete C30/37 class N and can be seen in the figure below.

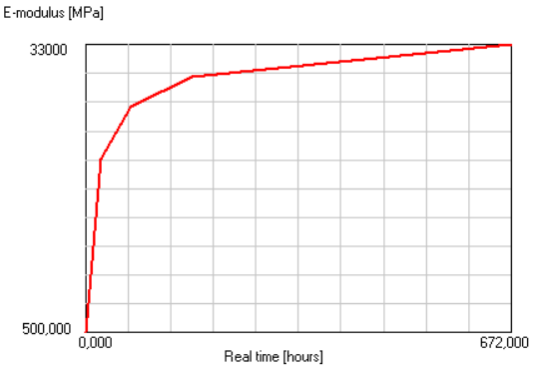

figure 65 Young's Modulus development according to the Eurocode

- **Compressive strength development**

The development of the mean concrete compressive strength is calculated from the 28-day compressive strength according to NEN-EN 1992-1-1 for C30/37 class N. The resulting curve can be seen in the figure below.

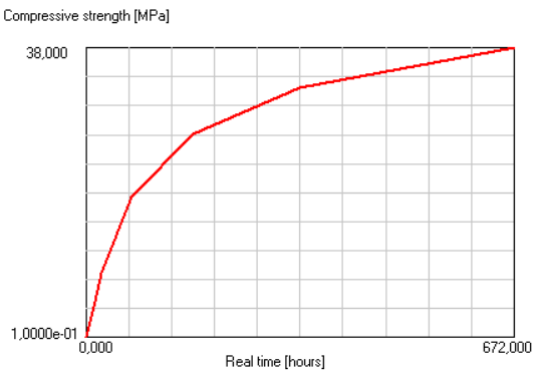

figure 66 Compressive strength development according to the Eurocode

- **Tensile strength development**

The mean tensile strength development is calculated from the 28-day tensile strength according to NEN-EN 1992-1-1 for C30/37 class N. The resulting curve can be seen in the figure below.

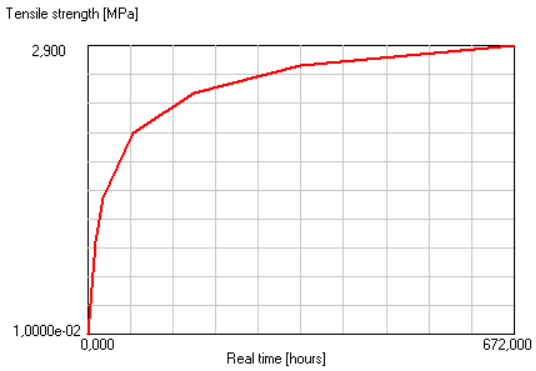

figure 67 Tensile strength development according to the Eurocode

- **Autogenous shrinkage**

The autogenous shrinkage is initially calculated according to NEN-EN 1992-1-1 for concrete C30/37 class N. As is concluded during the literature study, the Eurocode tends to underestimate the autogenous shrinkage significantly. However it is decided to initially use the Eurocode for calculating the autogenous shrinkage. The resulting curve can be seen in the figure below:

figure 68 Autogenous shrinkage development according to the Eurocode

- **Initial mix temperature**

The initial mix temperature can only be guessed using a rule of thumb as in reality it depends on the ambient conditions and the conditions at the manufacturer. As a rule of thumb it is decided to use an initial mix temperature of the mean ambient temperature + 5℃ (VWICC). This means that for a mean ambient temperature of 5℃, the initial mix temperature is assumed to be 10 ℃.

3.3.2.3 Convection and radiation

- **Wind speed**

The wind speed is retrieved from KNMI measurements over the period of 1981 to 2010 for the month of February. The resulting wind speed equals 4 on the scale of Beaufort.

- **Formwork**

NOE Top formwork will be used for casting the concrete walls. The plating material consists of plywood with a thickness of 21 mm (NOE B.V., 2017). The top of the walls will not be covered by any

formwork. According to the building schedule the formwork will be removed after 72 hours, where after the concrete will remain uncovered.

- **Solar radiation**

The solar radiation is determined according to data of the KNMI (Velds, 1994).

- Average daily sum for February in de Bilt = $4.63\ MJ/m^2 = \frac{4.63*10^6}{24*3600} = 53.6\ W/m^2$
- Maximum radiation is $228\ W/m^2$ at noun
- This modelled as a periodic function in MLS heat as can be seen in the figure below:

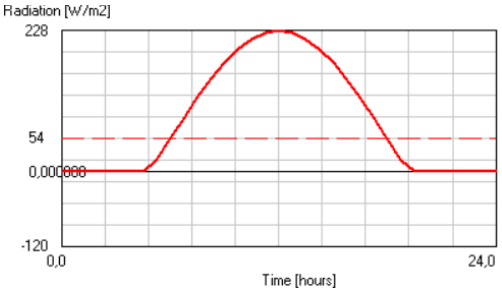

figure 69 Periodic radiation function following from KNMI weather data

- **Radiation coefficients**

The radiation coefficients are retrieved from tables in the MLS Heat database for the materials 'concrete' and 'plywood':

- $\varepsilon_r = 0.8\ dark\ grey\ NOEply$
- $\varepsilon_r = 0.65\ concrete$
- $\varepsilon_s = 0.9\ \ wood$
- $\varepsilon_s = 0.9\ concrete$
- $\varepsilon_a = \varepsilon_s * c_1 = 0.9 * 0.94\ (with\ clouds) = 0.846$

3.3.2.4 Remaining properties:

- **Mean ambient temperature and amplitude**

The mean ambient temperature and amplitude are derived from measurements from the KNMI for the month of February over the years 1981-2010. The mean ambient temperature then becomes 5°C. The amplitude becomes 3°C. The daily temperature cycle is modelled as an oscillating function as can be seen in the figure below.

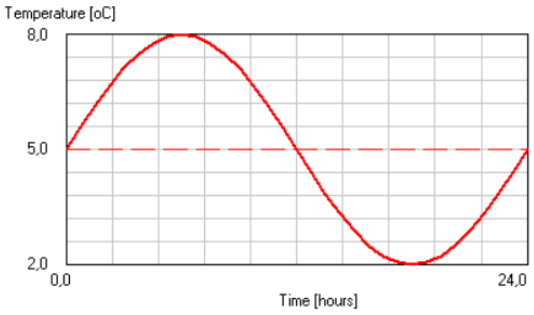

figure 70 Periodic temperature function according to KNMI data

- **Poisson's ratio**

The Poisson's ratio is assumed to be 0.2 [-] as is in correspondence with the recommendations of P. Bamforth (2007).

3.3.3 Calculation procedure

Once the input parameters have been defined, the finite element analysis can be performed. To be able to adequately interpret the results of such an analysis it is relevant to gain more insight in the calculation procedure that lies behind it. The calculation procedure is therefore discussed in more detail here. This will be discussed in a global manner where the main steps of the calculations and their input parameters are described. Details on the actual mathematics will not be given as providing a detailed description of the finite element method lies outside of the scope of this study. In the end the calculation procedure is visualized by means of a flow diagram as can be seen in figure 71.

- Runtime specifications

The finite element analysis for assessment of the risk of cracking is a time dependent analysis. The material properties, temperature and stresses vary of time. For this reason the calculations are performed in an incremental way which means that they are repeated for each time step. The magnitude of the time increments and the total timespan are defined based on the purpose of modelling. The calculations are performed for each node of the finite element mesh as can be seen in figure 63.

- Temperature calculations

At the beginning of each time step the temperature in calculated in each node. This is done based on the initial mix temperature and the adiabatic evolution which is mix dependent. This calculated temperature varies over the cross-section as heat is lost to the environment by means of convection, conduction and radiation. The magnitude of heat loss depends on the location in the cross-section, the formwork material, the ambient temperature, wind speed and amount of radiation.

Next to the temperature, also the unrestrained temperature dilation increment which is equal to the product of the change in temperature and the coefficient of thermal expansion is calculated in each node.

- Maturity calculations

When the temperature for the specific timestep is known, the maturity can be calculated. This is done through the relations as described in the literature study. The maturity can be calculated directly from the temperature history and the activation energy of the concrete mixture. The maturity is needed to determine the strength- and stiffness evolution in each node and is therefore denoted as the 'equivalent concrete age'.

- Strength calculations

As can be seen in the previous section, the strength- and stiffness evolution as a function of time are defined prior to the analysis. This is the evolution for concrete hardening at a constant temperature of 20 °C. The for each node calculated temperature will however not be constant and therefore the strength- and stiffness development in each node will be different from the pre-defined evolution.

The actual strength- and stiffness for each timestep is calculated by means of the 'equivalent concrete age' as defined above. If the temperature history of the concrete will for instance on

average be higher than 20 ℃, then the strength for this timestep will be higher than the strength corresponding to this actual point in time when using the pre-defined strength evolution curve. The strength and stiffness thus follow from the maturity.

- Stress calculations

After the stiffness of the concrete wall and the thermal dilation are known, the stress in the concrete can be calculated for this timestep. There are several other parameters that are needed to perform this calculation. These are listed here:

  - The total strain increment is composed of the thermal strain, autogenous deformation strain and the viscoelastic strain. The viscoelastic strain is composed of the elastic strain and creep strain and is retrieved from the Maxwell chain data.
  - Because these strains are being restrained, stresses will develop. There are two types of restraint, internal and external restraint as is discussed in more detail in the literature study. The internal restraint follows from temperature differentials over the cross-section and the external strain is derived from the geometry of the slab, the mechanical- and kinematic boundary conditions and the difference in stiffness between the slab and wall.
  - The stress is subsequently calculated in each integration point of the finite elements. The total stress at a specific timestep is calculated using the principle of superposition. This is discussed in more detail in the literature study.

As stated before, these calculations are repeated for each timestep and the development of strength and stress are compared to determine the risk of early-age cracking. The total calculation procedure is visualized by means of a flow diagram as can be seen in figure 71.

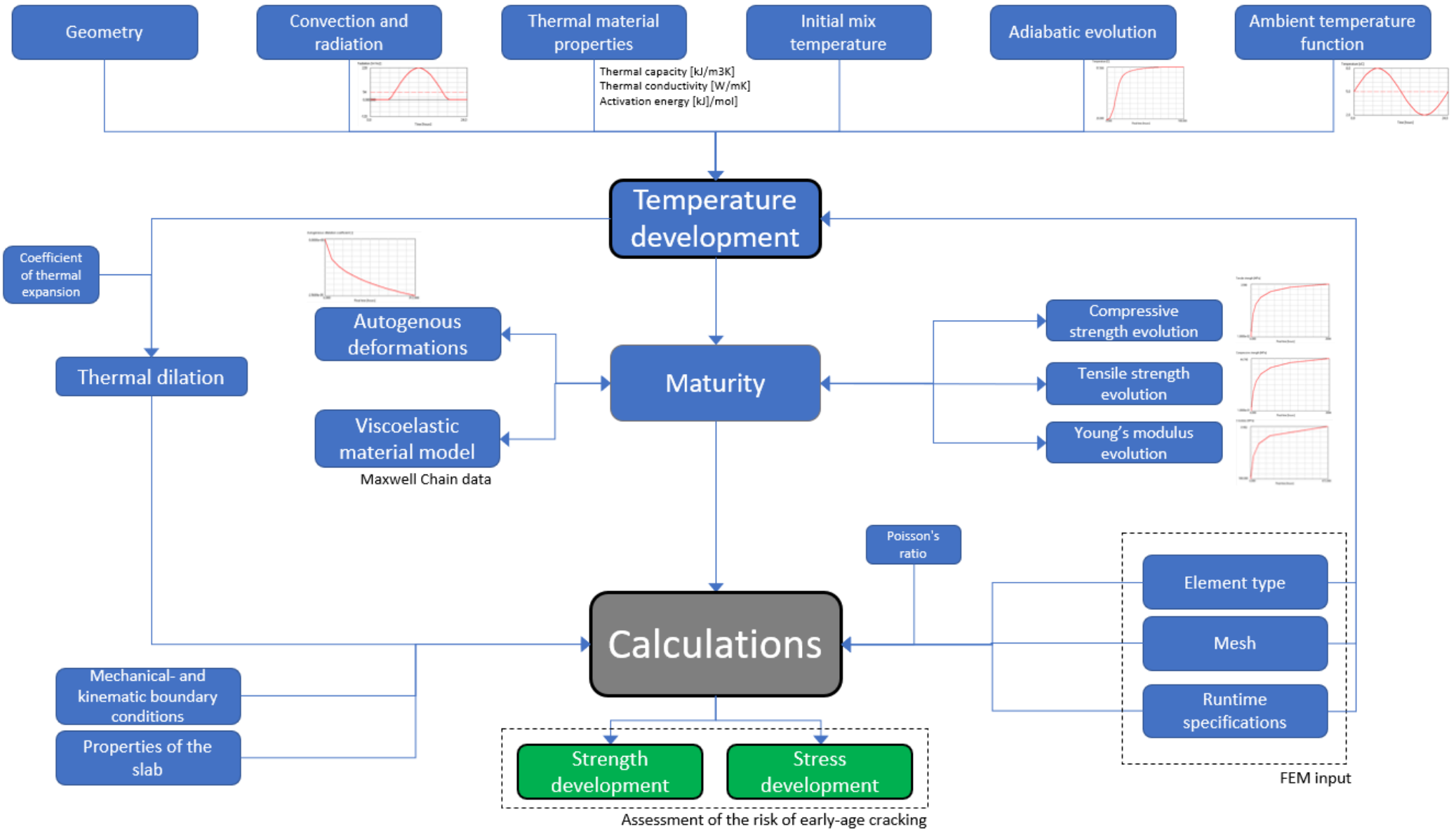

figure 71 Flow diagram of FEM calculations

3.3.4 Runtime specifications

Before the finite element calculations can start, the runtime specifications have to be set. It is decided to use the following specifications:

- The computation time equals 300 hours. From the results can be seen that this timespan is sufficient for the concrete to cool down completely and thus includes the points in time where early-age cracking might occur.
- The stresses are smoothened over the elements
- The time increment is decided to be 0.33 hours, and the results are stored each 3 hours.
- The element type used are fully integrated quadrilateral elements

4 Parameter study

For some of the input of the analysis into the risk of early-age cracking holds that there is accurate data available which can directly be used in the finite element analysis. For some other parameters this cannot be said, which means that these parameter values have to be obtained from literature or even be guessed. This introduces uncertainties in the analysis which in turn may decrease the accuracy of the results. It is therefore important to gain more insight into the effects of variations of these input parameters on the results of the analysis.

4.1 Defining the parameters with high uncertainty

Here parameters are listed that are used in the analysis but have a high uncertainty due to lack of accurate data and/or measurements. For these parameters a study is performed into the effects of variations of these parameters on the output of the finite element analysis. Viscoelastic behaviour (creep and stress relaxation) is not included in this parameter study as this behaviour is discussed later in this research.

Concrete mixture properties:

- Activation energy $[kJ/mol]$
- Initial mix temperature [°C]
- Poisson's ratio $[-]$
- Autogenous shrinkage $[\mu\varepsilon]$

Thermal properties:

- Thermal conductivity $[W/mK]$
- Thermal capacity $[kJ/m^3K\ ]$
- Expansion coefficient $[\mu\varepsilon/°C]$

Boundary conditions:

- Ambient temperature function [°C]
- Radiation coefficients $[-]$
- Solar radiation function $[W/m^2]$

Formwork:

- Striking time $[h]$
- Convection coefficient $[W/m^2K]$

4.2 Initial values

The influence of variations of the parameters will be investigated by running the analysis for different values of the parameters and analysing the results. To be able to do this, initial values for the parameters should be defined. The initial values are derived from literature and/or available information regarding the project that is treated in the case study as is discussed in a previous section.

Concrete mixture properties:

- Activation energy = 50 kJ/mol
- Initial mix temperature = 10 ℃
- Poisson ratio = 0.2
- Young's modulus development according to CEB-FIP MC10 for slow hardening cement
- Autogenous shrinkage according to EN1992-1-1 for $f_{ck} = 30\ N/mm^2$

Thermal properties:

- Thermal conductivity = 3.0 W/mK
- Thermal capacity = 2496 kJ/m^3K
- Expansion coefficient = 12 $\mu\varepsilon$/℃

Properties of the slab:

- No maturity model used for the slab. It is considered as 'hardened concrete'.

Boundary conditions:

- Ambient temperature function
  - Mean temperature = 5 ℃
  - Amplitude = 3 ℃
- Radiation coefficients
  - ε_r = 0.8 for NOE Top formwork
  - ε_r = 0.65 for uncovered concrete
  - ε_s = 0.9
  - $\varepsilon_a = \varepsilon_s * c_1 = 0.9 * 0.94\ (assuming\ cloudy\ weather) = 0.846$
- Solar radiation function
  - Average radiation = 54 W/m^2
  - Maximum radiation = 228 W/m^2

Formwork:

- Striking time = 72 h
- Convection coefficient
  - NOE Top formwork = 6.612 W/m^2K
  - Uncovered concrete = 36.1 W/m^2K

4.3 Method

As described before, the influence of variations of the different input parameters on the output of the FEA will be investigated by running the analysis for the different values and analysing the results. To be able to do this, deviations from the initial values have to be defined which is done here. For some parameters it can be argued that the deviations will most likely lie within the range of -30 to +30% from the initial value, while for other parameters the deviations can be smaller or larger. The variations that will be used in the analyses are listed here.

Parameter for which -30 and +30% variations will be investigated:

- Activation energy
- Poisson ratio
- Thermal conductivity
- Thermal capacity
- Expansion coefficient
- Radiation coefficients ε_r, ε_s and ε_a
- Maximum solar radiation
- Convection coefficients

For some of the parameters above a variation of +- 30% may not be realistic, while for other parameters it could be quite realistic. The aim of this parameter study is however just to compare the effects of variations of the different input parameters. This means that it is more relevant to use the same variations for each of the parameters rather than defining realistic deviations for each parameter individually.

Parameter for which a specific variation is investigated:

For the following parameters holds that it is not sufficient to investigate variations of the same relative magnitude because in reality the variations will most likely be much larger. For these parameters specific variations are defined.

- Initial mix temperature

For the initial mix temperature a standard value of 10℃ was adopted. This value has a high uncertainty as the ambient temperature at the moment of casting and thus also the initial mix temperature cannot easily be predicted. Therefore it is chosen to investigate variations of -5 and +5 ℃.

- Ambient temperature function

For the ambient temperature it also holds that accurate prediction is not possible, therefore here it is chosen to investigate variations of -3 and +3 ℃ with respect to the mean ambient temperature (5 ℃).

- Striking time

The striking time depends on the difference between the temperature of the concrete and the ambient temperature. When this difference reduces and comes within certain predefined limits, the formwork can be struck. According to the schedule this will be done after 3 days, however the moment in time where the temperature criterium is reached may vary. Therefore it is chosen to investigate variations of -1 and +1 day with respect to 3 days.

- Autogenous shrinkage

For the initial analysis autogenous shrinkage is included using the calculation method according to EN1992-1-1 Design of concrete structures – General rules and rules for buildings. However as was concluded in the literature study, the Eurocode tends to underestimate the autogenous shrinkage. For this reason the effect of using different calculation methods for autogenous shrinkage is investigated using the calculation methods according the Model Code 2010 and the Japanese Society of Civil Engineers (JSCE).

A point in the cross-section has to be defined for which the analyses will be compared. It is chosen to use the governing point in the middle of the cross section lying in the bottom region of the wall. In this region of the wall the tensile stresses will be the largest due to the restraining effect of the concrete slab as can be seen in the figure below where the stresses σ_{zz} are plotted during the cooling phase.

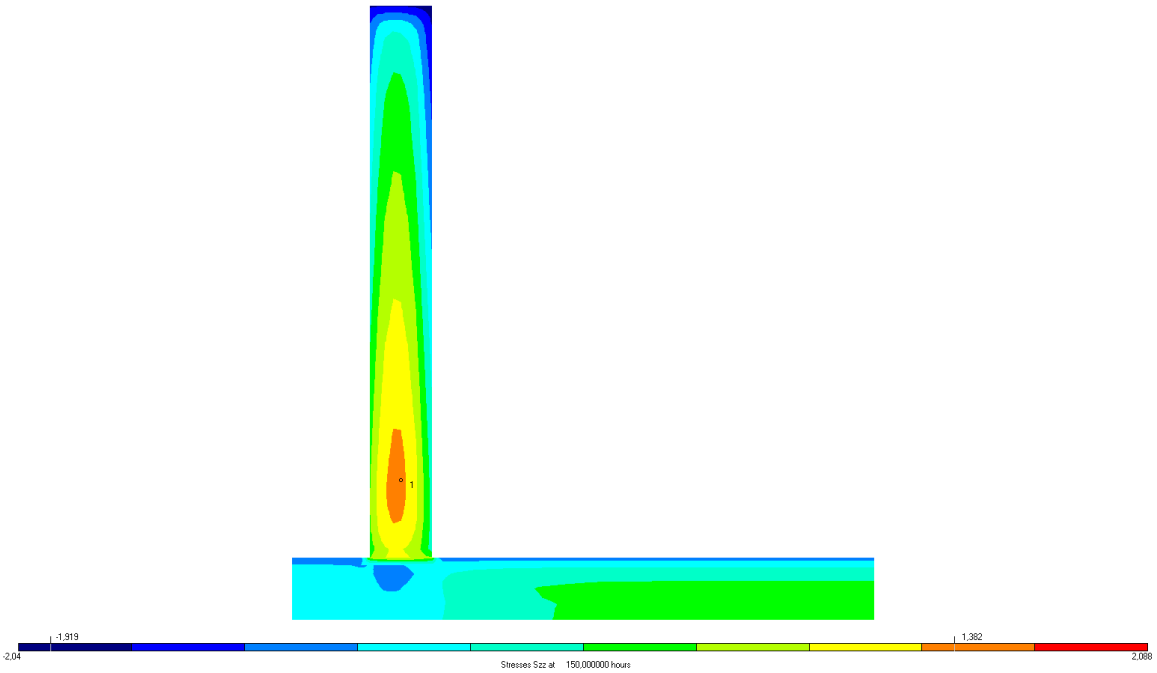

figure 72 Example of a stress distribution over the wall for a moment in time during cooling and indication of the governing point in the bottom of the cross-section

For the purpose of this research it is relevant to analyse several parts of the output of the FEA. First of all the temperature development is important, this because temperature rise and subsequent drop are closely linked to the risk of cracking. Besides that, the stress- and strength development at the point of interest is important. In fact, it is the ratio between the stress and strength which determines the safety against cracking. The output as described above will be visualized by means of graphs and will also be analysed quantitatively.

4.4 Results

First of all the output that is obtained using the initial parameter values is plotted. In figure 73 below the temperature development over time can be seen for the governing point in the centre of the wall.

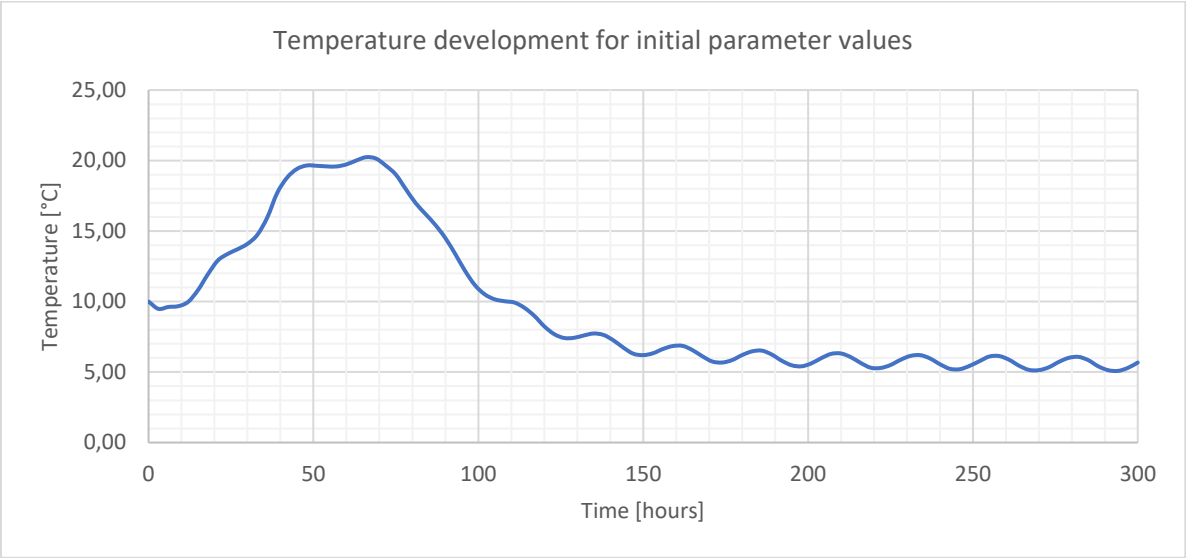

figure 73 Temperature development in the wall according to the FEA using the initial parameters

As can be seen in the figure below which displays the strength and stress development in the governing point over time, the critical point in time where the ratio between the stress and strength is the largest lies around 150 hours. After analysing the results of all different parameter variations it is stated that it can be assumed that this holds for all parameters variations. This means that this point in time will also be used in the remainder of this parameter study.

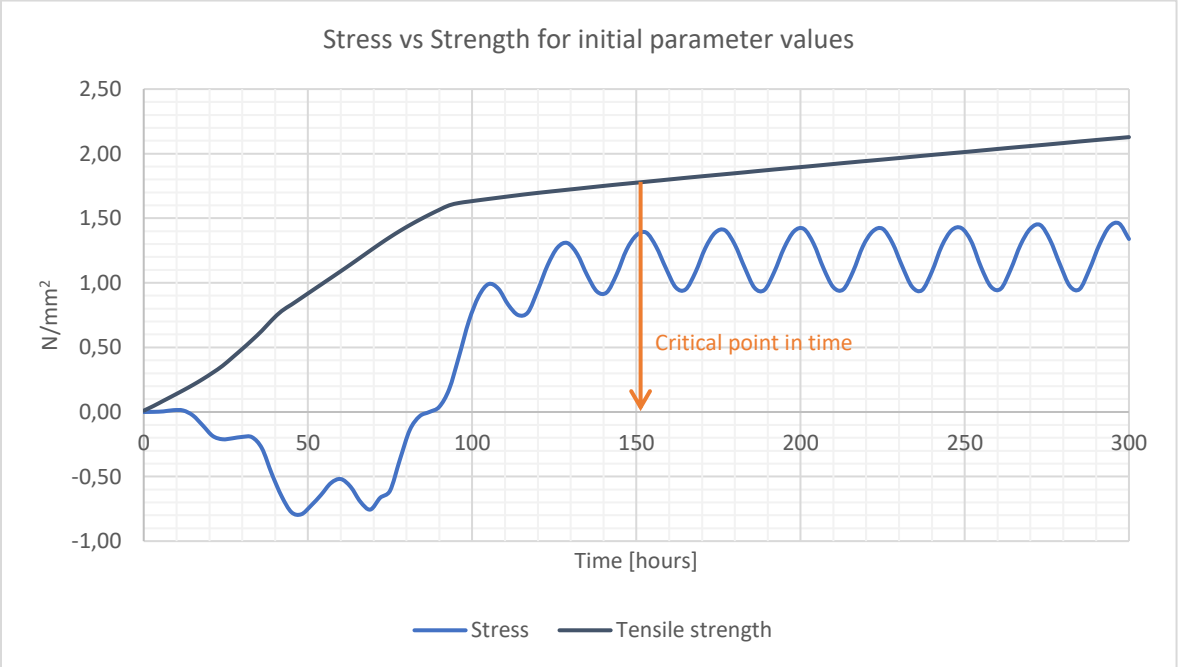

figure 74 Stress vs strength development over time for the governing point in the cross-section according to the FEA

In appendix A the same two graphs can be seen for variations of each input parameter that is investigated in this study.

The resulting data which can be seen in appendix A in more detail, can best be analysed by comparison in a single diagram. This is first done for the maximum temperature during hardening. In this bar diagram the effect of the parameter variations on the maximum temperature during hardening can be seen. This is expressed as the relative change with respect to the maximum temperature that is obtained using the initial values, in percentages.

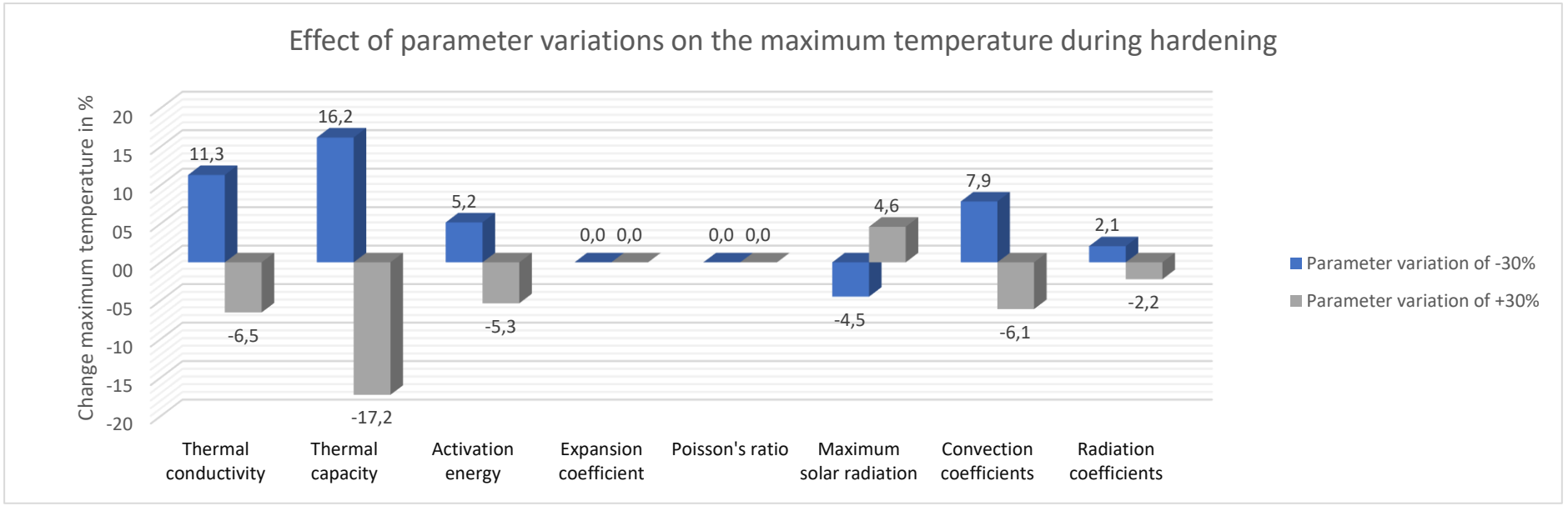

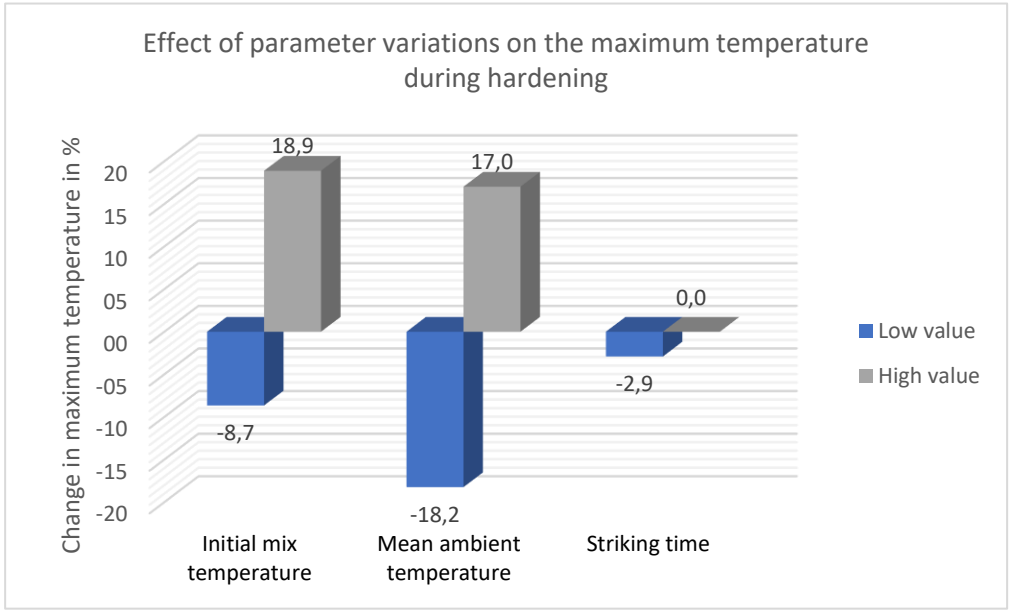

Figure 75 Relative effect of parameter variations on the maximum temperature during hardening

Next, the changes in maximum tensile strength are considered. This is the strength that is obtained at the end of the analysis after 300 hours. Changes in strength development are directly related to maturity and thus temperature. In the bar diagram below the effect of the parameter variations on the maximum tensile strength can be seen. This is again expressed as the relative change with respect to the maximum tensile strength that is obtained using the initial values, in percentages.

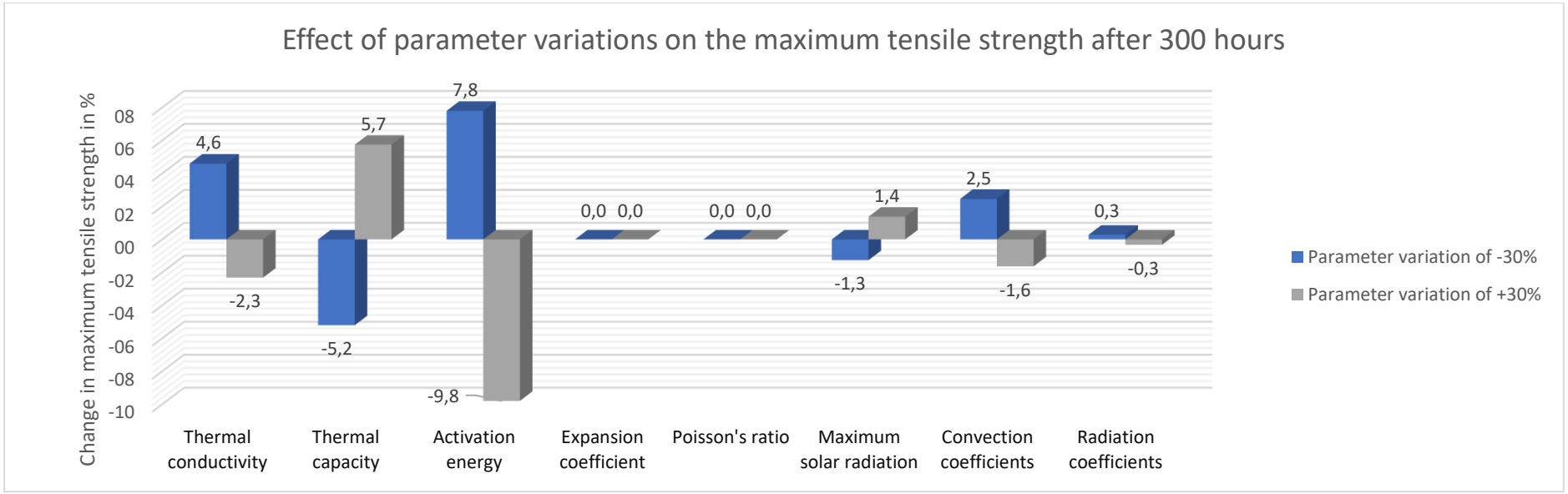

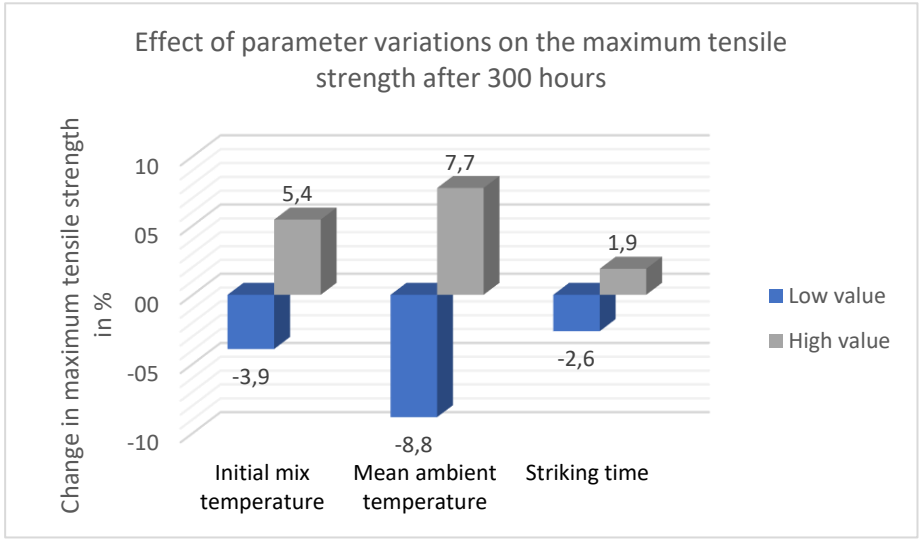

Figure 76 Relative effect of parameter variations on the maximum tensile strength after 300 hours of hardening

Subsequently the changes in maximum tensile stress are considered. This is the stress that is obtained at the end of the analysis after 300 hours. In the bar diagram below the effect of the parameter variations on the maximum tensile stress can be seen. This is again expressed as the relative change with respect to the maximum tensile stress that is obtained using the initial values, in percentages.

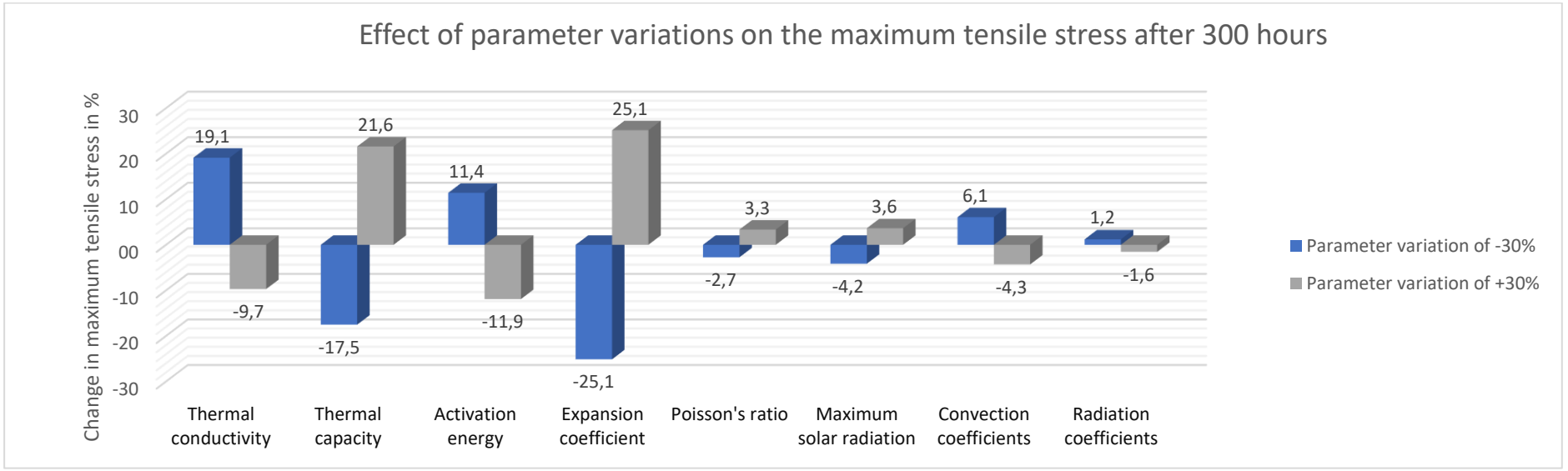

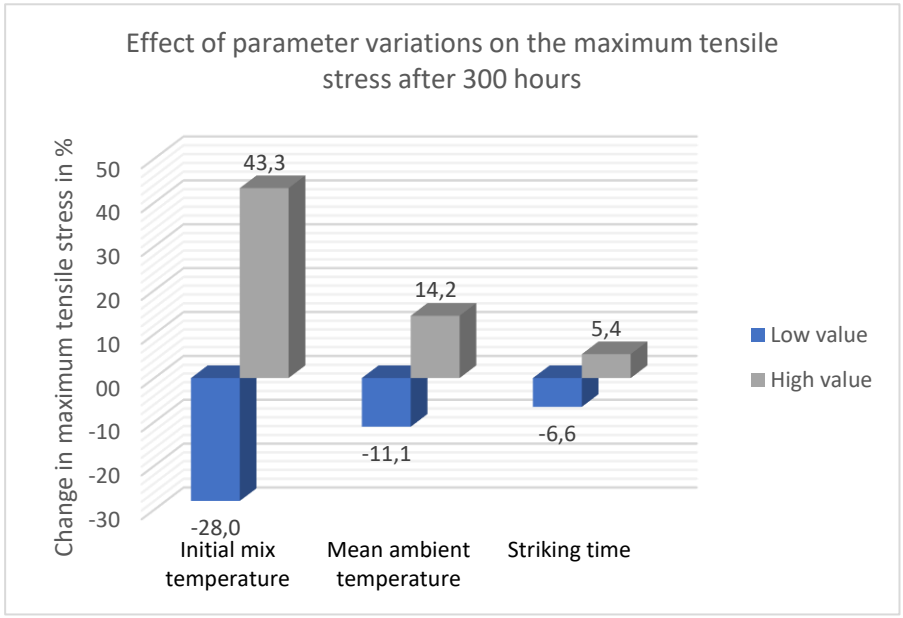

Figure 77 Relative effect of parameter variations on the maximum tensile stress after 300 hours of hardening

The changes in stress and strength cannot be linked directly to changes in safety against cracking when regarded individually. For this reason the ratio between stress and strength at the critical moment in time (150 hours) is calculated for each analysis here. This ratio is then compared with the ratio that is obtained using the initial values. The result is again a percentual change as can be seen here. Positive values (green bars) mean that the ratio between the stress and strength decreases, whereas negative values (red bars) mean an increase in the ratio between stress and strength which increases the risk of early-age cracking.

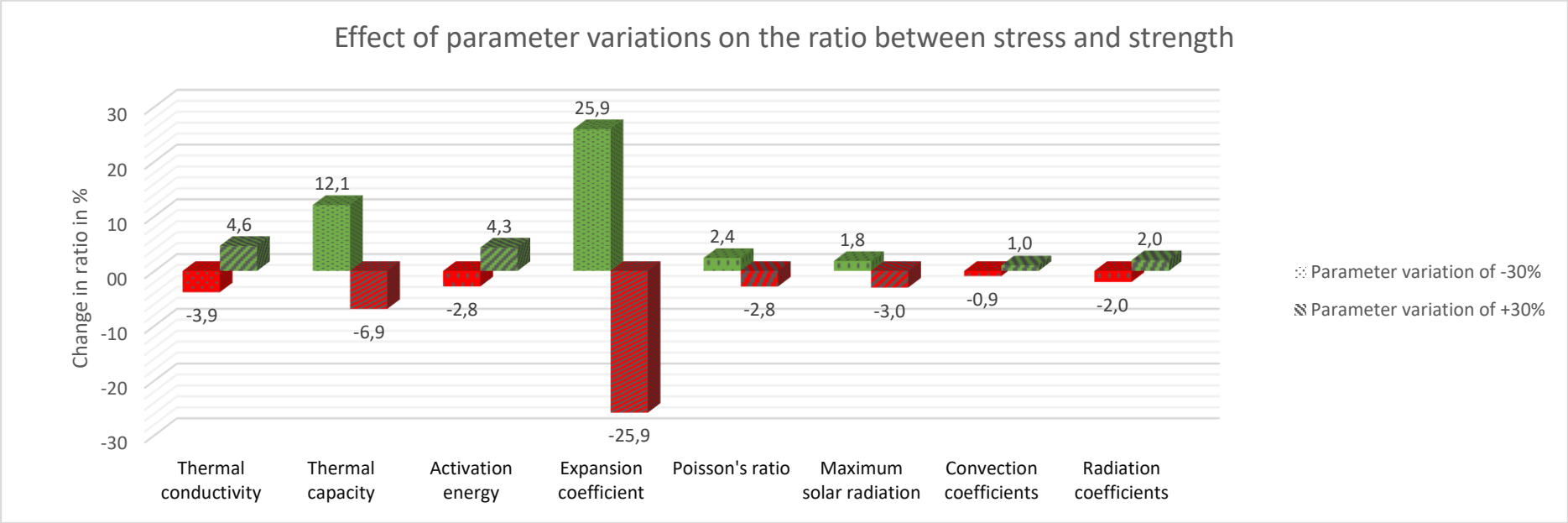

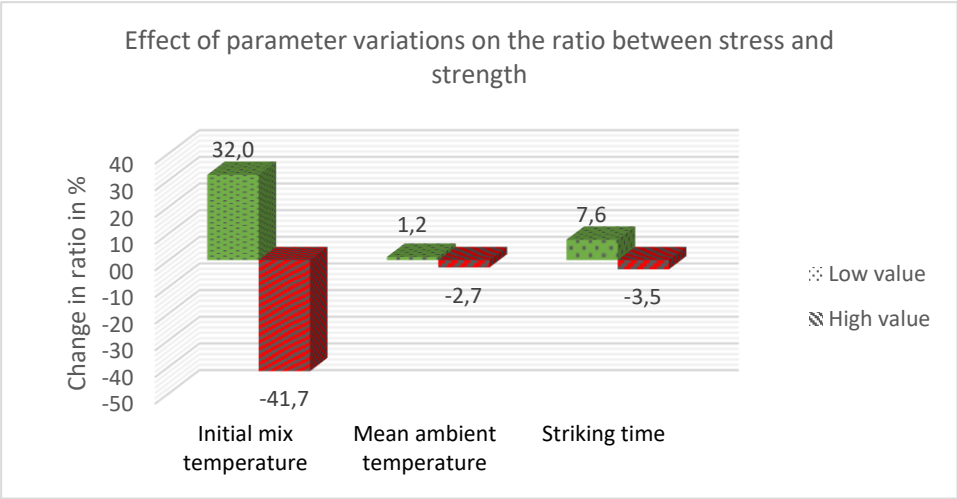

Figure 78 Effect of parameter variations on the ratio between stress and strength for a critical point in time during hardening

- The results for the autogenous shrinkage can be seen in the figures below. In the first figure the stress vs the strength development over time can be seen for variations of autogenous shrinkage calculation methods.

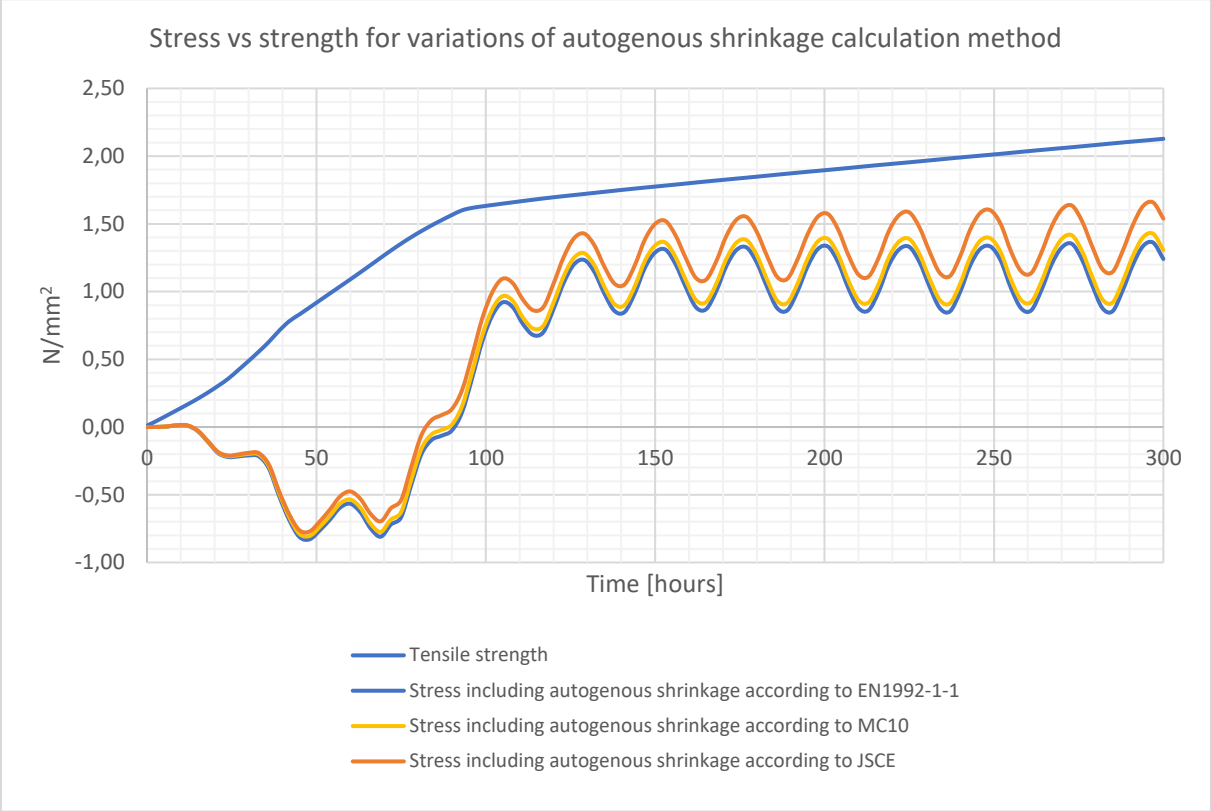

figure 79 Effect of variations in autogenous shrinkage on the stress development over time

In the bar diagram below the influence of using different calculation methods on the ratio between stress and strength can be seen. This is expressed as the relative change in ratio between stress and strength with respect to the ratio for EN1992-1-1. For both variations holds that the ratio increases which means a decrease in safety against cracking

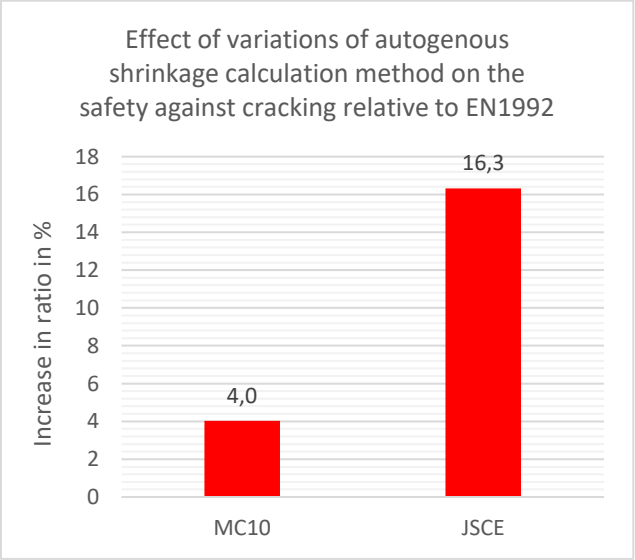

figure 80 Relative increase in ratio between stress and strength for using different autogenous shrinkage calculation methods

4.5 Conclusions

The goal of this parameters study was to gain more insight in the effects of variations of uncertain input parameters on the results of the finite element analysis. This was done by first defining initial parameter values and their possible variations and then running the analysis for each parameter value. The following conclusions can be drawn from the results:

- The *coefficient of thermal expansion* has a large influence on the ratio between stress and strength. Increasing this coefficient results in an equal relative increase of the stresses suggesting an almost linear relation between the two. The temperature- and maturity development over time is not influenced by this parameter which means that also the ratio between stress and strength increases linearly with increasing coefficient of thermal expansion.
- The *thermal capacity* also has a relatively large influence on the ratio between stress and strength. Increasing the thermal capacity increases the maximum temperature and subsequent temperature drop, this increases the tensile stresses which causes an increase in the ratio between stress and strength.
- The *mean ambient temperature* has a very limited impact on the ratio between stress and strength. While variations in mean ambient temperature have a large impact on the maximum temperature during hardening, the temperature drop, which is most important for the development of tensile stresses, remains somewhat constant. Also, an increase in maximum temperature also increases the maturity and thus the tensile strength of the material.
- The *initial mix temperature* however does have a large impact on the ratio between stress and strength. Because in contrast to the mean ambient temperature, changes in initial mix temperature do lead to significant changes in temperature drop during cooling, which increases the tensile stresses in this phase.
- Reducing the *striking time* has a positive influence on the ratio between stress and strength. This is caused by an increase of heat convection to the surroundings reducing the maximum temperature during hardening and thus the subsequent temperature drop. This result is counterintuitive as in practice it is often chosen to increase the striking time to reduce the temperature differentials over the cross-section and thus the risk of early-age cracking. The parameter study however does not show this expected result.
- For the *autogenous shrinkage* holds that a significant increase in tensile stresses is obtained when using the calculation method according to MC10 and JSCE. It is therefore concluded that to be able to accurately model the autogenous shrinkage, measurements are needed. This will be done through laboratory testing and will be discussed in more detail later.
- For the remaining parameters that were investigated in this study it is concluded that realistic variations of these parameters have limited effect on the ratio between stress and strength and thus the risk of early-age cracking.

5 Analysis of creep measurements

Next to the parameters that have been treated in the parameter study, the early-age viscoelastic behaviour (creep) of the material can also only be quantified with a relatively high uncertainty. To able to define this behaviour, early-age creep measurements from literature have to be analysed. This is done using the 'NU Database of laboratory creep data' as main source (Bažant et al., 2014). In this database a large amount of creep test data is assembled based on laboratory tests from the past. The following conclusions are drawn based on the analysis of available creep data:

- Many laboratory creep tests are performed on hardened concrete, for the purposes of this research only creep tests that are performed on young concrete are of relevance. This strongly reduces the amount of usable data
- The binder type of the concrete that is used in the case study is CEM III/B 42,5N which contains blast furnace slag (BFS) cement. Because BFS is mainly used in the Netherlands, the amount of available creep data based on laboratory testing of young concrete containing BFS cement is relatively small.
- Because the viscoelastic behaviour of the material is one of the main unknowns in this research, the question is raised whether it is required to only use creep data based on measurements of young concrete containing CEM III/B cement. As there is little to no data available which meet these requirements, it is decided to no longer exclude creep data for concrete containing OPC cement.

Next to the suitability of the available creep data, it has to be determined what a realistic range of creep values is that should be used in the analysis of early-age cracking in this research. Here the following is concluded:

- Initially, three files containing Maxwell chain data to represent the viscoelastic behaviour of the material were provided, namely 'Maxwell low, Maxwell high and Maxwell average'. As was concluded from available analyses on early-age cracking using MLS Heat in the past, 'Maxwell average' was generally used to account for the viscoelastic behaviour of the material.
- However, when analysing creep data it was found that the 'Maxwell low- and high creep data' lie within a limited range. In literature a larger range of creep values is found. This implies that for this research, a larger range of creep values should be taken into account.
- This is done by selecting two sets of creep data from the NU database, one representing the possible 'low creep' behaviour of the material, and one representing the possible 'high creep' behaviour of the material. For both data sets holds that the ages at loading are 1 day, 3 days, 7 days and 28 days which means that the tests are performed on young concrete.

The 'high creep' data set is based on basic creep measurements as performed by Lee (2006) on concrete containing OPC with a 28 day mean compressive strength of $f_{cm} = 35\ MPa$. The 'low creep' data set is based on basic creep measurements as performed by Le Roy (1996) on concrete containing OPC with a 28 day mean compressive strength of $f_{cm} = 93\ MPa$.

The selected creep data sets can be seen in figure 81 and figure 82 where the creep compliance is plotted against the time in days on a logscale. The creep compliance $J\ [1/MPa]$ is defined as the total load strain per unit of stress and is the sum of the elastic strain and the specific creep (Page et al., 2007).

High creep:

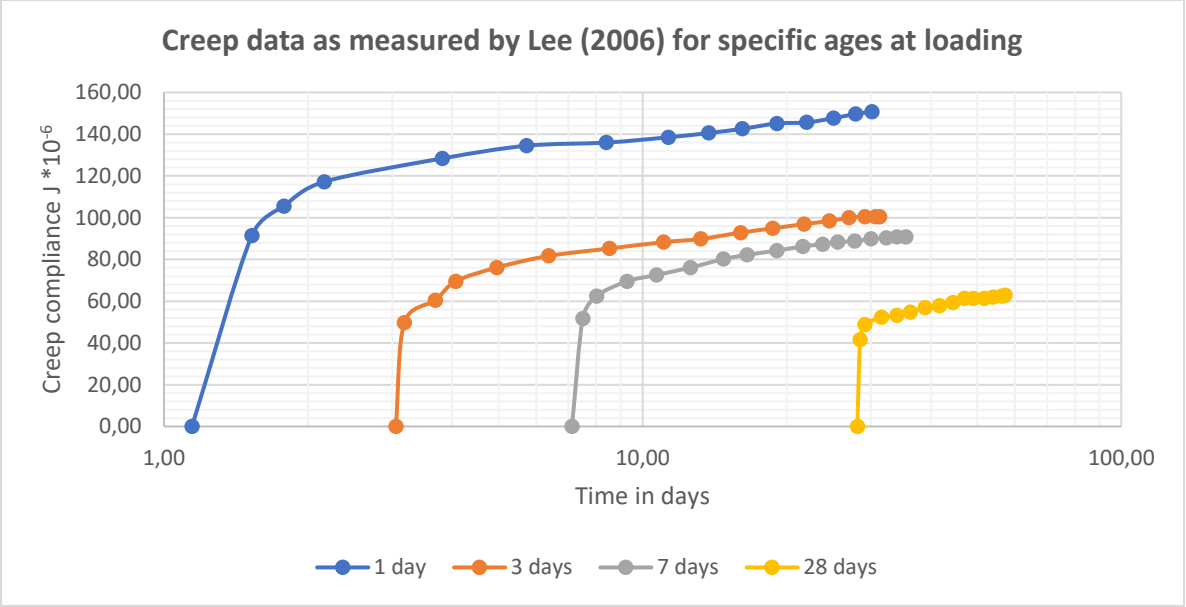

figure 81 Creep data according to the defined 'high creep' data set for young concrete

Low creep:

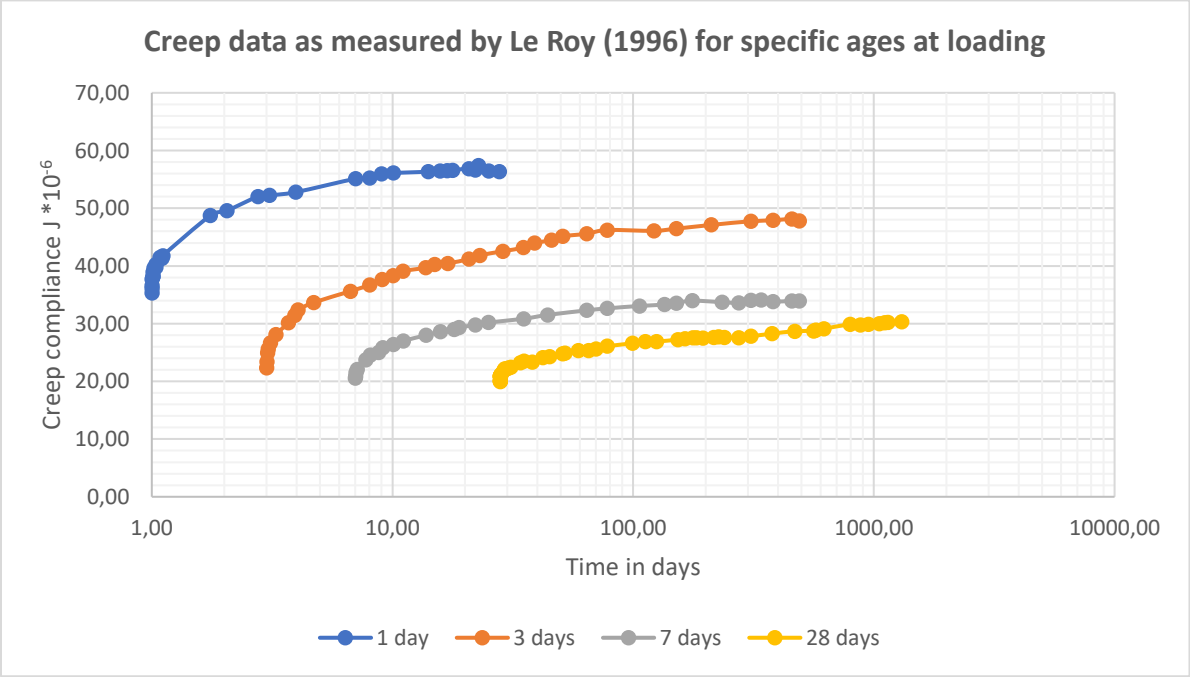

figure 82 Creep data according to the defined 'low creep' data set for young concrete

6 Evaluation of the Maxwell chain model

As stated before, from the analysis of creep measurements in literature it can be concluded that a relatively wide spread is measured. Two sets of creep measurements performed on young concrete have been selected and will be used in the analysis of this research. To be able to do so, the selected creep curves have to be fitted using the Maxwell chain model. MLS Heat requires creep data input in the form of a table containing Maxwell chain data where distribution coefficients are assigned to the different retardation times for several maturities at loading. To be able to do this, a derivation of the Maxwell chain model is needed. This is discussed in more detail in the literature study and will here be mentioned again briefly.

6.1 Model

As discussed in the literature study, the Maxwell chain model consist of units of springs and dampers connected in series. To describe the viscoelastic behaviour of the material, several Maxwell units in parallel are needed. In general it is stated that 4 to 5 units are needed to accurately describe the material behaviour (Reinhardt, 1985). In figure 83 a mechanical scheme of k units in parallel can be seen. Each unit has its own Young's modulus and retardation time, where the Young's modulus depends on the maturity of the material that is being regarded and the distribution coefficients for the different units. As one can imagine, the viscoelastic behaviour of the material changes as the maturity increases. This is simulated by distributing the Young's modulus of the material over the different units. This distribution is different for each maturity and depends on the properties of the material that is regarded. The retardation time of a specific unit is generally set as 10^{k-1} where k is the number of the unit that is regarded.

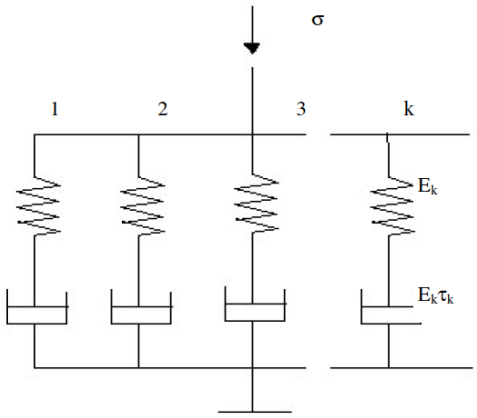

figure 83 General representation of the Maxwell chain model where different units are connected in parallel

To solve a system of k Maxwell units in parallel one has to solve a system of first order ordinary differential equations. The initial conditions can be retrieved from the static system at $t = 0$ by making use of the properties of a parallel system. The system can subsequently be solved by making use of the Laplace method. The Laplace method reduces the system of ODE's to a system of algebraic equations which can be solved using either substitution or linear algebra. In appendix B a system of two Maxwell units is solved by hand. In the end also the derivation of a system of 5 Maxwell units is performed including the initial conditions needed to solve the system.

6.2 Maple sheet and validation

The system of ODE's corresponding to a parallel system of 5 Maxwell units is solved using Maple. This is done using the Laplace method. Also, because the aim is to fit creep data from literature, the Young's modulus and distribution coefficients should remain unknown when solving the system. As a consequence the solution should be found partially symbolic. Details on the Maple sheet can be found in appendix C.

The Maple sheet that is compiled based on the derivations of the Maxwell chain model should be validated before it can be used to fit creep curves from literature. This is done by comparing the creep curves as can be evaluated in the Maple sheet with the creep curves in MLS Heat for the same creep data.

MLS Heat requires creep data input in the form of a table where distribution coefficients are assigned to the retardation times. This is done for a set of maturities where the coefficients change as the maturity increases. MLS heat then produces creep curves for each maturity. Using the same coefficients as input for the Maple sheet should result in creep curves that corresponds with the curves obtained with MLS Heat. The curves are compared by calculating the error at $t = 672\ h$.

This is done for some random maturities from the 'Maxwell average' file which has been used in many analyses in the past. In the table below the Maxwell chain data of this file can be seen. The results of the validation can be seen in appendix D. In the end it was found that the accuracy is sufficient for the purposes of application of this research.

Maxwell Chain Data Retardation times with distribution coefficients

Maturity	E-modulus	1,0	10,0	100,0	1000,0	10000,0	100000,0
[hours]	[MPa]	[hours]	[hours]	[hours]	[hours]	[hours]	[hours]
0	500	0,0000	0,0000	0,2000	0,8000	0,0000	0,0000
12	16685	0,0000	0,3000	0,2000	0,3000	0,2000	0,0000
24	21943	0,0000	0,2500	0,2500	0,2000	0,3000	0,0000
72	29021	0,0000	0,2000	0,2500	0,1500	0,4000	0,0000
168	33112	0,0000	0,2000	0,1500	0,2000	0,4500	0,0000
336	35628	0,0000	0,2000	0,1000	0,2000	0,5000	0,0000
672	37521	0,0000	0,1500	0,1500	0,1000	0,6000	0,0000
1344	38920	0,0000	0,1500	0,1000	0,1500	0,6000	0,0000
2688	39941	0,0000	0,1000	0,1500	0,0500	0,7000	0,0000

Table 10 Maxwell chain data of 'Maxwell average creep behaviour' as provided by the TU Delft

6.3 Curve fitting

The aim of deriving and solving the system of Maxwell units was to fit the distribution coefficient to selected creep data from literature. This is done by altering the distribution coefficient corresponding to each Maxwell unit and plotting the resulting curve together with the curve from literature in the same graph. Fitting of the creep data has to be done for each creep curve separately. The maturity at loading for a specific creep curve corresponds to a Young's Modulus of the material as can be calculated using the relations for the development of the Young's Modulus according to MC10. When the Young's Modulus is determined, the distribution coefficients are altered until the calculated curve fits to the curve from literature for this maturity at loading. This is done in Maple. Each selected set of creep curves consists of 4 curves, this means that in total 8 curves have to be fitted.

In figure 84 and figure 85 below the result of the curve fitting for two of these curves can be seen. In figure 84 the creep curve as measures by Le Roy (1996) where the age of loading equals 3 days can be seen. The creep data is shown as the unbroken line and the fitted curve is displayed as the dotted line. In figure 85 two similar curves can be seen for creep data as measured by Lee (2006). Next to that the error at $t = 672\ h$ is calculated to indicate the accuracy of the fitted curves.

figure 84 Fitting of the creep curve as measured by Le Roy (1996) where the age at loading equals 3 days

The error at $t = 672\ h$ equals 0.9%.

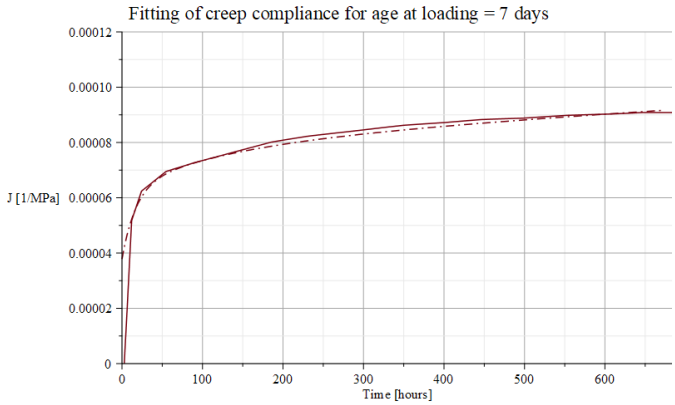

figure 85 Fitting of the creep curve as measured by Lee (2006) where the age at loading equals 7 days

The error at $t = 672\ h$ equals 0.91%.

This is done for all creep curves as selected to represent the 'Low creep' and 'High creep' Maxwell chain data sets. The resulting data can be seen in the figures below.

Maxwell Chain Data		Retardation times with distribution coefficients					
Maturity	E-modulus	1,0	10,0	100,0	1000,0	10000,0	100000,0
[hours]	[MPa]	[hours]	[hours]	[hours]	[hours]	[hours]	[hours]
0	500	0,0000	0,0000	0,2000	0,8000	0,0000	0,0000
24	14138	0,0000	0,2000	0,0000	0,0000	0,8000	0,0000
72	21623	0,0000	0,1600	0,1100	0,0000	0,7300	0,0000
168	26423	0,0000	0,1000	0,0700	0,0000	0,8300	0,0000
672	31952	0,0000	0,0600	0,0300	0,0000	0,9100	0,0000

Table 11 Maxwell chain data for the 'Low creep' file as evaluated through curve fitting

Maxwell Chain Data		Retardation times with distribution coefficients					
Maturity	E-modulus	1,0	10,0	100,0	1000,0	10000,0	100000,0
[hours]	[MPa]	[hours]	[hours]	[hours]	[hours]	[hours]	[hours]
0	500	0,0000	0,0000	0,2000	0,8000	0,0000	0,0000
24	14138	0,0000	0,4000	0,1000	0,0000	0,5000	0,0000
72	21623	0,0000	0,3700	0,1500	0,0000	0,4800	0,0000
168	26423	0,0000	0,4200	0,1000	0,1100	0,3700	0,0000
672	31952	0,0000	0,3600	0,0700	0,1300	0,4400	0,0000

Table 12 Maxwell chain data for the 'High creep' file as evaluated through curve fitting

Next to the high- and low creep data sets, it was decided to manually create a third set, the ‘Average creep’ set. This set represents average viscoelastic material behaviour in relation to the high- and low creep sets. The resulting Maxwell chain data can be seen in the figure below. As said before, the aim of creating these creep data sets is to simulate possible creep behaviour of the material as reviewed in the case study.

Maxwell Chain Data	Retardation times with distribution coefficients						
Maturity	E-modulus	1,0	10,0	100,0	1000,0	10000,0	100000,0
[hours]	[MPa]	[hours]	[hours]	[hours]	[hours]	[hours]	[hours]
0	500	0,0000	0,0000	0,2000	0,8000	0,0000	0,0000
24	14138	0,0000	0,2400	0,0600	0,0000	0,7000	0,0000
72	21623	0,0000	0,3000	0,0000	0,1700	0,5300	0,0000
168	26423	0,0000	0,2000	0,1000	0,1000	0,6000	0,0000
672	31952	0,0000	0,0500	0,1000	0,1500	0,7000	0,0000

Table 13 Maxwell chain data for the 'Average creep' file as evaluated manually

6.4 Implications of viscoelastic analysis

The Maxwell chain model is used to describe viscoelastic material behaviour as is described in the literature study and in this section. The aim of this study is to be able to predict early-age cracking of concrete by using appropriate models and input for the different processes in hardening concrete. Because the material behaviour of the concrete after the moment of cracking lies outside the scope of this study, it is sufficient to perform a viscoelastic analysis without including any damage- or fracture models. This however has certain implications for the results. In reality there will be a redistribution of forces after the moment of cracking. This results in activation of the steel reinforcement and in a drop of stresses in the concrete surrounding the crack. In a viscoelastic analysis cracking behaviour is not modelled so the analysis is no longer valid after the tensile strength of the concrete is exceeded. Also for large deformations the linear analysis is no longer valid as geometrical nonlinearities should then be added to the model. It is important to keep these limitations in mind when analysing the results of the finite element analysis.

7 First evaluation of risk of early-age cracking for selected case

As the required parameter input is now complete, the finite element analysis for determining the risk of early-age cracking can be performed. All input parameters as defined in the sections above are used to evaluate the temperature, stress and strength development over time for governing point in the wall. After analysing the results it can be concluded that there are two governing points regarding early-age cracking:

- One point in the bottom region of the wall (1), around 1.0 m measured from the top of the slab. In this point the tensile stresses reach a maximum during the cooling phase as shrinkage is restrained by the slab.
- One point in the top of the wall (2). In this point the tensile stresses reach a maximum during the heating phase as this part of the wall has a high cooling rate compared to the centre of the wall. The temperature during hardening will therefore remain relatively low here.

Both point 1 and 2 can be seen in figure 86 below. In this figure the temperature distribution of the wall and slab can be seen at the end of the heating phase at $t = 69\ h$.

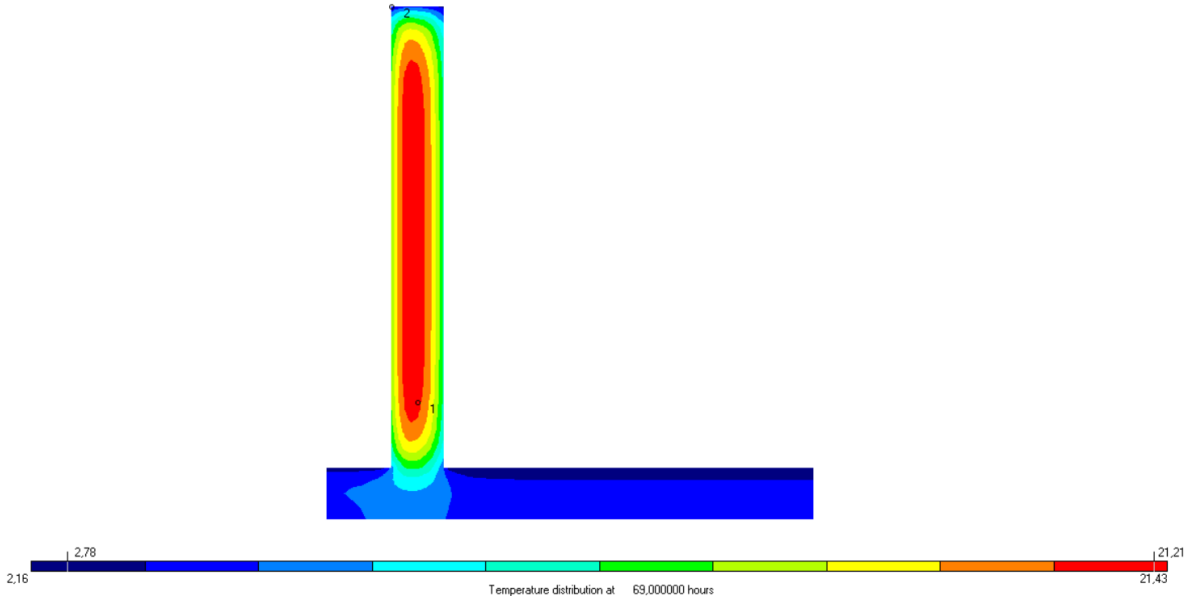

figure 86 Stress distribution in the wall and slab for a moment in time during the cooling phase

First of all the temperature development for the governing point in the bottom of the wall is plotted. This can be seen in figure 87. It can be concluded that the maximum temperature in the wall becomes $20.2°C$. The oscillating behaviour of the curve is caused by fluctuations in temperature and radiation due to the day-night cycle.

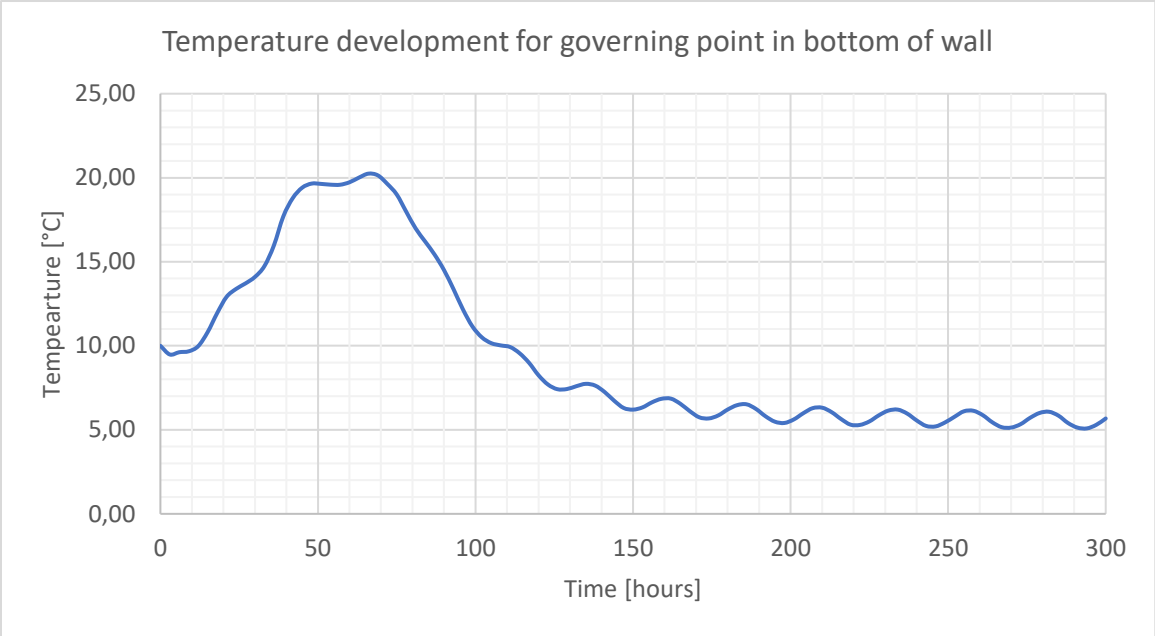

figure 87 Temperature development for a governing point in the bottom of the wall according to the FEA using the initial parameters

Next the stress- and strength development for both governing points are plotted in figure 88 and figure 89. For point 1 the effect of varying the characteristics of the viscoelastic behaviour of the material can be seen. In both figures three strength curves are plotted, f_{ctm}, $0.85f_{ctm}$ and $0.5f_{ctm}$. As is already discussed in the literature study, the probability of cracking for tensile stresses reaching $0.5f_{ctm}$ is 0.02%. This is therefore defined as the limit below which early-age cracking is not likely to occur. The probability of failure for several other specific limits is summarized in the table below.

Stress limit:	**Probability of cracking:**
$0.5f_{ctm}$	0.02 %
$0.7f_{ctm}$	7 %
$0.85f_{ctm}$	50 %

Table 14 Probability of cracking for several stress limits (van Breugel et al., 1996).

It can be concluded that for point 1 in the bottom region of the wall the maximum stress for 'low creep' lies in between $0.85f_{ctm}$ and f_{ctm}, which indicates a high probability of cracking. The stress curve for 'high creep' however lies closer to the $0.5f_{ctm}$ limit, which indicates that for this viscoelastic material behaviour the probability of cracking is significantly lower. However this difference between the different curves only becomes evident for $t > 125\ hours$. The probability of cracking can be determined more accurately when the correct viscoelastic material behaviour has been determined. This will be done by means of laboratory testing and will be discussed later.

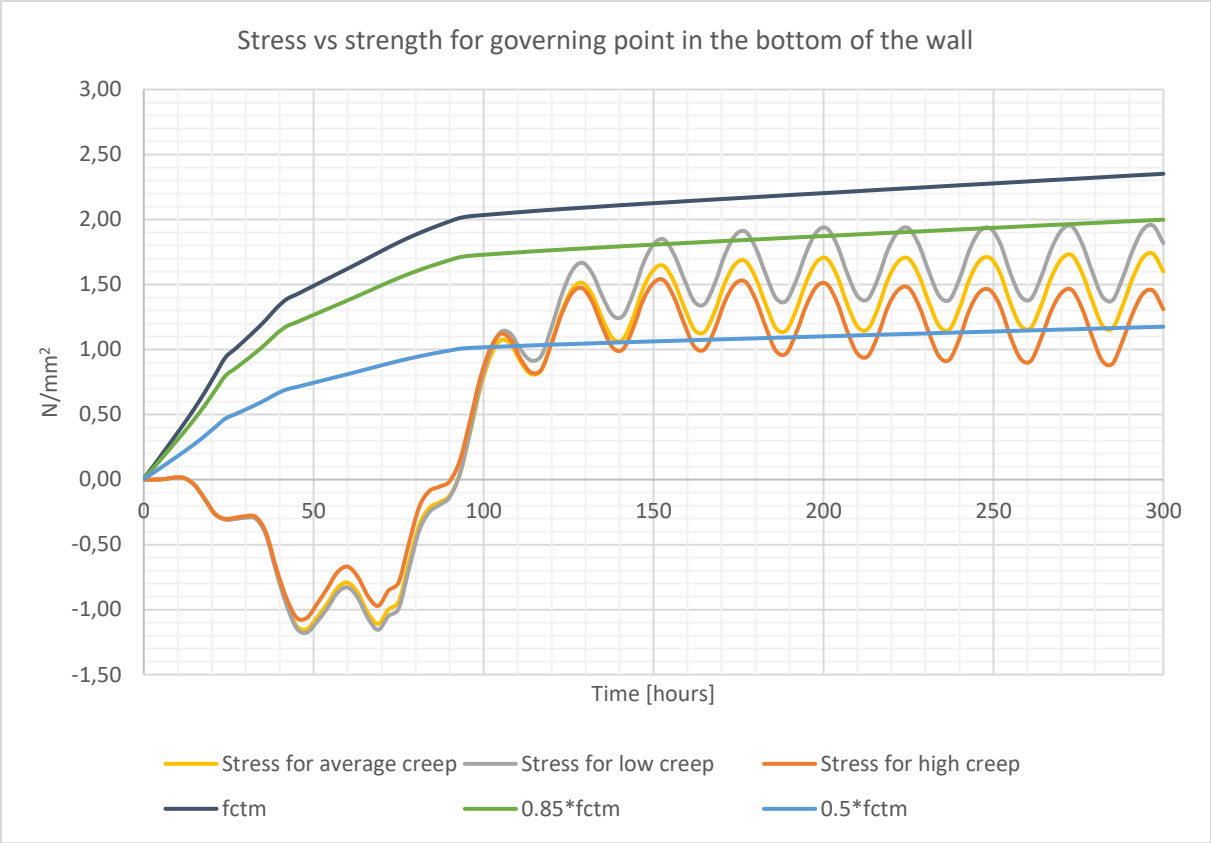

figure 88 Stress vs strength for the governing point in the bottom of the wall for different Maxwell chain data sets

For point 2 in the top of the wall it can be concluded that based on the input as used in this analysis, early-age cracking will definitely occur as the tensile strength f_{ctm} is clearly exceeded for 'stress for average creep'.

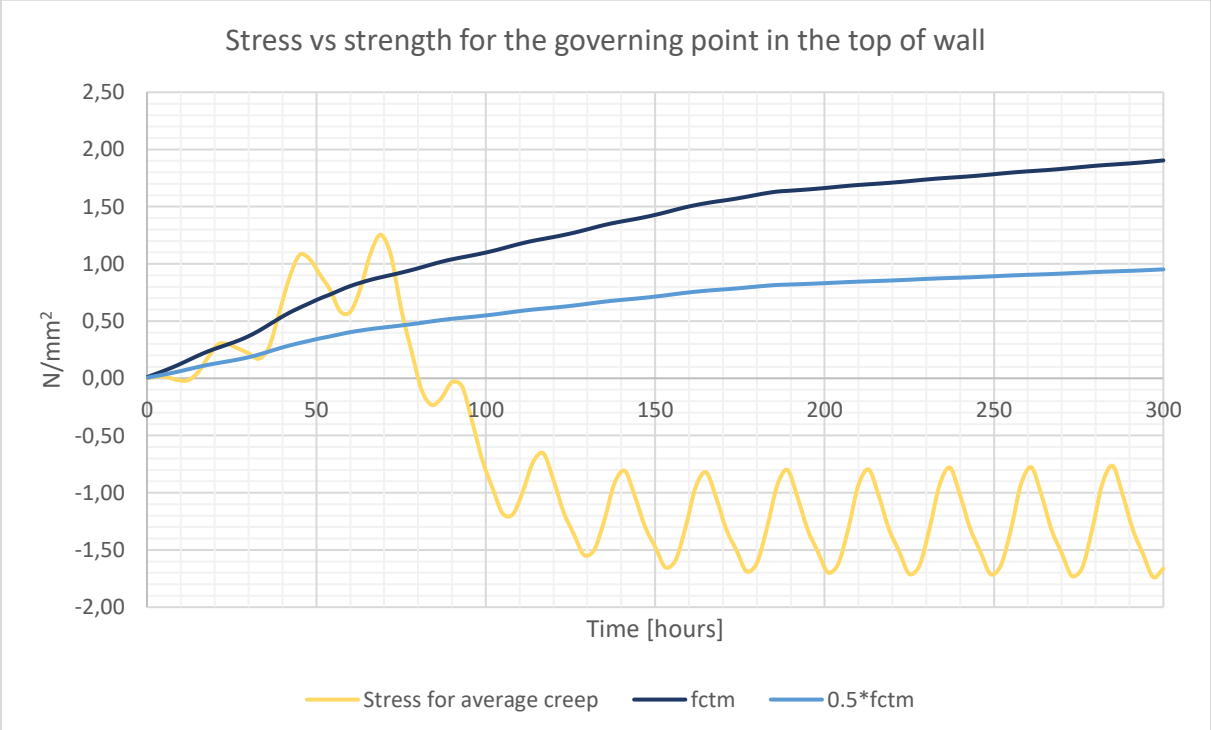

figure 89 Stress vs strength for the governing point in the top of the wall

8 Longitudinal section

As was mentioned before in the section on modelling of the cross-section of the wall and slab of a segment of the dive-under, a longitudinal section will also be modelled based on the results of the cross-sectional modelling. The longitudinal section of the wall of modelled to gain more insight in the stress development over the length of the wall. As is known from literature, the degree of restraint builds up from the edges towards the centre of the wall (in the longitudinal plane) and the stress development over the height is a function of the length/height ratio. It is therefore relevant to consider a longitudinal section of the wall and slab corresponding to a segment of the dive-under as part of this study.

As the modelling of the longitudinal section is based on the results of the FEA of the cross-section, this analyses can only be performed after the FEA of the cross-section is complete.

8.1 Model

The finite element model including dimensions, supports and mesh can be seen in figure 90. The relevant characteristics of the model will here be discussed in more detail.

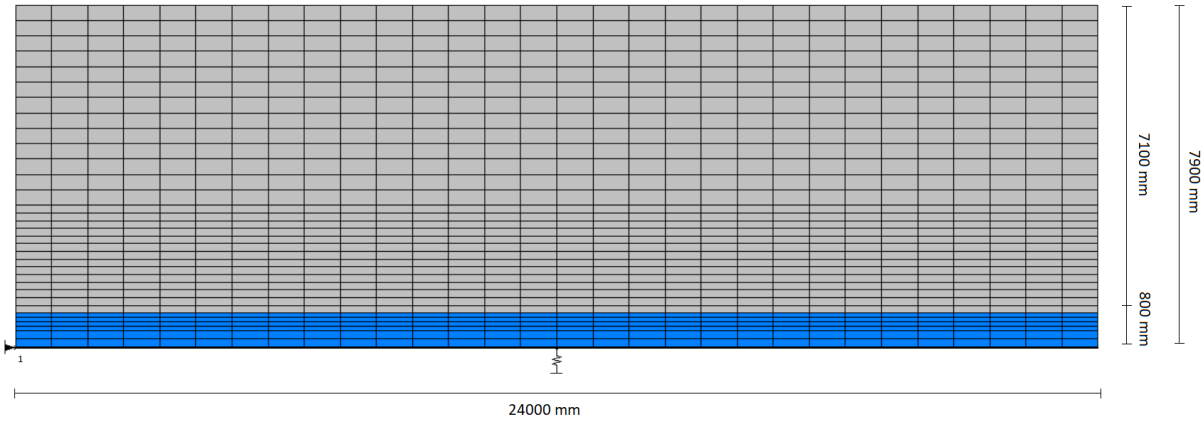

figure 90 FEM of longitudinal section of the wall- and slab of a segment of the dive-under

- All segments of the dive-under have a shallow foundation. Bending of the segments will partly be restrained by the soil and this effect should be included in the model. The foundation is modelled by means of a line support consisting of linear springs as can be seen in the figure. The stiffness of the springs is constant and can be derived from the subgrade modulus of the specific soil.
- The individual segments of the dive-under are not structurally connected and they are therefore able to bend and dilate independently with respect to each other. This is incorporated in the model by using a horizontal support at a single edge of the wall only. In this way free dilations and independent bending of the wall are ensured.
- A situation of plane stress is modelled which means that only stresses that act in the XY plane are regarded. As a consequence the stress component in the outward z-direction S_{zz} is assumed to be equal to zero. This is justified by the fact that the length of the wall is much larger than the dimensions in the outward z-direction.
- The outward dimension of the slab is larger than that of the wall and it will therefore have a higher axial- and bending stiffness compared to the wall. This is incorporated in the model by defining the dimension of the slab in z-direction as the ratio between the dimensions in z-direction of the slab and wall.

- In the end a mesh refinement study was performed which proved that the mesh size as presented here is sufficient

8.2 Input parameters

The material properties of the slab and wall are defined in correspondence with the FEM model of the cross-section of the dive-under segment as described in a previous section. However because the temperature development over the thickness and height of the wall during hardening cannot be evaluated when regarding a longitudinal section using this software, this has to be determined from the FEM of the cross-section. This is discussed here in more detail. Also, the spring stiffness of the shallow foundation should be defined.

- The temperature development during hardening is implemented in the model using prescribed areas as can be seen in figure 91 below. There are three prescribed areas that are used instead of one area for the entire wall to take into account any variations in temperature over the height of the wall. The areas are indicated by the three rectangles covering the wall as can be seen below.

figure 91 Prescribed areas for temperature development

- The temperature function for each prescribed area is derived from the FEM of the cross-section of the wall and slab. For each area, the temperature for each point in time is calculated as the linear average temperature over the thickness of the wall and is calculated from 5 equally distributed points as can be seen in figure 92.a below. The resulting temperature functions can be seen in figure 92.b. It can be concluded that the average temperature difference over the height of the wall is small and that the temperature is the highest for the middle third.

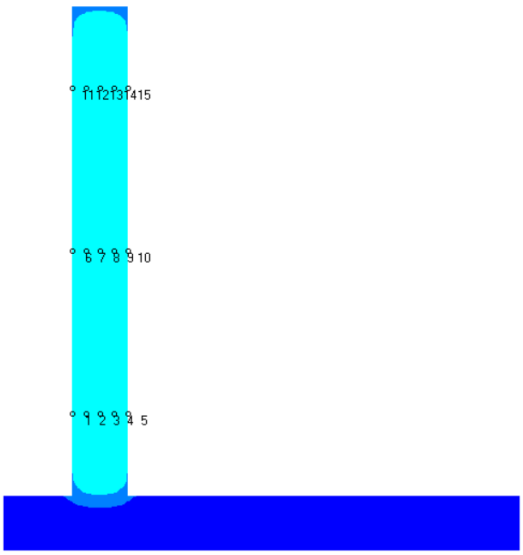

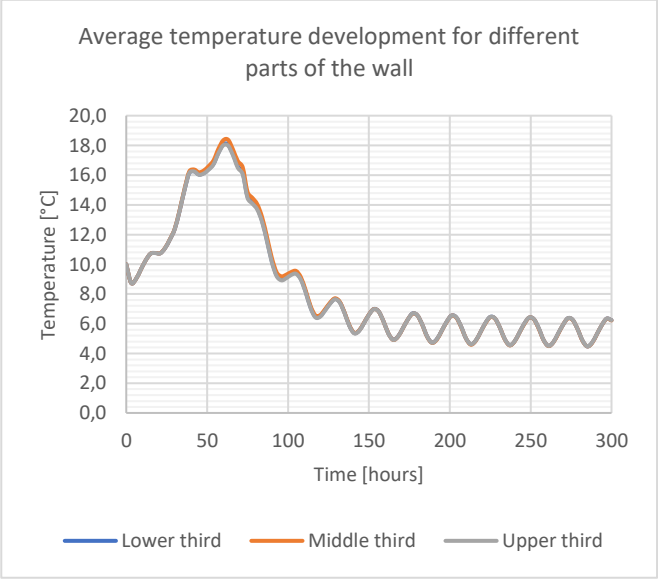

figure 92.a (left), Point in cross-section for calculation of average temperature. figure 92.b (right) Temperature curve for each prescribed area.

- Because the temperature development of the wall is already prescribed, convection and radiation properties do not have to be defined for this case. Also the ambient temperature is not relevant for this analysis.
- The subgrade modulus of the soil is determined based on cone penetration tests (CPT). The soil can be classified as relatively 'loose sand' and the lower bound value of the subgrade modulus is measured to be:

$$c = 7.5\ MN/m^3 = 7.5 * 10^{-3}\ N/mm^3$$

8.3 Runtime specifications

It is decided to use the following runtime specifications for the analysis:

- The computation time equals 200 hours. As can be seen from the evaluated stresses, this time period is sufficient to incorporate the possible moments of each cracking
- The stresses are smoothened over the elements
- The time increment is decided to be 0.33 hours, and the results are stored each 3 hours.
- The element type used are fully integrated quadrilateral elements

8.4 Results

The results of the FEA are presented by means of figures and graphs showing the stress- and strength development over time and the deformations of the wall- and slab. In figure 93 below the tensile stress S_{xx} $[N/mm^2]$ can be seen over the length of the wall for a governing moment in time during cooling. As shrinkage of the wall is being restrained by the slab, tensile stresses develop in the bottom region of the wall. Also, bending of the wall and slab occurs causing compressive stresses in the top of the wall. The tensile stress trajectories in the bottom region of the wall are consistent with figures from literature as the restraint builds up from the edges of the wall towards the centre. The governing point regarding early-age cracking is located at around 500 mm height measured from the top of the slab.

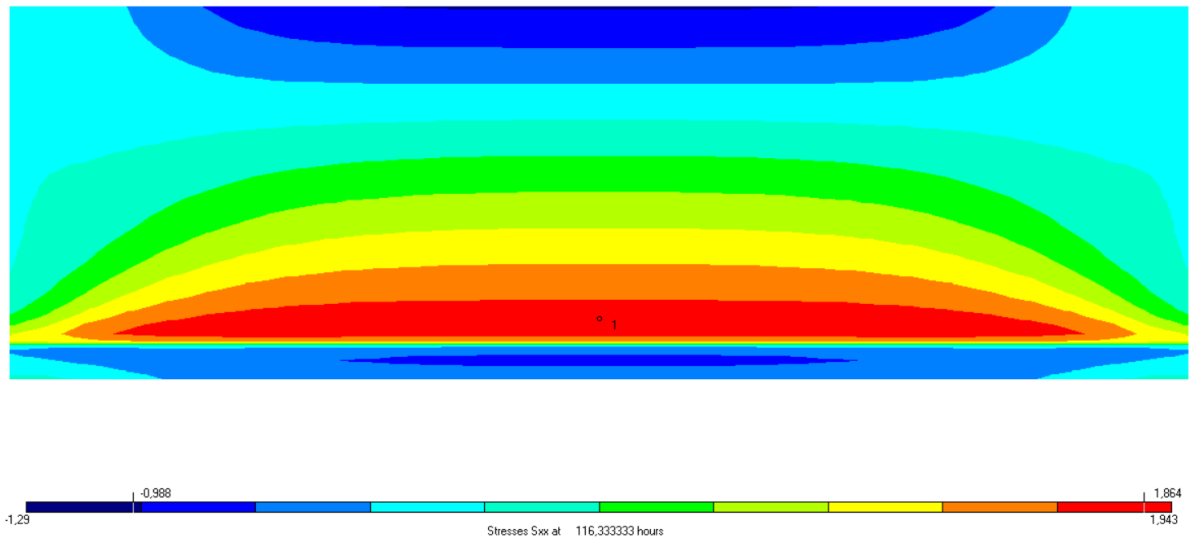

figure 93 Tensile stress trajectories over the length of the wall during cooling

In figure 94 the stress- and strength development for a governing point in the bottom of the wall can be seen. The trend of the stress development is similar to that of the FEA of the cross-section of the wall. The obtained values however have to be interpreted with care as will be discussed later.

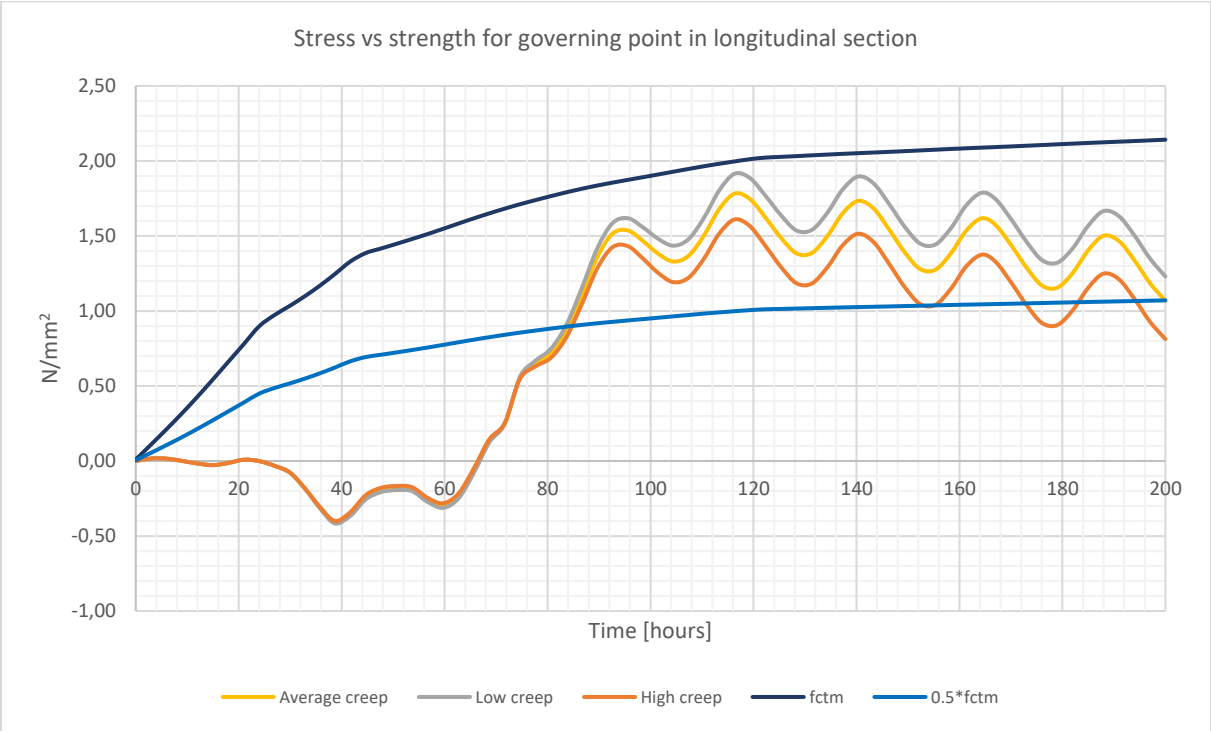

figure 94 Stress and strength development for a governing point in the bottom of the longitudinal section of the wall

The displacements of the wall and slab are visualized by means of the deformed mesh at a certain moment in time during cooling. The values are scaled in order to be able to properly view the deformations. As can be seen from the deformed mesh, restrained shrinkage of the wall results in bending of the wall and slab.

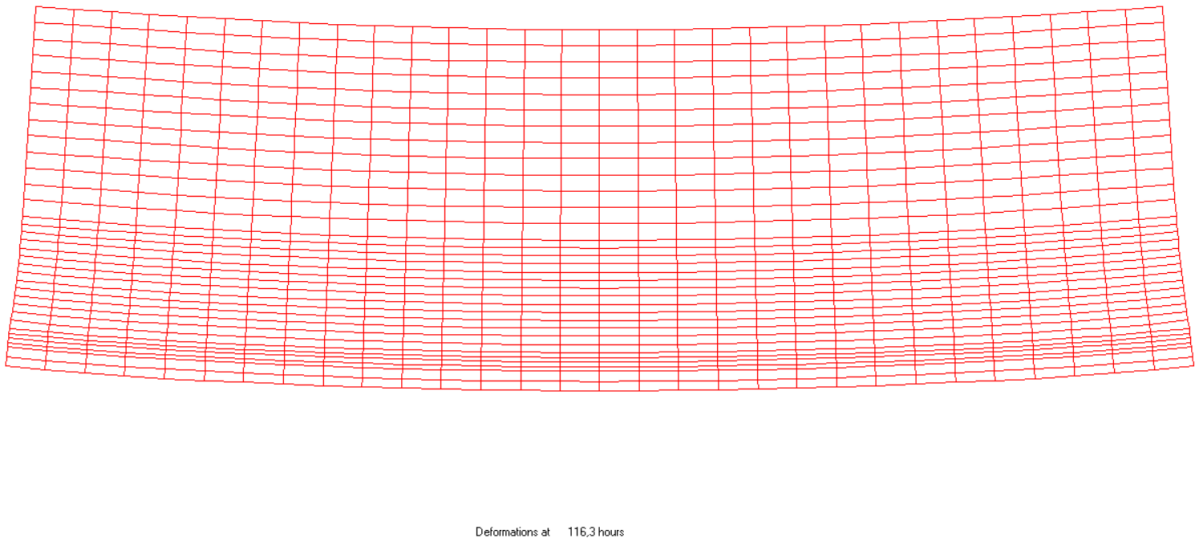

figure 95 Deformed mesh during cooling

The reaction forces of the springs can be seen in figure 96 below for a certain moment in time during cooling. As can be seen from this figure, bending is partly being restrained by the soil as the reaction forces counteract the bending deformations as visualized by means of the deformed mesh. The present model allows for tensile reactions forces to develop while in reality these forces cannot develop. This implies that the applicability of the model is limited and that the results should be interpreted with care. Nevertheless if the self-weight of the structure would have been included in the model these tensile forces would not have occurred.

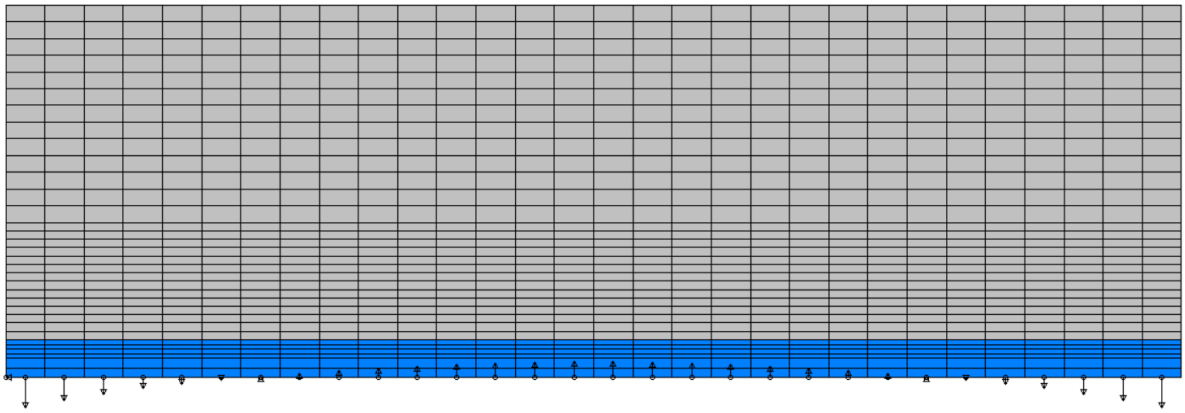

figure 96 Reaction forces for a certain moment in time during cooling

8.5 Discussion

The accuracy and/or applicability of the model and obtained results are discussed here in more detail.

- The temperature functions of the prescribed areas are derived from the average temperatures in the cross-section of the wall. In this way the temperature gradients over the cross-section of the wall are being neglected which reduces the accuracy of the model. In reality the temperature gradients may cause additional stresses in the wall. The obtained stress values as presented in the figures above should therefore be interpreted with care.

- It can be concluded that the prescribed temperature function is relatively accurate for the middle third of the wall (over the height). However at the top and the bottom of the wall, the temperature deviates from the prescribed temperature function because in these regions additional heat is lost to the environment (at the top) and to the slab (at the bottom) as can be seen in figure 93.a. These effects are disregarded when using the average temperature functions for the wall.

- In the current analysis, temperature variations of the slab due to variations in ambient temperature are not taken into account. In reality the temperature development of the slab is influenced by the ambient temperature. Taking this effect into account will reduce the temperature difference between the slab and wall and could therefore reduce the stresses in the wall.

- The length/height ratio for the wall is equals to $24/7.1 = 3.4$. According to van Breugel et al. (1996) the restraint at the top of the wall will for this ratio be close to 0.1. This implies that during cooling tensile stresses will develop at the top. However because in this case the slab is

relatively thin (800 mm) and therefore has a relatively low stiffness, bending of the slab will reduce the tensile stresses at the top of the wall and will even cause compressive stresses to occur in this region. This effect can also be observed in figure 93. A higher stiffness of the slab would lead to a reduction in bending and to an increase in tensile stresses in the wall. Besides, bending of the wall and slab is partly be restrained by the soil. However because in this case the subgrade modulus c $[N/mm^3]$ is relatively low, this effect is limited.

- The shallow foundation is modelled by means of linear springs. This means that in this model both compressive- and tensile reaction forces can develop. In reality however the foundation can only exert compressive forces on the structure. This makes that the applicability of the model is somewhat limited. It should be noted that in practice tensile reaction forces will never occur because of the self-weight of the structure which counteracts these forces. This is however not included in the present model. Besides, because the subgrade modulus of the soil is relatively low, the restraining effect on the bending deformations of the wall and slab will be limited. This implies that any inaccuracies in modelling of the shallow foundation will also have a limited effect on both the deformations and the stresses in the wall.

- When considering the stress development as presented in figure 94, it can be concluded that for this FEA the maximum tensile stress is reached after 116 hours. This deviates from the FEA of the cross-section where the maximum tensile stress is reached after around 150 hours. This could be due to the fact that temperature gradients over the cross-section during cooling cause the tensile stress to develop for a larger time period compared to this analysis where this effect is neglected.

- Stress relaxation seems to have a larger effect on the tensile stresses for this analysis compared to the analysis of the cross-section. This can be concluded from the fact that the decrease in tensile stress over time at later ages is larger for the analysis of the longitudinal section compared to the cross-sectional analysis.

9 Laboratory testing

Laboratory tests are performed at the Stevin laboratory of the TU Delft as part of this research. The different tests will be described in more detail in this section. First of all the aim of the experiments will be discussed followed by a description of the different testing methods and set-ups. The results of all tests will be analysed and statements will be made on the accuracy and applicability of the results regarding the assessment of the risk of early-age cracking of the walls of the case study. In the end the overall testing procedure will be evaluated.

9.1 Aim of the experiments

The aim of the experiments is on the one hand to simulate the imposed deformations- and stress development in the walls of the dive-under of the case study and on the other hand to determine several material properties that can subsequently be used to increase the accuracy of the finite element analysis regarding the assessment of the risk of early-age cracking. This will be done for a specific concrete mixture that will be used for casting of the concrete walls of the dive-under in practice.

The results of the experiments will also be compared with the results of the finite element analysis to subsequently be able to make statements on the accuracy of the finite element analysis and the accuracy of the input parameters of this analysis.

9.2 Methods

There are several testing methods that will be used. The tests are performed in parallel and with the supervision of the staff of the Stevin laboratory. The different testing methods are discussed in more detail in appendix F. Here a short description of the different tests can be found.

9.2.1 TSTM

The Temperature Stress Testing Machine (TSTM) is used to perform a deformation controlled experiment on a hardening concrete specimen in a temperature controlled mould. An overview of the test set-up can be seen in figure 97 below. The aim of this test is to simulate the hardening process of the concrete walls of the dive-under. This is done by restraining the deformations of the concrete specimen during hardening and regulating the temperature of the specimen to fit the temperature development over time of a governing point in the centre of the bottom of the wall as is modelled in a previous section. The output of this test is stress curve which can be used to compare with the output of the finite element models. More details on the testing procedure can be found in appendix F.

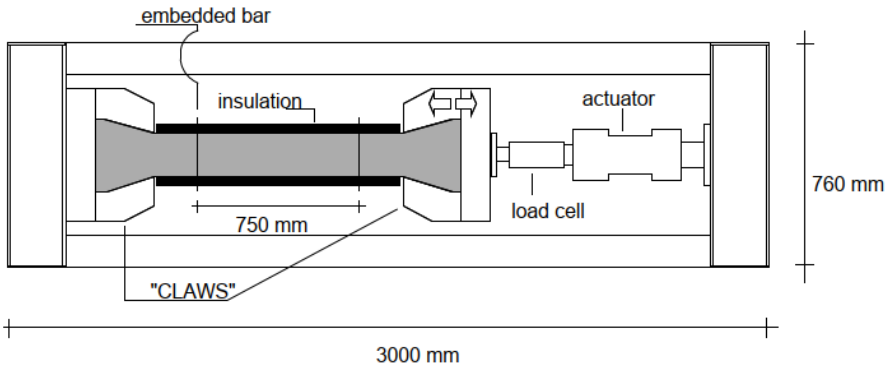

figure 97 Overview of the TSTM testing set-up (Lokhorst, 2001).

9.2.2 ADTM

Parallel to the TSTM test a Autogenous Deformation Testing Machine (ADTM) test is performed. The aim of performing this test is to measure the autogenous deformations for the specific concrete mixture as will also be used in the construction of the dive-under. Because the development of the autogenous deformation is one of the main unknowns in the finite element analyses, the results of this test will be used to increase the accuracy of the FEA regarding the assessment of the risk of early-age cracking. A more detailed description of the test set-up can be found in appendix F.

9.2.3 Cube tests

In the end also standard cube tests will be performed. There are two parameters that will be determined, namely the cube compressive strength and the tensile splitting strength. The cubes will be tested at several predefined ages to be able to determine the development of the material parameters over time. More details on the cube tests can be found in appendix F.

9.3 Mixture specifications

As is stated before, the laboratory tests are performed using the concrete mixture that will also be used in the construction of the dive-under. This concrete mixture is provided by Mebin B.V.. Details on the mixture are however confidential and can therefore not be published here. Nevertheless the general properties of the mixture can be seen in the table below.

Property:	**Value/remarks:**
Cement manufacturer	ENCI B.V.
Concrete manufacturer	Mebin B.V.
Concrete strength class	C30/37
Slump class	S3
Binder type	CEM III/B 42,5 N
w/c ratio	0.45
Binder content	350 kg/m^3
Fillers	-
Admixtures	Cugla PCE plasticizer, 3rd generation admixtures
Aggregate type	River gravel / sand
Grading	Gravel 4-16mm
	Sand 0-4mm
Minimum content ‘fine material’	>125 kg/m^3

Table 15 Details on the concrete mixture of the walls of the dive-under

9.4 Results

In this section the results of the different laboratory tests can be seen. The results will be compared to the input parameters as derived from literature and the results of the finite element analyses of the cross-section of the wall of the dive-under. The results are displayed here in the form of graphs. More details on test data can be found in appendix H.

9.4.1 TSTM

The TSTM test is carried out in a displacement controlled manner where the displacements are kept constant. This means that the measured force is the most relevant output parameter of the test. Also, it is relevant to analyse the measured temperature development in the test specimen and compare with the prescribed temperature function.

The temperature development that is measured during the test can be seen in figure 98 below. In this figure also the prescribed temperature function can be seen. The temperature of the specimen is controlled based on the measured temperature in the middle of the prismatic part of the concrete. This implies that the temperature curve of the measurement in the middle of the specimen should match the prescribed temperature curve. As can be seen from the figure, the two curves coincide up until $t = 140\ hours$. The reason why the curves do no longer coincide from this moment on is that the prescribed temperatures become too low for the cryostat device to be able to cool the specimen to the same temperature. This results in the fact that from this moment on the temperature of the specimen is kept constant at 7℃ and does no longer follow the prescribed temperature curve. This should be kept in mind when analysing the force output of the TSTM test and comparing to the output of the FEA.

Also, as can be seen from the curve corresponding to the average concrete temperature of the prismatic part of the specimen based on the three measurement locations, the average temperature is slightly higher compared to the individual temperature in the middle of the specimen.

In the end it must be noted that the initial temperature of the concrete is higher compared to the assumed initial mix temperature as taken into account in the prescribed temperature function. This difference is however no longer present from $t = 2\ hours$.

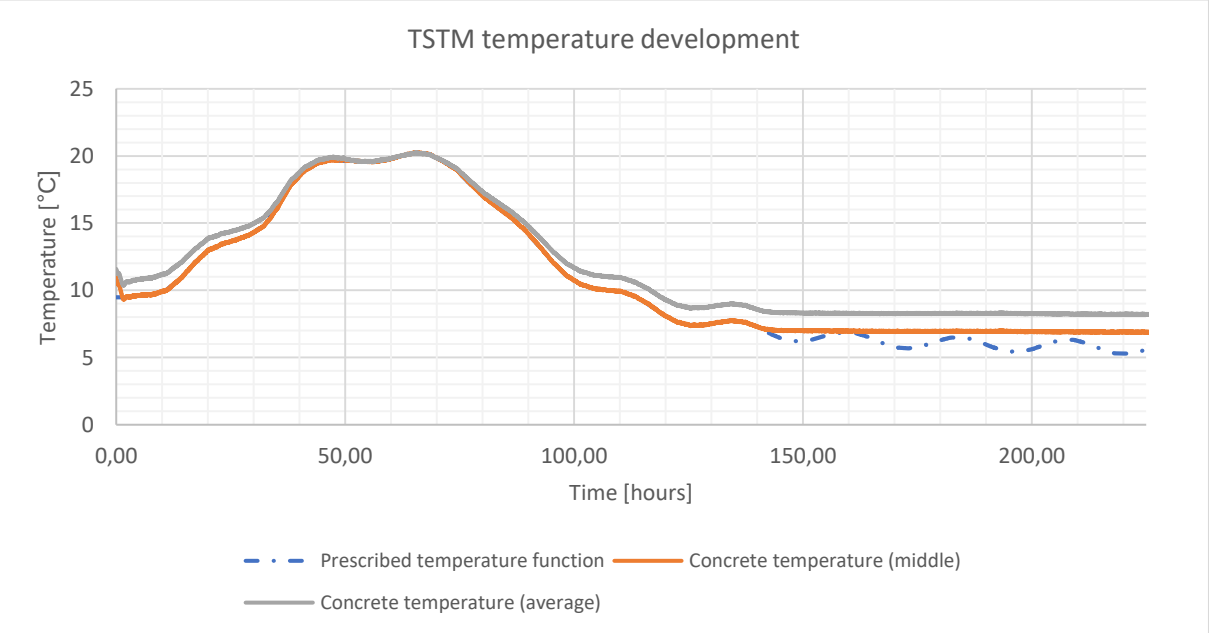

figure 98 Comparison between the measured temperature during the TSTM test and the prescribed temperature function

The force that is needed to perform a displacement controlled TSTM test where the dilatations of the prismatic part of the specimen are kept constant is continuously measured. The stress in the concrete can subsequently be calculated from the dimensions of the specimen. As the TSTM test is performed as a simulation of the hardening process of the governing point in the bottom region of a wall of the dive-under, the obtained stresses are compared with the stress output of the FEA of the wall. This can be seen in figure 99 below. The comparison between the results of the TSTM test and the FEA wall cannot be justified completely because the input- and boundary conditions of both tests are different. The TSTM test will be compared to an actual model of this test later in this study.

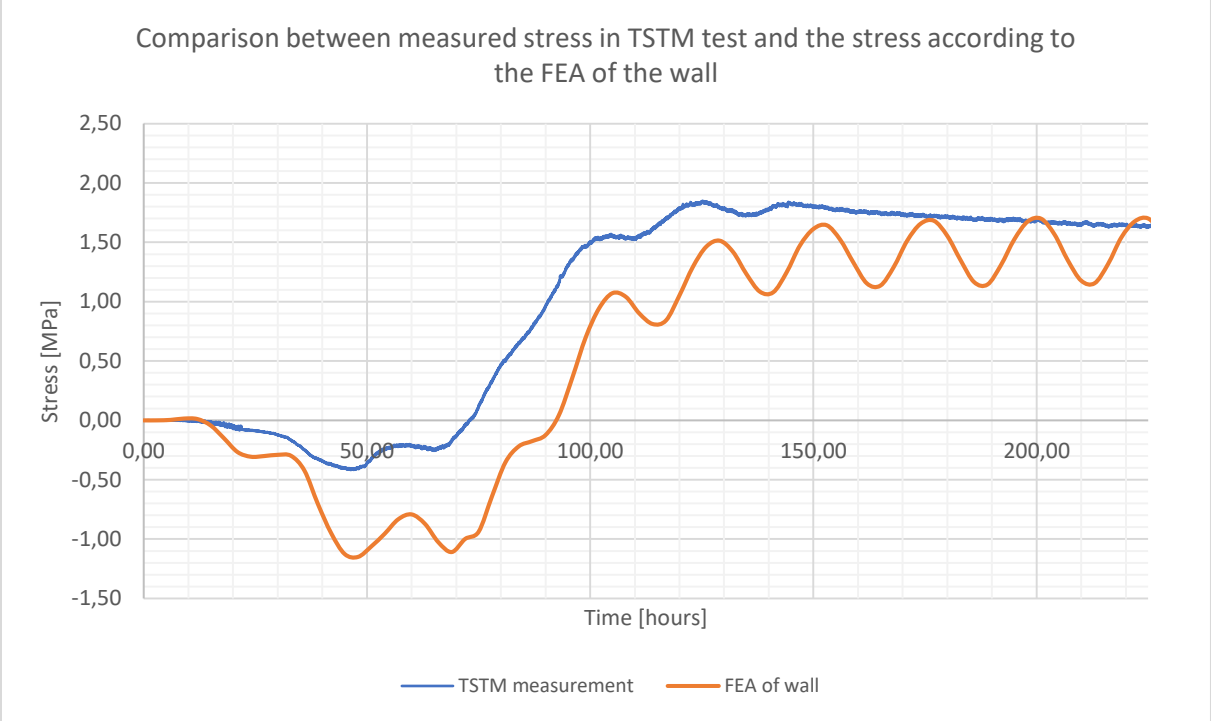

figure 99 Comparison between the measured stress in the TSTM test and the stress according to the initial FEA of the wall

There are several statements that can be made based on the comparison of the two stress curves. First of all, the compressive stresses that develop during the heating phase are much larger for the FEA than for the TSTM measurement. Second, the tensile stresses during the cooling phase are lower for the FEA than for the TSTM measurements. However the change in stress from compression to tension is similar, but the curves seem shifted relative to each other.

The stress curve of the FEA of the wall oscillates as a result of the temperature day-night cycle. This oscillation can also be seen in the stress curve of the TSTM test but has a smaller amplitude. This difference in amplitude is caused by the fact that the prescribed temperature function of the TSTM test is based on the temperature in the centre of the wall only. This means that temperature variations at the edges of the wall are not taken into account in this test. The temperature variations at the edges of the wall however cause additional temperature gradients over the thickness of the wall which results in an increase of the amplitude of the stress oscillations for the centre of the wall. These additional temperature gradients are included in the FEA of the wall but are not taken into account in the TSTM test which results in a smaller amplitude of the stress oscillations during this test.

Also, because the prescribed temperature curve is no longer followed for $t > 140\ hours$ and from that point in time the temperature of the TSTM specimen is kept constant, the stress oscillations of

the TSTM test are no longer present for $t > 140\ hours$. This can also be seen from the stress curve in the figure above.

As can be seen from the stress curve for $t > 140\ hours$, the effect of stress relaxation seems to be larger in the TSTM test compared to the FEA of the wall. This is concluded from the fact that the stresses of the TSTM are reduced over time, while for the FEA of the wall the average stress does not decrease significantly. This implies that the viscoelastic material behaviour that was assumed in the FEA is not correct. This will be discussed in more detail in the section on modelling of the TSTM test.

It is observed that the concrete did not crack during the TSTM test. Also, because the stresses were being reduced over time due to relaxation effects it is not likely that the concrete would have cracked if the TSTM test would have been carried out for a longer period than is done now. Cracking cannot be observed in the stress curve corresponding to the FEA of the wall as fracture models are not taken into account in this analysis and only a viscoelastic material model is used.

In the end it should be mentioned that to be able to compare the results of the TSTM test with the FEA regarding the assessment of early-age cracking in more detail, the TSTM test itself should be modelled using finite element software. When the TSTM test is modelled using the temperature curve as measured in the concrete specimen during the test, the resulting stress output can be compared to the results of the TSTM test in more detail. Conclusions can then be drawn on the accuracy of the FEA and the accuracy of the material properties as used in the analysis. This will be done in the next section.

After the TSTM test is modelled in a FEA, the causes of the differences between the stress output of the test and the FEA will also be discussed in more detail.

9.4.2 ADTM

For the ADTM holds that the relevant output consist of the temperature development and the deformations of the concrete specimen. As the aim of this test is to measure the autogenous deformations, the temperature is kept constant at 20℃ to avoid thermal strains. In figure 100 below the average concrete temperature of the specimen can be seen. Next to that the temperature of the water that is running through the temperature regulating mould can be seen. The temperature of this water is constantly adjusted to ensure a constant concrete temperature. As can be seen from the water temperature curve in the figure below, for the time period of $5 < t < 40$ hours holds that cooling of the concrete specimen is needed to keep the concrete temperature constant. This indicates that the rate of hydration is the highest in this period. For $t > 40$ hours holds that heating of the specimen is required, this is caused by the fact that the ambient temperature is slightly below 20℃.

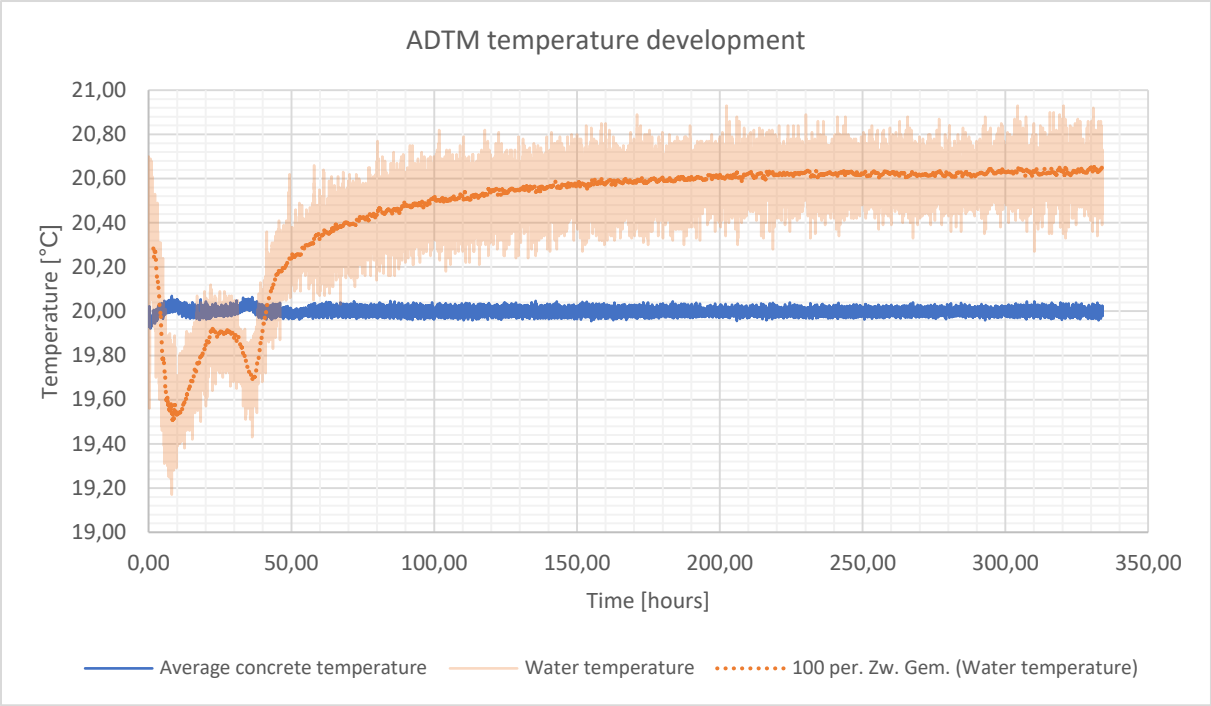

figure 100 Comparison between the measured concrete temperature and the water temperature during the ADTM test

The main output of the ADTM test is the deformation which is continuously measured at the locations of the embedded bars. Since the length over which the deformations are measured is known, these deformations can be converted to strains. The results can be seen in figure 101 below.

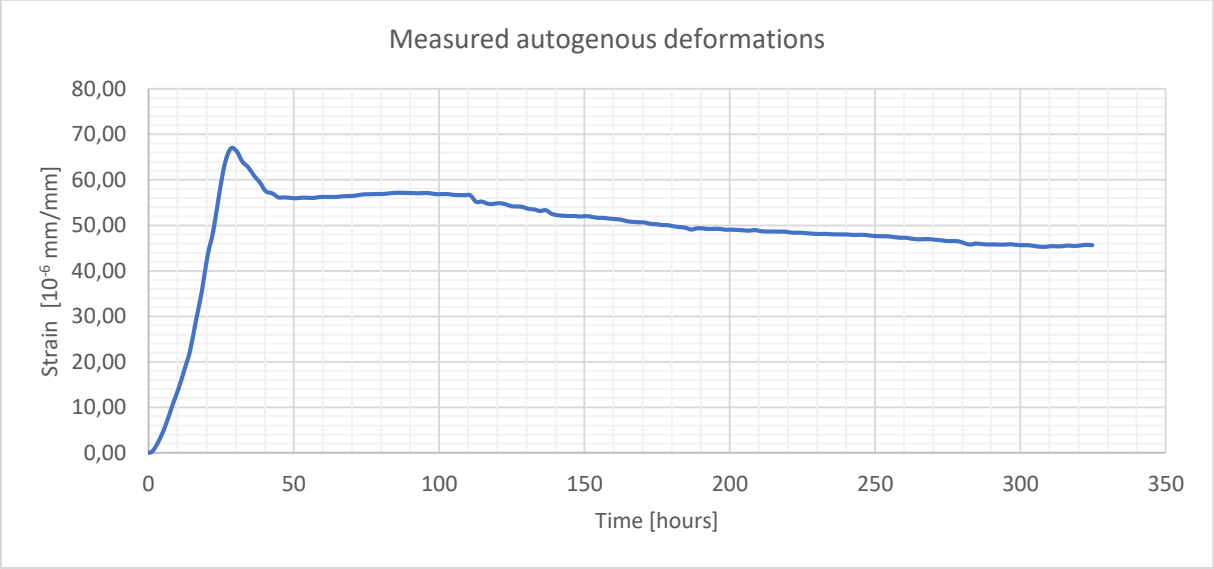

figure 101 Measured autogenous deformations during the ADTM test

As a side note to these measurements it should be mentioned that as in the first hours after casting of the concrete measurements cannot yet be done as the concrete is required to have a certain stiffness for the LVDT's to be placed in between the embedded bars. The point $t = 0$ in this graph therefore equals to 9 hours after the moment of casting of the concrete.

As can be seen from the figure above, in the period of $0 < t < 30$ hours autogenous swelling of the concrete specimen is measured, this swelling is of significant magnitude and is equals about $68\ \mu\varepsilon$. From $t \geq 30$ hours the concrete starts to shrink. The total amount of shrinkage is equal to $21\ \mu\varepsilon$.

The measured autogenous shrinkage can subsequently be compared to the autogenous shrinkage according to the Eurocode for the same concrete mixture. This can be seen in figure 102. Here the measured shrinkage is isolated and moved to the origin of the figure. It can be concluded that the measured autogenous shrinkage is slightly overestimated by the Eurocode but the curves follow a similar trend. It should however be noted that according to the Eurocode the concrete starts to shrink immediately after casting while in reality the shrinkage started after 30 hours.

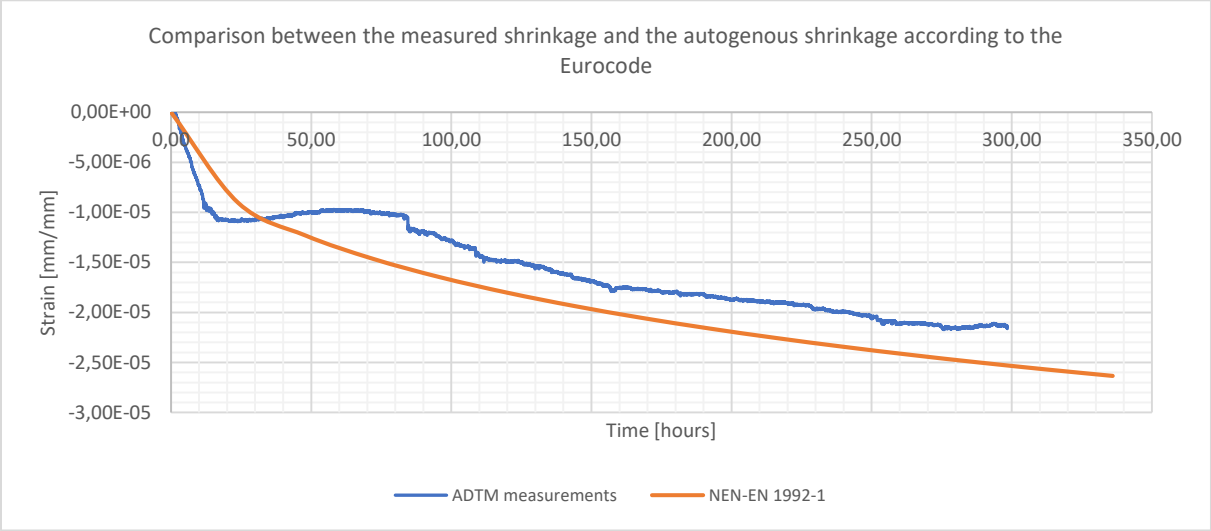

figure 102 Comparison between the isolated measured autogenous shrinkage and the autogenous shrinkage according to the Eurocode

In the end the measured autogenous strains, the water temperature and the average concrete temperature can also be plotted in a single figure. This is done in figure 103 below. The origin is set equal to the starting point of the temperature measurements. As mentioned before, the strain measurements were initiated several hours later.

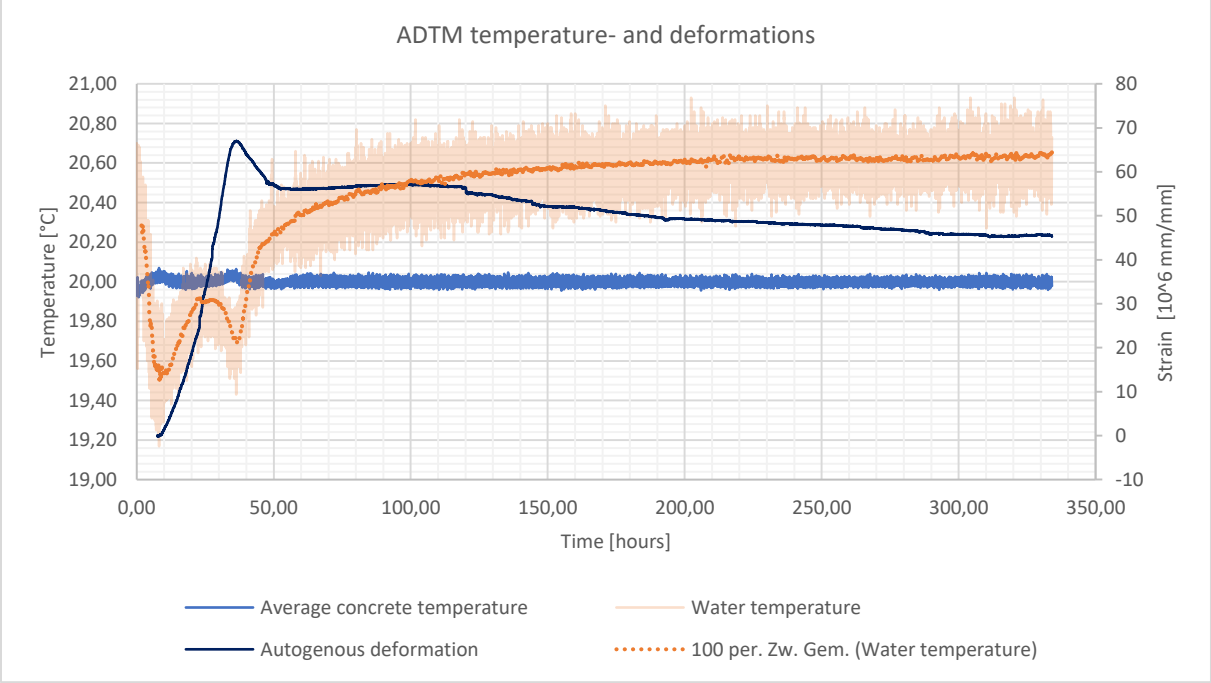

figure 103 Comparison between the measured temperatures during the ADTM test and the measured autogenous deformations

As can be seen from the figure above, the period of autogenous swelling coincides with the period for which the rate of hydration of the concrete specimen is the highest. This can be concluded from the fact that the water temperatures are lower than the average temperature of the concrete specimen in this period which means that cooling of the specimen is required.

Also, the turning point in time ($t \approx 36$ hours) for which the autogenous swelling turns into shrinkage corresponds to the moment in time for which cooling of the specimen turns into heating. This can be seen from the water temperature curve because from this point on the temperature rapidly increases.

9.4.3 Cube compression tests

The cube compressive strength is determined through standard compression tests. Cubes are tested after 1,2, 5, 8, 14 and 28 days of hardening. The results can be seen in figure 104 below. In this figure the measurements are plotted together with the mean compressive strength development according to the Eurocode and the Model Code for the same concrete mixture. More details on the test data can be seen in Appendix H.

It can be concluded from this figure that according to the measurements the early-age strength of the concrete is lower compared to the predictions of the Eurocode and the Model Code. However from $t = 120\ hours = 5\ days$ the measured concrete strength is larger.

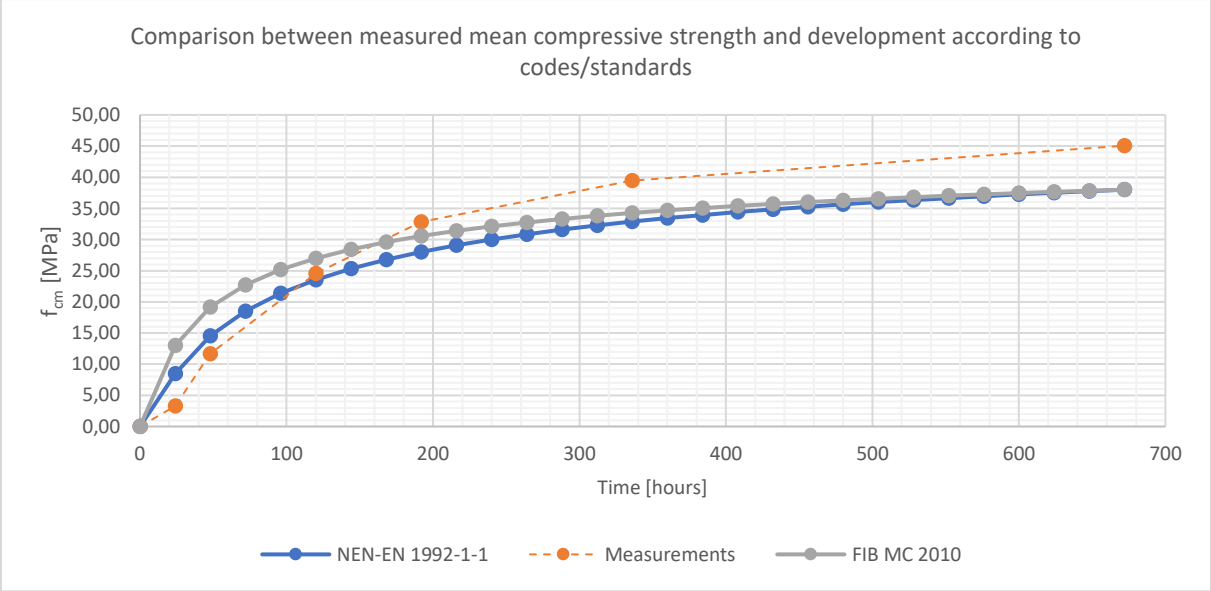

figure 104 Comparison between the measured compressive strength and the compressive strength development according to the Eurocode and the Model Code

The development of the E-modulus can subsequently be derived from the measured compressive strength according to the following equation which can be found in the Eurocode:

$$E_{cm}(t) = 22 * \left(\frac{f_{cm}(t)}{10}\right)^{0.3}$$

In figure 105 the derived development according to the Eurocode can be seen. In this figure also the development of the E-modulus according to the Eurocode and the Model Code can be seen. It can be concluded that the two curve follow the same trend as for the mean compressive strength. The E-modulus is thus slightly lower at early-ages and slightly higher at later ages.

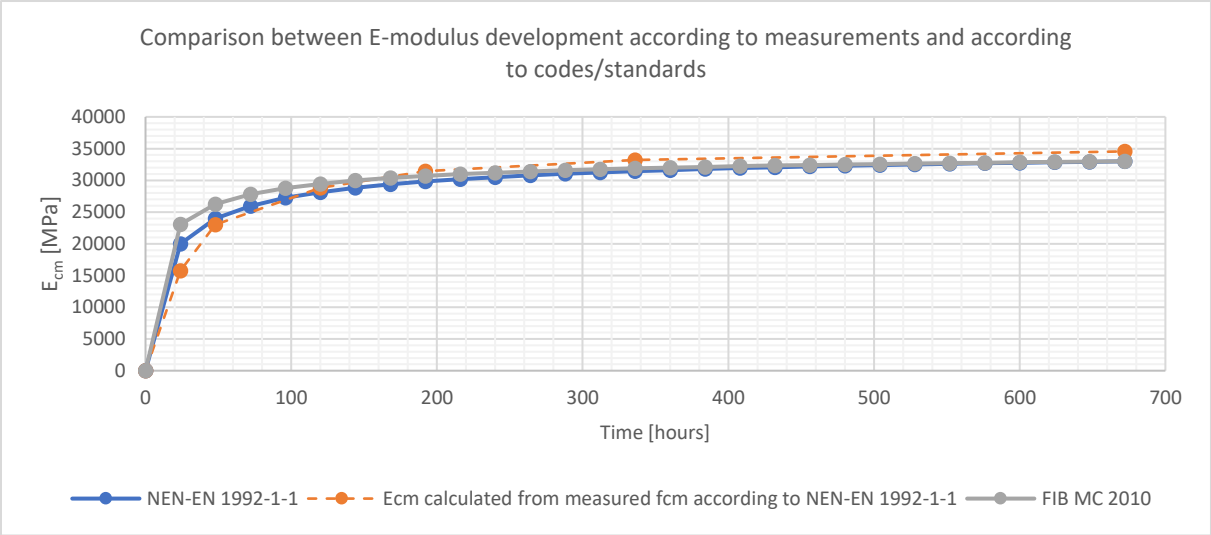

figure 105 Comparison between the derived E-modulus and the E-modulus development according to the Eurocode and the Model Code

9.4.4 Tensile splitting tests

Tensile splitting tests are performed parallel to the compressive strength tests. The results of these tests can be seen in figure 106 below. In this figure also the tensile strength development according to the Eurocode and the Model Code can be seen for the same concrete mixture. More details on the test data can be seen in Appendix H.

As for the compressive strength, the measured early-age tensile splitting strength is lower compared to the predictions of the Eurocode and the Model Code for the mean tensile strength. The measured tensile splitting strength at later ages is however significantly higher compared to these codes. The tensile splitting strength in general is about 10% higher compared to the mean tensile strength (TU Delft, 2020). The difference in these measurements however is much greater. It can also be concluded that for this concrete mixture the strength development as predicted by the Eurocode is more accurate compared to the predictions by the Model Code. This holds for both the compressive- and tensile strength development.

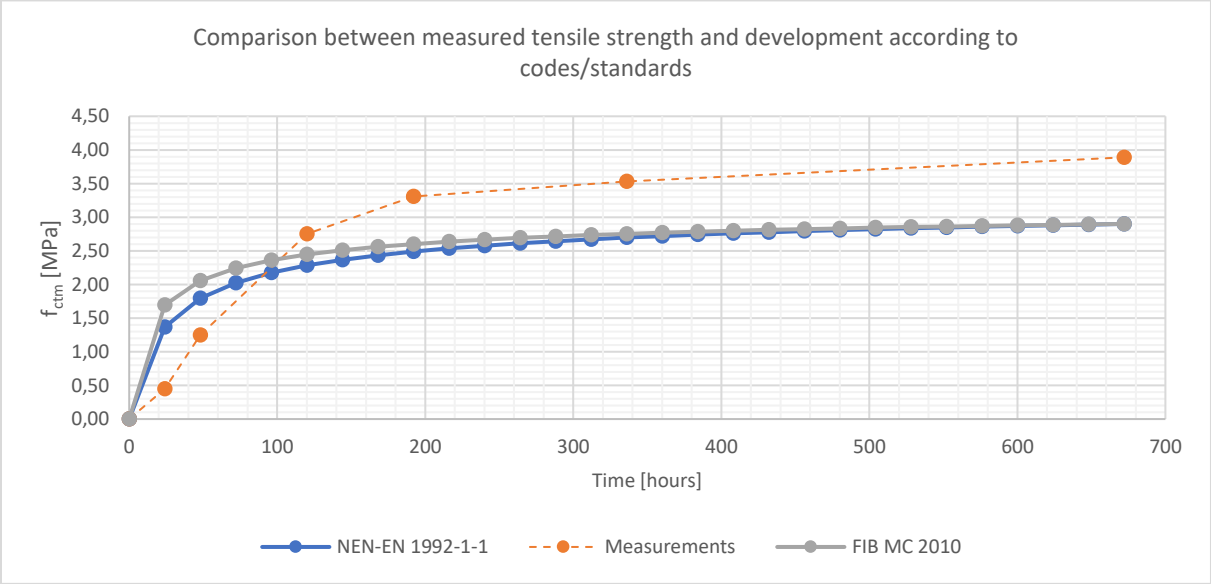

figure 106 Comparison between the measured tensile splitting strength and the tensile strength development according to the Eurocode and the Model Code

In the end the measured tensile strength and derived E-modulus can be used in to increase the accuracy of the FEA regarding the assessment of early-age cracking. This will be discussed in more detail later in this study.

9.5 Discussion and evaluation

There are certain limitations to the results as presented in the figures above and they should therefore be analysed with care. In this section the validity and limitations of the results are discussed in more detail. Besides, the overall testing procedure is discussed. The aim here is to reflect on the parts of the testing procedure that could be improved.

Concrete mixture:

- It is common practice to determine some basic properties of the concrete mixture in the laboratory. Several parameters were measured, that is the slump, density and the air content of the concrete mixture. The measured air content was 4,3% which is significantly higher than was specified by the manufacturer. Up to now, the cause of this increase in air content remains unknown. In general holds that an increase in air content could lead to a reduction of strength, however this effect is not observed in the cube tests when comparing to the strength development according to the Eurocode. It is therefore assumed that the effect of the increased air content on the results of the laboratory tests is limited.

TSTM test:

- As stated before, the average temperature of the concrete specimen is slightly higher compared to the prescribed temperature function as the temperature control system is linked to the temperature in the middle of the specimen only. In reality the overall specimen will therefore have slightly higher temperature compared to the prescribed temperature function
- It must be noted that the starting point of the TSTM test data is around 2.5 hours after the casting of the concrete. Besides, the prescribed temperature function was activated around 1.5 hours prior to the starting point of the data. This results in the fact that the oscillation peaks of the stress curves of the TSTM test and the FEA are shifted with respect to each other. This has to do with the fact that the starting points are not exactly the same
- In the prescribed temperature function the initial mix temperature was assumed to be equal to 10℃. As can be seen from the temperature measurements the initial mix temperature in practice was around 16℃. The difference between these two temperatures was no longer present 2 hours after the starting point of the data. This means that for the first 4.5 hours the temperature of the concrete mixture has been higher compared to the concrete temperature in the FEA. This should be taken into account when comparing the results. This could be improved if the TSTM test were to be repeated.
- The TSTM test was disrupted after 225 hours because of a technical error in the pump system of the actuator. Therefore no more accurate data is obtained beyond this point in time
- The TSTM test was carried out in a displacement controlled manner where the displacements as measured at the locations of the embedded bars are kept constant. However because the LVDT's were not calibrated correctly there is a small deviation in the order of 1-10 μm. This should be taken into account when modelling the TSTM test. Also, if the TSTM test were to be repeated, the calibration of the LVDT's should be redone to minimize the displacement error.
- Because the embedded bars are cast is with the concrete, stress concentrations will develop at these locations which could lead to cracking. The concrete of the TSTM test did however not crack so this effect did not affect the stress at the moment of cracking.

ADTM test:

- As is already discussed in the section on the results of the measurements, the displacements can only be measured after the concrete has a certain stiffness. For this reason the starting point of the measurements corresponds to 9 hours after the moment of casting of the concrete. As the concrete swells in the early-ages of hardening, it could be that due to the limitations of the test some of this swelling is not measured.
- The shrinkage of the concrete starts at around 30 hours after the starting point of the measurements. However according to the Eurocode the autogenous shrinkage starts immediately after the moment of casting of the concrete. This implies that the calculation method that is described in the Eurocode could be incorrect and that in practice the period of autogenous swelling should also be taken into account.
- The temperature of the concrete specimen is measured in the centre of the cross-section, at three locations over the length of the specimen. Because the temperature is measured at a single point in the cross-section only, possible temperature gradients over the cross-section cannot be measured. In the current set-up it is therefore not possible to determine whether as a result of possible temperature gradients over the cross-section, thermal strains are being included in the measurements. In any future ADTM tests, the temperature should also be measured at several locations over the cross-section.

Compressive and tensile strength tests:

- As only single cubes are tested at the different ages at which the concrete is tested, there could be a relatively large error in the obtained values. It is therefore the trend of the measurements that is important instead of the individual measurements.
- In general the Eurocode predicts a higher early-age strength and stiffness compared to the measured values. It is observed that even though the cement classification of the concrete mixture is N (‘Ordinary early strength’), the measured early-age strength and stiffness are lower compared to the estimated development according to the Eurocode for ordinary cement. It can therefore be concluded that for the first days after casting of the concrete these material properties are overestimated by the Eurocode.

10 TSTM modelling

The aim of performing the TSTM test is to simulate the hardening process of the wall from the case study and to gain more insight in the material behaviour regarding imposed deformations and early-age cracking. The results of the TSTM test can best be analysed by making use of a finite element model of the TSTM test which will be used to compare with the test results. The FEA is first performed using the initial input parameters as determined in a previous section on the case-study. Second the actually measured material properties (autogenous shrinkage, tensile- and compressive strength and corresponding E-modulus) are implemented in the FEA and the results are compared with the actual TSTM results. The differences- and/or agreements will then be discussed and statements will be made on the accuracy of the input parameters of the finite element analysis.

10.1 Model

The TSTM test is modelled using MLS Heat. The test is modelled in 2D as can be seen in figure 107 below. In this figure the complete model including dimensions, mesh and boundary conditions can be seen. The characteristics of the model will here be discussed in more detail.

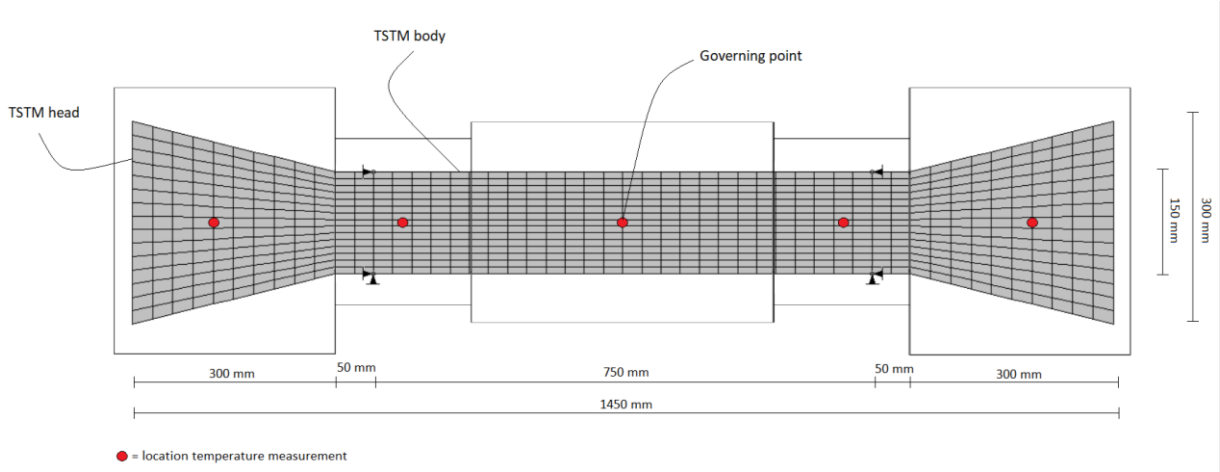

figure 107 FEM of TSTM test including boundary conditions and mesh

- In reality the transition from the 'heads' to the 'body' of the specimen is rounded and distributed over a certain length. In the model this is neglected and this transition is made abrupt as can be seen in the figure.
- As discussed before in the description of the laboratory testing, during the TSTM test the temperature is measured at five locations in the specimen as is indicated in the figure above. To be able to accurately model the TSTM test, these measured temperatures should be prescribed to areas of the specimen. These areas are indicated in the figure above by squares that surround the model. Each square corresponds to a temperature measurement lying in this area as indicated by the red dots in the figure. The temperature function corresponding to the specific measurement is prescribed to that area.
- Only stresses that act in the XY plane are relevant for this analysis and therefore a situation of plane stress is modelled. As a consequence the stress component in the outward z-direction S_{zz} is assumed to be equal to zero. This is justified by the fact that the length of the specimen is much larger than the dimensions in the outward z-direction.
- In reality, the restraining force is introduced in the heads of the specimen which are clamped by the 'claws' of the machine. As discussed before in the description of the laboratory tests,

deformations of the concrete specimen are being restrained by controlling the displacements at the locations of the embedded bars. The displacements are constantly measured and should be kept constant to ensure a fully restrained system during the test. However due to imperfections in the system the displacements are not kept constant completely and deviations occur. These deviations are registered.

- In the FEA the displacements at the locations of the embedded bars should be equal to the measured deviations during the test. To be able to do this, the supports should be placed at the positions of the embedded bars. A displacement function is subsequently assigned to these supports to ensure the same displacements over time as are measured during the test. By placing the supports at the locations of the embedded bars the restraining forces are introduced at these locations. This differs from the actual test where the forces are introduced in the heads of the testing machine. However as can be seen in the figure, the governing point lies in the middle of the specimen. The effects of changing the way in which the restraining force is introduced in the specimen on the force distribution in the governing point in the middle of the specimen are assumed to be negligible. This is checked by regarding the stress distribution of the specimen in state of compression and tension.

As can be seen in figure 108 below, the stress distribution at the point of interest in the middle of the cross section can be considered as uniform both in compression and in tension. The disturbances in stress distribution caused by the introduction of the restraining forces at the location of the supports do not have a large effect on the stress distribution at the point of interest. It can therefore be concluded that changes in supporting conditions with respect to the actual testing machine are justified.

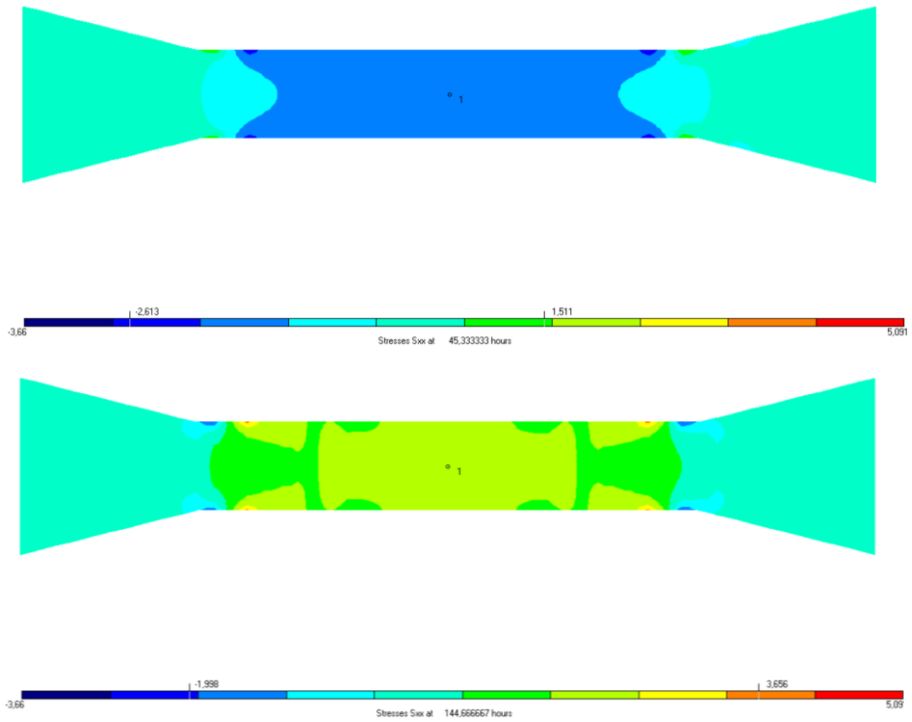

figure 108 Uniform stress distributions in compression (top figure) and in tension (bottom figure) at the point of interest

10.2 Symmetry

The finite element model as presented above consists of two symmetry axes. By making use of these symmetry axes the size of the model can be reduced. A reduction of the size of the model in turn results in a reduction of the computation time. The two symmetry axes and the reduced model can also be seen in figure 109 below.

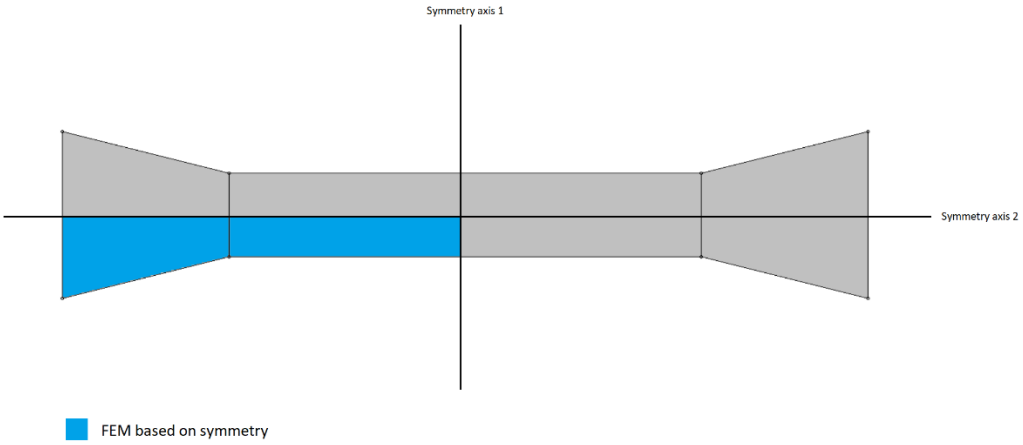

figure 109 The two symmetry axes that can be used to reduce the model size

Because use is made of symmetry, additional boundary conditions should be used at along the symmetry axes to ensure that the behaviour of the reduced model corresponds to the behaviour of the full model. Also, the point of interest of the model is the point in the middle of the TSTM specimen as can be seen in figure 108. This point should lie outside of the region in which disturbances in the force distribution could be present that could occur from the introduction of the restraining force at the location of the point support. The resulting model can be seen in figure 110 below.

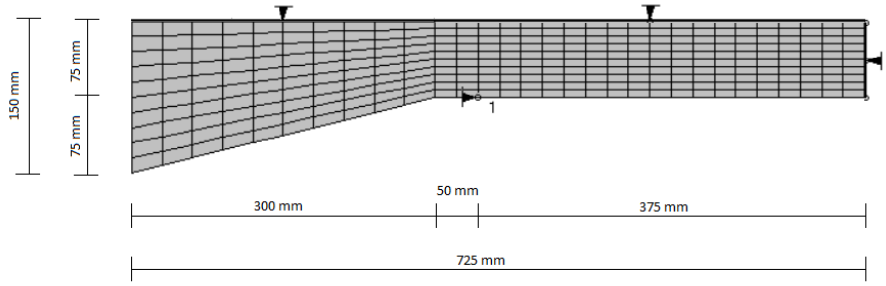

figure 110 The reduced FEM of the TSTM test, where use is made of symmetry to reduce the model size

The reduced model as presented here will be used in the remainder of this section. The results of the reduced model were validated through comparison with the results of the full model.

10.3 Input parameters

Initially the material properties are defined in correspondence with the FEM of the wall- and slab as is discussed in a previous section. However because in this case the temperature development during hardening is already prescribed, convection and radiation properties can be disregarded. The ambient temperature therefore also has no influence on the temperature development during the FEA. Subsequently, the measured material properties will be used. In this way the output of the TSTM test can be compared to the finite element model of this test.

10.3.1 Measured parameters

After the FEA is performed using the initial material properties, the material properties as measured by testing are implemented. As the measured properties are implemented, the accuracy of the FEA with respect to the actual TSTM testing should increase. There are several material properties of which the development over time has been measured and that therefore will be used in the analysis:

- Autogenous deformations ε_{au}
- Tensile strength f_{ctm}
- Compressive strength f_{cm}
- E-modulus E_{cm} (calculated from measured compressive strength)

10.4 Runtime specifications

Before the finite element calculations can start, the runtime specifications have to be set. It is decided to use the following specifications:

- The computation time equals 225 hours. This corresponds to the duration for which accurate results could be obtained from the TSTM test.
- The stresses are smoothened over the elements
- The time increment is decided to be 0.33 hours, and the results are stored each 3 hours.
- The element type used are fully integrated quadrilateral elements

10.5 Results

The results of the FEA can be seen in several figures as presented here below. In both figures the results of the FEA of the TSTM model are shown in relation to the actual TSTM test results. In figure 111 the results of the FEA using the initial parameter values can be seen. The viscoelastic behaviour of the material is varied between 'high creep', 'low creep' and 'average creep' as defined in a previous section on viscoelastic behaviour. In the end also the effect of not taking viscoelastic material behaviour into account can be seen (linear elastic analysis).

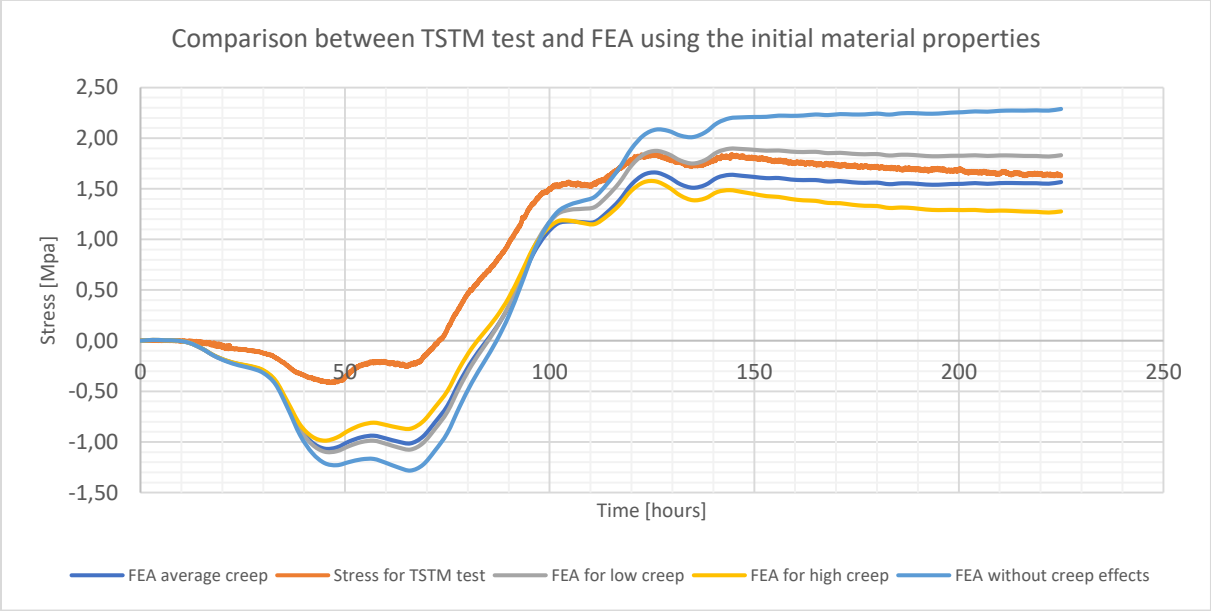

figure 111 Comparison between the measured stress in the TSTM test and the stress resulting from the FEA of the TSTM test for different types of viscoelastic material behaviour

As specific material properties have been determined through laboratory testing, the FEA is also performed using the measured material properties. The results can be seen in figure 112. In this figure also the curve of the FEA using the initial parameter values for average creep can be seen.

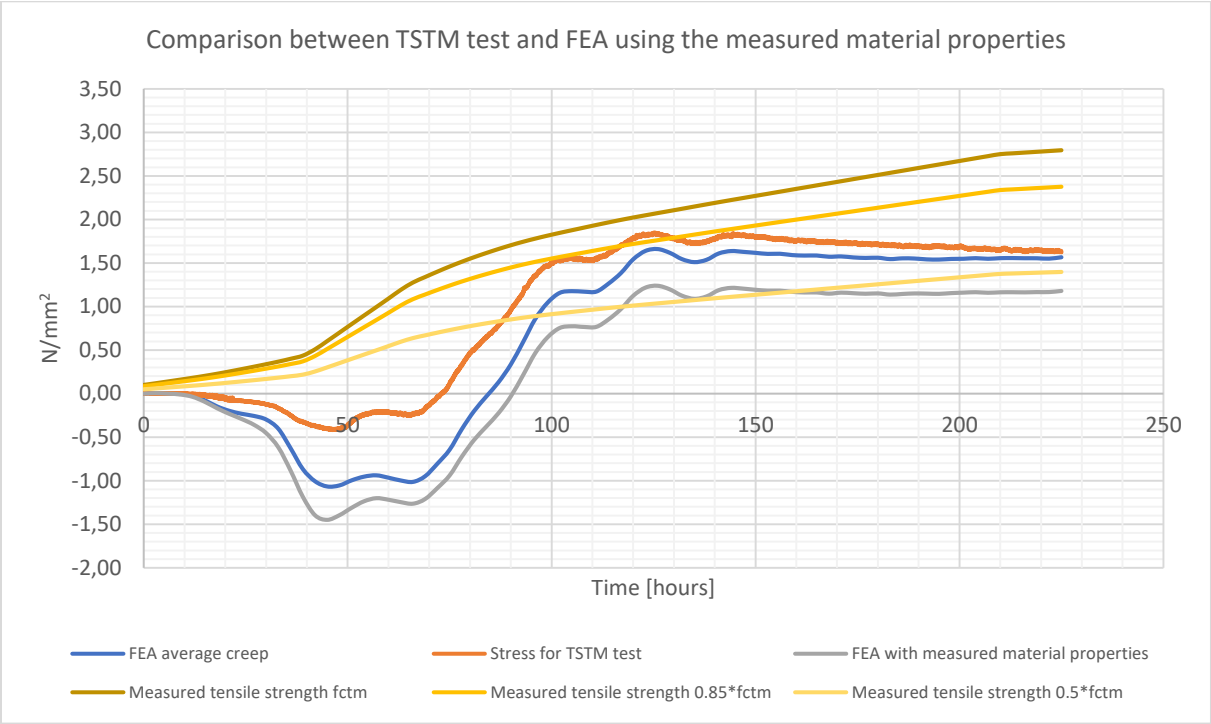

figure 112 Comparison between the measured stress in the TSTM test and the stress resulting from the FEA of the TSTM test using the measured material properties

10.6 Discussion

Here the results as shown in the figures above are discussed. The results of the FEA are compared with the results of the TSTM test and the effect of varying specific material properties will be discussed.

FEA results using the initial parameter values as displayed in figure 111:

- In general can be concluded that the curves of the FEA of the TSTM test follow the same trend. However because the compressive stresses are larger for the FEA, the curves are shifted with respect to each other. The absolute difference in stress from maximum compressive stress to maximum tensile stress is similar, but as the compressive stresses are larger subsequently the tensile stresses are lower.
- The increase in compressive stresses in the FEA with respect to the TSTM test could in part be caused by the fact that in reality the E-modulus of the material is smaller at early-ages compared to the E-modulus development according to the Eurocode. This is confirmed by the compressive- and tensile strength tests.
- The increase in compressive stresses in the FEA with respect to the TSTM test could also in part be caused by the fact that the creep- and relaxation effects at early-ages are larger than is taken into account in the FEA.
- As can be seen from the FEA in which viscoelastic material behaviour is not taken into account, the trend of this stress curve does not correspond to the measured stresses in the TSTM test. This is most evident for stresses in the range of $140 < t < 225$ hours. Also the compressive stresses at early-ages are significantly higher. It can therefore be concluded that viscoelastic

material behaviour cannot be neglected and that it has a significant effect on the risk of early-age cracking.

- When the trends of the different curves of the FEA are considered, it is observed that the trend of the 'high creep' FEA curve corresponds best to the TSTM measurements. Especially when the effects of stress relaxation are considered for $140 < t < 225$ hours, the 'high creep' curve corresponds best with the TSTM test curve. Also, for the 'high creep' curve the compressive stresses at early-ages are the smallest of all FEA curves which corresponds best to the TSTM test curve.

FEA results using the measured parameters as displayed in figure 112. Here the measured E-modulus, autogenous deformations and tensile- and compressive strength developments are used in the analysis:

- Using the E-modulus development as derived from the compressive strength measurements has the effect of decreasing the compressive stresses at early-ages because the E-modulus develops slower than was estimated using the initial parameter values. However as relatively large autogenous swelling was measured in the ADTM tests this effect has vanished and the resulting compressive stress at early-ages is larger than for the FEA using the initial parameter values.
- Using the tensile strength development as measured through tensile splitting cube tests in the FEA results in the tensile strength curve as a displayed in the figure. As can be seen in this figure the tensile stress of the TSTM test exceeds the limit of $0.85 * f_{ctm}$. According to van Breugel et al. (1996) this means that the probability of cracking is just over 50%. However as is discussed in the section on laboratory testing, the TSTM specimen did not crack during the test.
- Because using the measured parameter values in the FEA results in high compressive stresses at early-ages and therefore also lower tensile stresses during the cooling period, the stress curve of this FEA does not correspond to the measured stress curve from the TSTM test. It can hence be concluded that using the present material properties and model the TSTM test is not simulated correctly. Changes in the material properties and/or model are therefore needed to be able to simulate the TSTM test in a correct manner and to accurately determine the material behaviour in practice.
- To achieve the above, changes will be made in the viscoelastic material behaviour in the finite element model. The effects of creep and stress relaxation should be increased especially at early-ages to reduce the compressive stresses in this period. This is an iterative process in which the stress curve of the FEA will be fitted to the stress curve of the TSTM test and where the actual material behaviour can be determined.

10.7 Fitting of the viscoelastic material behaviour

As is mentioned in the discussion of the results of the finite element modelling of the TSTM test, changes will be made in the viscoelastic material behaviour in order to fit the stress curve of the FEA to the results of the TSTM test. The result of this iterative procedure can be seen in figure 113 below. In this figure the fitted stress output of the FEA using the measured material properties can be seen together with the stress output of the TSTM test. Next to these two curves the stress curve for the FEA using the 'high creep' viscoelastic behaviour as defined in a previous section can be seen.

From the stress curves as presented in the figure the effect of increasing the viscoelastic material behaviour at early-ages can clearly be seen as the compressive stresses are strongly reduced when the fitted material behaviour is used. Increasing the effect of stress relaxation at early-ages

subsequently causes an increase in tensile stresses at higher ages and the resulting stress curve therefore seems a reasonable fit to the stress curve of the TSTM test.

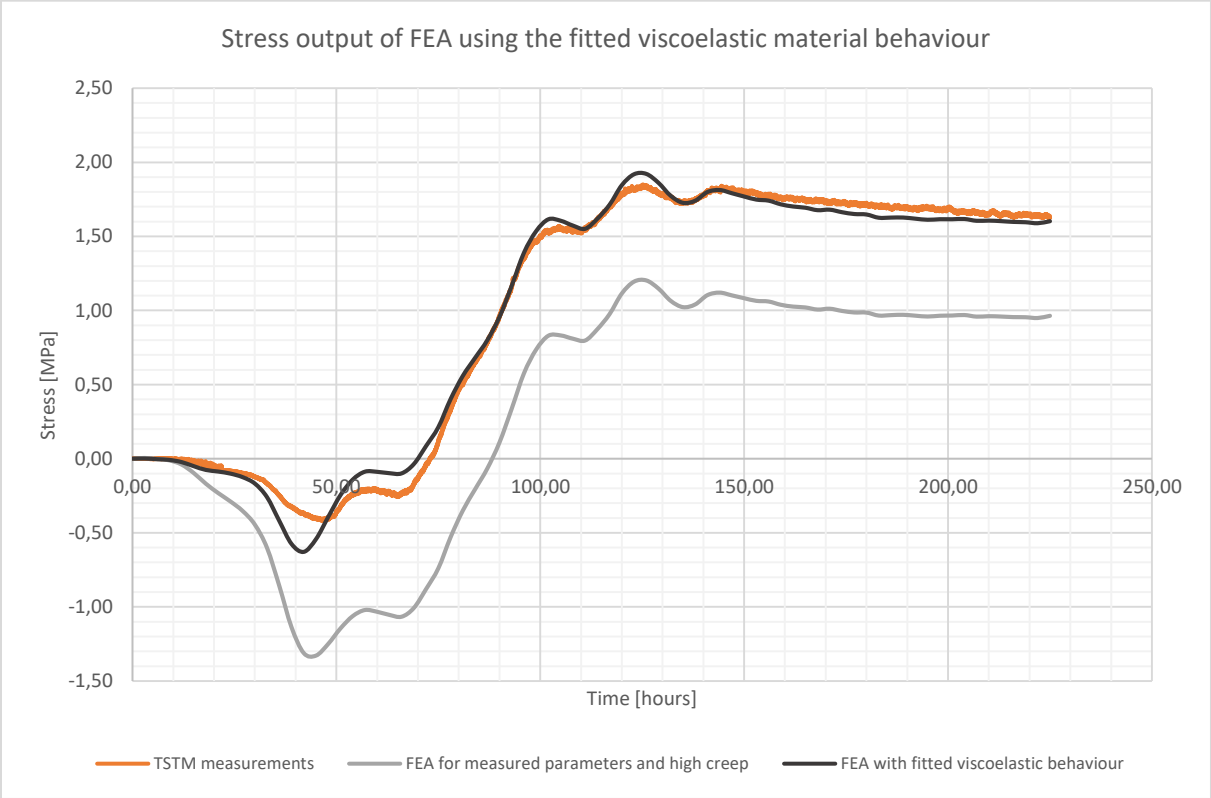

figure 113 Comparison between the measured stress in the TSTM test and the stress according to the FEA using the fitted viscoelastic material behaviour

The resulting viscoelastic material behaviour can be compared with the initially assumed behaviour named the 'high creep' data by comparing the creep compliance curves for certain ages at loading. More details on this comparison can be seen in appendix G. The results are summarized in the table below.

In this table the creep data sets are compared by means of the creep compliance at $t = 672$ hours after loading. As can be concluded from the multiplication factors, the fitted creep compliance is significantly higher compared to the 'high creep' compliance for 0 and 24 hours maturity at loading. It should be noted that the elastic response is equal for both creep data, so the multiplication factor as shown here is the actual increase in viscoelastic response at early-ages.

Maturity at loading: [hours]	Creep compliance for fitted creep behaviour: $[J * 10^{-6}]$	Creep compliance for 'high creep': $[J * 10^{-6}]$	**Multiplication factor: [-]**
0	4650.0	1707.1	**2.72**
24	288.7	117.7	**2.45**
72	88.1	84.2	**1.05**
168	55.1	76.4	**0.72**

Table 16 Multiplication factors following from the comparison between the initial 'high creep' behaviour and the fitted viscoelastic material behaviour

It can be concluded that the effects of creep and stress relaxation are significantly larger at early-ages than was initially assumed. This will have also have an effect on the assessment of the risk of early-age cracking.

The increased effects of creep and stress relaxation at early-ages can also be illustrated by means of the creep factor. The creep factor is here defined as the ratio between the stress that results from a linear elastic analysis and the stress that results from the analysis where the fitted creep behaviour is taken into account. The stress curves can again be seen in figure 114.

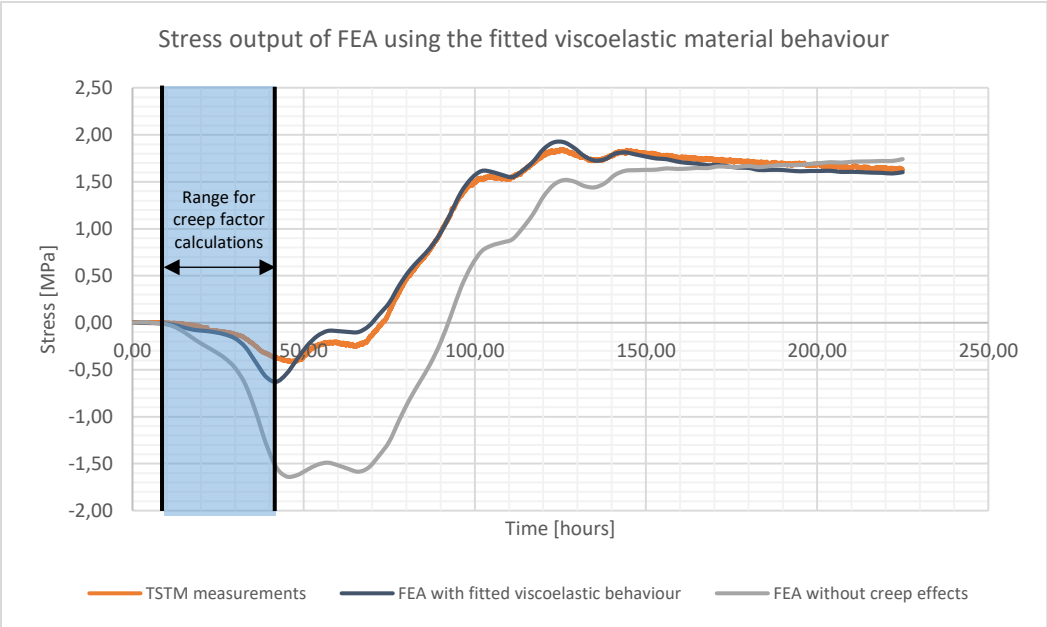

figure 114 Definition of the usable range for the calculations of the creep factor

As was already concluded, the effects of creep and relaxation at early-ages (0-50 hours) for a large part determine the stress development at higher ages. The creep factor is therefore calculated only for this specific range in time as can be seen from the figure above. The range is however limited by the specific point in time where the stress-rate changes sign (42 hours) as from this point on the values do no longer have significant meaning.

The aim of calculating the creep factor over time is purely to illustrate the effect of creep and stress relaxation in this analysis. The results can be seen in figure 115. It can be concluded that the average creep factor equals to 2.38 for this period in time. It must be noted that this factor cannot be compared creep factors as presented in NEN-EN 1992-1-1. In the current Eurocode only creep corresponding to structural loading of hardened concrete is considered. There is no guidance on effects of creep on stresses due to imposed deformations in hardening concrete.

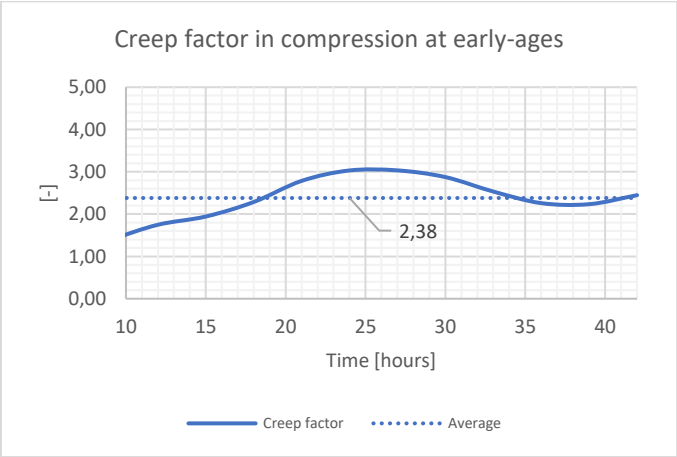

figure 115 Creep factors that follow from the fitted viscoelastic material behaviour at early-ages

11 Measurements and inspections

In-situ measurements and inspections are performed will be performed as part of this research. This is done specifically for the walls of segment 12 of the dive-under as is discussed in the section on the definition of the case study. The measurements and inspection are done both to verify and to compare with the results of the finite element analyses and the laboratory testing as described in the previous sections. In the end the measurements will be used to increase the accuracy of the finite element analyses regarding the assessment of the risk of early-age cracking. The inspections are performed to be able to make statements on the probability of early-age cracking in practice

11.1 Temperature measurements

First of all temperature measurements will be done for the southern wall of segments 12 of the dive-under. There are two types of measurements that will be done:

- Temperature measurements inside of the wall. As the initial mix temperature is an input parameter of the FEA which has a relatively high uncertainty, it is relevant to be able to measure the temperature of the wall during hardening. This is done by measuring the temperature at 4 specific locations as can be seen in figure 116 below. The locations are selected in the area of the governing point in the bottom region of the cross-section of the wall at 1000 mm height measured from the top of the slab.
- Temperature measurements outside of the wall. Next to the temperature development inside of the wall, the ambient temperature is also an input parameter of the FEA which has a relatively high uncertainty. For this reason the ambient temperature will be measured during hardening.

The output of these in-situ measurements will be used to calibrate the finite element model and increase the accuracy of the finite element analysis regarding the assessment of the risk of early-age cracking of the walls of the dive-under.

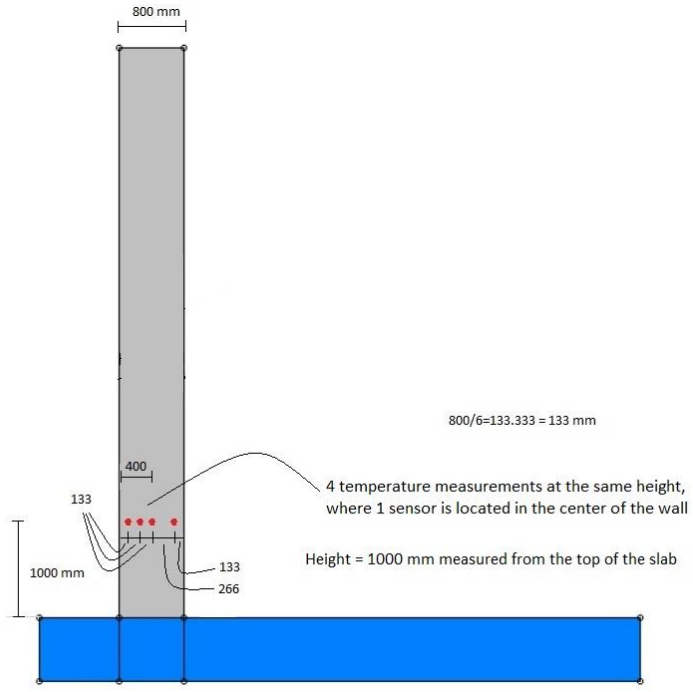

figure 116 Locations of the temperature measurements in the Southern wall of segment 12 in practice

11.2 Visual inspections

Next to the temperature measurements, visual inspections will be performed. The aim of these inspections is to validate the finite element analyses and laboratory testing by visually determining whether early-age cracking occurs in the walls of the dive-under. When it is determined if and when the concrete will crack in practice, conclusions can be drawn on the accuracy of the finite element modelling with respect to the assessment of early-age cracking.

11.2.1 Method

The inspections will be carried out by means of an inspection schedule based on the construction schedule and the critical moments in time regarding early-age cracking. At predefined moments in time after casting of the wall a visual inspection will be carried out. During such an inspection the bottom region of the wall (governing points regarding early-age cracking lie at 500-1000 mm height measured from the base of the wall) will be checked for cracks by means of a strong light to create a visible shadow at the locations of the cracks.

The focus of the inspection will be at the middle third of the wall (along the length) as this is the region where the imposed deformations are fully restraint. This can also be seen in the section on finite element modelling of the longitudinal section. As has already been described in the literature study, there is a typical crack pattern that can be expected for the case of 'base restraint' as can be seen in figure 117 below. This should be taken into account when performing the inspections.

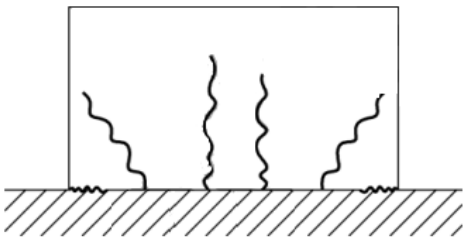

figure 117 Expected early-age crack pattern in the walls of the dive-under

11.2.2 Critical moments in time

The inspection schedule is determined based on critical moments in time regarding early-age cracking. These critical moments are determined by the FEA, TSTM testing and the construction schedule. In figure 118 the stress according to the TSTM test can be seen together with the measured tensile strength of which the development during the TSTM test is evaluated in the FEA of the TSTM. From these curves can be seen that the critical moment in time regarding early-age cracking lies within the range of $120 < t < 150$ hours after casting the concrete as the ratio between the stress and strength is the greatest here.

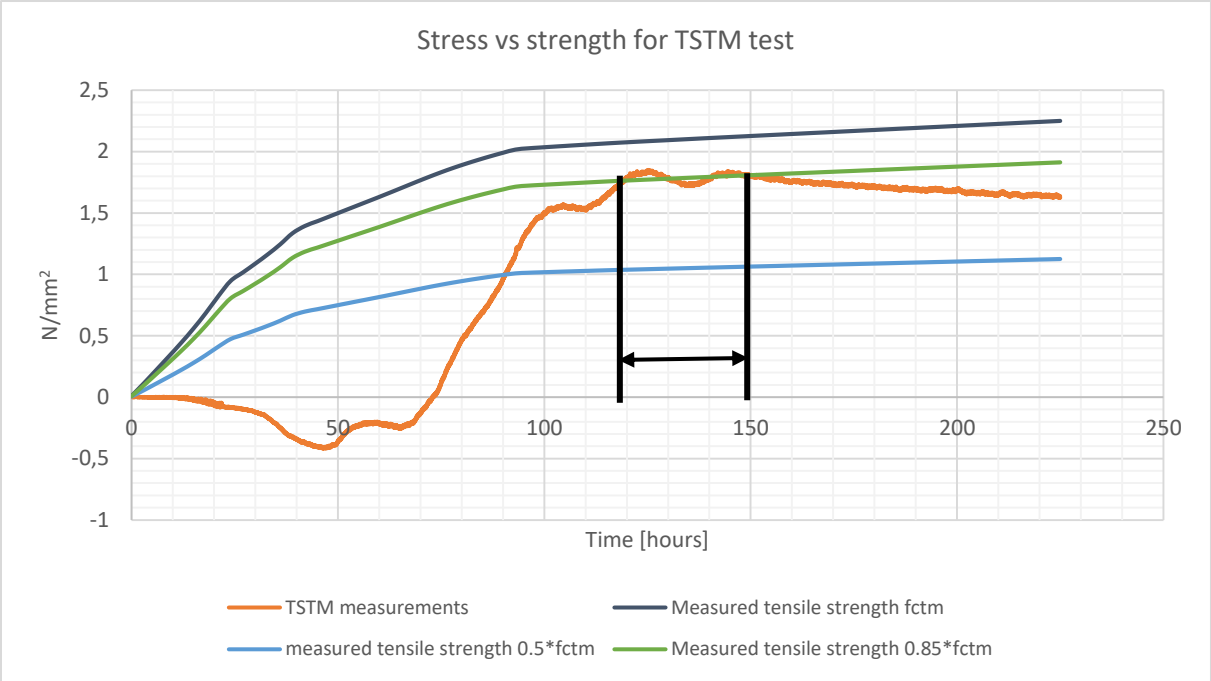

figure 118 Critical time period regarding early-age cracking according to the TSTM test

In figure 119 below the stress and strength development for the governing point in the bottom of the wall can be seen based on the FEA of the cross section of the wall. In these analyses the viscoelastic material behaviour is varied. It can be concluded from these analyses that the critical moment in time regarding early-age cracking lies within the range of $150 < t < 200$ hours.

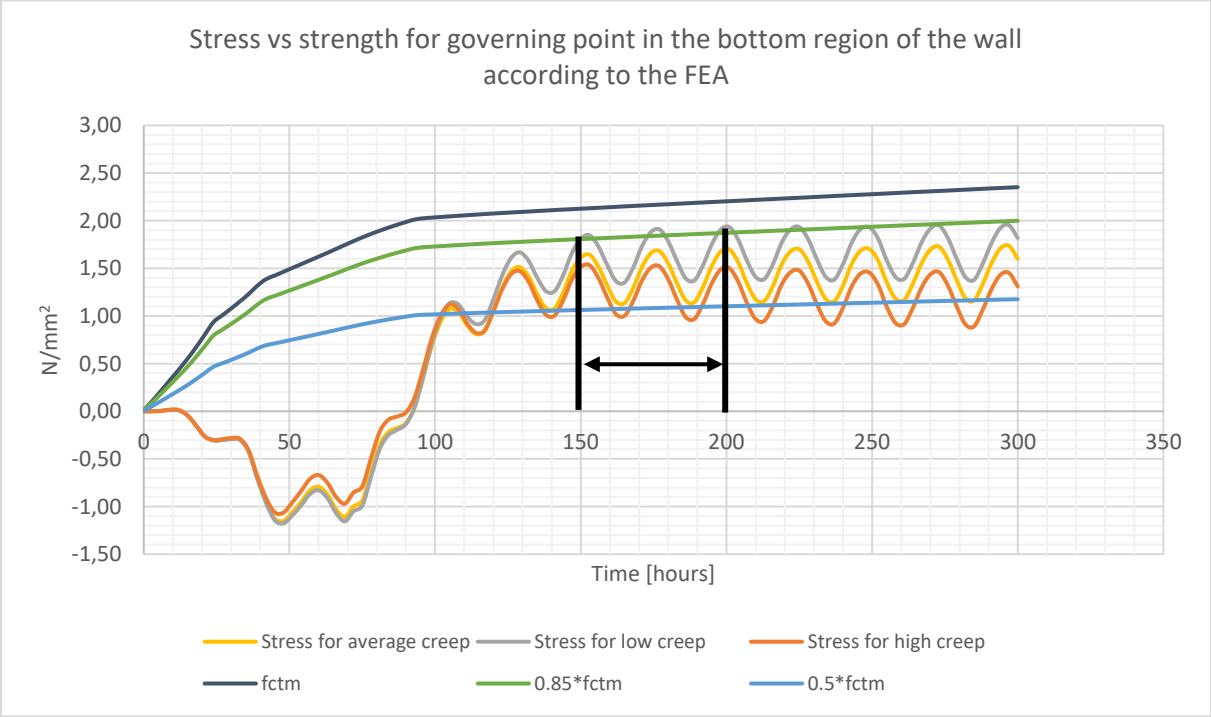

figure 119 Critical time period regarding early-age cracking according to the FEA

Besides, critical moments in time can also be derived from the construction schedule of the wall. The construction schedule for the southern wall of segment 12 can be seen in the table below:

Activity	Duration [days]	Begin date	End date	Time after casting [hours]
Preparing of formwork and reinforcement	16	24-01-2020	14-02-2020	-
Casting of the concrete	1	17-02-2020	17-02-2020	-
Hardening	3	17-02-2020	20-02-2020	0-72
Demoulding	1.5	20-02-2020	21-02-2020	72-96

Table 17 General construction schedule for the Southern wall of segment 12

The faces of the wall will only be visible after striking of the formwork. This means that the first opportunity to inspect the bottom region of the wall is after the formwork has been removed. This will probably be started after 72 hours which makes this another critical moment in time. The time after which the formwork will be struck cannot be determined exactly in advance because striking of the formwork can only be started when two main criteria are met:

- The maximum concrete temperature during hardening should have been reached
- The temperature difference between the centre of the concrete wall and the environment should be $\leq 15℃$.

11.2.3 Inspection schedule

The inspection schedule is based on the critical moments in time. When cracks are discovered during an inspection, the timespan in which the cracks might have occurred can be determined. Because the construction schedule is subject to change and the inspections are only possible from Monday till Friday, the inspection schedule may change. Also, because the period of $120 < t < 150$ hours after casting lies in the weekend there is no possibility to perform an inspection in this period. A preliminary schedule is presented in the table below.

Inspection number	Date	Description of critical moment in time	Time after casting [hours]
1	Friday 21-02-2020	The formwork has been removed at this point	96
2	Wednesday 26-02-2020	Check for early-age cracking at the end of the cooling period of the hydration process	216
3	Thursday 26-03-2020	Last check for imposed deformation induced cracks	912

Table 18 Inspection schedule regarding early-age cracking of the Southern wall of segment 12

The inspection window regarding early-age cracking as follows from the table above can be seen in figure 120 below. In this figure the inspection window is indicated with respect to the stress- and strength curves corresponding to the TSTM test. The first two individual inspection moments are also indicated.

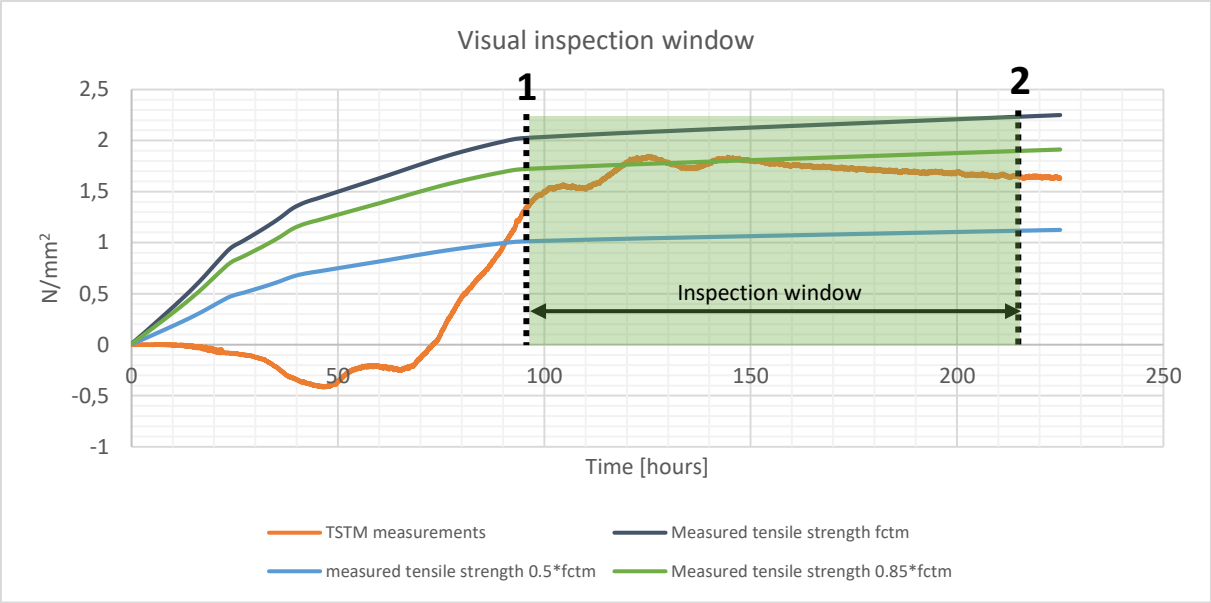

figure 120 The inspection window regarding early-age cracking indicated in the stress/strength diagram of the TSTM test

11.3 Results

11.3.1 Visual inspections

The visual inspections are performed based on the method and schedule as described in the beginning of this section. The focus of the inspections was on the Southern wall of segment 12 of the dive-under as can be seen in figure 61. However, because this wall is not the first wall that is constructed there were several other walls that were available for inspection which have the same dimensions and properties. The walls have been casted in sequence which means that they all have a different age. The additional walls that were inspected are listed here:

- Northern wall of segment 14, casted on Thursday 23-01-2020
- Northern wall of segment 12, casted on Thursday 30-01-2020
- Southern wall of segment 14, casted on Thursday 6-02-2020

Inspection number	Date	Time after casting [hours]	Was (early-age) cracking observed? [YES/NO]	Comments
1	21-02-2020	96	NO	All 4 walls were available for inspection. An additional wall, the Northern wall of segment 15 was being casted during this inspection
2	26-02-2020	216	NO	The Northern wall of segment 15 was also available for inspection. In total 5 walls have been inspected, none of which suffered from early-age cracking
3	26-03-2020	912	YES	After a cold clear night where temperatures below 0 °C were reached, cracking of the walls was observed. The moment at which the concrete cracked however lies outside of the time window for early-age cracking and therefore also outside of the timespan of the FEA for this study

Table 19 Results of the visual inspections

figure 121 Demoulding of the Southern wall of segment 12 of the dive-under during inspection number 1

In figure 122 below one of the cracks that was found during the third inspection can be seen. It is indicated by arrows. The moment at which cracking occurred however lies outside of the time window of the analysis regarding early-age cracking that is performed in this study.

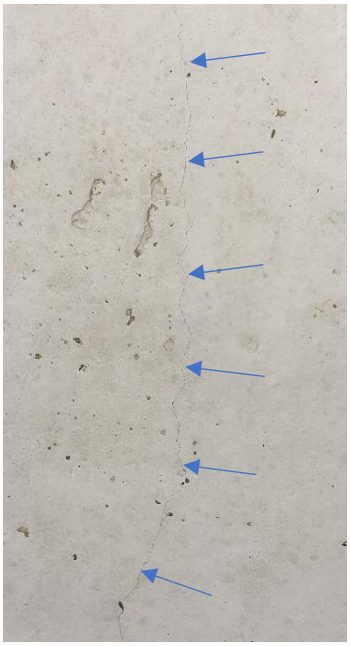

figure 122 Crack in the Southern wall of segment 12 that was discovered during inspection number 3

11.3.2 Temperature measurements

Temperature measurements were done at 4 different locations over the cross-section of the Southern wall of segment 12 as described in figure 116. In practice however, turned out that the locations at which the sensors had been placed could not be determined afterwards and only the temperature measurement in the centre of the cross-section can be used. The results can be seen in figure 123 below. In this figure the measured temperature in the centre of the cross-section can be

seen together with the temperature curve for the same point according to the initial FEA of the cross-section of the wall.

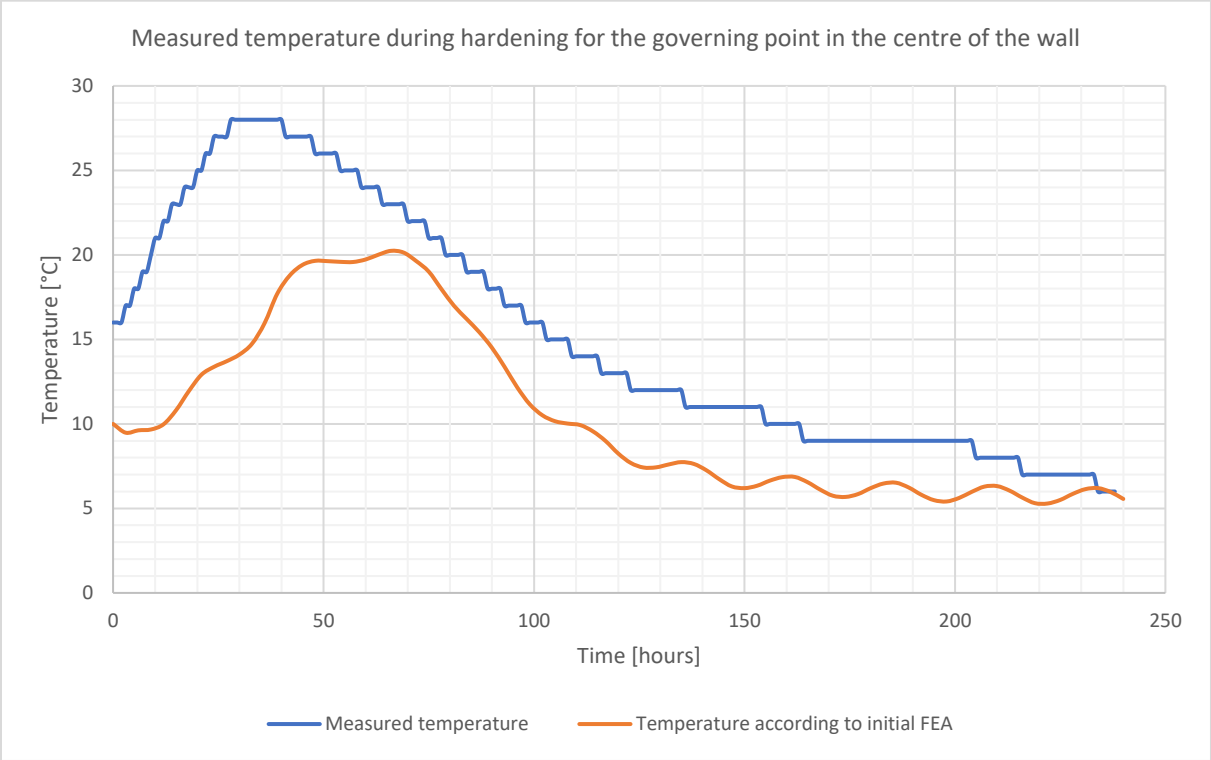

figure 123 Comparison between the measured temperature in the core of the wall and the results of the initial FEA

Besides, the ambient temperature during hardening of the Southern wall of segment 12 is measured. The resulting temperature curve can be seen in figure 124 below. In the initial FEA of the cross-section of the wall it was assumed that the average ambient temperature was equal to 5℃. It can be concluded that the measured ambient temperatures are significantly higher.

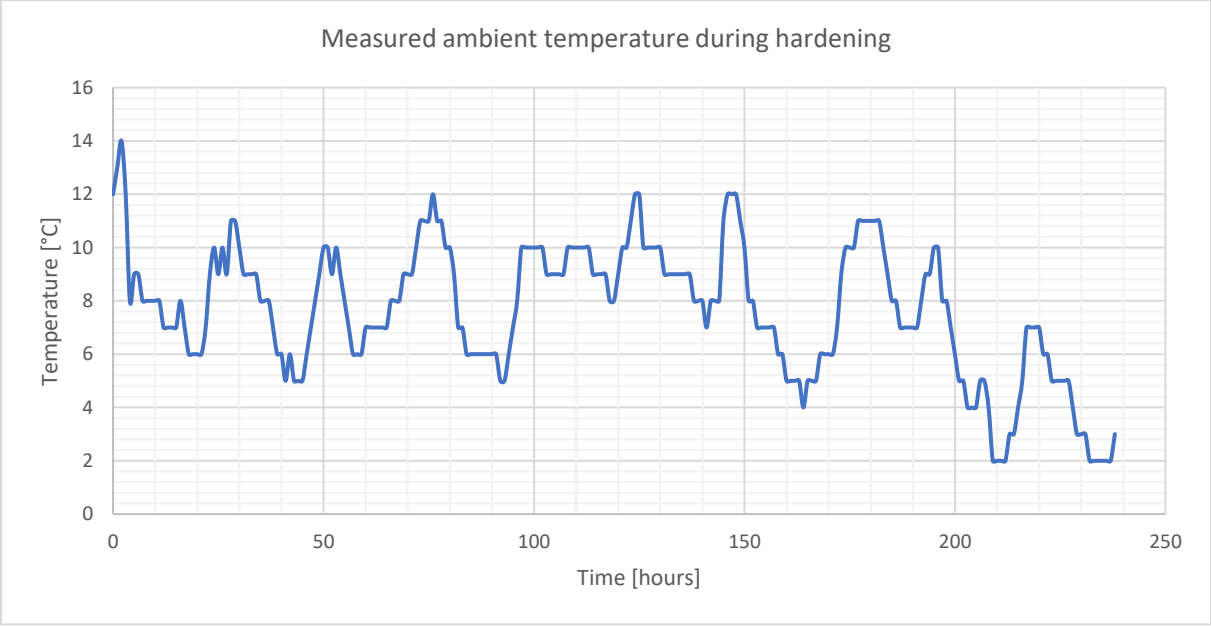

figure 124 Measurement results of the ambient temperature in practice

11.3.3 Concrete mixture

In the end it must be checked whether the concrete mixture that was used in casting of the concrete wall corresponds to the mixture that was used in the laboratory tests. There were several different mixtures that could have been used which all have a different aggregate gradation. The aggregate gradation varies between 4-16 mm and 4-32 mm. In the end was decided to use the fine concrete mixture (4-16 mm) for the bottom ~1.5 m of the wall and to use the coarse mixture (4-32 mm) for the remainder of the wall.

The concrete mixture that was used in the laboratory tests corresponds to the fine mixture that was used in the bottom region of the wall. Also, the bottom region of the wall is most relevant regarding early-age cracking. It can therefore be concluded that the laboratory tests are applicable in the assessment of early-age cracking of the wall.

11.4 Discussion

The results of the visual inspections and temperature measurements will be discussed here. The way in which the results can be used in the analysis of early-age cracking and the calibration of the finite element model will also be discussed.

- The measured temperatures in the core of the wall do not correspond to what was initially assumed in the FEA. This has to do not only with the initial mix temperature, but also with the rate of hydration. This is concluded from the fact that the measured temperature increase is higher than was initially assumed and the maximum temperature is also reached earlier. To ensure that the temperature development of the wall in the FEA corresponds to the measurements, changes should be made in the material parameters and the model.
- The measured ambient temperature can directly be used in the FEA regarding early-age cracking. This will increase the accuracy of the model and will be done in the next section.
- For the time period that was considered in the current analysis, early-age cracking was not observed in any of the walls that were inspected. The fact that the concrete did not crack during hardening in this period indicates that the tensile strength of the concrete was not exceeded at any point in time. This should be taken into account when analysing the results of the FEA of the wall using the updated model and material parameters as will be done in the next section.
- Cracking of concrete wall was observed after a period of cold clear nights after around 38 days of hardening. Cooling of the wall due to the low ambient temperatures would have increased the tensile stress. The fact that the wall subsequently cracked indicates that the stresses that developed during the cooling phase of the hydration process were (to a large extent) still present. This implies that the effect of stress relaxation at higher ages is limited. To further investigate this effect however lies outside of the scope of this study.
- The fact that during the inspections a total of 5 walls were considered instead of only 1 wall as was initially assumed, increases the reliability of the conclusion that early-age cracking of the Southern wall of segment 12 did not occur within the time window regarding early-age cracking.
- As is already discussed above, in the next section the finite element model of the cross-section of the wall will be modified to correspond to the measurements as presented in this section. Subsequently the assessment of the risk of early-age cracking will be redone. The results will then be compared with the results of the visual inspections and the TSTM test. In this way conclusions can be drawn on the accuracy of the model and the input parameters.

12 Final assessment of the risk of early-age cracking

Now that the results of the laboratory tests have been processed, the viscoelastic material behaviour has been derived and the temperature development in the wall during hardening is known, the assessment of the risk of early-age cracking in the wall can be redone. Because the uncertainties in the relevant material parameters have been reduced, the accuracy of this assessment will increase.

12.1 Updated temperature development in the wall

As is discussed in the previous section on the temperature measurements, the temperature development in the wall according to the initial FEA does not correspond to the measured temperature development during hardening in practice. This is on the one hand caused by a difference in initial mix temperature and on the other hand by a difference in maximum temperature increase.

To be able to accurately model the hardening process of the wall, the temperature development according to the FEA for the centre of the cross-section should correspond to the measured temperature development in practice. To achieve this, changes are made in the thermal properties of the concrete mixture and the thermal boundary conditions of the cross-section of the wall. The parameters that are adjusted are listed here:

- Adiabatic temperature rise
- Convection coefficient

The parameters are varied in an iterative process to fit the temperature curve of the centre of the wall to the measured temperature curve. In this iterative process the adiabatic curve was adjusted by increasing the total temperature rise and the rate of hydration. The convection coefficients at the edges of the wall were adjusted to fit the temperature development at later ages. This process was repeated until the temperature development of the analysis corresponded to the measured temperature development. There are several possible combinations of the above described parameters that result in similar temperature curves for the centre of the cross-section. The temperature gradient over the cross-section may however vary for each possible combination. To investigate the effect of possible variations in temperature gradient over the wall, there are two parameter combinations that will be considered. The resulting temperature curves can be seen in figure 125.

As can be seen from the figure, the temperature curves that result from the FEA of the cross-section of the wall now corresponds to the measured temperature curve. This holds for both combinations of adiabatic temperature rise and convection coefficient. The used combinations will not be discussed in more detail because they are comprised only to be able to fit the measured temperature curve and not to derive the actual thermal properties of the material.

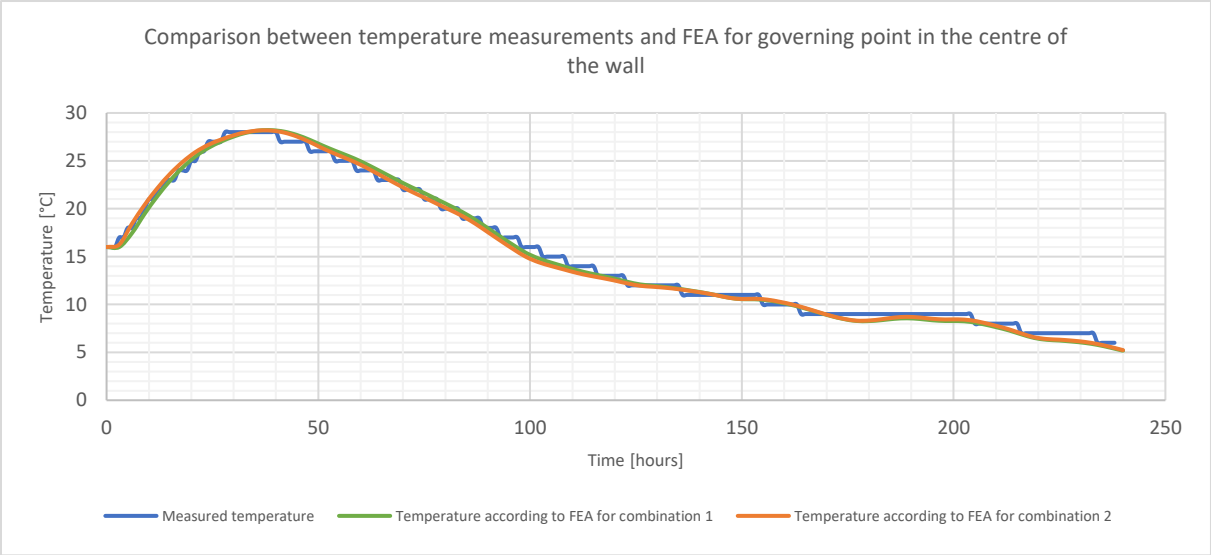

figure 125 Comparison between the measured temperature curve and the temperature curves according to the FEA using the adjusted thermal properties

12.2 Results

Because the temperature development in the centre of the cross-section of the wall according to the FEA now corresponds to the measured temperature, the analysis regarding early-age cracking can be redone. In this analysis the measured material parameters and the viscoelastic material behaviour that is fitted from the TSTM test are used. The results can be seen in figure 126 below. In this figure also the stress development that results from the analysis in which the initially assumed 'high creep' viscoelastic material behaviour is used can be seen.

Because the stress development over time is almost identical for both thermal parameter combination 1 and 2, the effect of variations in these parameters on the stress development can be assumed to be negligible. It is therefore decided to not use the distinction between the two combinations in the figure below.

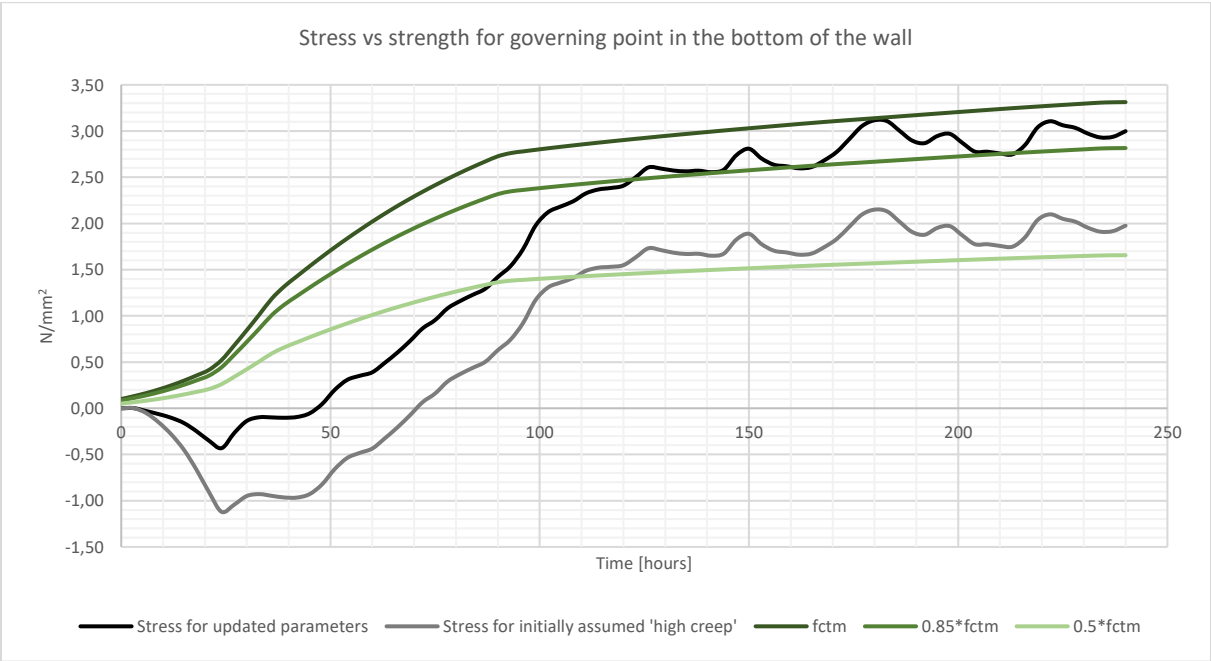

figure 126 Stress and strength development resulting from the FEA using the updated model- and material properties

As can be seen from the figure, using the fitted viscoelastic material behaviour strongly reduces the compressive stresses in the wall which is in correspondence with the results of the TSTM test. However, as a result during the cooling period the tensile stresses are increased. The tensile stress exceeds the $0.85f_{ctm}$ limit and at a certain moment in time even the f_{ctm} limit is almost exceeded. As is confirmed by van Breugel et al. (1996), this indicates a very high probability of cracking.

12.3 Discussion

Here the results of the assessment of early-age cracking using the updated model and material properties as presented in the figures above will be discussed. Also, they will be compared to the observations from the visual inspections and the results of the TSTM test. Conclusions will be drawn on the accuracy of the model and the input parameters.

Combinations of thermal properties:

- There are two combinations of adiabatic temperature rise and convection coefficients that are considered when fitting the temperature curve as follows from the FEA to the temperature curve as measured in practice. As is stated before, for both combinations holds that the resulting temperature development corresponds to the measurements in practice.

- The reason that two different combinations of the above described thermal properties are used is that while the temperature development for the centre of the cross-section may be equal, the temperature gradient over the thickness of the wall may be different. A difference in temperature gradient over the thickness of the wall could subsequently lead to a change in stress development for the governing point in the centre of the cross-section

- As is already mentioned during the presentation of the results, the effect of using different combinations of the above described thermal properties on the stress development turns out to be negligible. A distinction between the different combinations is therefore not made in the figure on the stress development in the wall.

Stress development and the risk of early-age cracking according to the FEA:

- As is stated before, using the viscoelastic material behaviour as is derived from the model of the TSTM test, the compressive stresses at early-ages are strongly reduced. As a results the stress curve is 'shifted' and the tensile stresses at higher ages are increased. This increases the probability of cracking.

- Because according to the FEA the $0.85f_{ctm}$ tensile stress limit is exceeded during hardening, early-age cracking is very likely to occur. However in practice early-age cracking did not occur in any of the inspected walls. It can therefore be concluded that the current model does not yet fully represent the hardening process of the wall in practice and that the stress development in the wall in practice is different from the stress development as evaluated in the FEA. There are several possible causes for this difference which will next be discussed in more detail.

Difference between the results of the FEA and the observations in practice:

- The fact that using the updated model- and material parameters results in an increase of tensile stresses and thus probability of cracking at higher ages is caused by the reduction of the compressive stress at early-ages as is explained before. The reduction of compressive stresses at early-ages is caused by the increase of the effects of creep and stress relaxation for this period

during hardening. The increase in the effects of creep- and relaxation at early-ages is derived from the TSTM modelling. During the TSTM test the measured compressive stresses were relatively low and together with the autogenous swelling that was taken into account in the model this resulted in the fact that the effects of creep and stress relaxation at early-ages had to be increased while fitting of the TSTM model to the measured stresses during the TSTM test. It could be that the due to friction in the TSTM, the measured compressive stresses at early-ages is lower than the stress that was actually developing in the concrete specimen. This possible reduction in stresses due to the effects of friction would then only affect the stress at early-ages. There is however not further evidence to support this theory.

- Following the above described theory, the effects of creep and stress relaxation at early-ages as are derived from the TSTM model could be incorrect and would be lower in practice. If the effects of creep- and stress relaxation at early-ages would be reduced in the FEA, the resulting tensile stress would also be reduced which could make that the results of the FEA then correspond to the observations in practice, as is currently not the case.

- As is discussed before, the viscoelastic material behaviour at early-ages is derived from the TSTM test. Because the actual temperature development in the wall was yet unknown when the TSTM test was performed, the prescribed temperature development in the test had to be based on the initial FEA of the wall. The temperature development during the test did therefore not correspond to the actual temperature development of the wall in practice. The finite element software makes use of a maturity model to determine the material properties over time based on the temperature history of the concrete. In this way the effect of the concrete temperature during hardening is taken into account. It could however be that the effect of the concrete temperature on the viscoelastic material behaviour is greater than is now taken into account in the model. This would cause a difference in the viscoelastic material behaviour that is observed in the TSTM test and the actual behaviour of the material in practice.

- Following the theory above, it must be noted that the concrete temperature during the TSTM test was lower compared to the temperature of the wall in practice. Because the effects of creep and stress relaxation on the stress formation in practice seem to be overestimated in this test, this would indicate that the effects of creep and stress relaxation would increase for decreasing temperature. The question however remains whether this behaviour could actually be occurring in practice.

- Something that was already mentioned in the discussion of the laboratory results but should also be discussed here is the fact that the aggregate distribution of the concrete mixture as used in the laboratory testing deviates from the concrete mixture that was used in casting of the walls of the dive-under. In the concrete mixture as was provided Mebin b.v., use was made of an additional 0-2 mm aggregate fraction, which was not available at the TU Delft. At the TU Delft this additional fraction was added up with the 0-4 mm aggregate fraction. It is however expected that the effect of this deviation on the results of the tests is limited.

- The thermal properties of concrete were discussed in more detail in the literature study. It was stated that the thermal conductivity, thermal capacity and the coefficient of thermal expansion are time dependent properties of which the magnitude varies over time during hardening. In the current analysis however, these properties were assumed to be constant. This could have a

negative effect on the accuracy of the analysis and could therefore contribute to the fact that the results do not correspond to the observations made in practice.

- The question arises whether there are any mechanisms that play a role in the hardening process which are not taken into account in the current model. Non-linear effects are for example not taken into account and also the moisture content of the material is not considered in the analysis. What additional mechanisms should be taken into account and their effect on the probability of early-age cracking is however yet to be determined.

13 Conclusions and recommendations

13.1 Conclusions

Based on the laboratory testing, the finite element analysis regarding the risk of early-age cracking and the observations from practice the following conclusions can be drawn:

- Overall it can be concluded that the material behaviour in the first two days after casting is very important for the overall stress development in the concrete when it is subject to imposed deformations.

- Based on the TSTM test it can be concluded that the effects of creep and stress relaxation in the early-ages of hardening are generally underestimated in engineering practice. New creep curves are derived, based on the TSTM model that describe the viscoelastic material behaviour at early-ages. More research is needed into this viscoelastic material behaviour at early-ages in general.

- From the finite element analyses that were performed it can be concluded that for the current case of imposed deformations, the increased effect of stress relaxation during the heating phase at early-ages is not beneficial regarding the risk of early-age cracking. Stress relaxation in this phase has the effect of decreasing the maximum compressive stress, but will cause an increase in maximum tensile stress during the subsequent cooling phase, increasing the risk of cracking.

- Using the current model, the risk of early-age cracking cannot be assessed accurately. This is concluded from the fact that the results of the FEA do not correspond to the results of the visual inspections in practice. According to the results of the FEA, early-age cracking should occur. This is however not observed in practice. It can be concluded that without the availability of accurate data on the viscoelastic material behaviour of the specific concrete mixture at early-ages (first 48 hours), the assessment of the risk of early-age cracking will be inaccurate and will not correspond to observations in practice.

- In the first days after hardening, autogenous swelling of the concrete was observed. The autogenous swelling as was measured during the ADTM cannot be neglected in the analysis because it has influence on the stress development in the material.

- For the specific concrete mixture that was used in the laboratory testing holds that the strength development at early-ages is overestimated by the Eurocode- and Model Code. The strength at higher ages is however underestimated.

- The coefficient of thermal expansion and the thermal capacity are thermal material properties that have a relatively large influence on the ratio between the stress and strength in the finite element analysis. Under- or overestimation of these parameters will have a negative influence on the accuracy of the assessment of the risk of early-age cracking. Also, the magnitude of these parameters is not constant over time. Assuming them to be constant in the analysis may lead to less accurate results.

- The initial concrete mix temperature has a relatively large influence on the stress development in the analysis. Overestimation of the initial mix temperature results in an increase of the

temperature drop in the cooling phase which, when restrained, causes an increase in tensile stress in the analysis. The initial mix temperature in the analysis should therefore always correspond to the initial mix temperature in practice.

- A cross-sectional analysis of the hydration process of the concrete wall and slab gives insights in the effects of temperature gradients over the wall and the restraining effects of the slab on the stress development over time. In this way the assessment of the risk of early-age cracking can be done for the governing point in the cross-section of the wall. When a longitudinal section of the wall and slab is modelled, insights are gained in the stress development over the length of the wall. Temperature gradients over the width of the wall are however not taken into account and only averaged temperature developments can be used. The results of both analyses do not fully correspond. The cross-sectional analysis is therefore considered to be most reliable in this study.

- The Maxwell chain model is used to model the viscoelastic material behaviour of the material in the analysis. To be able to accurately model the material behaviour, several units with different retardation times are needed. When too little units are used, the results become inaccurate and the material behaviour cannot be modelled properly. The actual material behaviour is fitted from the TSTM model using the Maxwell chain data. New creep curves are derived based on this chain data.

13.2 Recommendations

1. More research is needed on the effects of creep and stress relaxation on concrete stresses at early-ages. This viscoelastic material behaviour at early-ages turns out to be highly important for the stress development in the material at higher ages. However in literature only limited data is available on this particular material behaviour.

2. For the early-age creep data that is available holds that the data is mainly based on concrete containing OPC, there is little data available on concrete containing blast furnace slag cement CEMIII/B as is used in this study. More early-age creep measurements on concrete containing BFS cement are therefore needed.

3. The fact that cracking of the walls was observed at later ages (around 30-40 days after hardening) which lie outside of the scope of this study, indicates that the stresses that develop during the initial cooling phase as part of the hydration process are (to a large extent) still present at later ages. This implies that the effect of stress relaxation at later ages is limited. More research is therefore needed on the effect of stress relaxation at later ages. In this way a better understanding could be gained in the fact that cracking of the walls only occurred at higher ages.

4. The effect of concrete temperature on the viscoelastic material behaviour should be investigated in more detail. The concrete temperature could have an even greater effect on the effects of creep- and stress relaxation than is taken into account using the maturity model in the current FEA.

5. The analysis as is performed in this study where the results of laboratory testing and a finite element analysis are compared with observations in practice should be done for more cases in which young concrete is subjected to imposed deformations. By repeating the method of this study for several similar cases the conclusions that are drawn in this study can be supported and/or rejected.

6. To ensure that thermal strains are not included in the ADTM measurements, multiple temperature measurements over the cross-section of the concrete specimen are needed. This should be taken into account when performing a ADTM test in the future.

7. In the Eurocode autogenous shrinkage is assumed to develop instantly after the moment of casting of the concrete. This is however contradicted by the laboratory tests which suggest that the period of autogenous swelling prior to the period of shrinkage should also be taken into account. Taking the period of autogenous swelling into account influences the stress development during hardening.

8. Using the current set-ups of the ADTM and TSTM test, measurements can only be initiated after the concrete has gained some stiffness. This moment in time is however difficult to determine which could lead to incorrect measurements in this first hours of measuring. If the testing set-ups could be modified to be able to initiate the measurements sooner after casting of the concrete, more data could be collected on the material behaviour at early-ages.

9. Thermal properties of the concrete mixture like the thermal conductivity, thermal capacity and coefficient of thermal expansion are time dependent which means that their magnitude changes during hardening. In the current analysis these parameters were however assumed to be constant because accurate data on the development of these properties was not available. To increase the accuracy of similar analyses in the future, measurements should be done to determine the development of these thermal properties over time during hardening. For these measurements also holds that the first days of hardening are of high importance.

10. It can in the end be concluded that it is the combination of the different material properties and model parameters that determine the stress development during hardening. For all parameters holds that the magnitude at early-ages is of high importance. It should therefore be considered to do measurements more measurements on material properties at very early-ages (0-48 hours).

Bibliography

1. Al-Gburi, M. (2015). Restraint effects in early-age concrete structures.
2. Bamforth, P.B. (2007). Early-age thermal crack control in concrete. Publication C660, CIRIA.
3. Bamforth P.B. (1980). In situ measurement of the effect of partial Portland cement replacement using either fly ash or ground granulated blast-furnace slag on the performance of mass concrete.
4. Barnett, S.J. & Soutsos, M.N. & Millard, S.G. & Bungey, J.H. (2006). Strength development of mortars containing ground granulated blast-furnace slag: Effect of curing temperature and determination of apparent activation energies.
5. Bažant, Z. & Wendner, R. & Hubler, M. (2014). NU Database of laboratory creep and shrinkage data. Northwestern University.
6. Bažant, Z.P. & Wu, S.T. (1991). Rate-type creep law of aging concrete based on Maxwell chain
7. Bažant, Z.P. & Osman, E. (1989). Double power law for basic creep of concrete.
8. Bažant, Z.P. (1988). Mathematical modelling of creep and shrinkage of concrete, Chapter 2: Material models for structural creep analysis.
9. Bentz, D.P. & Weiss, W.J. (2010). Internal curing: A 2010 State-of-the-art review.
10. Bentz, D.P. & Sant, G. & Weiss, J. (2008). Early-age properties of cement-based material I: Influence of cement fineness.
11. Bouquet, G.Chr. (2019). Effect of relaxation on eigenstresses and microcracking in concrete under imposed deformation.
12. CEB-FIB (2012). Model Code 2010.
13. Chengju, G. (1989). Maturity of Concrete: Method for predicting early-age strength.
14. de Schutter, G. (2003). Applicability of degree of hydration concept and maturity method for thermo-visco-elastic behaviour of early age concrete.
15. Fairbairn, E. et al. (2013).Thermal cracking of massive concrete structures. RILEM TC 254 CMS.
16. Femmasse B.V. (2006). User manual MLS version 8.5.
17. Femmasse B.V. (1996). HEAT version 6.2 manual : Material models.
18. Fernandez-Jimenez, A. & Puertas, F. (1997). Alkali-activated slag cements : Kinetic studies.
19. Giatech Scientific (2017). The history of concrete. Retrieved from https://www.giatecscientific.com/education/the-history-of-concrete/
20. Habel, K. (2004). Structural behaviour of elements combining ultra-high performance fibre reinforced concretes (UHPFRC) and reinforced concrete.
21. Holt, E.E. (2001). Early age autogenous shrinkage of concrete.
22. Japan Society of Civil Engineers (2007). Standard specifications for concrete structures: Design.
23. Jensen, O.M. (2000). Influence of cement composition on autogenous deformation and change of the relative humidity.
24. Kelly, P.A. (2015). Solid Mechanics part I: An introduction to Solid Mechanics. Chapter 10: Viscoelasticity.
25. Kim, S.G. (2010). Effect of heat generation from cement hydration on mass concrete placement.
26. Kim, K.H. & Jeon, S.E. & Kim, J.K. & Yang, S. (2002). An experimental study on thermal conductivity of concrete
27. Lee, K.M. & Lee, H.K. & Lee, S.H. & Kim, G.Y. (2006). Autogenous shrinkage of concrete containing granulated blast-furnace slag.
28. Lokhorst, S.J. (2001). Deformational behaviour of concrete influenced by hydration related changes of the microstructure.

29. Lu, T. (2019). Autogenous shrinkage of early age cement paste and mortar.
30. Lu, T. & Koenders, E. (2014). Modelling and analysing autogenous shrinkage of hardening cement paste.
31. Lura, P. & Jensen, O.M. & van Breugel, K. (2003). Autogenous shrinkage in high-performance cement paste: An evaluation of basic mechanisms.
32. Mors, R.M. (2011). Autogenous shrinkage: Cementitious materials containing BFS.
33. Mazloom M. & Ramezanianpour, A.A. & Brooks, J.J. (2004). Effect of silica fume on mechanical properties of high-strength concrete.
34. Maekawa, K. & Ishida, T. & Kishi, T. (2003). Multi-scale modelling of concrete performance: Integrated material and structural mechanics.
35. Mindess, S. & Young, J.F. & Darwin, D. (2003). Concrete, 2nd edition.
36. Naghdi, R. (2013). Evaluation of autogenous shrinkage of high-performance concrete.
37. NEN-EN 197-1. Cement – Part 1: Composition, specifications and conformity criteria for common cements
38. NEN-EN 1992-1-1+C2, Eurocode 2: Design of concrete structures – Part 1-1: General rules and rules for buildings.
39. NEN-EN 1992-3, Eurocode 2: Design of concrete structures - Part 3: Liquid retaining and containment structures.
40. Neville, A.M. 2011). Properties of Concrete, 5th edition.
41. NOE B.V. (2017). Product information NOE top panel. Retrieved from https://www.noe.de/NOE_Downloadbereich/public/productgroup/13?pgid=11&agid=13
42. Page, C.L. & Page, M.M. (2007). Durability of concrete and cement composites.
43. Punkki, J. (2010). CIV-E2020 Concrete technology, Lecture 2: Portland cement
44. Reinhardt, H.W. (1985). Beton als constructiemateriaal – eigenschappen en duurzaamheid.
45. Smithsonian (2011). The Secrets of ancient Rome's buildings. Retrieved from https://www.smithsonianmag.com/history/the-secrets-of-ancient-romes-buildings-234992/
46. Tazawa, E. & Miyazawa, S. (1995). Influence of cement and admixture on autogenous shrinkage of cement paste.
47. The American Society of Mechanical Engineers (2017). Ancient roman concrete stands the test of time. Retrieved from https://www.asme.org/topics-resources/content/ancient-roman-concrete-stands-test-time
48. van Beek, A. & Baetens B.E.J. & Schlangen, E. (2001). Numerical model for prediction of cracks in concrete structures.
49. van Breugel, K. et al. (2018). CIE5130 Capita Selecta of concrete structures. TU Delft.
50. van Breugel, K. et al. (2017). CIE5110 Concrete – Science and Technology. TU Delft.
51. van Breugel, K. et al. (1996). Concrete structures under imposed thermal and shrinkage deformations - Theory and Practice. Betonpraktijkreeks 2.
52. van Breugel, K. (1980). Relaxation of young concrete.
53. Velds, C.A. (1994). Zonnestraling in Nederland. Koninklijk Nederlands Meteorologisch instituut, de Bilt.
54. Wu, L. & Farzadnia, N. & Shi, C. & Zhang, Z. & Wang, H. (2017). Autogenous shrinkage of high performance concrete: A review.
55. Wu, X. & Roy, D.M. & Langton, C.A. (1983). Early age hydration of slag-cement
56. Yeon J.H. & Choi, S. & Won, M.C. (2013). In situ measurement of coefficient of thermal expansion in hardening concrete and its effect on thermal stress development.
57. 99% Invisible, Kohlstedt, K. (2017). Cracking the case: science solves ancient mystery of durable roman concrete. Retrieved from https://99percentinvisible.org/article/cracking-case-secret-ingredient-explains-durability-roman-concrete/

Appendix A: Results of parameter study

- **Thermal conductivity**

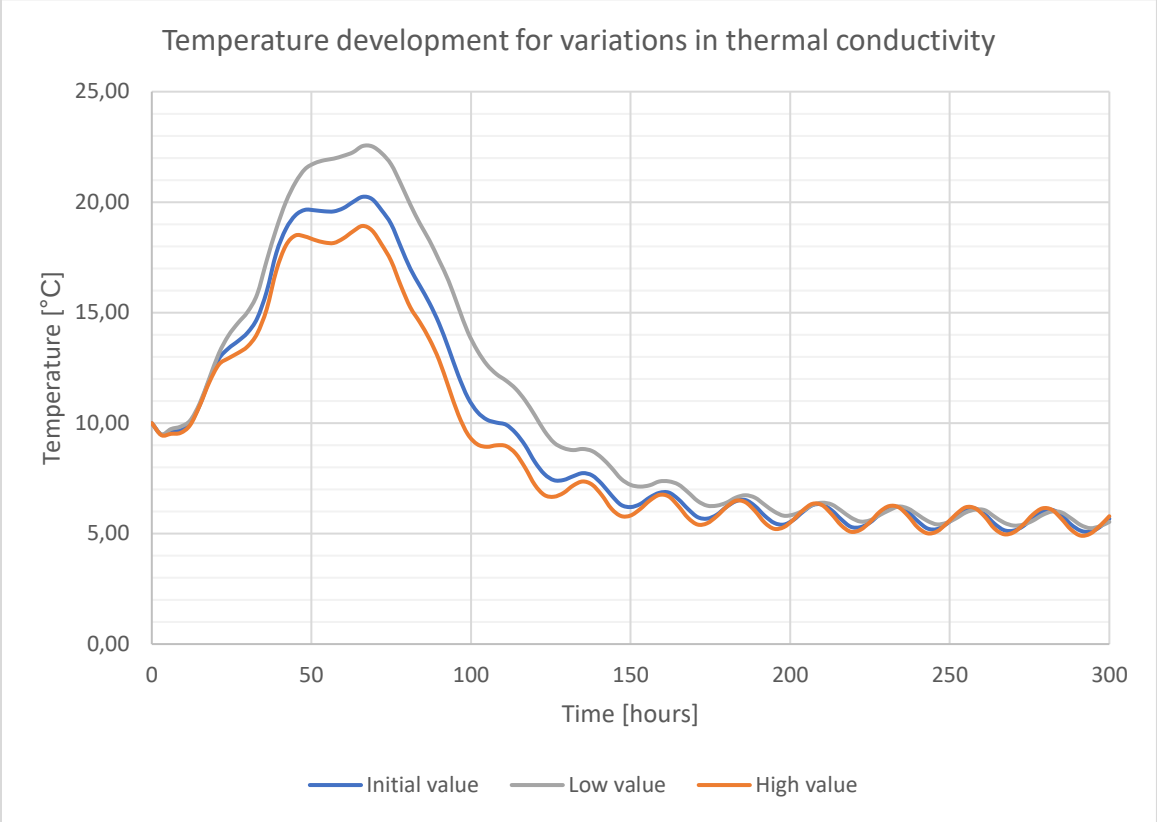

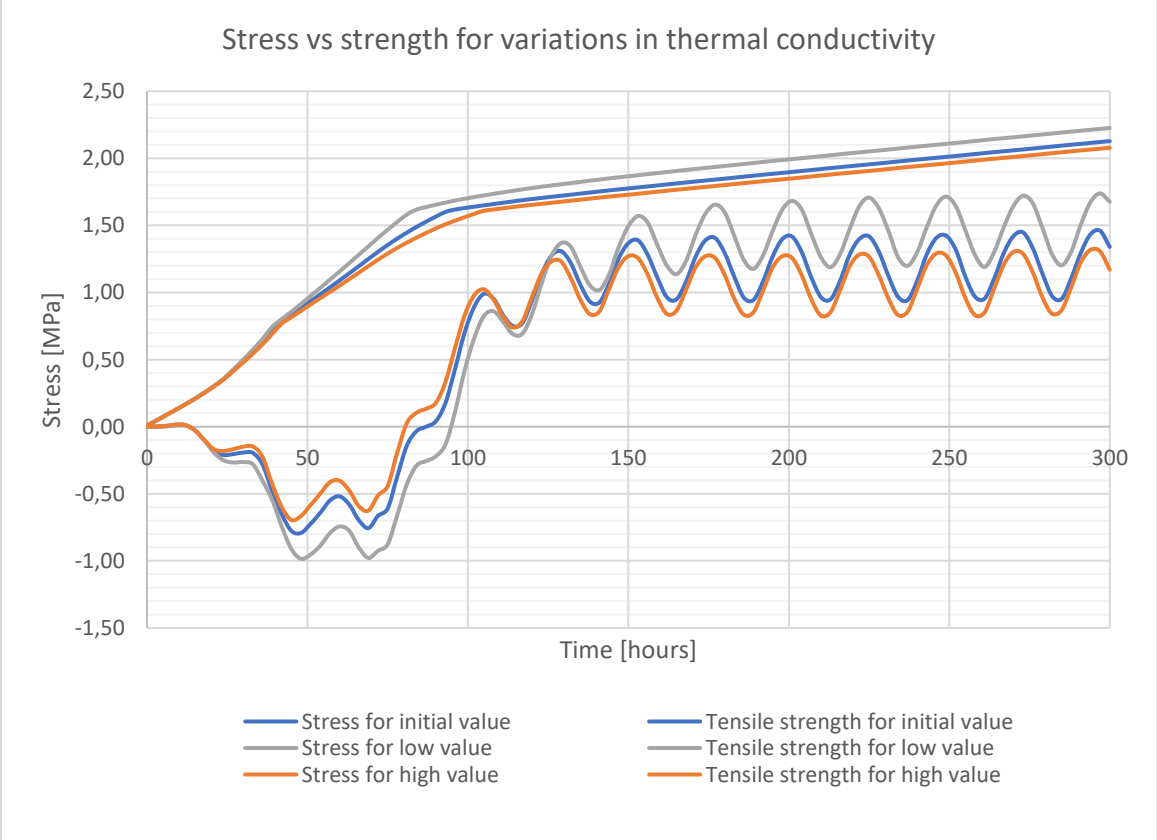

- **Activation energy**

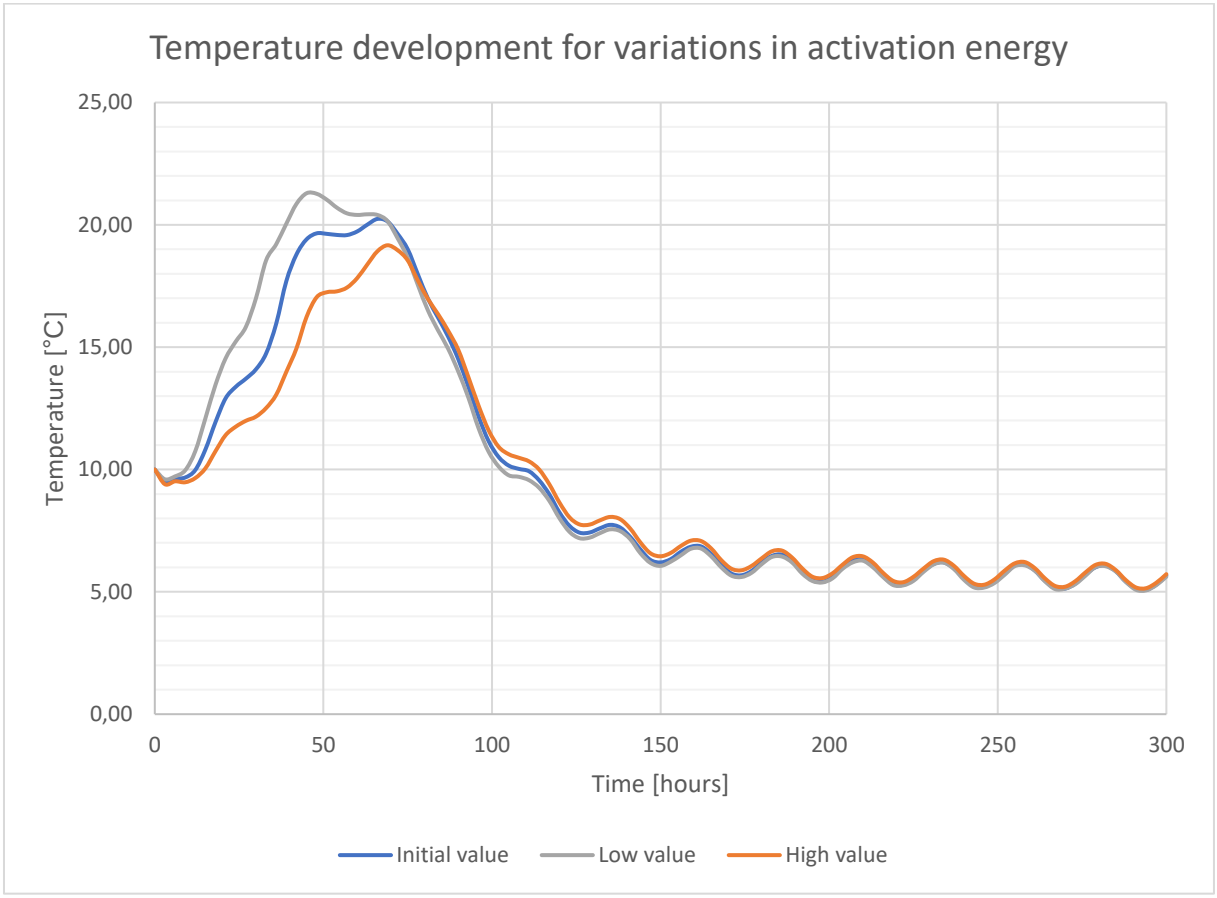

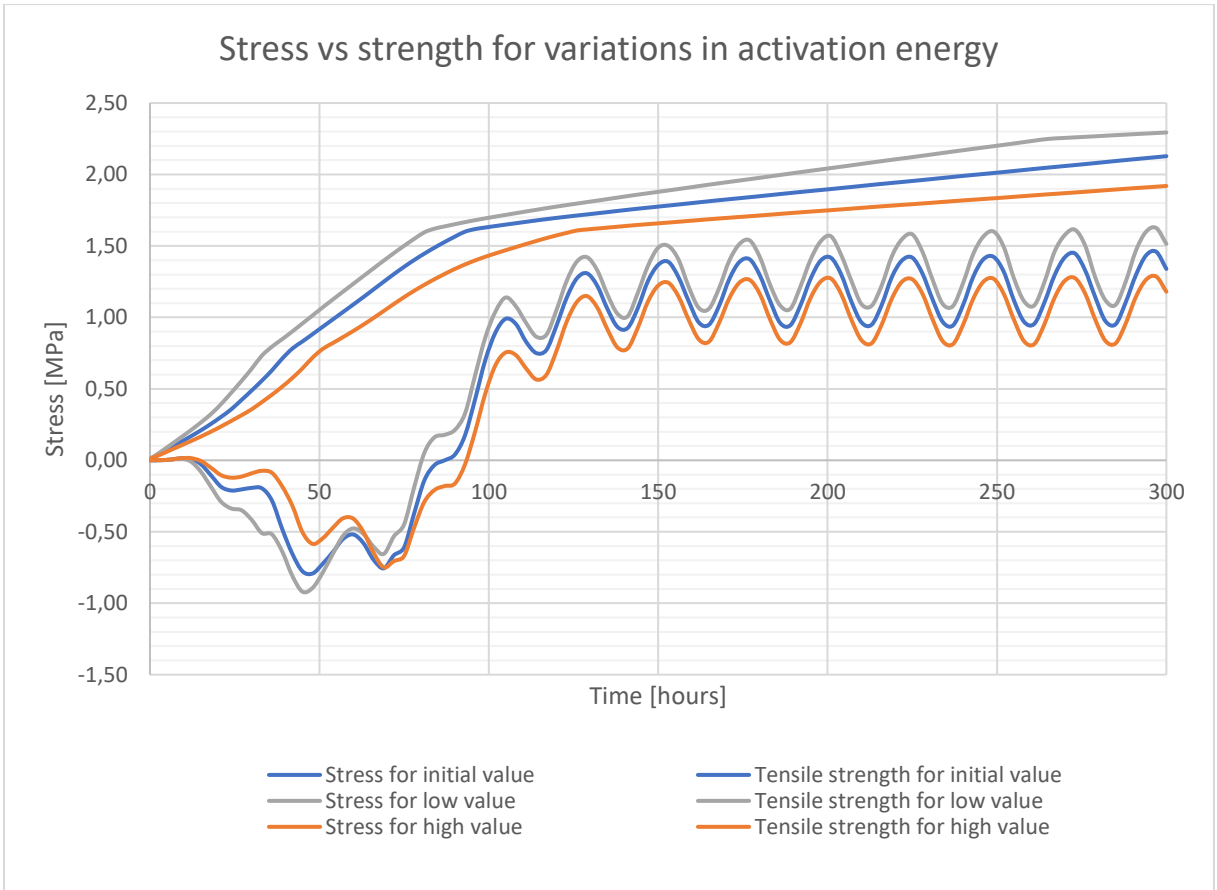

- **Thermal capacity**

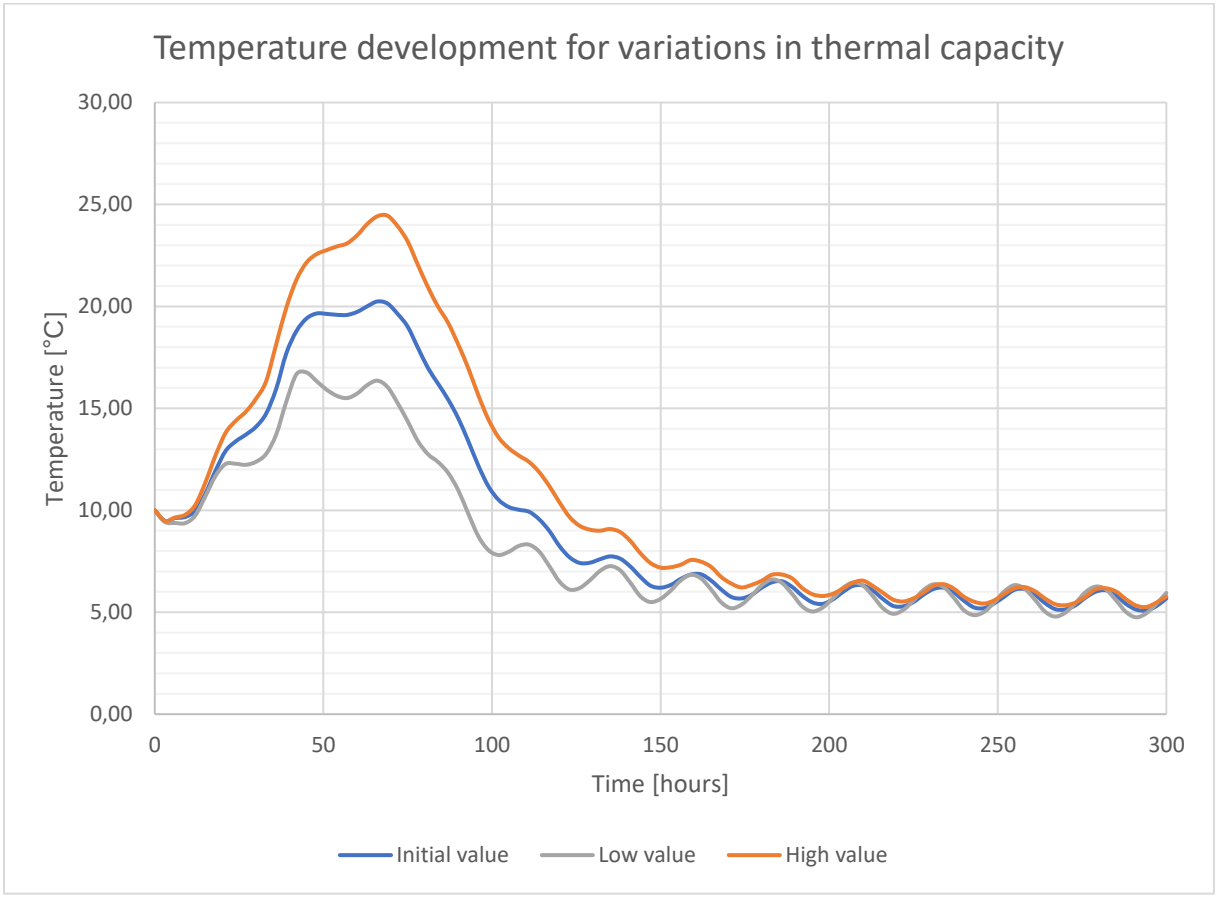

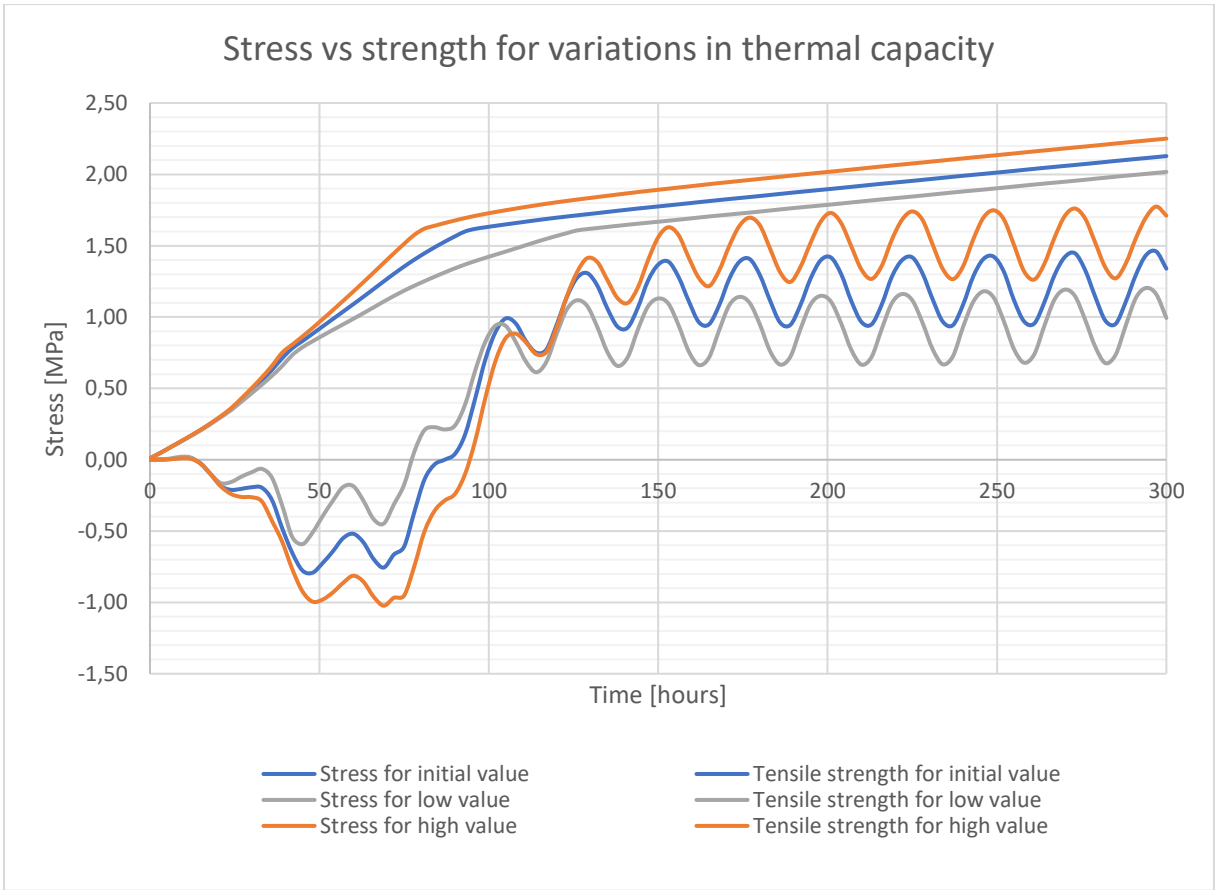

- **Poisson's ratio**

Variations in the Poisson's ratio do not result in changes in temperature development. Therefore only the strength- and stress development is shown here. Besides, because the temperature development does not change, neither does the strength develop change. This can be seen in the figure below.

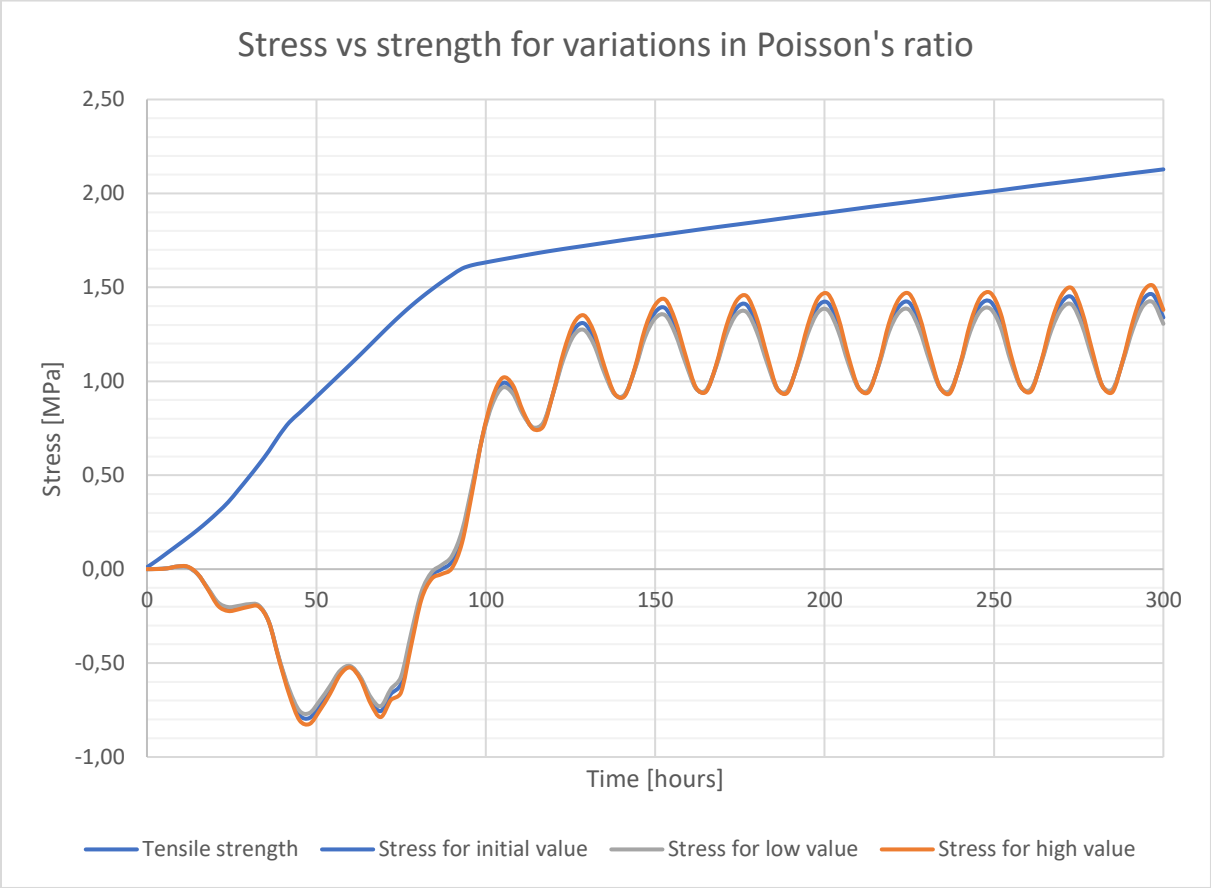

- **Expansion coefficient**

Like for the Poisson's ratio, for the expansion coefficient also holds that the temperature development and subsequent strength development does not change.

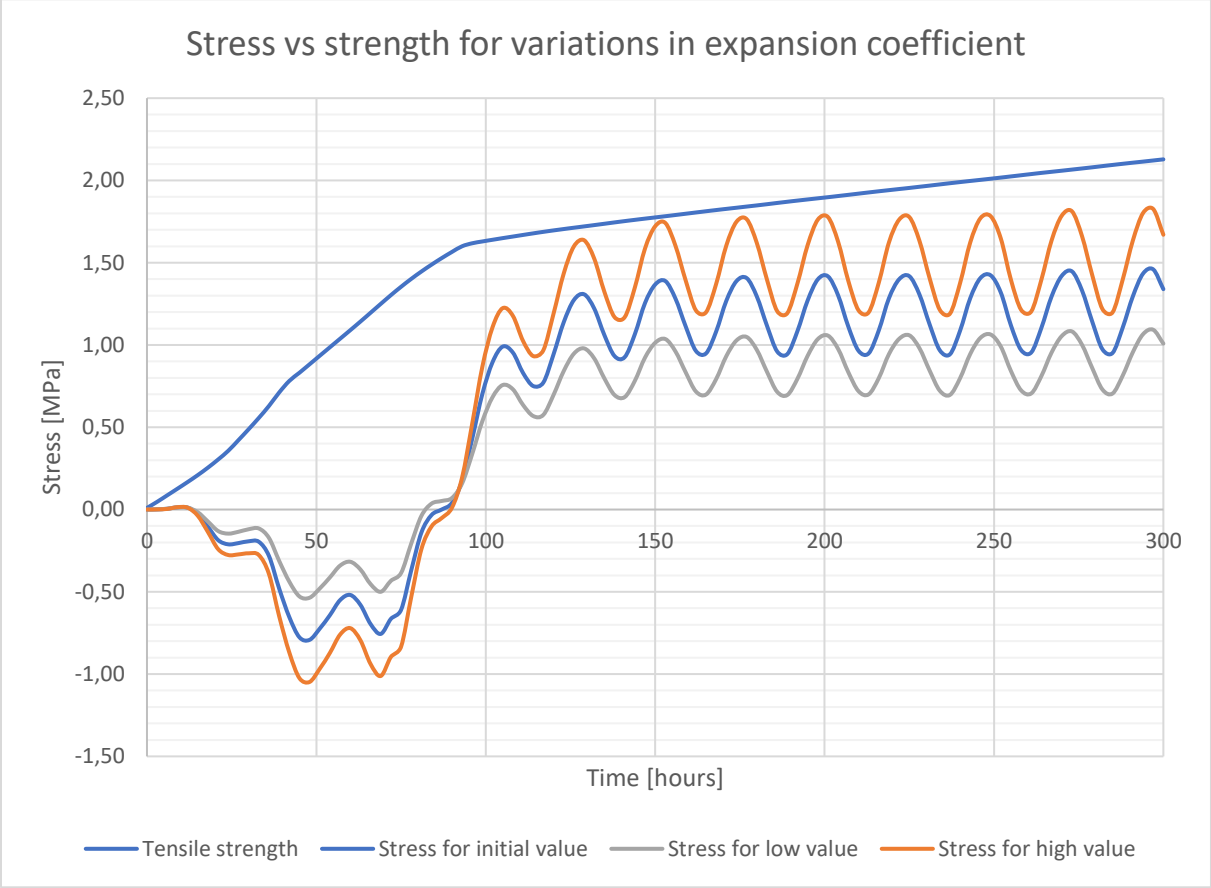

- **Initial mix temperature**

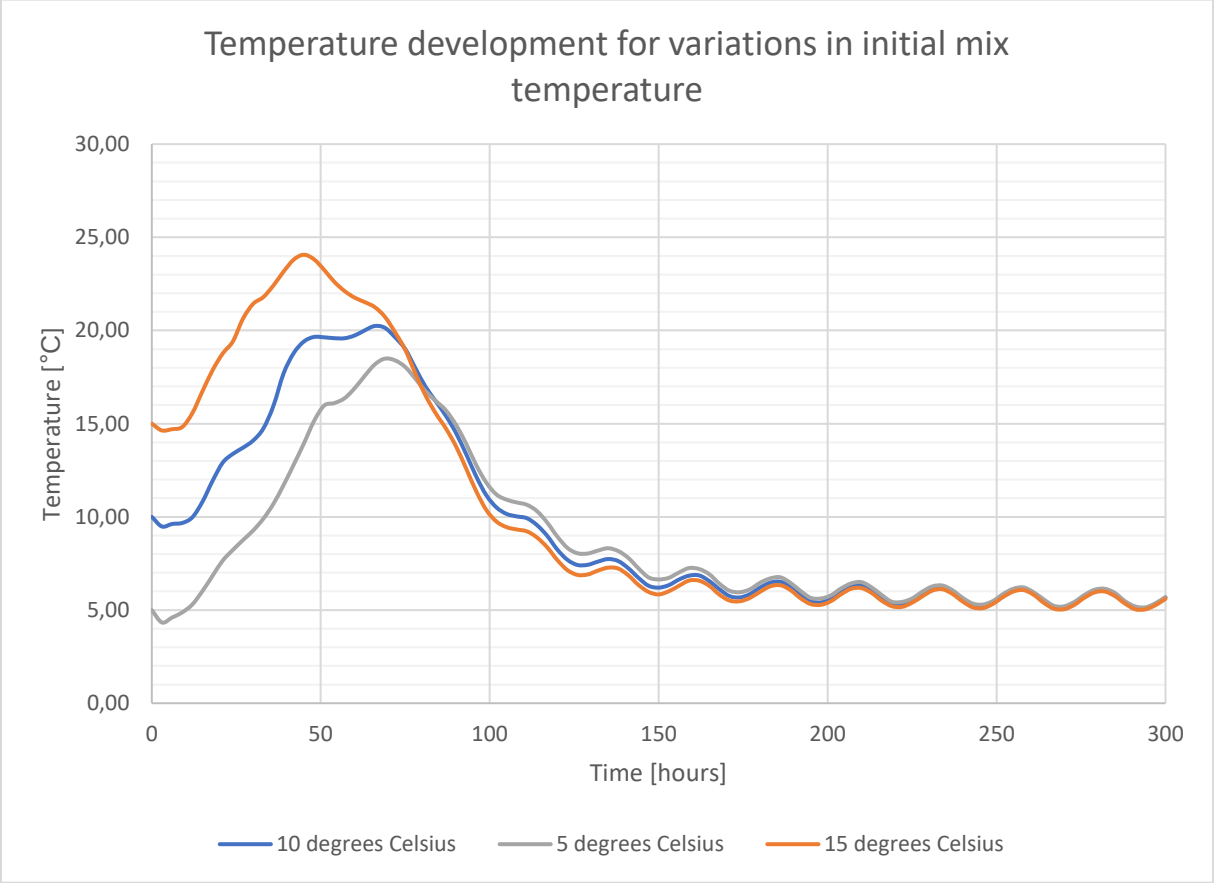

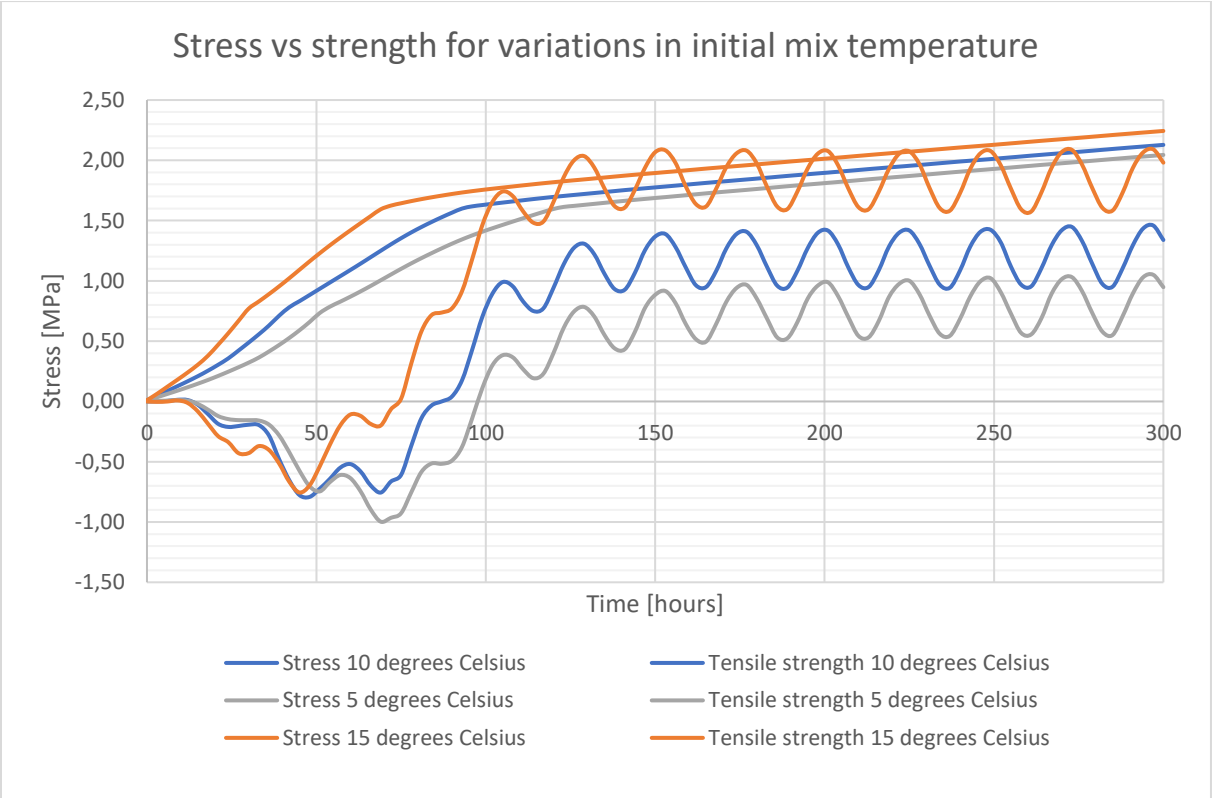

- **Mean ambient temperature**

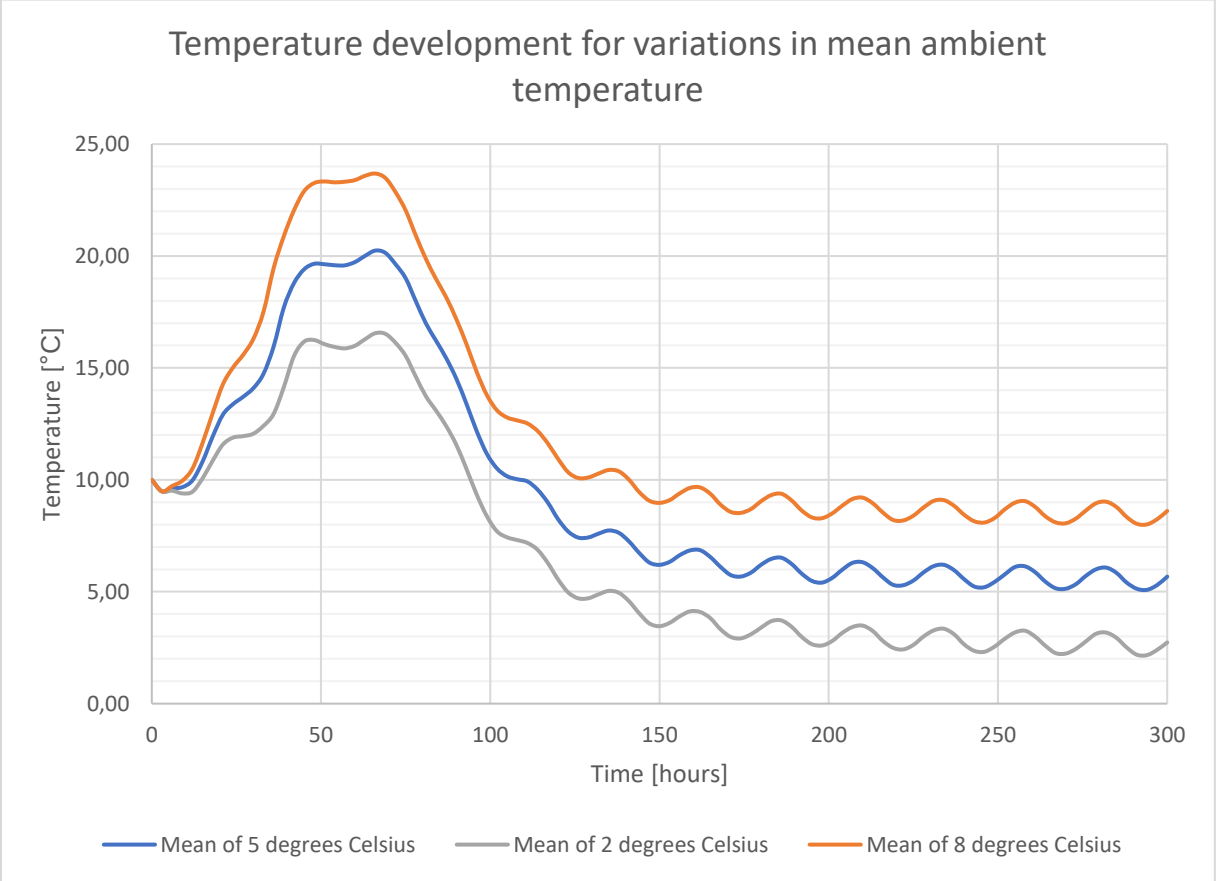

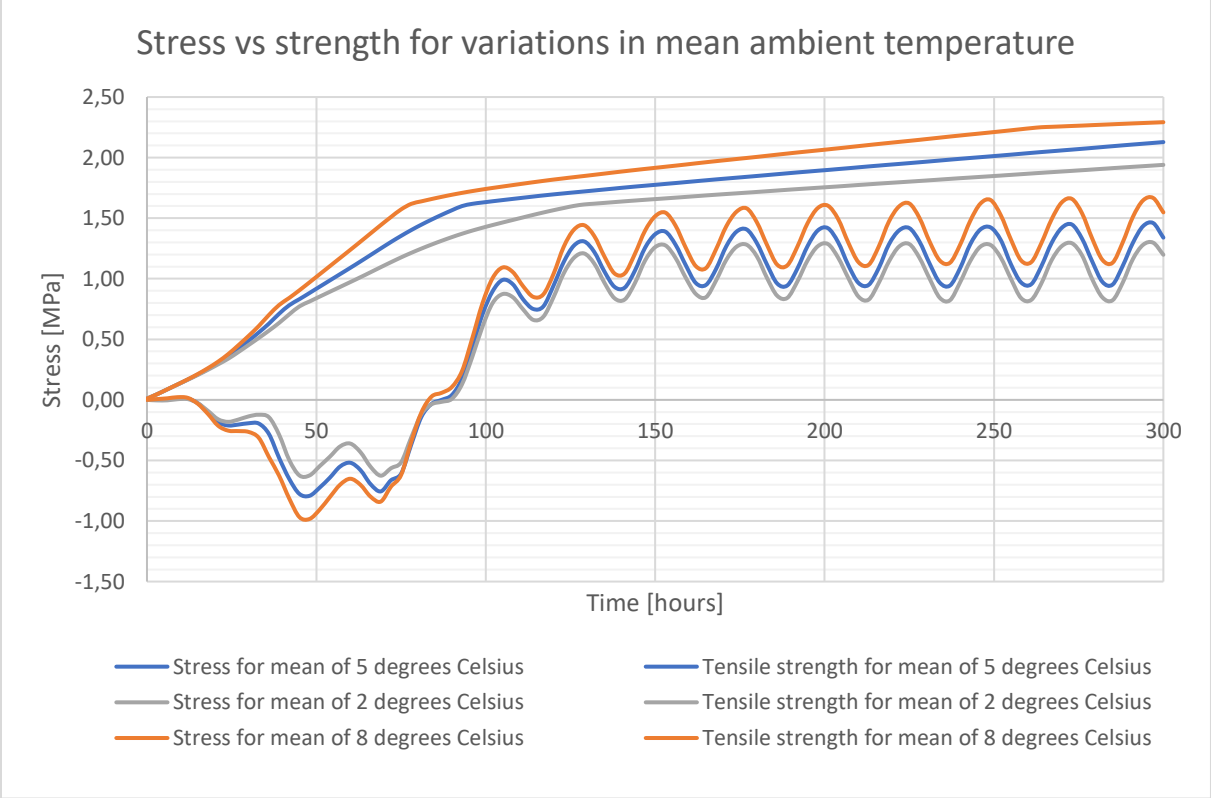

- **Striking time**

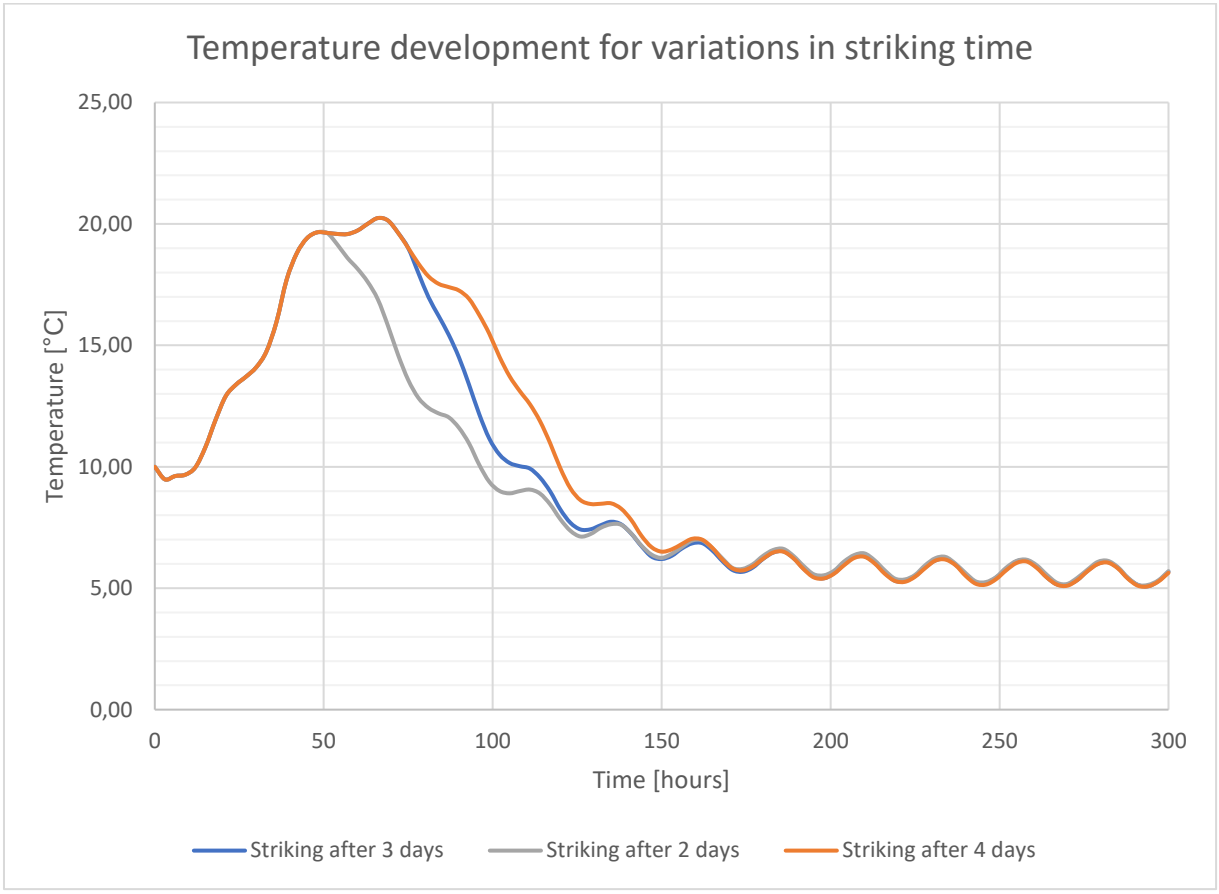

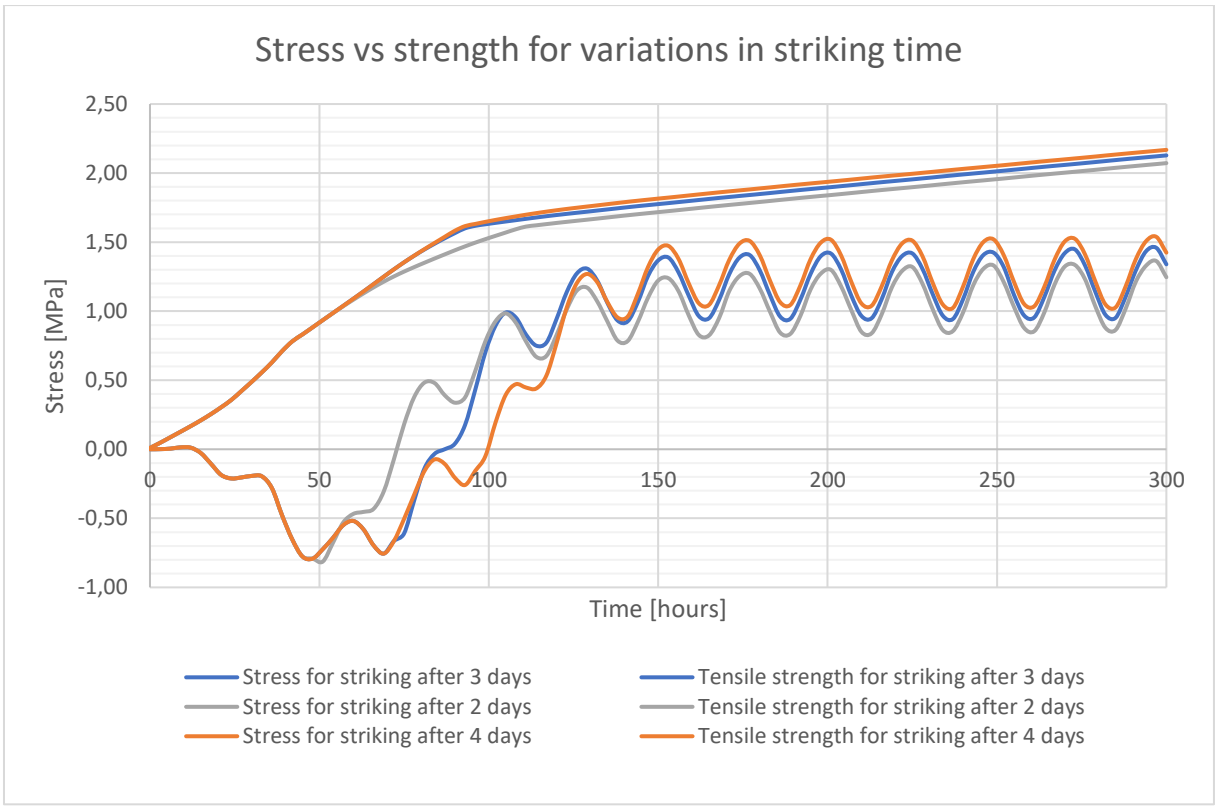

- **Maximum solar radiation**

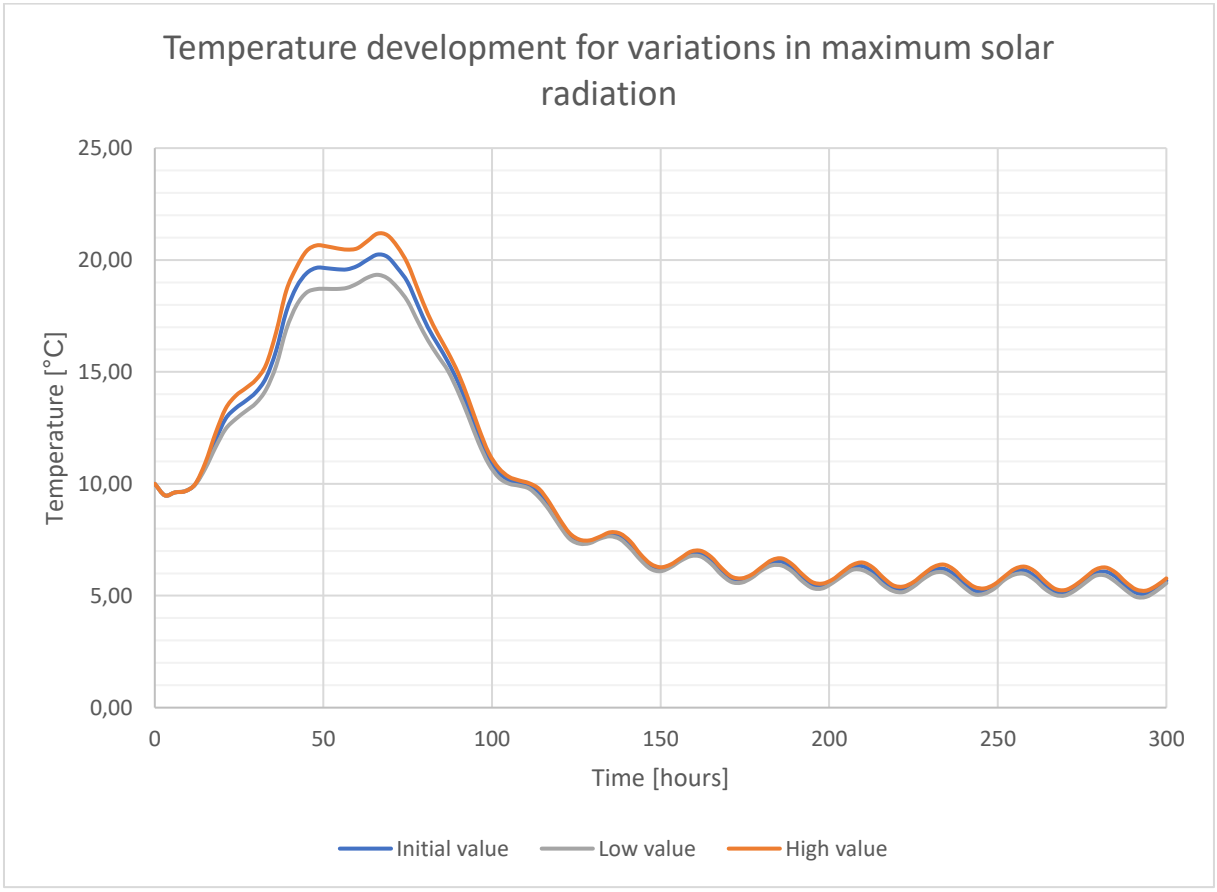

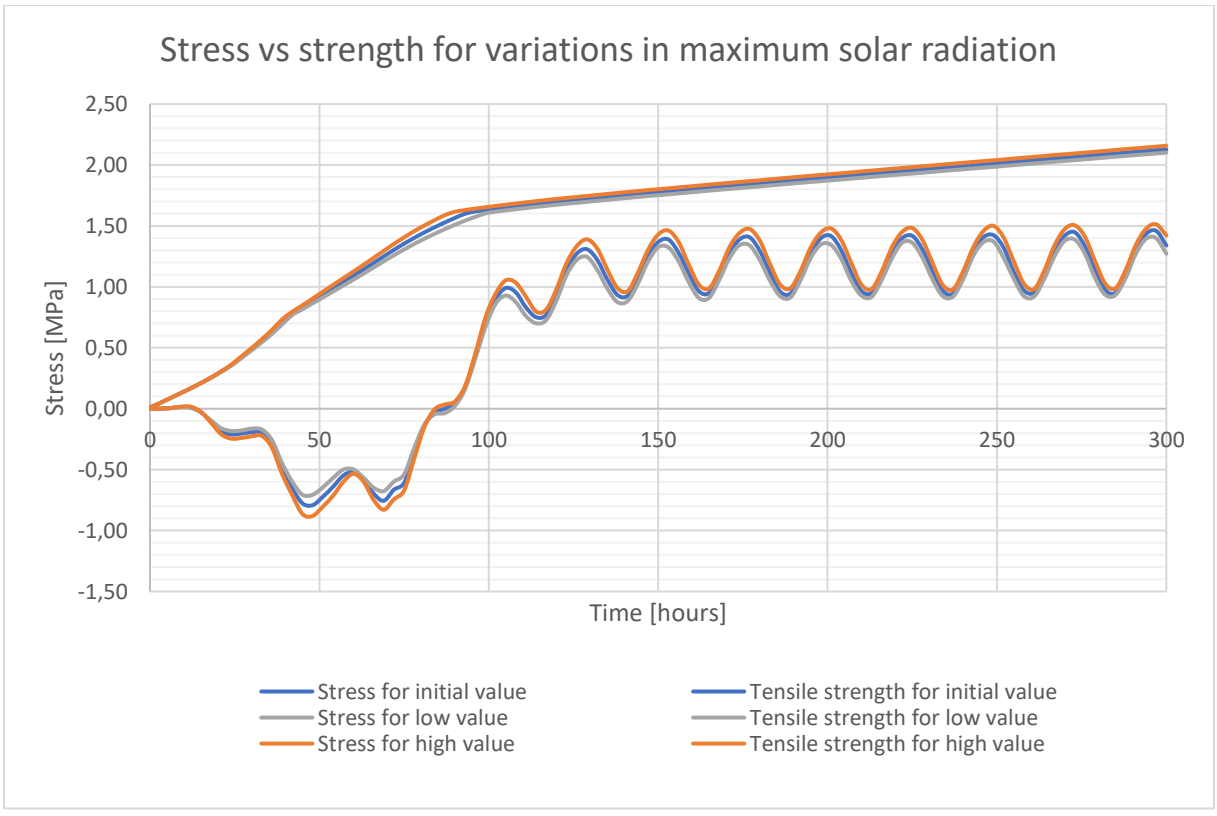

- **Convection coefficient**

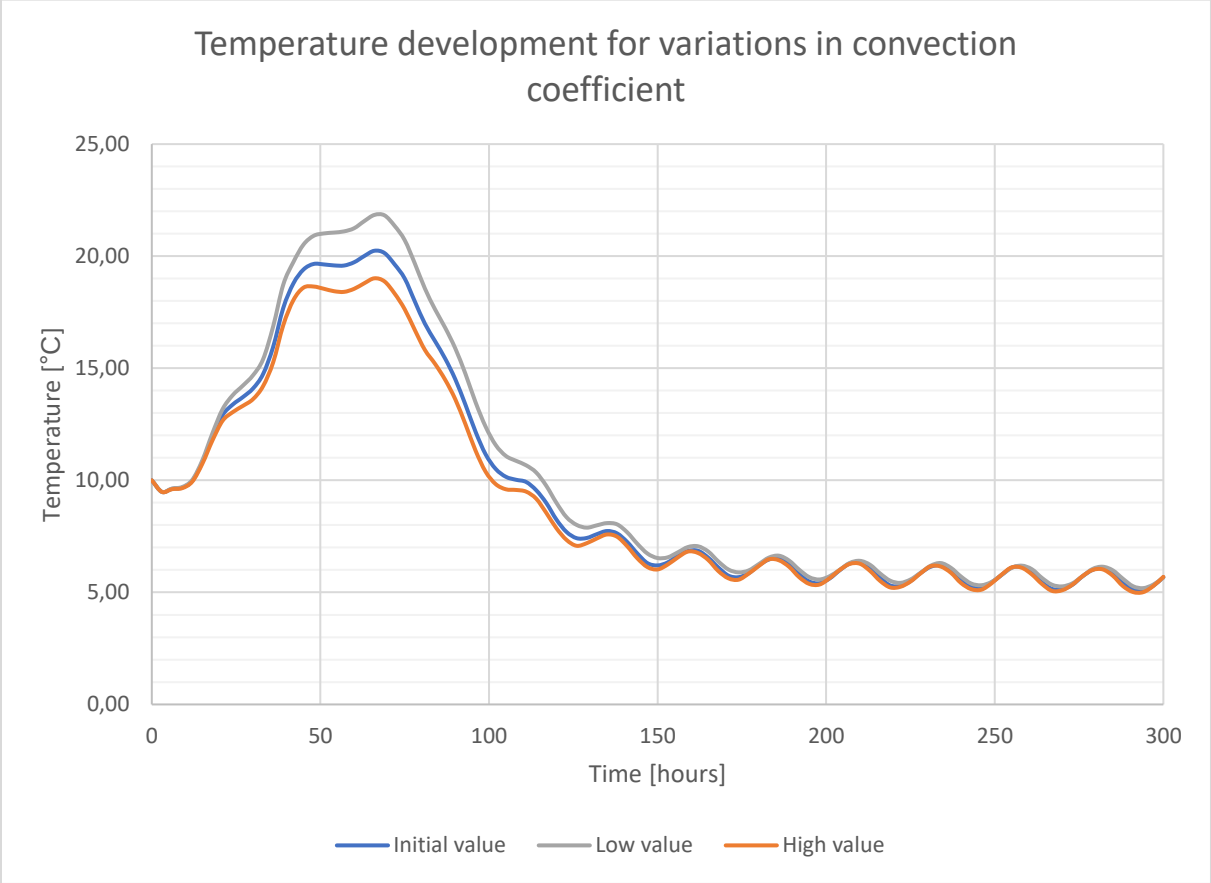

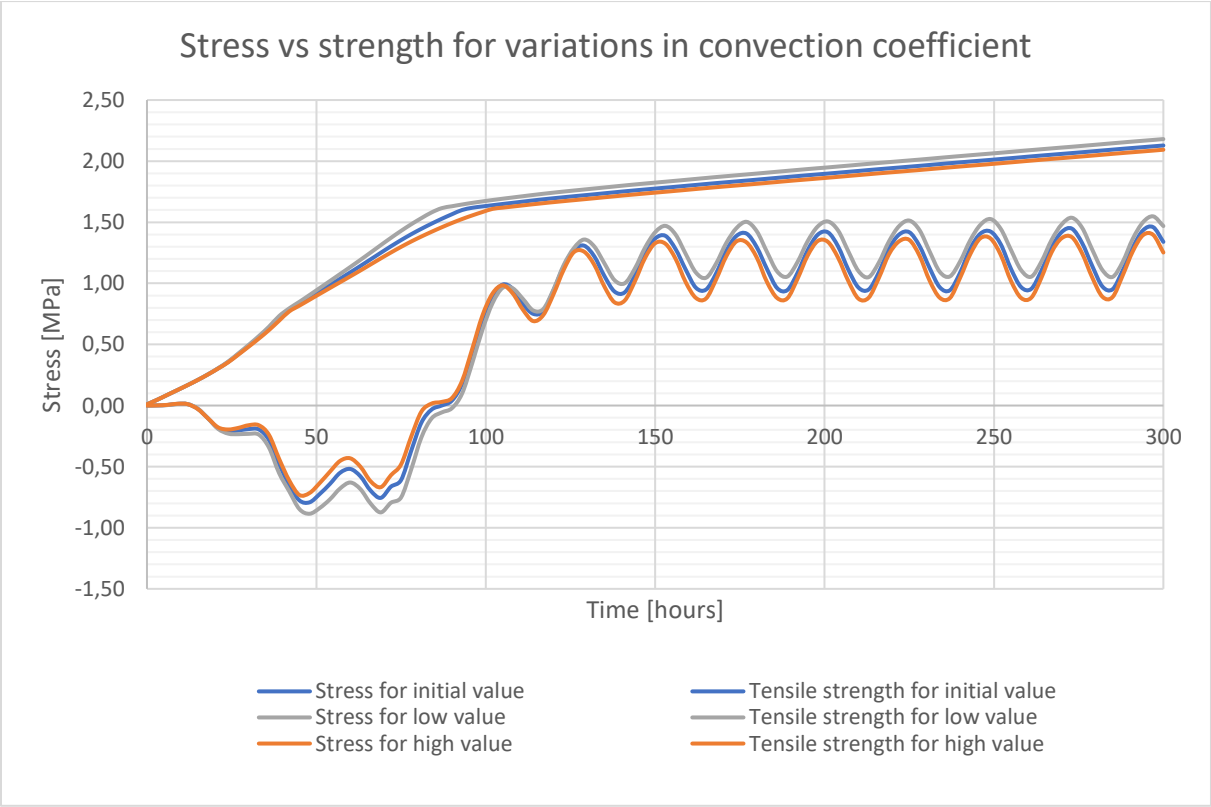

- **Radiation coefficients**

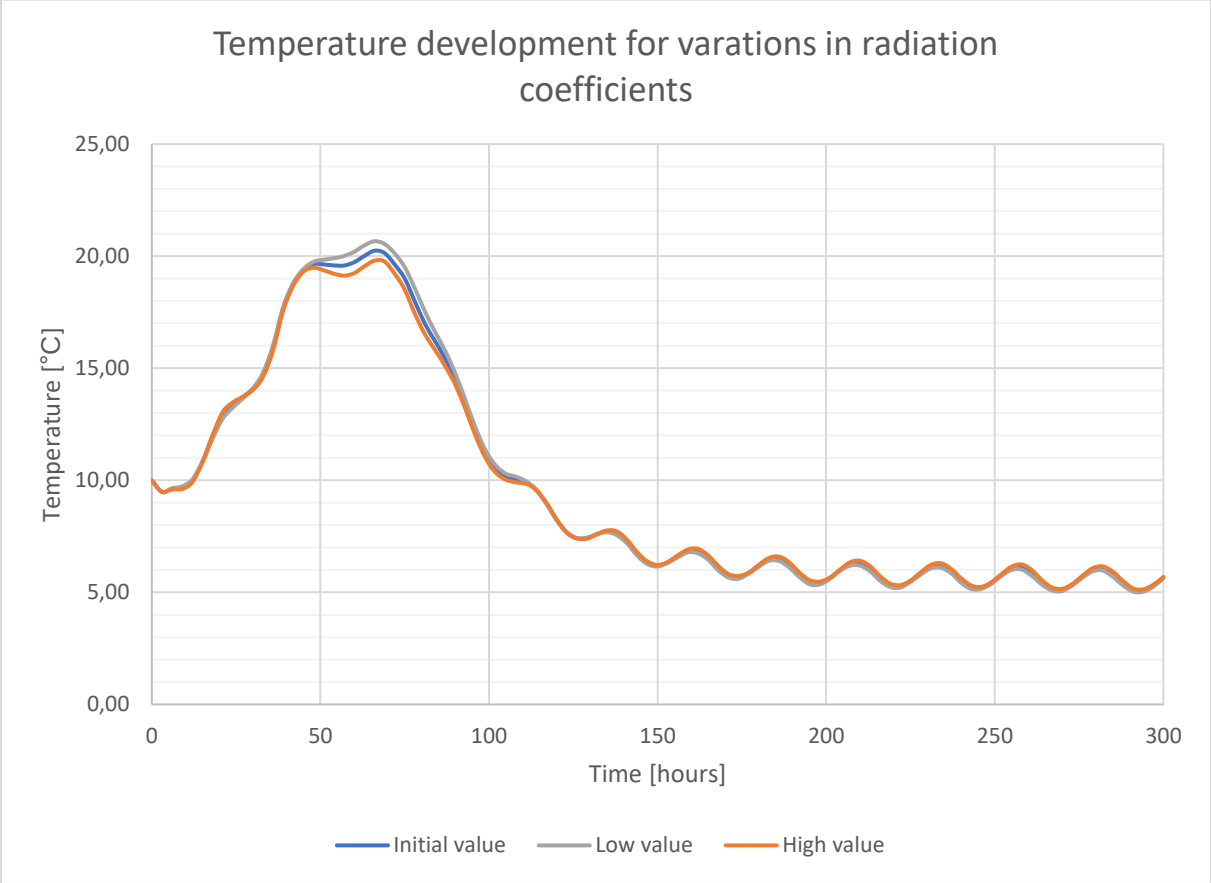

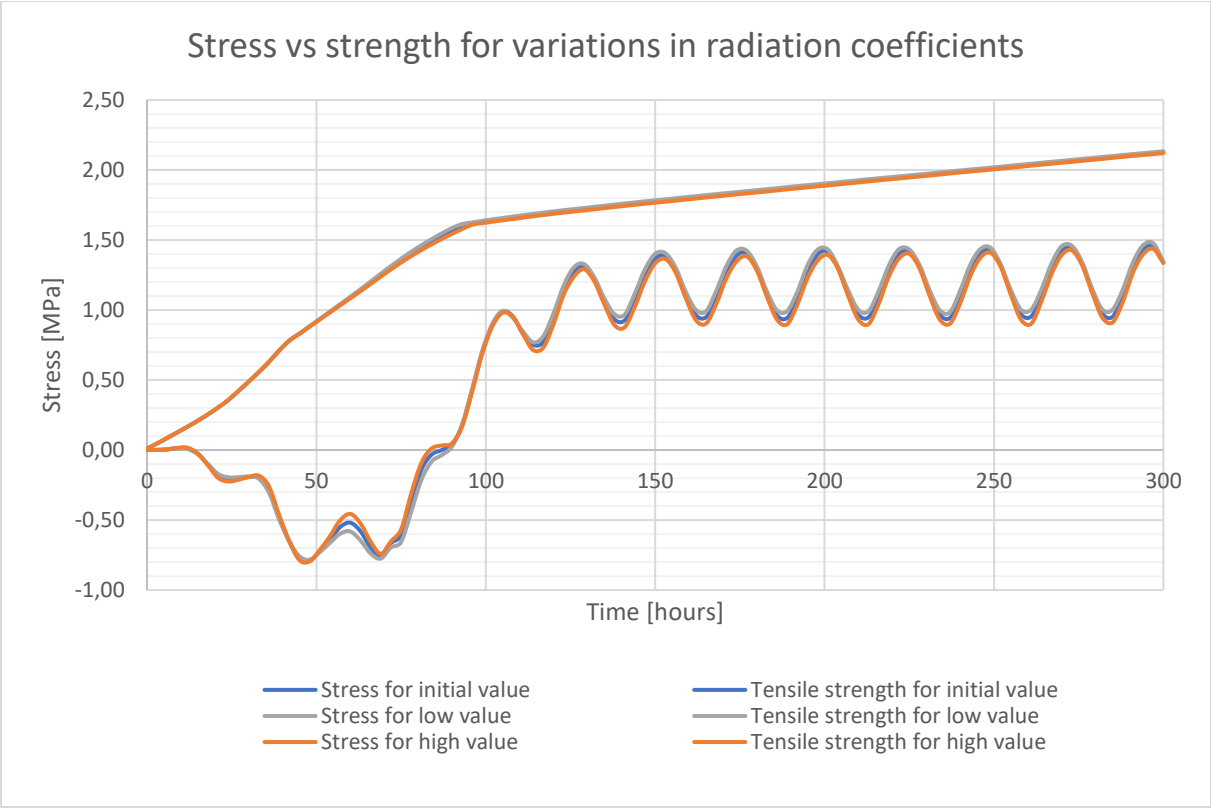

Appendix B: Derivation of Maxwell chain model

Here the hand written evaluation of the Maxwell chain model can be seen. This is first done for a single unit, then for two units and in the end also for 5 units.

Deriving the standard form of the Maxwell chain model

- **1 unit: spring and dashpot connected in series:**

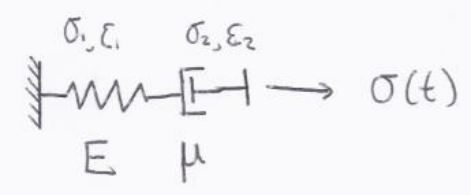

Constitutive relations:

Spring: $\varepsilon_1 = \frac{1}{E}\sigma_1$ (Hook's law)

Dashpot: $\dot{\varepsilon}_2 = \frac{1}{\mu}\sigma_2$

Equilibrium conditions:

$$\begin{cases} \sigma = \sigma_1 = \sigma_2 \\ \varepsilon = \varepsilon_1 + \varepsilon_2 \end{cases}$$

- **Substitution gives:**

$$\dot{\varepsilon} = \dot{\varepsilon}_1 + \dot{\varepsilon}_2 = \frac{1}{E}\dot{\sigma}_1 + \frac{1}{\mu}\sigma_2 = \frac{1}{E}\dot{\sigma} + \frac{1}{\mu}\sigma$$

$$\sigma + \frac{\mu}{E}\dot{\sigma} = \mu\dot{\varepsilon}$$

$$\boldsymbol{\sigma + \tau\dot{\sigma} = \mu\dot{\varepsilon}}$$

With:

$$\tau = \frac{\mu}{E} = \text{retardation time in seconds}$$

This first order differential equations is the standard form of the Maxwell chain model. The parameters σ and ε are a function of time.

2 Maxwell units in parallel

- For describing the viscoelastic material behaviour, several Maxwell units are used in parallel. The derivation of a system consisting of 2 units connected in parallel is shown here.

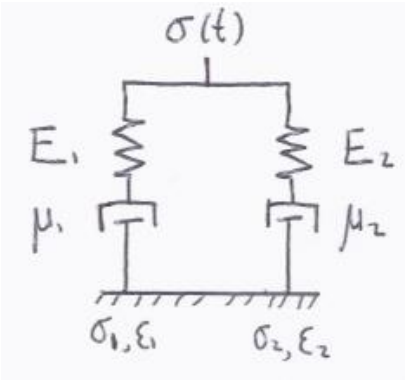

Parallel system:

$$\varepsilon(t) = \varepsilon_1 = \varepsilon_2 \quad (1)$$

$$\sigma(t) = \sigma_1 + \sigma_2 \quad (2)$$

Using property (1) of the parallel system and the standard form for the single units we end up with a system of 2 coupled first order ODE's:

$$\begin{cases} \sigma_1 + \tau_1 \dot{\sigma}_1 = \mu_1 \dot{\varepsilon} \\ \sigma_2 + \tau_2 \dot{\sigma}_2 = \mu_2 \dot{\varepsilon} \end{cases}$$

Then by also making use of property (2), we are able to eliminate σ_2:

$$\begin{cases} \sigma_1 + \tau_1 \dot{\sigma}_1 = \mu_1 \dot{\varepsilon} \\ \sigma - \sigma_1 - \tau_2 \dot{\sigma}_1 = \mu_2 \dot{\varepsilon} \end{cases}$$

We end up with 2 coupled first order ODE's. This means that two initial conditions are needed to solve the system: $\sigma_1(0)$ and $\varepsilon(0)$.

- We consider the case of a creep test where the load remains constant:

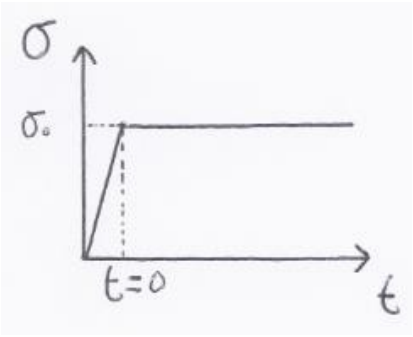

Also, we assume an instant application of the load σ_0 at $t = 0$.

- The initial conditions needed to solve the problem can be derived considering the static system at $t = 0$.
- For the static system only the springs act:

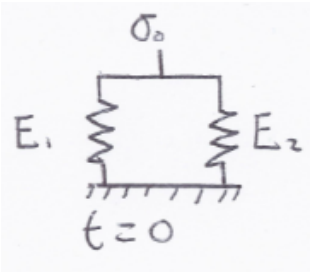

$$\sigma_i = E_i \varepsilon_i = E_i \varepsilon_0$$

$$\sigma_0 = \sum_{i=1}^{2} \sigma_i = E_1 \varepsilon_0 + E_2 \varepsilon_0$$

So we are able to formulate the first initial condition:

$$\boldsymbol{\varepsilon_0 = \frac{\sigma_0}{E_1 + E_2}} \qquad (\mathbf{1})$$

Also:

$$\sigma_1 = E_1 \varepsilon_1 = E_1 \varepsilon \rightarrow \varepsilon = \frac{\sigma_1}{E_1}$$

$$\sigma_0 = E_1 \varepsilon + E_2 \varepsilon = \sigma_1 + \frac{E_2}{E_1} \sigma_1$$

So the second initial condition becomes:

$$\boldsymbol{\sigma_1(0) = \frac{\sigma_0}{1 + \frac{E_2}{E1}}} \qquad (\mathbf{2})$$

The initial value problem can be solved analytically by making use of the Laplace method, which reduces the ODE's to a system of algebraic equations.

Solving the system of first order ODE's for 2 units

Previously, we arrived at the following system:

$$\begin{cases} \sigma_1 + \tau_1\dot{\sigma}_1 = \mu_1\dot{\varepsilon} \\ \sigma - \sigma_1 - \tau_2\dot{\sigma}_1 = \mu_2\dot{\varepsilon} \end{cases}$$

With two initial conditions at $t = 0$:

$$\varepsilon(0) = \frac{\sigma_0}{E_1 + E_2} \quad ; \quad \sigma_1(0) = \frac{\sigma_0}{1 + \frac{E_2}{E1}}$$

Use is made of realistic values for the input parameters regarding the viscoelastic material behaviour:

$$\tau_1 = 100\ hours$$
$$\tau_2 = 1000\ hours$$
$$E_1 = 5000\ MPa$$
$$E_2 = 10000\ MPa$$
$$\sigma_0 = 2\ MPa$$
$$\mu_1 = \tau_1 * E_1 = 500000 = 5.0 * 10^5\ MPa * h$$
$$\mu_2 = \tau_2 * E_2 = 1000000 = 1.0 * 10^7\ MPa * h$$

This changes the problem into:

$$\begin{cases} \sigma_1 + 100\dot{\sigma}_1 = 5.0 * 10^5\dot{\varepsilon} \\ 2 - \sigma_1 - 1000\dot{\sigma}_1 = 1.0 * 10^7\dot{\varepsilon} \end{cases}$$

With:

$$\varepsilon(0) = \frac{2}{10000 + 5000} = \frac{1}{7500} \quad ; \quad \sigma_1(0) = \frac{2}{1 + \frac{10000}{5000}} = \frac{2}{3}\ MPa$$

- **Now we use the Laplace Transform:**

$$L\{\dot{\sigma_1}\} = s * \hat{\sigma}_1 - \sigma_1(0)$$
$$L\{\dot{\varepsilon}\} = s * \hat{\varepsilon} - \varepsilon(0)$$

And substitute:

$$\begin{cases} \hat{\sigma}_1 + 100\big(s\hat{\sigma}_1 - \sigma_1(0)\big) = 5.0 * 10^5\big(s\hat{\varepsilon} - \varepsilon(0)\big) \\ \frac{2}{s} - \hat{\sigma}_1 - 1000\big(s\hat{\sigma}_1 - \sigma_1(0)\big) = 1.0 * 10^7\big(s\hat{\varepsilon} - \varepsilon(0)\big) \end{cases}$$

Using the initial conditions, we end up with the following system:

$$\begin{cases} \hat{\sigma}_1 + 100s\hat{\sigma}_1 - \frac{200}{3} = 5.0 * 10^5 s\hat{\varepsilon} - \frac{200}{3} \\ \frac{2}{s} - \hat{\sigma}_1 - 1000s\hat{\sigma}_1 + \frac{2000}{3} = 1.0 * 10^7 s\hat{\varepsilon} - \frac{4000}{3} \end{cases}$$

Now we rewrite the system to arrive at an expression for $\hat{\sigma}_1$:

$$\begin{cases} \hat{\sigma}_1(1+100s) - \hat{\varepsilon}(5.0*10^5 s) = 0 & (1) \\ \hat{\sigma}_1(-1-1000s) - \hat{\varepsilon}(1.0*10^7 s) = -\frac{2}{s} - \frac{6000}{3} & (2) \end{cases}$$

$$\mathbf{(2) - 20 * (1) =}$$

$$-\hat{\sigma}_1 - 1000s\hat{\sigma}_1 - 20\hat{\sigma}_1 - 2000\hat{\sigma}_1 s = -\frac{2}{s} - \frac{6000}{3}$$

$$\hat{\sigma}_1(-1-20-1000s-2000s) = -\frac{2}{s} - \frac{6000}{3} = -\frac{6}{3s} - \frac{6000s}{3s} = -\frac{6+6000s}{3s}$$

$$\hat{\sigma}_1 = -\frac{6+6000s}{3s(-3000s-21)} = \frac{6+6000s}{3s(3000s+21)}$$

$$\hat{\sigma}_1 = \frac{6+6000s}{9000s^2+63s} = \frac{6+6000s}{s(9000s+63)} = \frac{\frac{6}{9000}+\frac{2}{3}s}{s\left(s+\frac{63}{9000}\right)}$$

Partial fraction decomposition is used to rewrite the expression above into a more convenient form:

$$\frac{A}{s} + \frac{B}{s+\frac{63}{9000}} = \frac{\frac{6}{9000}+\frac{2}{3}s}{s\left(s+\frac{63}{9000}\right)}$$

$$A*s + \frac{63}{9000}A + B*s = \frac{6}{9000} + \frac{2}{3}s$$

$$\frac{63}{9000}A = \frac{6}{9000} \rightarrow A = \frac{6}{63}$$

$$A + B = \frac{2}{3} \rightarrow B = \frac{4}{7}$$

Now:

$$\hat{\sigma}_1 = \frac{\frac{6}{63}}{s} + \frac{\frac{4}{7}}{s+\frac{63}{9000}} = \frac{6}{63}\left(\frac{1}{s}\right) + \frac{4}{7}\left(\frac{1}{s+\frac{63}{9000}}\right)$$

Use the inverse Laplace transform:

$$\begin{cases} L\{e^{at}\} = \frac{1}{s-a} \\ L\{1\} = \frac{1}{s} \end{cases}$$

Gives the solution for $\sigma_1(t)$:

$$\boldsymbol{\sigma_1(t) = \frac{2}{21} + \frac{4}{7}e^{-\frac{7}{1000}t}}$$

Now use (1) again to find an expression for $\hat{\varepsilon}$:

$$\hat{\varepsilon}(5.0 * 10^5 s) = (1 + 100s)\hat{\sigma}_1$$

Use the expression for $\hat{\sigma}_1$:

$$\hat{\varepsilon}(5.0 * 10^5 s) = (1 + 100s)\left(\frac{2}{21}\left(\frac{1}{s}\right) + \frac{4}{7}\left(\frac{1}{s + \frac{63}{9000}}\right)\right)$$

$$\hat{\varepsilon}(5.0 * 10^5 s) = \frac{2}{21}\left(\frac{1}{s}\right) + \frac{4}{7}\left(\frac{1}{s + \frac{63}{9000}}\right) + \frac{200}{21} + \frac{400}{7}\left(\frac{s}{s + \frac{63}{9000}}\right)$$

$$\hat{\varepsilon} = \frac{2}{21 * 5.0 * 10^5}\left(\frac{1}{s^2}\right) + \frac{200}{21 * 5.0 * 10^5}\left(\frac{1}{s}\right) + \frac{400}{7 * 5.0 * 10^5}\left(\frac{1}{s + \frac{63}{9000}}\right) + \frac{4}{7}\left(\frac{1}{s + \frac{63}{9000}}\right)\left(\frac{1}{5.0 * 10^5 s}\right)$$

Use partial fraction decomposition again on the last term:

$$\frac{4}{7}\left(\frac{1}{s + \frac{63}{9000}}\right)\left(\frac{1}{5.0 * 10^5 s}\right) = \frac{1}{6125}\left(\frac{1}{s}\right) - \frac{1}{6125}\left(\frac{1}{s + \frac{7}{1000}}\right)$$

And use the inverse Laplace transform:

$$\begin{cases} L\{e^{at}\} = \dfrac{1}{s - a} \\ L\{1\} = \dfrac{1}{s} \\ L\{t^n\} = \dfrac{n!}{s^{n+1}} \end{cases}$$

Gives:

$$\boldsymbol{\varepsilon(t) = \frac{1}{5250000}t + \frac{67}{367500} - \frac{3}{61250}e^{-\frac{7}{1000}t}}$$

The solutions for $\varepsilon(t)$ and $\sigma_1(t)$ as derived above are checked using Maple and turn out to be correct.

5 Maxwell units

In general 4 to 5 Maxwell units are used to describe the viscoelastic material behaviour. The derivations for a system of 5 Maxwell units can be seen here.

We use 5 units in parallel:

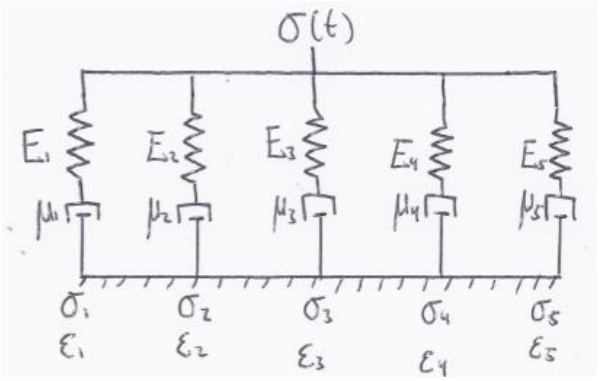

The retardation time for each unit is:

$$\tau_i = \frac{\mu_i}{E_i}$$

Properties of the parallel system:

$$\sigma = \sigma_1 + \sigma_2 + \sigma_3 + \sigma_4 + \sigma_5 = \sum_{i=1}^{5} \sigma_i \qquad (1)$$

$$\varepsilon = \varepsilon_1 = \varepsilon_2 = \varepsilon_3 = \varepsilon_4 = \varepsilon_5 \qquad (2)$$

Using the second property (2) of the parallel system and the standard form for the Maxwell chain units, we arrive at the following system of coupled first order ODE's:

$$\begin{cases} \sigma_1 + \tau_1 \dot{\sigma}_1 = \mu_1 \dot{\varepsilon} \\ \sigma_2 + \tau_2 \dot{\sigma}_2 = \mu_2 \dot{\varepsilon} \\ \sigma_3 + \tau_3 \dot{\sigma}_3 = \mu_3 \dot{\varepsilon} \\ \sigma_4 + \tau_4 \dot{\sigma}_4 = \mu_4 \dot{\varepsilon} \\ \sigma_5 + \tau_5 \dot{\sigma}_5 = \mu_5 \dot{\varepsilon} \end{cases}$$

We are able to eliminate 1 unknown by using the first property (1) of the parallel system:

$$\sigma_1 = \sigma - \sigma_2 - \sigma_3 - \sigma_4 - \sigma_5$$

Which gives:

$$\begin{cases} \sigma - \sigma_2 - \sigma_3 - \sigma_4 - \sigma_5 + \tau_1(-\dot{\sigma}_2 - \dot{\sigma}_3 - \dot{\sigma}_4 - \dot{\sigma}_5) = \mu_1 \dot{\varepsilon} \\ \sigma_2 + \tau_2 \dot{\sigma}_2 = \mu_2 \dot{\varepsilon} \\ \sigma_3 + \tau_3 \dot{\sigma}_3 = \mu_3 \dot{\varepsilon} \\ \sigma_4 + \tau_4 \dot{\sigma}_4 = \mu_4 \dot{\varepsilon} \\ \sigma_5 + \tau_5 \dot{\sigma}_5 = \mu_5 \dot{\varepsilon} \end{cases}$$

- 5 first order ODE's: 5 initial conditions needed to solve the system
- 5 unknowns: $\varepsilon(t)$, $\sigma_2(t)$, $\sigma_3(t)$, $\sigma_4(t)$ and $\sigma_5(t)$.

The initial conditions can be found from the static system at $t = 0$, where only the springs act:

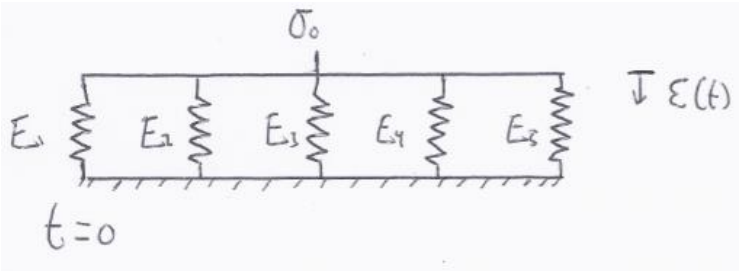

$$\sigma_i = E_i \varepsilon_i \quad ; \quad \varepsilon_i = \varepsilon$$

$$\sigma(0) = \sigma_1 + \sigma_2 + \sigma_3 + \sigma_4 + \sigma_5 = E_1\varepsilon + E_2\varepsilon + E_3\varepsilon + E_4\varepsilon + E_5\varepsilon$$

So the first initial condition becomes:

$$\varepsilon_0 = \frac{\sigma_0}{E_1 + E_2 + E_3 + E_4 + E_5} = \frac{\sigma_0}{E_{total}} \qquad (1)$$

- Now for the forces:

$$\sigma_2 = E_2\varepsilon \rightarrow \varepsilon = \frac{\sigma_2}{E_2}$$

Substitute in:

$$\sigma(0) = \sigma_1 + \sigma_2 + \sigma_3 + \sigma_4 + \sigma_5 = E_1\varepsilon + E_2\varepsilon + E_3\varepsilon + E_4\varepsilon + E_5\varepsilon$$

Gives:

$$\sigma(0) = \frac{E_1}{E_2}\sigma_2 + \sigma_2 + \frac{E_3}{E_2}\sigma_2 + \frac{E_4}{E_2}\sigma_2 + \frac{E_5}{E_2}\sigma_2$$

So the second initial conditions becomes:

$$\sigma_2(0) = \frac{\sigma_0}{1 + \frac{E_1 + E_3 + E_4 + E_5}{E_2}} = \frac{E_2\sigma_0}{E_{total}} \qquad (2)$$

Initial conditions (3), (4) and (5) for $\sigma_3(0), \sigma_4(0)$ and $\sigma_5(0)$ are found in the same way.

The initial value problem can subsequently be solved using the Laplace method like is done for a system of 2 units. For the 5 units here, this is done using Maple.

Appendix C: Maple sheet for Maxwell chain model

Here the Maple sheet for solving the Maxwell Chain model can be seen. Next to that, fitting of the distribution coefficients to creep data from literature can be seen.

```
> restart;
```

Solving the system of differential equations with the initial conditions

```
>
> eq1 := sig_total - sig2(t) - sig3(t) - sig4(t) + T1·(-diff(sig2(t),
      t)-diff(sig3(t), t)-diff(sig4(t), t)) = u1·diff(eps(t), t) :
> eq2 := sig2(t) + T2·diff(sig2(t), t) = u2·diff(eps(t), t) :
> eq3 := sig3(t) + T3·diff(sig3(t), t) = u3·diff(eps(t), t) :
> eq4 := sig4(t) + T4·diff(sig4(t), t) = u4·diff(eps(t), t) :
>
>
>
> sig_total := sig_0 :
> desys := {eq1, eq2, eq3, eq4} : ic := {sig2(0) = sig2_0, sig3(0)
      = sig3_0, sig4(0) = sig4_0, eps(0) = eps_0} :
>
> solution := combine(dsolve(desys union ic, {eps(t), sig2(t), sig3(t),
      sig4(t)}, method = laplace)) : assign(solution) :
> #eps(t);
```

High: Lee fcm = 35 MPa for t = 7 days

```
> a :='a': b :='b': c :='c': d :='d':
> E1 := a·E_total : E2 := b·E_total : E3 := c·E_total : E4 := d
      ·E_total : T1 := 10 : T2 := 100 : T3 := 1000 : T4 := 10000 :
      u1 := T1·E1 : u2 := T2·E2 : u3 := T3·E3 : u4 := T4·E4 :
      sig_0 := 1 :
>
```

> $sig2\_0 := \frac{sig\_0}{1 + \frac{E1 + E3 + E4}{E2}} : sig3\_0 := \frac{sig\_0}{1 + \frac{E1 + E2 + E4}{E3}} :$
$sig4\_0 := \frac{sig\_0}{1 + \frac{E1 + E3 + E2}{E4}} : eps\_0 :=$
$\frac{sig\_0}{E1 + E2 + E3 + E4} :$

> $###eval(eps(t));$

Input data:

>
$$X1 := 24 \cdot \begin{bmatrix} 0.12 \\ 0.50 \\ 1.01 \\ 2.28 \\ 3.68 \\ 5.58 \\ 7.75 \\ 9.53 \\ 12.07 \\ 14.61 \\ 16.77 \\ 18.55 \\ 20.71 \\ 23.00 \\ 25.29 \\ 26.94 \\ 28.47 \end{bmatrix} : Y1 := 10^{-6} \cdot \begin{bmatrix} 0.00 \\ 51.75 \\ 62.41 \\ 69.51 \\ 72.56 \\ 76.11 \\ 80.17 \\ 82.20 \\ 84.23 \\ 86.26 \\ 87.27 \\ 88.29 \\ 88.79 \\ 89.81 \\ 90.32 \\ 90.82 \\ 90.82 \end{bmatrix} : subplot5 := plot(X1, Y1) :$$

>

> **E_total** := 26423 :

> **a := 0.42 :**

> **b := 0.1 :**

> **c := 0.11 :**

> **d := 0.37 :**

> $a + b + c + d;$

>

> $E1 := a \cdot E\_total : E2 := b \cdot E\_total : E3 := c \cdot E\_total : E4 := d \cdot E\_total : T1 := 10 : T2 := 100 : T3 := 1000 : T4 := 10000 : u1 := T1 \cdot E1 : u2 := T2 \cdot E2 : u3 := T3 \cdot E3 : u4 := T4 \cdot E4 : sig\_0 := 1 :$

>

> $sig2\_0 := \frac{sig\_0}{1 + \frac{E1 + E3 + E4}{E2}} : sig3\_0 := \frac{sig\_0}{1 + \frac{E1 + E2 + E4}{E3}} : sig4\_0 := \frac{sig\_0}{1 + \frac{E1 + E3 + E2}{E4}} : eps\_0 := \frac{sig\_0}{E1 + E2 + E3 + E4} :$

> $subplot6 := plot(eps(t), t = 0 ..672, y = 0 ..0.0002, gridlines = true, linestyle = dashdot) :$

> $with(plots) : display(\{subplot5, subplot6\}, size = [0.5, 0.7]);$

>

> $eps672 := eval(eps(t), t = 672) :$

> $evalf(eps672) :$

Calculating the error at t=672 hours:

> $Y1\_end := 90.82 \cdot 10^{-6} :$

> $Digits := 5 :$

> $err\% := \mathrm{abs}\left(100 \cdot \left(\frac{eps672}{Y1\_end} - 1\right)\right); Digits := 10 :$

>

Appendix D: Results of validation Maple sheet Maxwell chain model

The Maxwell Chain data for the 'Maxwell Average' can be seen in figure D.1.

Maxwell Chain Data		Retardation times with distribution coefficients					
Maturity	E-modulus	1,0	10,0	100,0	1000,0	10000,0	100000,0
[hours]	[MPa]	[hours]	[hours]	[hours]	[hours]	[hours]	[hours]
0	500	0,0000	0,0000	0,2000	0,8000	0,0000	0,0000
12	16685	0,0000	0,3000	0,2000	0,3000	0,2000	0,0000
24	21943	0,0000	0,2500	0,2500	0,2000	0,3000	0,0000
72	29021	0,0000	0,2000	0,2500	0,1500	0,4000	0,0000
168	33112	0,0000	0,2000	0,1500	0,2000	0,4500	0,0000
336	35628	0,0000	0,2000	0,1000	0,2000	0,5000	0,0000
672	37521	0,0000	0,1500	0,1500	0,1000	0,6000	0,0000
1344	38920	0,0000	0,1500	0,1000	0,1500	0,6000	0,0000
2688	39941	0,0000	0,1000	0,1500	0,0500	0,7000	0,0000

Table D.1 Maxwell Average chain data file

The validation is performed for some random maturities in the table above. For each maturity that is used, the resulting curve that is obtained using MLS Heat is shown on the left, while the resulting curve as obtained using the Maple sheet can be seen on the right.

- **For maturity at loading = 24 hours**

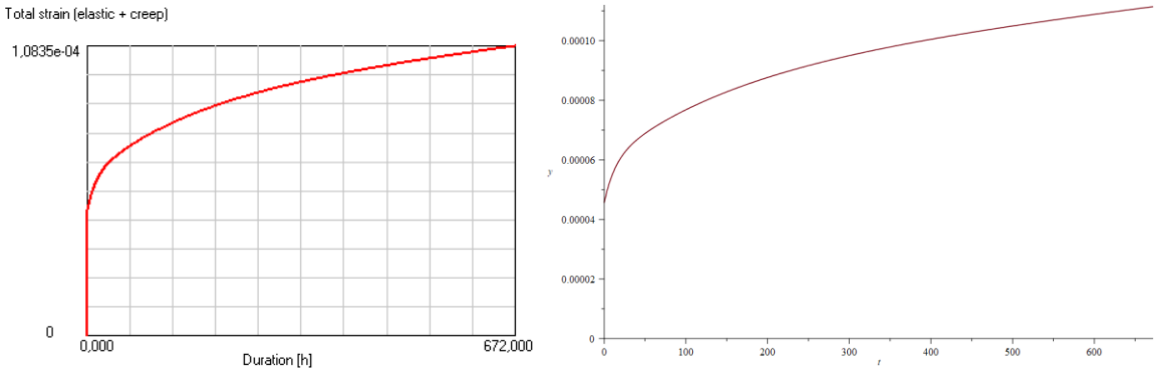

figure D.1 Total strain response to unit of stress according to MLS Heat (left) and according to Maple sheet (right) for a maturity of loading of 24 hours

The error at $t = 672\ h = \mathbf{2.8}\%$

- **For maturity at loading = 168 hours**

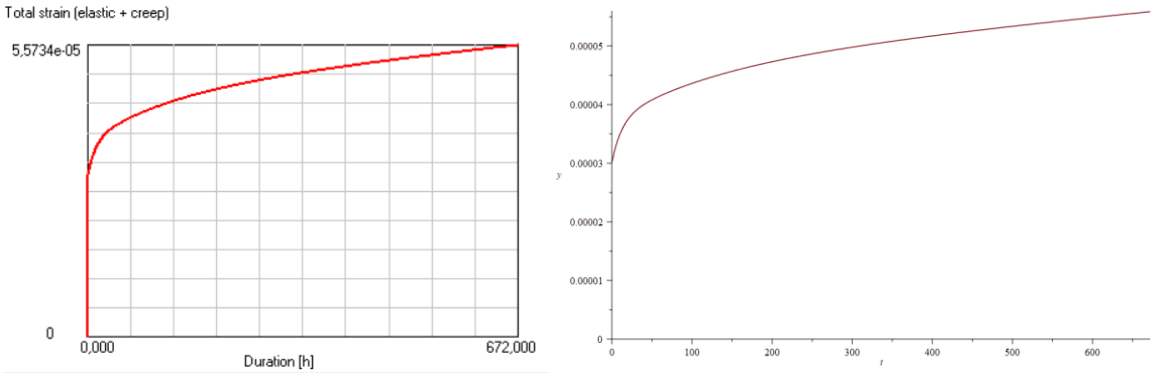

figure D.2 Total strain response to unit of stress according to MLS Heat (left) and according to Maple sheet (right) for a maturity of loading of 168 hours

The error at $t = 672\ h = \mathbf{0.2}\%$

- **For maturity at loading = 672 hours**

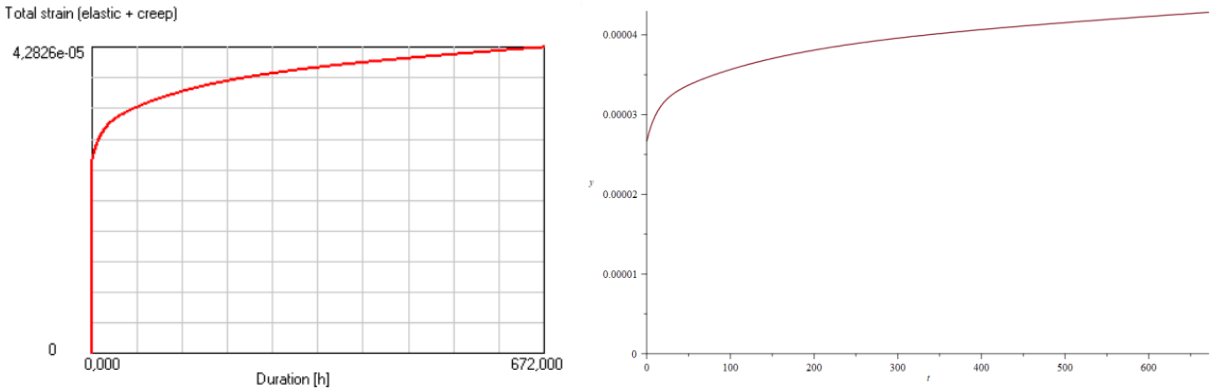

figure D.3 Total strain response to unit of stress according to MLS Heat (left) and according to Maple sheet (right) for a maturity of loading of 672 hours

The error at $t = 672\ h = \mathbf{0.02}\%$

Conclusion

Evaluation of the Maxwell chain model by solving the system of first order ODE's using the Laplace method in Maple gives accurate results for large maturities at loading (high E-modulus). For lower maturities at loading the error between the values computed using MLS Heat and the values computed using Maple increases. This could be due to the fact that the standard calculation error increases as the creep is larger at lower maturities at loading. Overall it can be concluded that the accuracy is sufficient for the purpose of application of this research.

Appendix E: Mesh refinement study

A mesh refinement study is performed as part of the Finite element modelling. This is done by decreasing the mesh size and comparing the results for a specific point in the cross section. The point that is regarded in this study is located in the middle of the wall at 1 m height measured from the top of the slab as can be seen in figure E.1 below.

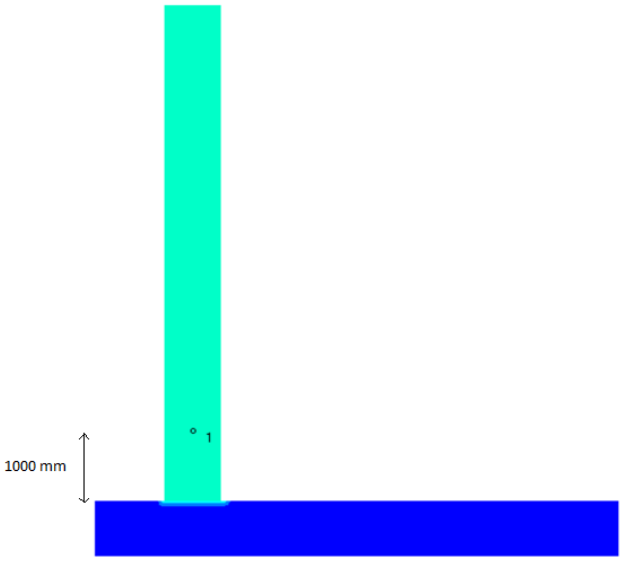

figure E.1 Governing point in the bottom of the wall

An initial mesh size is chosen from which the refinement study will start. This is chosen as half the thickness of the wall $= 800/2 = 400\ mm$. The FEA is performed using this mesh size where specific output is regarded, namely the maximum temperature during hardening and the maximum tensile stress during hardening.

Next, to determine whether the fineness of the mesh is sufficient, the mesh size is halved and the effect on the output is regarded. This is done for three mesh sizes as can be seen in the figure below where the initial mesh is the one on the left.

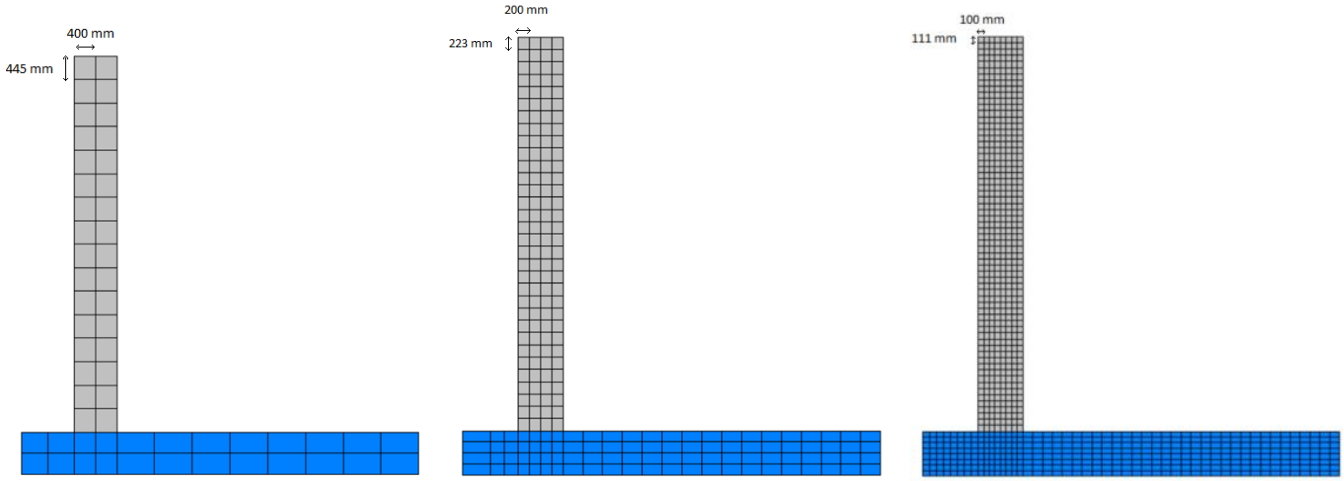

figure E.2 Three different mesh sizes that are considered

This results in the following table. In this table the percentual change of the temperature and tensile stresses after reducing the mesh size can be seen. When this change lies within certain limits, the mesh size is sufficient. For this study holds that when having halved the mesh size, the difference in the results remain below 5%, the previous mesh size was sufficiently small.

Mesh number:	Element size [mm]	Maximum temperature [°C]	Difference (absolute value)	Maximum stress [MPa]	Difference (absolute value)
1	400x445	20.82	-	1.69	-
2	200x223	20.63	**0.90 %**	1.58	**6.70 %**
3	100x111	20.93	**1.44 %**	1.53	**3.47 %**

Table E.1 results of the mesh refinement study

As can be seen from the table, for reducing the mesh size from 200 to 100 mm holds that the change in the results remains below the predefined limit. This means that mesh number 2 is sufficient.

Appendix F: Description of the different testing methods

TSTM test

The Temperature Stress Testing Machine (TSTM) is used to perform a deformation controlled experiment on a hardening concrete specimen in a temperature controlled mould. An overview of the test set-up can be seen in figure F.1 (Lokhorst, 2001). Next, the overall testing procedure will be described.

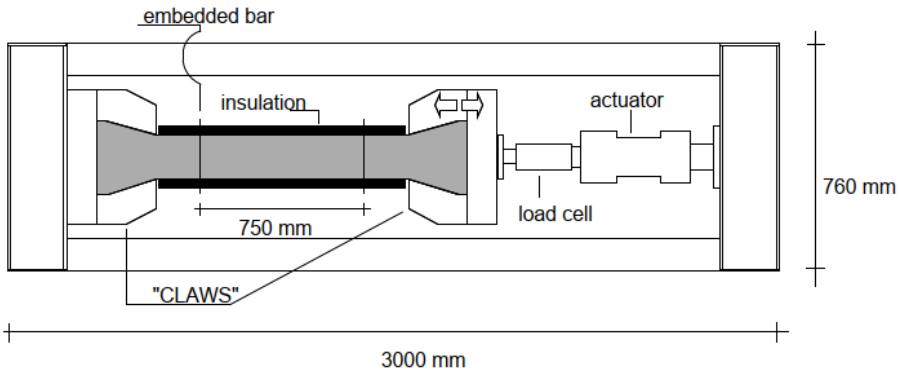

figure F.1 TSTM set-up (Lokhorst, 2001).

First of all the concrete mixture is poured into the mould. The mould is then sealed to prevent any moisture loss during hardening. During hardening the temperature of the specimen is measured at several locations and the temperature of the specimen can be controlled based on a prescribed temperature function by means of a system of water tubes running through the mould. The water temperature is regulated by a cryostat device (Lokhorst, 2001).

In this case it is decided to perform a displacement controlled test in which the displacements of the prismatic part of the specimen are kept constant at the locations of the embedded bars as can be seen in figure F.2. The displacements are measured using linear variable differential transformers (LVDT) at both sides of the specimens as can be seen in the figure below. The LVDT's are supported by a glass bar and are in constant contact with the embedded bars. In that way the deformations of the embedded bars (and thus concrete specimen) can be measured.

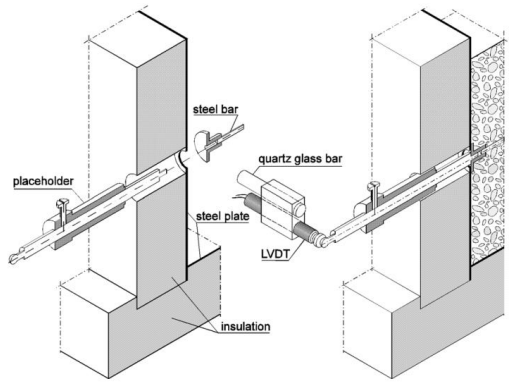

figure F.2 Embedded bars and LVDT's (Lokhorst, 2001).

The ends of the specimen are clamped by the ‘claws’ of the machine which means that the concrete specimen is fully restrained during hardening. The force that is needed to restrain the deformations of the concrete during hardening is measured by the load cell.

The aim of performing the TSTM test is to simulate the imposed deformations in the governing point in the bottom region of the walls of the dive-under. For this reason the temperature curve that is prescribed for this test corresponds to the temperature development in the wall as calculated in the FEA of the cross-section of the wall and slab as described in a previous section.

In figure F.3 below a schematisation of the concrete specimen of the TSTM test can be seen. In this figure the relevant dimensions of the specimen can be seen together with the locations of the embedded bars and the temperature measurements. There are five temperature measurements, two in the ‘heads’ of the specimen and three in the prismatic part of the specimen which are used for the temperature control. The height of the prismatic part of the specimen equals 100 mm.

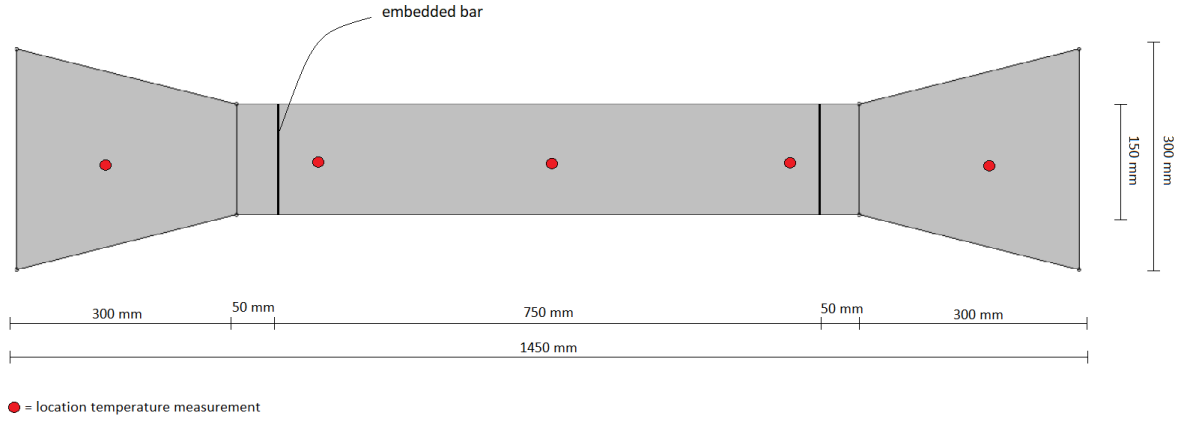

figure F.3 Schematisation of the concrete specimen of the TSTM test (Lokhorst, 2001).

In figure F.4 below the TSTM test as it is set-up in the Stevin laboratory at the TU Delft can be seen. As can be seen from the figure, the prismatic part of the specimen is fully covered by the temperature regulating mould.

figure F.4 TSTM test set-up in the Stevinlab at the TU Delft.

ADTM test

Parallel to the TSTM test, an Autogenous Deformation Testing Machine (ADTM) test is performed. The aim of performing this test is to determine the autogenous deformations for the specific concrete mixture. The results can subsequently be used to increase the accuracy of the FEA regarding the assessment of the risk of early-age cracking.

For the ADTM also holds that the concrete is poured into a temperature regulating mould. After compaction the concrete is again sealed and the mould is closed. The deformations of the specimen are measured on both sides of the specimen at the location of the embedded bars which are casted in with the concrete. This is again done by means of LVDT's as can be seen in figure F.5 below.

figure F.5 LVDT's and embedded bars of ADTM test

Since the aim of this test is to measure the autogenous deformations, the temperature of the specimen is kept constant at 20℃ to avoid any thermal strains during hardening. Also, measures are taken to avoid any influence of friction on the deformations of the specimen.

In figure F.6 a schematic representation of the ADTM can be seen. In this figure the relevant dimensions can be seen together with the locations of the temperature measurements and the locations of the embedded bars. As can be seen from the figure, the length over which the deformations are measured equals 500 mm. The height of the specimen equals 150 mm. The temperature is measured at three locations within the specimen.

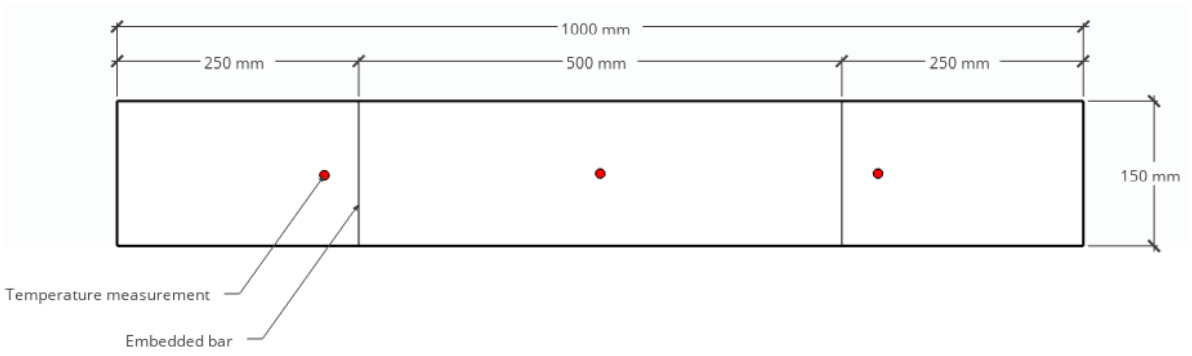

figure F.6 Schematisation of the concrete specimen of the ADTM test

In figure F.7 below the ADTM test as it was set-up at the Stevinlaboratory at the TU Delft can be seen. Here the closed mould can be seen together with the in- and outlet of the inner tube system for temperature regulation. Next to that one of the glass bars can be seen which suppors the LVDT's.

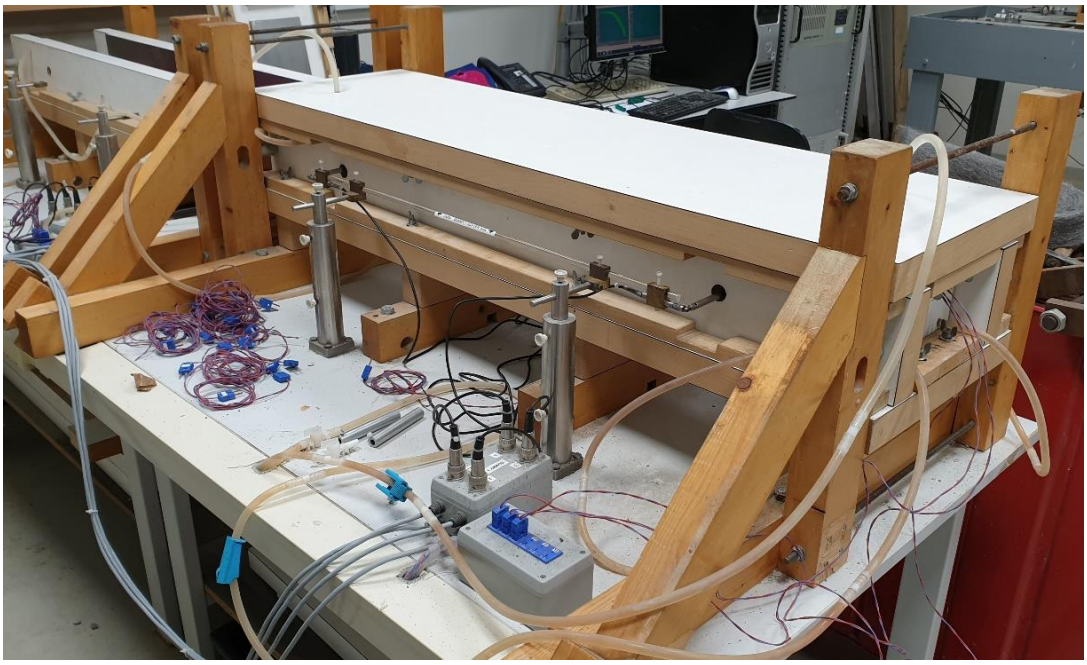

figure F.7 ADTM test set-up in the Stevinlab at the TU Delft.

Cube tests

To determine the compressive- and tensile strength development of the concrete, several standard cubes are casted (150x150x150mm). The cubes are casted in steel temperature regulating moulds as can be seen in figure F.8. The moulds have an inner tube system for temperature regulation and are sealed using a foil to prevent any moisture loss during hardening. The internal temperature of the cubes is continuously measured and is kept constant at 20℃.

figure F.8 Cubes in the temperature regulating malls

To determine the development of the mechanical properties of the concrete cubes, the cubes are tested at predetermined ages. This is done after 1, 2, 5, 8, 14 and 28 days of hardening. There are two types of cube tests that will be performed, namely cube compressive tests and tensile splitting tests. Both tests are carried out in line with NEN-EN 12390-4 respectively NEN-EN 12390-6. In figure F.9 below one of the concrete cubes can be seen in each of the test set-ups. In the figure F.9a the standard test set-up of a cube compression test can be seen. In figure F.9b the standard test set-up of a tensile splitting test can be seen. Here splitting of the cube is enabled by placing wooden ‘sticks’ in between the pressure plates and the cube on both the bottom and top side of the cube as can be seen in the figure.

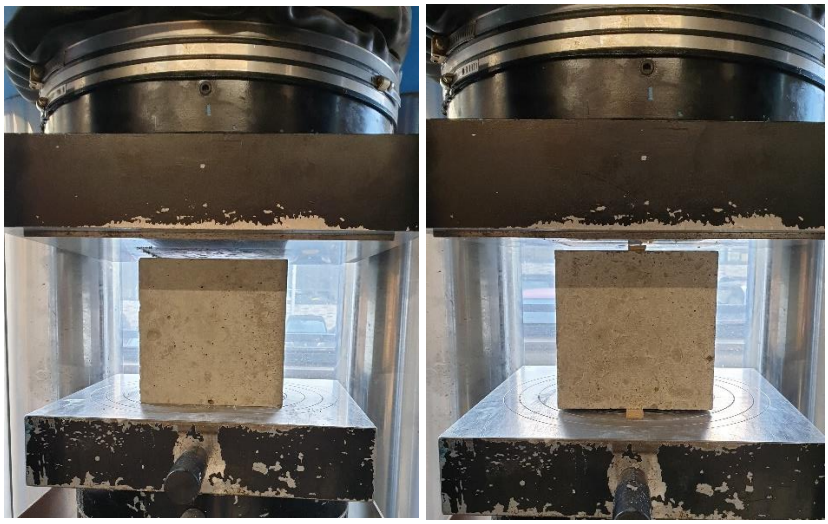

figure F.9a Cube compressive test and F.9b Tensile splitting test..

The development of the E-modulus can be derived from the compressive strength development based on relations as presented in NEN-EN 1992-1. Both the measured tensile- and compressive strength development and the development of the E-modulus will be used to increase the accuracy of the finite element analysis regarding the assessment of the risk of early-age cracking.

Appendix G: Comparison between initially assumed creep data and fitted creep data

In this appendix the creep data as initially defined named 'high creep' is compared with the creep data as results from the iterative fitting of the stress curve of the FEA of the TSTM test to the stress curve as results from the TSTM test. The finite element software requires the creep data in the form of 'Maxwell chain data'. The chain data for both the 'high creep' and the 'fitted creep behaviour' can be seen in the tables below.

- High creep

Maxwell Chain Data		Retardation times with distribution coefficients					
Maturity	E-modulus	1,0	10,0	100,0	1000,0	10000,0	100000,0
[hours]	[MPa]	[hours]	[hours]	[hours]	[hours]	[hours]	[hours]
0	500	0,0000	0,0000	0,2000	0,8000	0,0000	0,0000
24	15732	0,0000	0,4000	0,1000	0,0000	0,5000	0,0000
72	24958	0,0000	0,3700	0,1500	0,0000	0,4800	0,0000
168	30555	0,0000	0,4200	0,1000	0,1100	0,3700	0,0000
672	34559	0,0000	0,3600	0,0700	0,1300	0,4400	0,0000

Table G.1 Maxwell chain data for initial 'high creep'

- Fitted creep behaviour

Maxwell Chain Data		Retardation times with distribution coefficients					
Maturity	E-modulus	1,0	10,0	100,0	1000,0	10000,0	100000,0
[hours]	[MPa]	[hours]	[hours]	[hours]	[hours]	[hours]	[hours]
0	500	0,9000	0,1000	0,0000	0,0000	0,0000	0,0000
24	15732	0,1000	0,9000	0,0000	0,0000	0,0000	0,0000
72	24958	0,0000	0,4200	0,1800	0,0000	0,4000	0,0000
168	30555	0,0000	0,2200	0,1000	0,1100	0,5700	0,0000
672	34559	0,0000	0,3600	0,0700	0,1300	0,4400	0,0000

Table G.2 Maxwell chain data for 'fitted creep' behaviour

Next, the creep data sets are compared by means of the creep compliance $J\ [\frac{1}{MPa}]$ curves consisting of the elastic response and the specific creep response. This is done for specific maturities at loading as can be seen from the tables containing the Maxwell chain data above. It must be noted that for all maturities at loading the elastic response is equal for both creep data sets.

- **Loading at 0 hours maturity**

The E-modulus for 0 hours of maturity is assumed to be equal to 500 MPa. This is a fictional stiffness because in reality the concrete will not have any stiffness at 0 hours maturity. However because of computational limitations the concrete is required to have an initial stiffness.

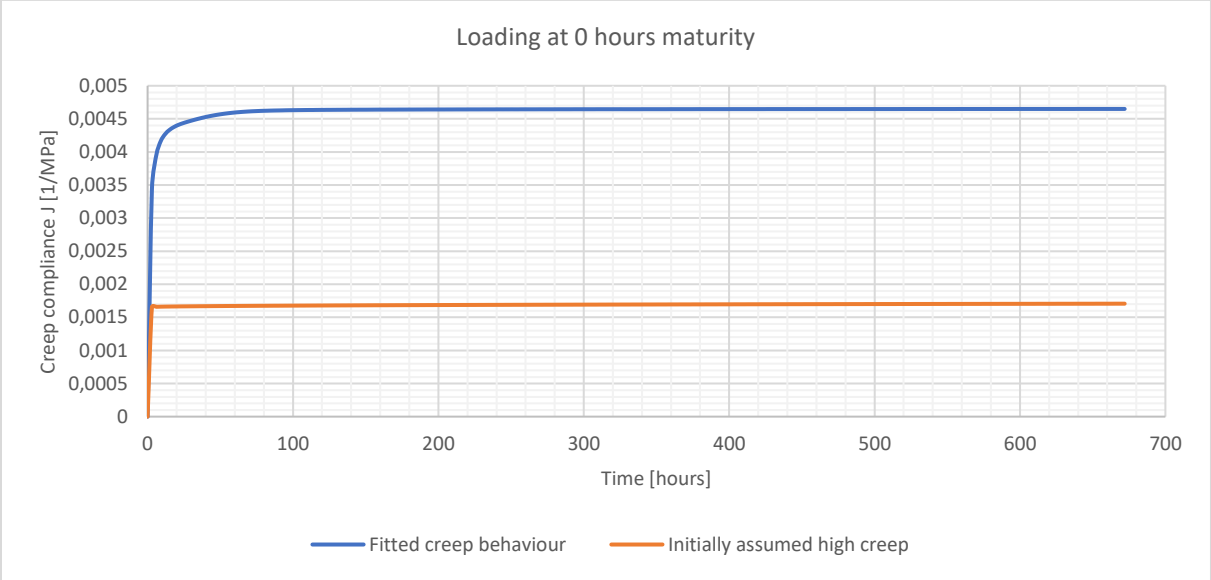

figure G.1 Comparison between the total strain response to unit of stress according to the fitted creep behaviour and the initially high creep behaviour for a maturity at loading of 0 hours

As can be seen from the figure above, the creep compliance at $t = 672$ hours after loading is significantly higher for the fitted creep behaviour. The multiplication factor between the two values equals:

$$\frac{J_{fittedcreep}}{J_{highcreep}} = \frac{4{,}65 * 10^{-3}}{1{,}71 * 10^{-3}} = \mathbf{2{,}72}\ [-]$$

- **Loading at 24 hours maturity**

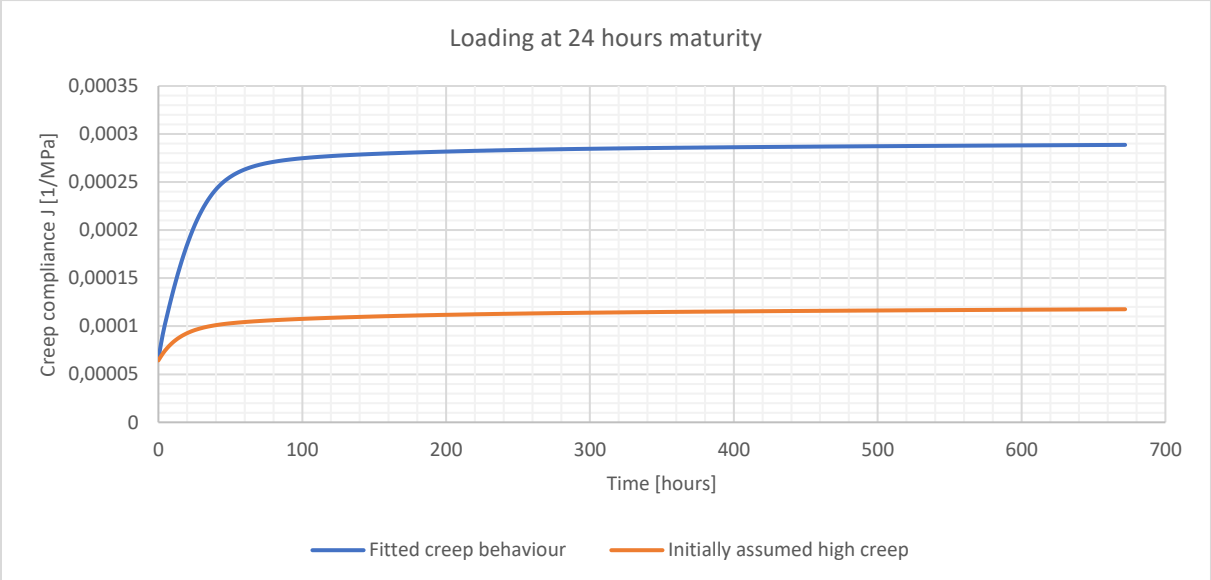

figure G.2 Comparison between the total strain response to unit of stress according to the fitted creep behaviour and the initially high creep behaviour for a maturity at loading of 24 hours

As can be seen from the figure above, the creep compliance at $t = 672$ hours after loading is significantly higher for the fitted creep behaviour. The multiplication factor between the two values equals:

$$\frac{J_{fittedcreep}}{J_{highcreep}} = \frac{2{,}89 * 10^{-4}}{1{,}18 * 10^{-4}} = \mathbf{2,45}\ [-]$$

- **Loading at 72 hours maturity**

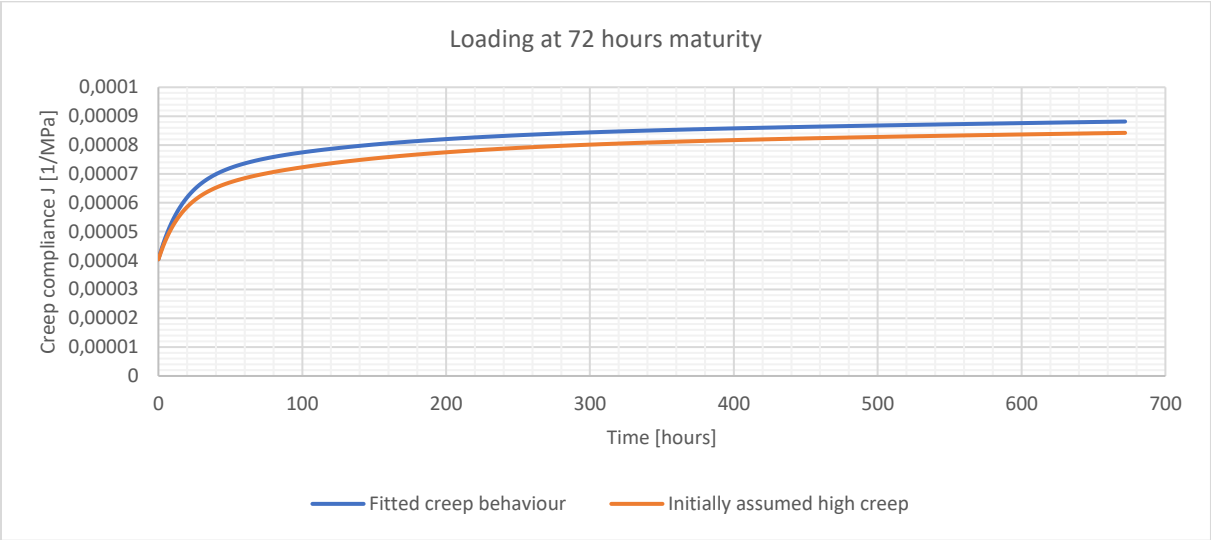

figure G.3 Comparison between the total strain response to unit of stress according to the fitted creep behaviour and the initially high creep behaviour for a maturity at loading of 72 hours

As can be seen from the figure above, the creep compliance at $t = 672$ hours after loading is higher for the fitted creep behaviour. The multiplication factor between the two values equals:

$$\frac{J_{fittedcreep}}{J_{highcreep}} = \frac{8{,}81 * 10^{-5}}{8{,}42 * 10^{-5}} = \mathbf{1.05}\ [-]$$

- **Loading at 168 hours maturity**

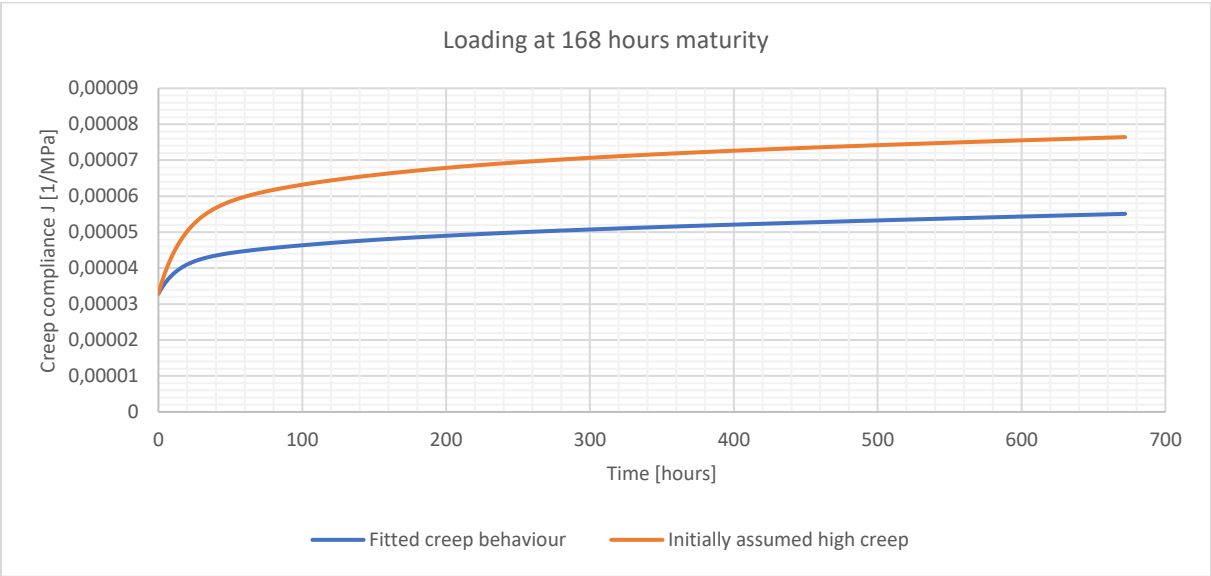

figure G.4 Comparison between the total strain response to unit of stress according to the fitted creep behaviour and the initially high creep behaviour for a maturity at loading of 168 hours

As can be seen from the figure above, the creep compliance at $t = 672$ hours after loading is higher for the initally assumed 'high creep' behaviour. The multiplication factor between the two values equals:

$$\frac{J_{fittedcreep}}{J_{highcreep}} = \frac{5.51 * 10^{-5}}{7.64 * 10^{-5}} = \mathbf{0.72}\ [-]$$

Appendix H: Laboratory test data

Details on the data resulting from the laboratory testing can here be seen.

- **TSTM and ADTM test:**

The raw data of the TSTM and ADTM tests is assembled in an Excel file. This file is added to this PDF report in the form of an attachment. In this Excel file the different sensor output over time can be seen for the different tests. This includes measurements of temperature, forces and displacements. The measurement interval is equal to 1 minute.

- **Cube tests:**

Details on the results of the cube tests are displayed here in the form of tables. Cubes were tested at specific moments in time after casting.

Cube compressive tests:

Hours	Days	$f_{cm}(t)$
24	1	3.27
48	2	11.65
120	5	24.57
192	8	32.83
336	14	39.46
672	28	45.06

Table H.1 Results of the cube compressive tests

Tensile splitting tests:

Hours	Days	$f_{ctm}(t)$
24	1	0.45
48	2	1.25
120	5	2.75
192	8	3.31
336	14	3.53
672	28	3.89

Table H.2 Results of the cube tensile splitting tests

Mean E-modulus as derived from the measured compressive strength:

Hours	Days	$E_{cm}(t)$
24	1	15732
48	2	23031
120	5	28810
192	8	31427
336	14	33210
672	28	34559

Table H.3 E-modulus development as derived from the measured compressive strength